ENERGY FACILITIES: MANAGEMENT AND DESIGN AND TECHNOLOGICAL INNOVATIONS

Collective monograph

E54   **Authors:**
Andriy Polishchuk, Volodymyr Kulyk, Vira Teptya, Sviatoslav Vishnevskyi, Yurii Hrytsiuk, Iryna Hrytsiuk, Viacheslav Komar, Petro Lezhniuk, Vladyslav Lesko, Yuliya Malogulko, Volodymyr Netrebskyi, Olena Sikorska, Volodymyr Khomenko, Oksana Chernysh, Viacheslav Barsukov, Viktor Tverdokhlib, Arkadij Berezovskij, Volodymyr Slobodianyk, Natalia Minska, Roman Shevchenko, Vasyl Servatyuk, Valery Strelets, Victoria Lukashenko, Yaroslav Kalchenko, Ernst Kussul, Tetyana Baydyk, Masuma Mammadova, Jorge Luis Rodriguez Mendoza

Energy facilities: management and design and technological innovations: collective monograph. – Kharkiv: PC TECHNOLOGY CENTER, 2022. – 224 p.

The collective monograph contains the results of scientific research on the management of energy facilities and the creation of elements of energy systems. A system for proactive control of reactive power flows in distributed electrical networks and an algorithm for coordinating schedules for the consumption of electricity and renewable energy sources in electrical networks to improve the reliability of the balance are proposed. Composite materials based on water-soluble binders for electrochemical capacitors are proposed as non-traditional rechargeable sources of electric current. Design and technological solutions for the creation of film solar cells for backup power supply of emergency protection systems, as well as design solutions for solar concentrators are given.
The monograph is intended for practitioners in the field of creating energy systems and managing power supply facilities, researchers and university professors.
Figures 132, Tables 38, References 298 items.

AUTHORS

CHAPTER 1

ANDRIY POLISHCHUK
PhD, CEO
JSC "Vinnytsiaoblenergo"
ORCID ID: https://orcid.org/0000-0003-4652-9113

VOLODYMYR KULYK
Doctor of Technical Sciences, Associate Professor
Department of Electric Stations and Systems
Vinnytsya National Technical University
ORCID ID: https://orcid.org/0000-0002-7594-5661

VIRA TEPTYA
PhD, Associate Professor
Department of Electric Stations and Systems
Vinnytsya National Technical University
ORCID ID: https://orcid.org/0000-0002-2792-0160

SVIATOSLAV VISHNEVSKYI
PhD
Department of Electric Stations and Systems
Vinnytsya National Technical University
ORCID ID: https://orcid.org/0000-0002-2159-603X

YURII HRYTSIUK
PhD, Associate Professor
Department of Electrical Engineering
Lutsk National Technical University
ORCID ID: https://orcid.org/0000-0002-6463-3910

IRYNA HRYTSIUK
PhD, Associate Professor
Department of Electrical Engineering
Lutsk National Technical University
ORCID ID: https://orcid.org/0000-0003-4472-306X

CHAPTER 2

VIACHESLAV KOMAR
Doctor of Technical Sciences, Professor
Department of Electrical Plants and Systems
Vinnytsia National Technical University
ORCID ID: http://orcid.org/0000-0003-4969-8553

PETRO LEZHNIUK
Doctor of Technical Sciences, Professor
Department of Electrical Plants and Systems
Vinnytsia National Technical University
ORCID ID: http://orcid.org/0000-0002-9366-3553

VLADYSLAV LESKO
PhD, Associate Professor
Department of Electrical Plants and Systems
Vinnytsia National Technical University
ORCID ID: http://orcid.org/0000-0002-5477-7080

YULIYA MALOGULKO
PhD, Associate Professor
Department of Electrical Plants and Systems
Vinnytsia National Technical University
ORCID ID: http://orcid.org/0000-0002-6637-7391

VOLODYMYR NETREBSKYI
PhD, Associate Professor
Department of Electrical Plants and Systems
Vinnytsia National Technical University
ORCID ID: http://orcid.org/0000-0003-2855-1253

OLENA SIKORSKA
PhD, Senior Lecturer
Department of Electrical Plants and Systems
Vinnytsia National Technical University
ORCID ID: http://orcid.org/0000-0001-7341-9724

CHAPTER 3

VOLODYMYR KHOMENKO
Doctor of Technical Sciences, Associate Professor
Department of Electrochemical Power Engineering & Chemistry
Kyiv National University of Technologies and Design
ORCID ID: https://orcid.org/0000-0003-0013-8010

OKSANA CHERNYSH
PhD, Senior Researcher
Department of Electrochemical Power Engineering & Chemistry
Kyiv National University of Technologies and Design
ORCID ID: https://orcid.org/0000-0002-9402-1595

VIACHESLAV BARSUKOV
Doctor of Chemical Sciences, Professor, Honored Worker of Science and Technology of Ukraine, Head of Department
Department of Electrochemical Power Engineering & Chemistry
Kyiv National University of Technologies and Design
ORCID ID: https://orcid.org/0000-0002-3041-2474

VIKTOR TVERDOKHLIB
PhD, Associate Professor
Department of Electrochemical Power Engineering & Chemistry
Kyiv National University of Technologies and Design
ORCID ID: https://orcid.org/0000-0002-5764-9842

ARKADIJ BEREZOVSKIJ
PhD, Head of Department
Research Department
Central Scientific Research Institute of Armament and Military Equipment of Armed Forces of Ukraine
ORCID ID: https://orcid.org/0000-0001-9328-6586

VOLODYMYR SLOBODIANYK
PhD, Senior Researcher
Research Department
Central Scientific Research Institute of Armament and Military Equipment of Armed Forces of Ukraine
ORCID ID: https://orcid.org/0000-0001-5901-873x

CHAPTER 4

NATALIA MINSKA
Doctor of Technical Science, Associate Professor
Department of Special Chemistry and Chemical Engineering
National University of Civil Defence of Ukraine
ORCID ID: https://orcid.org/0000-0001-8438-0618

ROMAN SHEVCHENKO
Doctor of Technical Science, Professor
Department of Automatic Security Systems and Information Technologies
National University of Civil Defence of Ukraine
ORCID ID: https://orcid.org/0000-0001-9634-6943

VASYL SERVATYUK
Doctor of Military Sciences
Professor
Institute of State Military Administration
National Defence University of Ukraine named after Ivan Cherniakhovskyi
ORCID ID: https://orcid.org/0000-0001-8438-0618

VALERY STRELETS
PhD
The International Humanitarian Organization The Halo Trust in Ukraine
ORCID ID: https://orcid.org/0000-0003-1913-7878

VICTORIA LUKASHENKO
PhD, Associate Professor
Department of Computer Systems and Networks
National Aviation University
ORCID ID: https://orcid.org/0000-0002-8898-2269

YAROSLAV KALCHENKO
Doctor of Philosophy
Department of Fire and Technogenic Safety of Facilities and Technologies
National University of Civil Defence of Ukraine
ORCID ID: https://orcid.org/0000-0002-3482-0782

CHAPTER 5

ERNST KUSSUL
Doctor, Profesor, Investigador Titular C de T.C.
Instituto de Ciencias Aplicadas y Tecnología
Universidad Nacional Autonoma de México
ORCID ID: https://orcid.org/0000-0002-2849-2532

TETYANA BAYDYK
Doctor, Profesor, Investigador Titular C de T.C.
Instituto de Ciencias Aplicadas y Tecnología
Universidad Nacional Autonoma de México
ORCID ID: https://orcid.org/0000-0002-3095-2032

MASUMA MAMMADOVA
Doctor, Professor, Head of Department
Department of Number 15
Institute of Information Technology of Azerbaijan National Academy of Sciences
ORCID ID: https://orcid.org/0000-0002-2205-1023

JORGE LUIS RODRIGUEZ MENDOZA
PhD student
Facultad de Ciencias Químicas
Universidad de Colima
ORCID ID: https://orcid.org/0000-0001-6000-3623

ABSTRACT

The collective monograph contains the results of scientific research on the management of energy facilities and the creation of elements of energy systems. A feature of the proposed approaches is the consideration of objects in several aspects: process control in distributed networks, the balance of production and consumption of electricity, innovative materials and technological solutions focused on the concept of using renewable and non-traditional energy sources.

Chapter 1 presents a solution to the problem of improving the methods and tools for optimizing reactive power flows in distribution networks with significant daily volatility in generation and consumption of electricity.

Chapter 2 proposes an algorithm for the method of matching the generation schedules of photovoltaic power plants with the electric load of the network as a possible solution for improving the balance in the electricity grid with renewable energy sources.

Chapter 3 describes the results of research and development of environmentally friendly methods for producing composite materials for electrochemical capacitors related to non-traditional rechargeable electric current sources.

Chapter 4 presents the results of a study of solar cells based on CdS/CdTe, intended for backup power supply of security systems and facility management in conditions of damage to the power supply system. Ways to improve the efficiency of such film solar cells are proposed.

Chapter 5 presents the development of several prototypes of compact, lightweight, and inexpensive solar concentrators, and proposes two assembly methods that overcome the main problem associated with automating the solar concentrator assembly process.

KEYWORDS

Advanced heating, power distribution system, renewable energy sources, power balance, electrochemical capacitor, porous carbonaceous material, film solar cell, solar concentrator.

CIRCLE OF READERS AND SCOPE OF APPLICATION

The monograph is intended for practitioners in the field of creating energy systems and managing power supply facilities, engineering and technical specialists, and designers. The monograph will also be useful for researchers and university teachers who use advanced research developments in the educational process in the relevant specialties, developing the skills of working with scientific information in future young professionals to generate new practical solutions.

CONTENTS

LIST OF TABLES

LIST OF FIGURES

INTRODUCTION

The creation of modern energy supply systems and the management of the processes of generation, distribution and consumption of energy require integrated approaches that take into account various aspects. Among them are promising and environmentally friendly materials for power facilities, the design of elements of the corresponding systems that meet operational requirements, their manufacturing technologies, as well as systems for the optimal control of such facilities.

Consideration of energy objects in such planes makes practically useful solutions obtained in the course of relevant scientific research, which determines the relevance of such research. The concepts and data presented in the monograph allow us to speak about a comprehensive consideration of problems, since they can provide a solution to the problems of managing processes in distributed grids and balancing the production and consumption of electricity; selection of innovative materials and technological solutions, including those based on renewable and non-traditional energy sources.

The relevance of research aimed at using such an integrated approach is explained by the possibility of integrating the results obtained for different aspects of the problem. In particular, the following aspects of the development of energy facilities and their management were reflected:

– improvement of methods and tools for optimizing reactive power flows in distribution grids with significant daily volatility in generation and consumption of electricity;

– development of a method for coordinating the schedules for the production of photovoltaic power plants with the electrical load of the grid;

– creation of environmentally friendly methods for obtaining composite materials for electrochemical capacitors related to non-traditional rechargeable sources of electric current;

– study of solar cells based on CdS/CdTe, intended for backup power supply of security systems and facility management in conditions of damage to the power supply system;

– development of prototypes of solar concentrators and methods for their assembly.

Improvement of methods and means of optimizing reactive power flows in distribution networks contributes to improving the quality of functioning of energy distribution systems.

The development of a method for matching the generation schedules of photovoltaic power plants with the electrical load of the grid is a possible solution to improve the balance in the electricity grid with renewable energy sources. At the same time, means of regulating reactive power in the electrical grid can also be found in order to maintain the voltage within acceptable limits.

The creation of environmentally friendly methods for producing composite materials for electrochemical capacitors can contribute to the improvement of such elements as non-traditional rechargeable electric current sources that can be quickly charged and discharged, have high power and a long service life. Having certain disadvantages in comparison with batteries in terms of capacity and energy density, they nevertheless have significant advantages over batteries in terms

of their power density, rate of charge-discharge processes and service life. Therefore, the search for effective solutions in the production of such electric current sources opens up additional prospects for expanding their representation in many practical applications: military and space technology, in energy storage systems at peak loads, for regulating wind generator turbines, etc.

The results of studies of solar cells based on CdS/CdTe open up new opportunities for creating backup power elements for security systems and facility management in conditions of damage to the power supply system. In particular, one of the key ones is the technological aspects of obtaining such elements.

The development of prototype solar concentrators and methods for assembling them is important in the context of maximizing the use of renewable energy sources. It should be noted that such solutions are promising for many regions of the world, the features of which are the abundance of solar radiation, the predominance of mountainous regions with remote and hard-to-reach settlements that need to create autonomous life support systems. Rational design decisions regarding the design of solar concentrators can achieve high efficiency solar energy for the respective regions.

The solutions presented in the collective monograph, obtained by considering objects in such planes, can be useful in practice and contain ideas that have the potential for development in the field of theory.

Andriy Polishchuk, Volodymyr Kulyk, Vira Teptya,
Sviatoslav Vishnevskyi, Yurii Hrytsiuk, Iryna Hrytsiuk

CHAPTER 1

CHAPTER 1

SYSTEM OF PROACTIVE CONTROL OF REACTIVE POWER FLOWS IN DISTRIBUTED ELECTRICAL GRIDS

ABSTRACT

The paper solves the urgent problem of improving the methods and means of optimizing reactive power flows in distribution grids with significant daily volatility in the generation and consumption of electricity. The object of research is the process of automated control of a set of reactive power sources (RPS) in distribution electrical grids (DEG). Coordination of their operation will contribute to the reduction of electricity losses in the DEG and improve the voltage quality. Based on the results of the analysis of modern trends in the construction of RPS control systems, the expediency of decentralization using local automatic control systems (ACS) is substantiated.

The operational determination of the optimal powers of the RPS and the calculation of the corresponding settings of local ACS are associated with objective difficulties. The study proposes a formalization of the problem of optimizing reactive power flows in DEG and a new way to solve it. It is shown that the problem can be reduced to the determination and periodic correction of the settings of local systems of automatic control of the RPS. The latter, by adjusting the energy flows according to local parameters, taking into account the specified settings, contribute to the achievement of the overall effect of reducing losses and stabilizing the voltage in the DEG. The proposed method contributes to a reasonable simplification and increase in the reliability of the distributed control system for reactive power flows in the DEG, taking into account technical limitations.

To solve the problem, the principle of advancing control, the method of "ideal" current distribution (according to power losses) was applied. Using the model of "ideal" current distribution, the problem of nonlinear optimization of reactive power flows in the DEG was reduced to a fundamentally simpler problem of finding current distribution in a step-by-step circuit with active resistances. To determine the time intervals between the adjustment of local ACS, it is proposed to analyze the correlation between the predictive graph of the optimal power of an individual RPS and local energy consumption based on the Pearson coefficient.

A block diagram and algorithms for the operation of the control system for the set of RPSs are proposed, which provide a minimum of computational operations and data exchange operations. At the same time, a response is provided to changes in the consumption and generation of electricity

in the conditions of short-term failures of information systems. This contributes to improving the quality of operation of energy distribution systems in modern conditions.

KEYWORDS

Proactive control, power distribution system, reactive power sources, optimization, "ideal" current distribution, losses, voltage quality.

The operation of modern distribution electrical grids (DEG) is characterized by a local increase in energy consumption, the appearance of two-way flows, increased requirements for ensuring reliability and controllability, as well as more stringent environmental restrictions [1]. To solve the problem of cost-effectiveness and environmental friendliness of the DEG operation, various energy-saving measures and innovative technologies are being developed and implemented.

In recent years, trends in the economical use of fossil fuels have led to the integration of renewable energy sources (RES) into distribution grids. Moreover, the share of the latter in the energy balance of some DEG already today is 30 % or more. Since DEGs were designed for centralized power supply, the development of dispersed generation gives rise to new problems and tasks [2]. From a technical point of view, the main tasks are to maintain the balance of active and reactive power.

The transmission of reactive power by grids is associated with an increase in current loads, an increase in voltage drops, an increase in electricity losses, etc. A feature of reactive power compensation in modern DEG is that optimal decisions have to be made in conditions of significant volatility of active and reactive power consumption, as well as unstable local generation. At the same time, individual RES can provide additional means to improve the efficiency of electricity distribution.

The implementation of information technologies in DEG has created the basis for the development and improvement of the operating efficiency of reactive power sources (RPS) with automatic control. However, the solution of a complex problem requires the application of efficiency criteria that link the energy efficiency of the DEG, the quality of electricity, the reliability of grids and the RPS payback. The complexity of the problem statement, the dynamism of the processes and the dispersal of reactive power sources in the DEG requires constant improvement of approaches to automated and automatic control.

Therefore, the problem of improving the methods and means of optimizing reactive power flows in distribution grids, which have significant daily volatility in the generation and consumption of electricity, turns out to be relevant.

Traditionally, to search for solutions to optimize reactive power flows in DEG, numerous methods of linear and nonlinear programming are used [3]. For the practical implementation of solutions, uncontrolled RPS or automated reactive power compensation installations are used. The latter

automatically adjust the output power according to local parameters. The general disadvantage of this approach is that it gives partial solutions. To eliminate it, it is proposed to determine the optimal parameters of the RPS based on the mutual influence of all sources and consumers in the DEG. And a dispersed control system for a set of local RESs should be built on the basis of the Hamilton-Ostrogradsky principle [4] to achieve a system-wide effect.

The aim of the study is to improve the efficiency of managing a set of dispersed reactive power sources, which is manifested in reducing power losses and improving the quality of voltage in distribution grids.

To achieve the aim, the following objectives are solved:

— well-known methods for optimizing the modes of electrical grids in terms of reactive power are analyzed;

— the conditions for the optimal operation of reactive power compensation means in distribution grids are determined;

— a block diagram and algorithms for the operation of the control system for a set of RPS equipped with local automatic control systems have been developed;

— the effectiveness of the automated reactive power flow control system was tested on the example of 10 kV urban distribution grids.

The object of the study is the normal modes of distribution electrical grids with dispersed sources of electricity.

The subject of the study is methods and means of optimizing power flows by means of proactive control of reactive power compensation installations.

For the analysis and solution of the tasks set, the principle of least action in the formulation of Hamilton-Ostrogradsky, methods of linear and non-linear programming are used. The established DEG modes were modeled on the basis of the nodal voltage method. Electricity losses were determined by the method of average loads and numerical integration. Matrix algebra, graph theory and decomposition were used to develop algorithms for optimizing reactive power flows in and the formation of adjustment parameters for automatic control systems of the RES, matrix algebra, graph theory and decomposition were used. To develop an automated control system, the provisions of the theory of automatic control were used.

The conducted studies have shown the feasibility of using the Hamilton-Ostrogradsky principle to solve the problem of optimizing reactive power flows in distribution grids with a sharply changing load. In particular, using the mentioned principle, the possibility of raising the problem of nonlinear optimization of reactive power flows according to the criterion of maximum profit to the calculation of the "ideal" mode of the distribution grid is substantiated. This significantly reduced the number of calculations and increased the reliability of obtaining a solution.

The proposed approach to the calculation of the optimal reactive powers made it possible to develop an algorithm for proactive control of a set of RESs. It ensured the coordination of the RPS operation in the grids of power supply companies by preventive adjustment of the adjustment parameters of their control systems. According to the developed block diagrams and control algo-

rithms, an automated control system for the existing RPS was created to maintain optimal reactive power flows, taking into account the rapid changes in the operating parameters of the DEG, in particular, the generation of renewable sources.

1.1 METHODS FOR OPTIMIZING REACTIVE POWER FLOWS IN MODERN DISTRIBUTION GRIDS

Optimization of reactive flows in modern DEG has certain features. In addition to traditional sources of reactive power, in particular, power plants, transmission lines and specialized devices, dispersed installations for the conversion of energy from renewable sources (RES) should be considered. Their operation is determined by the influence of the environment, so it is difficult to predict. As a result, reverse flows occur periodically, which affect the reliability and efficiency of electricity transportation. Since the pace of renewable energy development is growing every year, these problems will only get worse. This is evidenced by the experience of Western countries. In [5], using the example of Germany, it is shown that the output of RES power can cause an unacceptable increase in voltage levels.

At the same time, using inverter converters, synchronous or asynchronous RES generators can generate or consume a given reactive power without active power limitation. For example, in [6] it is shown that the controlled supply of reactive power from RES can reduce losses in the distribution grid and facilitate the flexible exchange of reactive energy with the grids of transmission system operators (TSOs).

In addition to the RES implementation, electricity consumption is increasing locally in modern distribution grids. In Italy, for example, fast charging stations for electric vehicles have significant peak powers and low power factor. The random nature of this load, which grows with the demand for electric vehicles, has a negative impact on the energy efficiency of distribution grids [7].

Thus, changes in the nature of generation and consumption in distribution grids, especially reactive power, require improvements in methods and means to improve energy efficiency.

1.1.1 METHODS FOR SOLVING PROBLEMS OF OPTIMIZING REACTIVE POWER FLOWS

To solve problems related to the optimization of reactive power flows in DEG to achieve maximum profit or profitability, methods of decomposition, linear and nonlinear programming are traditionally used [8]. However, such methods use assumptions and simplifications, so they can direct the solution process to local extrema.

In a number of works, in particular [8], the possibility of moving from a complex problem of optimizing reactive power flows to a number of separate optimization problems is shown. This allows the use of classical optimization methods [8] and traditional software. However, this approach is

associated with the need for additional assumptions for the decomposition of the problem. This reduces the reliability and speed of obtaining a solution and degrades the efficiency of the operational control of the RPS [9].

The development of information technologies and computing facilities has created conditions for new approaches to solving the problem of optimizing reactive power flows. They are focused on increasing the level of automation of the DEG operation. Elements of artificial intelligence [10–12], including artificial neural grids [10], expert systems [5], genetic algorithms [11], and evolutionary programming [12], are actively used. However, the excessive time spent on finding optimal solutions in the case of using evolutionary and genetic algorithms limits their use for real-time problems [9].

For DEG, the problem of reactive power control is mainly due to its influence on the voltage deviation [13]. Therefore, the optimization of reactive power generation in DEG is often based on voltage sensitivity assessment methods. For this, in [13], a fragment of the Jacobian sensitivity matrix and voltage sensitivity index (VSI) are used. The latter is defined as the Euclidean norm of a fragment of the inverse Jacobi matrix [14].

In addition to determining the optimal powers of the RPS, an important aspect is the organization of their interaction in the DEG to ensure a systemic effect. In [15], an approach is presented to optimize the reactive power and voltage flows in the power system using game theory. It is shown that a complex interaction between the RPS is necessary to control the voltage in the DEG. For its reproduction and optimization, a non-commercial formal game was used. It is shown that the appropriate settings of the automatic control systems of individual DEGs allow their coordinated operation according to local parameters. This minimizes the total reactive power generation required to satisfy voltage limits.

Advances in information technology have made it possible to use parallel computing to optimize the DEG operation. Therefore, methods of multicriteria optimization of reactive power distribution have been developed [16]. The vast majority of them are based on well-known single-objective optimization methods, in particular, on genetic algorithms [17, 18], search engine optimization algorithms [19], and competitive algorithms [20, 21] in combination with decomposition methods [22].

In [23], a modified Pareto method was proposed to apply parallel computing to the problem of optimizing the distribution of reactive power. Three objective functions were chosen for multi-purpose operational optimization: reduction of power losses, reduction of voltage deviation and increase of voltage stability. To solve the problem, let's use the algorithm of strength Pareto multi-group search optimization (SPMGSO) [24]. The results of Pareto optimization are compared with other methods, in particular, with non-dominant sorting genetic algorithm II (NSGA II) [25], non-dominant sorting particle swarm optimization (NSPSO) [26]. The comparison confirmed the effectiveness of the method, which is manifested in a steady reduction in energy losses.

However, the practical implementation of this approach involves the prompt determination of the optimal powers of the RPS, as well as the possibility of permanent centralized control over them. The latter is mostly impossible for DEG due to the lack of a developed information infrastruc-

ture [27, 28]. Based on this, it is advisable to use distributed automated control systems based on local automatic control systems (ACS).

For such a control organization, specific approaches to solving optimization problems should be applied. In [29], it was proposed to use the iterative method of semi-definite programming (SDP) to solve the problems of optimizing the RPS power. Each iteration involves solving the optimization problem of determining the power of the RPS using SDP. Changes in the DEG parameters within the iteration are considered not critical for the adequacy of the model. After each iteration, the grid parameters are refined. The validity of this principle of distribution of the optimization process was confirmed by computational and full-scale experiments [29]. Therefore, it was used in our study to create algorithms for simulating DEG modes during the day and taking into account the influence of local systems of automatic control of the RPS.

1.1.2 OPTIMIZATION OF REACTIVE POWER FLOWS BASED ON THE "IDEAL" MODE OF THE DISTRIBUTION GRID

The objective function of the problem of optimizing the RPS powers according to the criterion of minimum power losses in the DEG is predominantly convex and has no gaps. To solve the problem, a number of methods have been developed that have confirmed their effectiveness. But the tasks of operational control of reactive power sources are more complicated. The reasons are the dynamism of the processes of the control object and severe time constraints for decision making. Based on this, the methods described above often cannot guarantee a solution to the problem. At the same time, the application of the Hamilton-Ostrogradsky principle [30] makes it possible to determine the coordinates of some "ideal" DEG mode, taking into account energy losses. After that, the search for the optimal regime is reduced to taking into account the limitations of the parameters. This approach increases the reliability and speed of the search for the optimal solution of energy problems. After all, the process of searching for a solution begins not with an arbitrary initial approximation, but with an extreme value corresponding to the "ideal" mode of the DEG (**Fig. 1.1**). In addition, the coordinates of the "ideal" mode can be determined by calculating the steady state after a certain adjustment of the calculation model [31].

The process of searching for the optimal solution is shown in the projection onto the X_1X_2 coordinate plane (**Fig. 1.1, a**) and in the projection onto the $P(X_1, X_2)$ coordinate plane obtained by the principal component method (PCM) (**Fig. 1.1, b**). Taking into account the peculiarities of determining the step of the gradient method, the process of finding a solution slows down significantly in the optimality region (**Fig. 1.1, a**) [31]. Thus, the time limits of operational control may be violated.

The optimal DEG mode in terms of reactive power (**Fig. 1.1, a**) is determined in two stages. First, the parameters of the "ideal" mode X_i [X_{1i}, X_{2i}] are calculated, which correspond to the minimum power losses at given loads and voltage levels in the DEG. The values of the optimized variables X_{1i}, X_{2i} and the objective function Z_i for such a regime are calculated by analytical expressions

obtained from the Euler-Lagrange equations [31]. In practice, such a regime generally cannot be implemented. Therefore, at the second stage, restrictions are imposed on the dependent and independent parameters of the regime. This ensures the transition to the optimal DEG mode X_o [X_{1o}, X_{2o}]. Losses of electricity for the optimal DEG mode, obviously, will be greater than for the "ideal".

CHAPTER 1
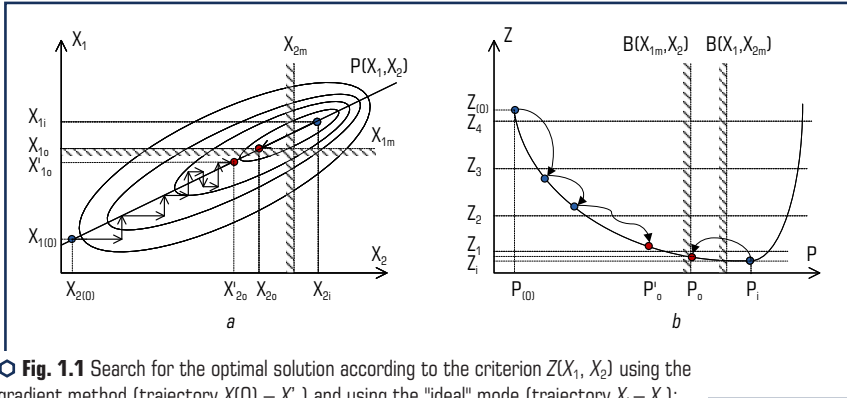
○ **Fig. 1.1** Search for the optimal solution according to the criterion $Z(X_1, X_2)$ using the gradient method (trajectory $X(0) - X'_o$) and using the "ideal" mode (trajectory $X_i - X_o$): a – projection onto the coordinate plane X_1, X_2; b – projection onto the plane $P(X_1, X_2)$

To form control laws and determine the debugging parameters of the ACS, one should take into account the uncertainty of individual independent parameters of the DEG. It is due to the dynamism of the regimes and the shortcomings of information support. Accounting for the mutual influence of the control actions of individual ACS and changes in the DEG parameters under the action of control is a particularly difficult task. It requires the use of simulation models and the principle of active control.

1.1.3 OPERATIONAL OPTIMIZATION OF REACTIVE POWER FLOWS USING PROACTIVE CONTROL

Decentralization of power supply in DEG and the growth of the total power of sources of dispersed generation complicate the planning of power grid modes. The existing supervisory control and automation systems were not ready to support this process. This resulted in the inability to take advantage of the potential benefits of the DESs. In particular, the use of subscriber energy sources for unloading DEG and reducing losses in them [32]. At the same time, technical problems associated with their integration emerged.

For example, power fluctuations at the inputs of powerful wind and solar power plants entail problems in energy transmission systems [33]. Traditional sources of reactive power are not able to constantly maintain the balance of reactive power in such transmissions. Therefore, it is

necessary to improve the means of managing the RPS to ensure the stability of distribution grids in terms of voltage.

For the development of automation systems for RPS, it is necessary to take into account the purpose of control, as well as the requirements of industry standards. On their basis, [4, 27, 34, 35] formulated the requirements for technical means, as well as the principles of RPS automatic control:

— reduction of electricity losses in consumer power supply systems in possible daily consumption modes;

— implementation of voltage restrictions in the DEG;

— the maximum attraction of the RPS, if there are no restrictions on the exchange of reactive power between the DEG and the subscriber;

— control of actual reactive power flows at the inputs of DEG subscribers and dispersed energy sources;

— determination and implementation of the optimal settings for the power factor at the inputs of subscribers and DES. Technical support for the possibility of their remote adjustment when changing the DEG modes;

— hourly registration of reactive power flows and power factors within the balance sheet of the DEG. Remote monitoring of the state of the information-measuring subsystem;

— centralized control in automated and automatic modes using local control devices.

Distributed objects, similar to the DEG properties, are constantly exposed to a significant number of influences from sources and consumers of electricity, local controls and emergency automation, as well as the environment. These perturbations affect the dynamic processes in a distributed object and require control coordination. The general structure of proactive control of such an object is shown in **Fig. 1.2** [36]. Local automatic control systems adjust the parameters of individual elements of a distributed object to ensure its optimal operation according to a certain criterion. The local control task comes from the coordinator. It determines the control actions for individual ACS, taking into account the dynamics of the object. The predictor predicts changes in the state of a distributed object as a response to registered disturbances and controls.

However, the optimal parameters of an individual controlled element depend not only on the perturbations recorded at its level or the influence of the local ACS [37]. Adjacent controlled elements and the external environment have a significant impact. Its settings at the local level are usually not logged. To ensure proactive control, the predictor and coordinator must mimic the response of distribution grids. In addition, they must reproduce the reaction of local ACS to the recorded changes in the parameters of the DEG mode, taking into account the possible dynamics of these changes. In this case, periodic debugging of local ACS will provide stable and consistent proactive control of a distributed object [38].

The scheme for organizing the control of dynamic modes of reactive power consumption, containing links of centralized and local control, has shown its effectiveness in practice [33].

Thus, in [33], it was proposed to use a coordinated adjustment of the parameters of DC converters of wind and solar power plants and RPS. Local automatic control of the RPS provides a

quick response to a decrease in reactive power flows. If the reactive power consumption exceeds the power of the RPS, then the AC filter is switched on. And the RPS is remotely reconfigured to maintain the power balance.
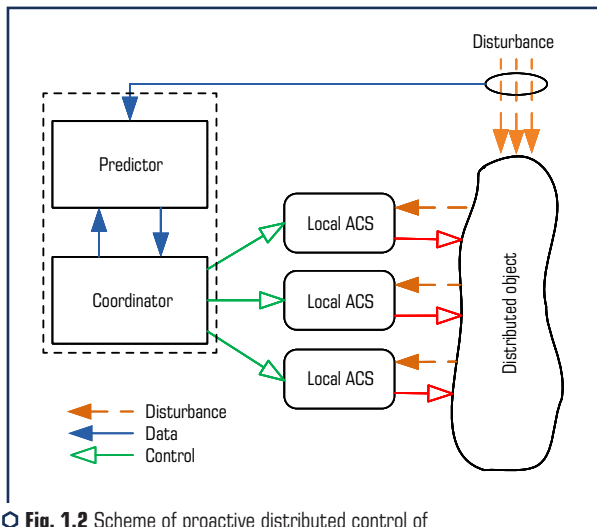
Fig. 1.2 Scheme of proactive distributed control of a distributed object

Similarly, the problems of power fluctuations for local photovoltaic stations (PVS) due to changes in insolation are solved. This leads to voltage fluctuations in the mains of the DEG and a violation of the quality of electricity. In [32], to solve this problem, PVS inverters were used as sources of reactive power. A method for local adjustment of the debugging parameters of PVSs inverters to maintain the specified voltage levels is proposed. Uncertainty of the schedule of electricity generation is taken into account.

Due to the insufficient equipment of modern DEG with data transmission tools, the use of a distributed control system was justified in [32] (**Fig. 1.2**). The system performs the main control functions autonomously according to local parameters. Communication of local systems with the distribution system operator is performed periodically to adjust their debugging parameters. To determine the necessary settings for the inverters, a short-term forecast of meteorological parameters is used. However, the described control system does not take into account the mutual influence between the local ACS of individual RPS. In addition, no attention is paid to the economic aspects of the problem of optimizing reactive power flows.

In [39], the need to take into account the mutual influence of local control systems of the RPS used to maintain the voltage profile is substantiated. The proposed approach makes it possible

to solve the problem of optimizing reactive power flows in DEG by minimizing the linearized target functions of power losses for local subsystems using the Lagrange decomposition method.

It is shown that after the decomposition of the problem of finding a global optimum for RPS as a multi-agent system of large dimensions, the main attention should be paid to the coordination of the operation of local subsystems for which the information infrastructure of the DEG dispatch center used for Thus, the reduction of losses, taking into account local constraints, is provided by distribution. The effectiveness of decisions made is periodically monitored at the top hierarchical level [35, 39]. The need to coordinate the actions of local ACS is determined by the available power reserve of the RPS after maintaining the voltage profile.

So, as the practice of operating DEG [27, 35] shows, the existing information infrastructure often does not support the possibility of implementing centralized control of individual RPSs. Therefore, it is expedient to use decentralized control and local ACS that respond to local consumption of reactive power or manifestations of its change.

To coordinate the work of local ACS, it is advisable to periodically adjust their debugging parameters. Thus, the exchange of reactive power between local subsystems and DEG can be reduced to the optimal one [35]. This will increase the efficiency of sharing the RPS in distribution grids.

Determining debugging parameters for local ACS is quite a difficult task. Let's note that these parameters will remain unchanged for a certain time (from several minutes to several hours). During this time, they must ensure the effective interaction of local ACSs that support the given mode of the dynamic system. To determine the settings of the ACS, not always adequate initial data are used.

To organize distributed control of reactive power flows in DEG, ACS with voltage drop control is often used [35]. Such a system maintains a close to optimal distribution of electricity in the DEG. But the exchange of reactive power is often suboptimal due to the fact that the mutual influence of individual ACS is not taken into account.

To solve the problem of matching the ACS [35], it was proposed to use some virtual impedance in the control controller of the RPS to clarify the optimal powers in the absence of operational information from the centralized control system. Such impedances for local ACS are proposed to be determined taking into account the ratio of the squares of systematically fixed reactive power flows. The proposed RPS controller will approximately take into account the flow in the coverage area of other ACS, using only locally measured information. Its participation in the performance of system functions, in particular, the reduction of power losses and the alignment of the voltage profile in the DEG, will be determined by the change in the virtual impedance.

In this paper, it is shown that the efficiency of using the reactive power of the DEG with coordinated control can be increased by 50 % compared with local control. However, in the study [35], when determining virtual impedances, the following was not taken into account:

– influence of joint flows of reactive power along the DEG mains;

– the economic aspect of attracting subscriber RPSs to the system control of reactive power;

– that DESs have different reactive power generation capabilities.

In [40], a modified virtual impedance method was proposed. Different installed powers of the DES were taken into account. It is proposed to determine the impedances for a partially equivalent grid, in particular, to reduce the number of nodes in the design scheme. However, this did not solve the problem of coordinating the operation of local ACS and taking into account economic factors in the organization of control.

The analysis of studies has shown that in order to improve the efficiency of DEG control, it is necessary to improve information systems, introduce innovative technologies with a gradual transition to the concept of Smart Grid [41]. Currently, the use of decentralized control systems remains relevant. The main method for coordinating the operation of the RPS in electrical grids is the periodic centralized adjustment of the debugging parameters of their ACS.

From the analysis of literary sources, the following conclusions can be drawn:

1. Due to the underdeveloped information infrastructure of modern DEG, reactive power flows are controlled under conditions of incomplete and unreliable information about regime parameters and external influences. In order to increase the efficiency of using the RPS resource, it is advisable to switch to proactive control with the involvement of local ACS. The latter operate according to local parameters, but provide a systemic effect of reducing losses by adjusting the debugging parameters.

2. In order for these parameters to ensure the ACS coordination, it is necessary to perform a significant number of optimization calculations to determine them. It is expedient to determine the optimal power of the RPS for a certain point in time in the forecast interval using the "ideal" mode method. The advantage of the latter is higher reliability and performance in comparison with the methods of optimized enumeration of variants.

3. Optimization of DEG modes in terms of reactive power requires taking into account the reliability and quality of power supply to consumers. Therefore, in mathematical models on which control actions are formed and checked, this feature of the control object must be taken into account. Accounting for restrictions on dependent parameters, in particular, voltage deviations, will make it possible to reasonably make decisions about changing the operating mode of individual RPSs and their sets.

1.2 CONDITIONS FOR OPTIMAL OPERATION OF REACTIVE POWER SOURCES IN DISTRIBUTION GRIDS

Optimization of reactive power flows is a purely technical task. However, in modern conditions, RPS, which provide a systemic effect of reducing electricity losses in DEG, may be owned by another energy entity. Therefore, when solving them, it is necessary to take into account economic factors. All subjects of the electric power industry are objectively interested in reducing electricity losses and improving the quality of voltage in the DEG. Calculations show that due to the RPS inclusion in distribution grids, it is possible to reduce losses by 5–8 % [32, 35, 42]. But the effect

of reducing losses is ensured not only by the introduction of RPS, but mainly by the quality of their further operation.

Automated RPS control is necessary for a number of reasons. For the consumer, it is economically justified to use automatic control systems for the RPS to reduce reactive power flows on the verge of the subscriber's balance sheet ownership. This helps to reduce the fee for the flow of reactive energy. But the main reason is the need for rapid implementation of control actions under conditions of a variable schedule of consumption and generation of reactive power in DEG. A number of studies are devoted to the development and implementation of automatic control systems for RPS, in particular [42–45]. Efficient in terms of speed and accuracy technical solutions for automating the operation of the RPS are proposed. They allow to maintain the optimal values of the reactive power factor in certain nodes of the DEG.

However, in order to optimize the reactive power flows in the DEG with the help of a set of RPSs, it is necessary to coordinate their operation. To do this, it is periodically possible to determine and change the settings for local ACS, taking into account the mutual influence of the DEG. Due to severe time constraints for such systems, it is necessary to improve the methods and algorithms for calculating the optimal powers of the RPS. They should take into account changes in the modes and configuration of the DEG during operation, as well as changes in electricity tariffs [31, 46].

1.2.1 DETERMINATION OF THE OPTIMAL RPS POWER BASED ON THE SIMULATION OF THE "IDEAL" MODE OF THE DISTRIBUTION GRID

In the simplest case, the problem of optimizing the RPS power can be represented as follows:

$$V_Q\left(Q_i\right) \rightarrow \min,\, i \in \left[1...n_q\right],\tag{1.1}$$

when balancing reactive power in the system

$$G = \sum_{i=1}^{n_q} Q_i - \sum Q_= - \Delta Q\left(Q_i\right) = 0,\, i \in \left[1...n_q\right],\tag{1.2}$$

and restrictions on parameters:

$$Q_i^{\max} \geq Q_i \geq Q_i^{\min},\, i \in \left[1...n_q\right];\tag{1.3}$$

$$U_j^{\max} \geq U_j \geq U_j^{\min},\, j \in \left[1...n\right],\tag{1.4}$$

where V_Q – the power loss in the DEG; n, n_q – the number of DEG nodes for which voltage restrictions apply and the number of installed RPSs; $\sum Q_n$ – total load of consumers; $\Delta Q(Q_i)$ – losses of reactive power in DEG; $\left[Q_i^{min}, Q_i^{max} \right]$ – power adjustment range of the i-th RPS; $U_j, \left[U_j^{min}, U_j^{max} \right]$ – respectively, the calculated value of the voltage in the j-th node of the DEG and the range of permissible voltage values.

The classical solution of such a problem by the Lagrange method is the need to maintain the equality of the relative increases in power losses [14, 27]:

$$\frac{\partial V_Q / \partial Q_i}{1 - \partial \Delta Q / \partial Q_i} = idem. \tag{1.5}$$

Using equation (1.5), problem (1.1), (1.2) under certain assumptions can be reduced to solving the system of $n_q + 1$ linear equations and quickly find the optimal values of the RPS power. However, taking into account the nonlinear dependence of $V_Q(Q_i)$ and $\Delta Q(Q_i)$, such a solution will require clarification. In addition, the formulation of the problem does not take into account the economic factors of the RPS operation.

To take into account these shortcomings, it is necessary to move to the objective function through the profit from the RPS operation during a certain reporting period:

$$AP(Q_i) \rightarrow \max, i \in \left[1 \ldots n_q \right]. \tag{1.6}$$

After substituting mathematical expressions for the components of profit and deductions, expression (1.7) took the form:

$$AP(Q_i) = \sum_t \left(\begin{array}{c} \Delta P_{(t)}^0 \Delta t\, C_{(t)} - \Delta P_{(t)} \Delta t \left(1 - \alpha_t \right) C_{(t)} - \\ - \left(\sum_{i=1}^{n_q} \alpha_{ei} Q_i \Delta t + \sum_{i=1}^{n_q} \alpha_{\Delta Wi} Q_i \Delta t\, C_{(t)} \right) \left(1 - \alpha_t \right) \end{array} \right),$$

or

$$AP(Q_i) = \sum_t \left(\begin{array}{c} \Delta P_{(t)}^0 - \\ - \left(\Delta P_{(t)} + \sum_{i=1}^{n_q} \left(\frac{\alpha_{ei}}{C_{(t)}} + \alpha_{\Delta Wi} \right) Q_i \right) \left(1 - \alpha_t \right) \end{array} \right) C_{(t)} \Delta t, \tag{1.7}$$

where ΔP^0, ΔP – the average power losses for the DEG modes during the time before and after the RPS inclusion into operation, taking into account the given schedule of their operation $Q_i(t)$; $C(t)$ – price of electricity on the intraday market during the t-th period; α_{ei} – specific costs for the production of reactive energy from the i-th RPS (for RPS on the balance sheet of DEG $\alpha_{ei} = 0$); $\alpha_{\Delta Wi}$ – specific energy losses in the i-th RPS; α_t – tax on balance sheet profit.

Based on the results of previous studies [4, 27, 31], it has been shown that it is advisable to determine the optimal power of the RPS according to the technical and economic criterion based on the "ideal" modes of the DEG. For this, spade circuits with active resistances are used (**Fig. 1.3**). The economic characteristics of the RPS operation are listed in equivalent supports, which are commonly referred to as economic. The economic pillars for individual RPSs are determined based on the fact that the cost of electricity losses should correspond to the operating costs of the RPS.
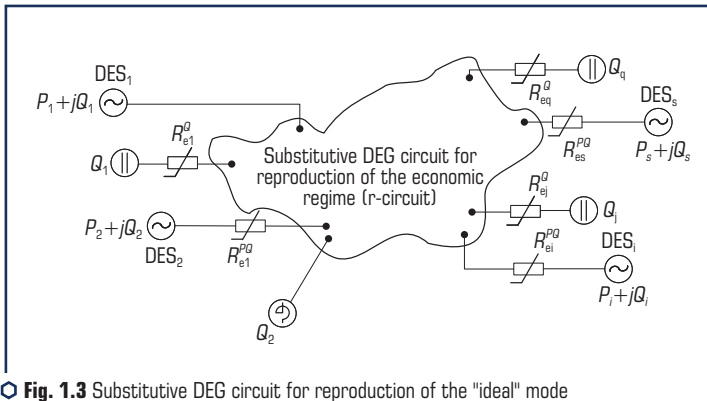
○ **Fig. 1.3** Substitutive DEG circuit for reproduction of the "ideal" mode according to the technical and economic criterion

This approach reduces the number of calculations and makes it possible to obtain a solution close to the global maximum of the objective function. This is achieved by reducing the problem of optimizing reactive energy flows to several calculations of the "ideal" mode with the adjustment of the DEG substitutive scheme. After that, restrictions (1.2)–(1.4) are imposed and the optimal powers of the RPS are specified.

Taking into account that the power losses ΔP^0 will not change due to the involvement of the RPS, problem (1.7) can be reduced to finding the minimum operating costs in the DEG:

$$OC\left(Q_i\right) = \sum_t \left(\Delta P_{(t)} \Delta t + \sum_{i=1}^{n_q} \left(\frac{\alpha_{ei}}{C_{(t)}} + \alpha_{\Delta Wi} \right) Q_i \Delta t \right) \left(1 - \alpha_t\right) C_{(t)}. \tag{1.8}$$

In (1.8), the price of electricity $C(t)$ is a series of positive, predetermined values. Therefore, the search for the minimum of the objective function (1.8) will be equivalent to the search for the minimum of some equivalent power losses:

$$\Delta W_{eq} = \frac{OC(Q_i)}{(1-\alpha_t)C_{(t)}} = \sum_t \Delta P_{(t)} \Delta t + \sum_t \sum_{i=1}^{n_q} \left(\frac{\alpha_{ei}}{C_{(t)}} + \alpha_{\Delta Wi} \right) Q_i \Delta t. \tag{1.9}$$

Thus, the function of equivalent losses of electricity in the DEG has been obtained. They take into account losses in the RPS and the costs associated with their operation. Their reduction due to the control of the RPS will allow to evaluate the effectiveness of such control. The decrease in losses (1.9) will correspond to the increase in profit (1.7). In addition, the extreme powers of the RPS for both functions will coincide due to the equivalence of the transformations.

Calculation of the current distribution in the interceptor circuit with active resistances (**Fig. 1.3**) will allow to determine the minimum power loss $\Delta P(t)\Delta t$ and the RPS power Q_i, which are needed for this. In order to take into account economic factors in determining the "ideal" mode, it is necessary to introduce additional supports into the spacing scheme (**Fig. 1.3**). Losses in them will be equivalent to the second component of expression (1.9):

$$\Delta W_{eq} = \Delta t \sum_t \frac{Q_i^2}{U_i^2} R_{ei}^Q = \Delta t \sum_t \sum_{i=1}^{n_q} \left(\frac{\alpha_{ei}}{C_{(t)}} + \alpha_{\Delta Wi} \right) Q_i,$$

where

$$R_{ei}^Q = \frac{U_i^2}{Q_i} \left(\alpha_{\Delta Wi} + \frac{\alpha_{ei}}{C_{(t)}} \right). \tag{1.10}$$

The expression for determining the economic resistance of the i-th RPS R_{ei}^Q contains its current power Q_i and economic indicators $\alpha_{\Delta Wi}$, α_{ei}, $C(t)$, as well as dependent mode parameters U_i. Therefore, these supports need to be iteratively refined during the search for the optimal solution.

Similarly, expressions were obtained for calculating the economic resistance of the RPS for different conditions of their use to optimize the reactive power flows in the DEG (**Table 1.1**). This made it possible, within the framework of solving one problem, to ensure the optimization of the RPS powers in a multicriteria setting. That is, the powers of individual RPS are optimized according to different criteria, providing a system-wide effect of increasing profits.

CHAPTER 1

The RPS powers, obtained after calculating the "ideal" DEG mode, provide the maximum profit (1.7), and usually cannot be included due to violations of the restrictions (1.3), (1.4). To move to the optimal mode, their values require adjustment.

● **Table 1.1** Economic resistances of the RPS for different optimality criteria

Optimality criterion for the *i*-th RPS	Economic resistance of the *i*-th RPS
Minimum loss of electricity in DEG	$R_{ei}^Q = 0$
Minimum cost of RPS operation	$R_{ei}^Q = \dfrac{\alpha_{ei} U_i^2}{Q_i^2 C_{(t)}}$
Maximum profit from the RPS operation	$R_{ei}^Q = \dfrac{U_i^2}{Q_i}\left(\alpha_{\Delta Wi} + \dfrac{\alpha_{ei}}{C_{(t)} Q_i}\right)$
Minimum loss for DES due to generation of excess reactive power	$R_{ei}^Q = \begin{cases} 0,\ if\ Q_i \leq Q_{i\max}; \\ \dfrac{\beta_{Pi} P_{Ri}(Q_i) U_i^2}{Q_i^2 C_{(t)}},\ if\ Q_i > Q_{i\max} \end{cases}$
Minimum cost of system services for voltage regulation	$R_{ei}^{PQ} = \dfrac{Q_{Ai} U_i^2}{\left(P_i^2 + Q_i^2\right)} \dfrac{\beta_{Qi}}{C_{(t)}}$

Note: In expressions: $\beta_i(Q_i)$ — unit costs for the RPS operation; β_{Pi}, $P_{Ri}(Q_i)$ — the price of electricity from the *i*-th source and the reduction in power output due to forced excess generation; $Q_i > Q_{i\max}$, β_{Qi}, Q_{Ai} — specific cost and volume of additional reactive power output at the request of the DEG operator.

Taking into account the restrictions on the limiting powers of the RPS (1.3) is not accompanied by significant algorithmic difficulties. If constraint (1.3) is violated, then to fulfill it, the value of the RPS power is fixed at the upper $Q_i^{\max}$ or lower $Q_i^{\min}$ boundaries of the range of values.

If the control of the RPS power is discrete, then the calculated value of the power Q_i is rounded off to an acceptable value. There can be two such values in the vicinity of Q_i. Then, for optimal selection, the enumeration of options is used with control over the value of the objective function (1.7).

The task of taking into account voltage restrictions (1.4) cannot be solved by a simple selection of values due to the significant number of RPSs and the complex effect of their powers on the voltage level in the DEG. To correct the RPS power, taking into account such limitations, it is

necessary to solve an additional optimization problem. Changing the RPS parameters to take into account restrictions is always associated with a decrease in profit from their operation. Indeed, at the same time, the RPS power deviates from "ideal". Therefore, the corrections ΔQ_i to the RPS powers must be determined so that after the restrictions on dependent variables (1.4) are met, the decrease in profit (1.7) is minimal:

$$
\begin{cases}
\Delta AP\left(\Delta Q_i\right) \to \min, i \in \left[1; n_q\right]; \\
\mathbf{J}_D^{-1}\Delta\mathbf{Q} = \Delta\mathbf{U},
\end{cases}
\tag{1.11}
$$

where $\mathbf{J}_D^{-1}$ – fragment of the inverse Jacobi matrix with the values of derivatives $J_{ij} = \partial Q_i / \partial U_j$. They relate changes in the RPS reactive power ΔQ_i to voltage deviations in the DEG nodes ΔU_j, for which the restrictions (1.4) are violated $j \in \left[1; n_?\right]$; $\Delta\mathbf{Q}$ – column vector of corrections of RPS reactive powers with dimension ; $\Delta\mathbf{U}$ – column vector of voltage deviations in the DEG nodes in excess of allowable limits. Each element of the vector is defined by an expression.

Given the relationship between objective functions (1.7) and (1.9), the formulation of problem (1.11) can be simplified. It can be reduced to the problem of minimizing the increase in equivalent losses (1.9) in the form $\Delta U_j = U_j - U_j^{\max}$:

$$
\Delta V_{Qeq}\left(\Delta Q_i\right) = \sum_{i=1}^{n_q}\left(\frac{\partial \Delta P_{(t)}}{\partial Q_i} + \frac{\alpha_{ei}}{C_{(t)}} + \alpha_{\Delta Wi}\right)\Delta Q_i \to \min .
\tag{1.12}
$$

Using the power loss distribution coefficients T_{Qi} [47], the objective function (1.12) was reduced to a linear one:

$$
\begin{cases}
\Delta V_{Qeq}\left(\Delta Q_i\right) = \sum_{i=1}^{n_q}\left(T_{Qi} + \frac{\alpha_{ei}}{C_{(t)}} + \alpha_{\Delta Wi}\right)\Delta Q_i \to \min; \\
\mathbf{J}_D^{-1}\Delta\mathbf{Q} = \Delta\mathbf{U}.
\end{cases}
\tag{1.13}
$$

Such a transition greatly simplifies the solution of the problem and reduces the number of calculations. Using the simplex method, from the list of corrections to the RPS powers ΔQ_i, those ensuring the fulfillment of voltage restrictions (1.4) with a minimum deviation from the extremum of function (1.7) were determined.

The studies carried out made it possible to obtain a reliable and high-speed method for searching for the optimal RPS powers. It can be used for simulation calculations in order to determine the debugging parameters of local ACS. However, for the formation of local control laws, a different approach was used, which makes it possible to obtain the conditions for the optimality of their operation in terms of local parameters.

1.2.2 CONDITIONS FOR THE OPTIMAL RPS OPERATION FOR CONTROLLING REACTIVE POWER FLOWS

As noted earlier, in order to optimize the RPS operation in the normal modes of the DEG, the task of automatically controlling their powers in order to obtain the maximum profit from their operation is relevant. Therefore, the problem of optimizing the daily regimes of the RPS with automatic control $Q_i(t)$, $i = 1,2…n$, taking into account the RPS modes with manual control, turns out to be relevant. The optimality criterion is the minimum of costs associated with compensating for electricity losses for DEG in the context of the dynamics of energy market tariffs $C(t)$ and technical restrictions on the part of consumers and RPS:

$$\int_{t_0}^{t_k} C(t)\Delta P\left(Q_i(t), i = 1..n_q\right)dt \rightarrow \min. \tag{1.14}$$

Problem (1.14) can be presented in more detail as follows [4]. A set of n_q automatically controlled RPSs and m manual RPSs is given. The total reactive power of the latter is Q_{PKj}. As controlled variables, the power of the automatic control of the RPS is taken. Losses from reactive power flows in the DEG are described as a non-linear function of the RPS powers. The composition and characteristics of the included RPS during the day are considered unchanged. Necessary on the time interval $[t_0; t_k]$ to find RPS modes with automatic control $Q_i(t)$ that would provide the maximum profit from reducing losses in the DEG, taking into account changes in tariffs in the energy market:

$$\int_{t_0}^{t_k}\left[C(t)\Delta\ \left(Q_i(t)\right) + \sum_{i=1}^{n_q}\left(\alpha_{ei}Q_i(t)\right)\right]dt \rightarrow \min, \tag{1.15}$$

subject to execution of the reactive power balance:

$$G = Q_{PKj}(t) + \sum_{j=1}^{m}Q_{PKj} + \sum_{i=1}^{n}Q_i(t) - Q_{nav}(t) = 0$$

and restrictions on parameters

$$Q_i^{\min} \leq Q_i(t) \leq Q_i^{\max}, i = 1..n,$$

$$U_i^{\min} \leq U_i(t) \leq U_i^{\max}, i = 1..n.$$

The values of the RPS powers at the beginning and end of the interval $Q_i(t_0)$ and $Q_i(t_k)$ are considered to be given.

Assuming that the dependence of losses on the RPS power, the dependences $Q_{nav}(t)$ and $C(t)$ are continuous and differentiated twice, the problem posed can be attributed to the limiting variational isoperimetric problems. In this case, the extremum (1.15) is achieved by the same functions $Q_i(t)$ as the extremum of the following expression:

$$\Phi = \int\limits_{t_0}^{t_k} \left[\begin{array}{l} C(t)\Delta \ \left(Q_i(t) \right) + \sum\limits_{i=1}^{n} \left(\alpha_{ei} Q_i(t) \right) + \\ + \lambda \varphi(t) + \sum\limits_{i=1}^{n} P_i^Q(t) + \sum\limits_{i=1}^{n} P_i^U(t) \end{array} \right] dt = \int\limits_{t_0}^{t_k} F(t) dt \Rightarrow \min, \tag{1.16}$$

where λ_i – indefinite Lagrange multipliers; $P_i^Q(t)$, $P_i^U(t)$ – penalty functions introduced into the objective function $F(t)$ to take into account constraints such as inequalities in the reactive power of the RPS and voltage in the DEG nodes.

According to Pontryagin's principle of minimum of continuous functions [14], the minimum (1.15) provides the value of $Q_i(t)$ for which the Euler equation is satisfied, as a necessary condition for the minimum (1.16):

$$F_{Q_i} - \frac{d}{dt} F_{\dot{Q}_i} = 0,\ i = 1, 2, \ldots n, \tag{1.17}$$

where $F_{Q_i} = \dfrac{\partial F}{\partial Q_i}$; $F_{\dot{Q}_i} = \dfrac{\partial F}{\partial \dot{Q}_i}$; $\dot{Q}_i = \dfrac{dQ_i}{dt}$.

Taking into account (1.16), equation (1.17) took the form:

$$F_{Q_i} - \frac{d}{dt} F_{\dot{Q}_i} = \left(C(t) - \frac{dC(t)}{dt} \right) \left[\frac{\partial \Delta}{\partial Q_i(t)} - \frac{d}{dt} \frac{\partial \Delta}{\partial \dot{Q}_i(t)} \right] + \alpha_{ei} +$$

$$+ \lambda + \frac{\partial P_i^Q}{\partial Q_i} + \frac{\partial P_i^U}{\partial Q_i} = 0,\ i = 1, 2 \ldots n. \tag{1.18}$$

For a non-degenerate system of equations (1.18), the necessary conditions for the optimality of the RPS powers of with automatic control are as follows:

$$z^*(t) = \frac{\lambda + \alpha_{e1} + q_1^P}{\sigma_1^*(t)} = \frac{\lambda + \alpha_{e2} + q_2^P}{\sigma_2^*(t)} = \ldots = \frac{\lambda + \alpha_{en} + q_n^P}{\sigma_n^*(t)}, \tag{1.19}$$

where $z^* = z + z'$, and $\sigma_i^* = \sigma_i + \sigma_i'$ provided that

$$\begin{cases} z = -C(t); \; z' = \dfrac{dC(t)}{dt}, \quad q_i^{\mathsf{H}} = \dfrac{\partial P_i^q}{\partial Q_i} + \dfrac{\partial P_i^U}{\partial Q_i}; \\[3mm] \sigma_i = \dfrac{\partial \Delta}{\partial Q_i}; \; \sigma_i' = -\dfrac{d}{dt}\dfrac{\partial \Delta}{\partial Q_i}. \end{cases} \tag{1.20}$$

If to neglect the changes in the operating RPS parameters during a certain time interval, for example, $\Delta t = 0.5$ h, then the condition for the optimal RPS power (1.20) will look like:

$$z_t = \frac{\lambda + \alpha_{e1} + q_1^P}{\sigma_{1t}} = \frac{\lambda + \alpha_{e2} + q_2^P}{\sigma_{2t}} = \ldots = \frac{\lambda + \alpha_{en} + q_n^P}{\sigma_{nt}}. \tag{1.21}$$

The variable λ is calculated iteratively using the boundary conditions. The main condition is to maintain the balance of reactive power in the DEG, in particular at the beginning and end of the integration time interval. In terms of physical content, λ characterizes the RPS effectiveness in the context of making a profit from reducing losses. It shows to what extent the costs of RPS operation will pay off due to a decrease in the cost of electricity losses in the DEG, if the power of the i-th RPS increases, for example, by 1 kvar.

$$\lambda = z_t \sigma_{it} - \alpha_{ei} = -C_t \left.\frac{\partial \Delta}{\partial Q_i}\right|_t - \alpha_{ei}. \tag{1.22}$$

The control of the set of RPSs in accordance with the optimality conditions (1.19) provides the maximum profit from reducing electricity losses in the DEG. Local automation systems will give a command to increase the RPS power only if the increase in costs is offset by a decrease in electricity losses, taking into account penalties for reducing voltage quality. Since the electricity losses in the DEG depend on voltage levels, the local control of the RPS will have a positive impact on the quality of electricity in the DEG. To ensure a system-wide effect, it is necessary to combine the set of local systems for automatic control of the RPS according to local parameters into a single system. The latter, thanks to the proactive adjustment of local ACS settings, will provide efficiency in the face of incomplete or unreliable information in data flows between the coordinator and local ACS (**Fig. 1.2**).

1.3 STRUCTURAL DIAGRAM OF PROACTIVE CONTROL OF REACTIVE POWER FLOWS IN DISTRIBUTION GRIDS

Automated systems with proactive control provide optimization of technological processes in conditions of incomplete or imperfect current information regarding the parameters of the control

object and external influences. Such features are typical for a complex of spatially distributed RPSs, which together should optimize the flow of reactive power to the DEG. Therefore, an automated RPS control system was proposed, which makes it possible to combine the set of RPS with automatic control according to local parameters into a single system (**Fig. 1.4**).
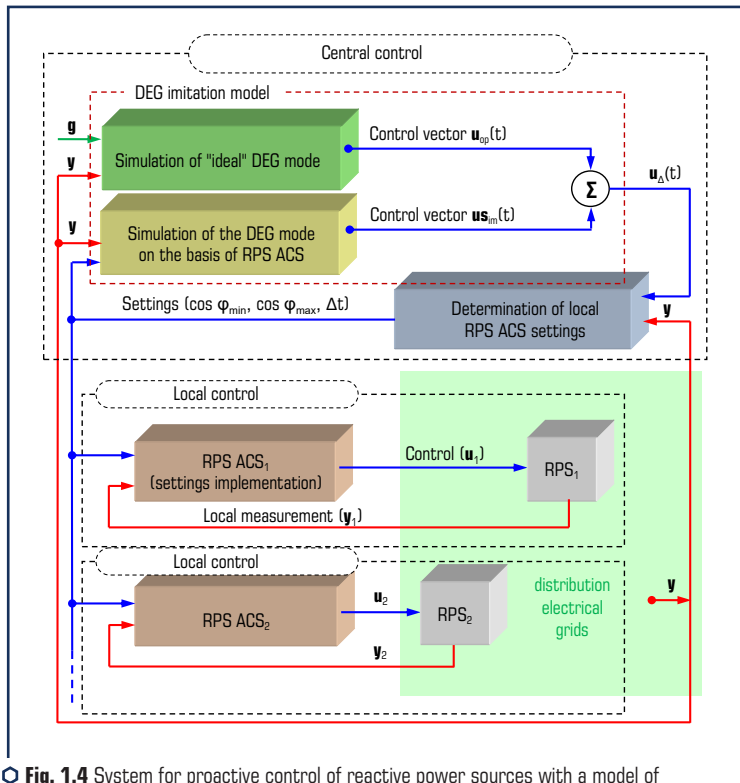
○ **Fig. 1.4** System for proactive control of reactive power sources with a model of the "ideal" DEG mode

1.3.1 STRUCTURAL DIAGRAM OF COORDINATED CONTROL OF DISPERSED REACTIVE POWER SOURCES

Coordination of the control of local ACS is provided by the hierarchical structure of the automated control system. At the level of centralized control, tasks for local ACS are formed and their implementation is controlled. At the level of local control, automatic adjustment of the RPS power

takes place according to the measured parameters (load voltages and currents). The operation of local subsystems is coordinated by periodic centralized adjustment of their debugging parameters.

Each local control loop [31] is formed by the RPS and the local automatic control system (**Fig. 1.4**). The operation of local ACS is periodically adjusted by a centralized system. The functions of coordinating centralized and local control are performed by the block for determining the ACS settings. The appropriate debug parameters are defined and passed here. They determine the frequency of control and control actions u_i for individual RPSs. Information support of centralized control is provided by the operational information complex. It measures the set of given DEG parameters and forms the observation vector **y**.

To simulate the "ideal" DEG modes, that is, the modes that provide maximum profit from the RPS operation, a simulation model is used. According to the optimality conditions (1.19), here the control actions are determined for each RPS $u_{sim}(t)$, which would ensure the transition from the current mode to the optimal one for the local control subsystem. Here, the settings of the local ACS and the dynamics of the measured parameters are taken into account.

Next, the simulation block of the "ideal" DEG mode generates control actions $u_{op}(t)$, which ensure the transition to the optimal DEG mode according to the optimality criterion (1.7). Further, for each RPS controller, debugging parameters are determined that minimize the inconsistency $u_{\Delta}(t)$ between the outputs $u_{op}(t)$ and $u_{sim}(t)$ of the simulation model [48]. The mode simulation block is also used as a source of pseudo-measurements of control parameters ui and individual local ACS. Since it is relatively simple to reproduce the processes of power transmission in DEG, the simulation model provides sufficient adequacy. This is controlled by feedback **y** [17, 48].

The decision to introduce into the centralized control circuit a block for simulating the DEG modes $u_{sim}(t)$ instead of remote measurement of the grid parameters **u** is economically justified for the distribution grids of Ukraine and European countries. The latter was shown on the basis of a technical and economic analysis in [28].

At the initial stage of the implementation of the control system, it is necessary to periodically coordinate operational control with automatic control. Then the simulation model provides an estimate of the effectiveness of the manual control commands **g**, including the consequences of changing the powers of the RPS. The model provides information support for manual formation and adjustment of the debugging parameters of local ACS, as well as reproduction of the predictive states of the DEG. After the accumulation of the base of typical DEG modes and the final implementation of the proposed control system, the simulation model becomes the main element of the coordination of local ACS and introspection.

The stability and efficiency of the centralized coordination of the RPS control depends on the frequency of updating the parameters of the DEG mode, as well as on the speed and intensity of changes in the observation parameters **y**. To ensure the stability of local control, it is necessary to optimize the time settings Δt for individual ACS. For the efficient use of the RPS resource, in particular switching devices, it is necessary to optimize the power factors $cos\phi_{min}$, $cos\phi_{max}$. They determine the RPS response to a change in the local load, and also determine the dead zone of the ACS.

The processes of determining and adjusting the settings are carried out by the corresponding block of the control system (**Fig. 1.5**).
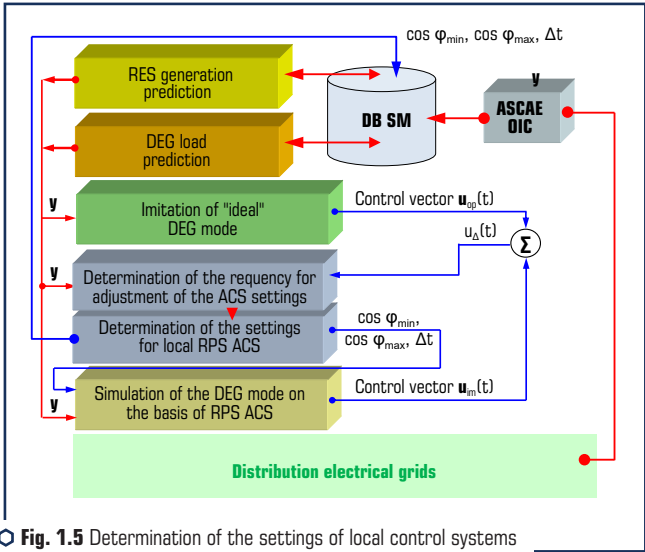
○ **Fig. 1.5** Determination of the settings of local control systems for reactive power sources

Considering that the ACS settings can only be changed periodically, the block includes blocks for short-term prediction of DEG loads and generation of local sources. To predict loads, the method of fractal analysis of statistical data on power consumption and weather conditions was used [49]. Short-term forecasting of energy production by local sources, in particular solar stations is performed by the method of neuro-fuzzy modeling [50]. The initial data comes from the operational information complex (OIC) of the DEG, automated systems for the commercial accounting of electricity (ASCAE) of the DEG and consumers, as well as forecast weather services Gismeteo, WetherBit, Meteoblu, RP5. The data is accumulated in the database of the simulation model (DB SM) and can be used by forecasting blocks at a random time with a given retrospective depth.

Based on the results of loading forecasting and generation, signals are simulated at the output of the "ideal" mode model $u_{op}(t)$ and the DEG mode simulation unit $\mathbf{u}_{sim}(t)$ taking into account the implementation of control actions of local ACS. Next, the intensity of the appearance of inconsistency between them $\mathbf{u}_\Delta(t)$ is analyzed and the necessary frequency of adjusting the debugging parameters of the local ACS is determined. This frequency will be different for individual local control systems of the RPS. Thus, information overload of communication channels does not occur.

Further, the block for determining the settings with a certain discreteness ensures the adjustment of the settings in time and $cos\phi_{min}$, $cos\phi_{max}$. The main difficulty here is the need for a

significant amount of calculations to optimize the reactive power curves of the RPS. In addition, it is necessary to evaluate the correlation of these graphs and the graphs of local reactive power consumption in the coverage area of the RPS in order to optimize the periods for updating the ACS parameters. Determining the debugging parameters of the ACS requires a significant investment of time. Therefore, it is carried out preventively based on the results of forecasting and typical load schedules for DEG [38].

Thus, to ensure automatic control of the RPS, it is possible to use a dispersed proactive control system with a simulation model. Local control systems are made on the basis of the optimality conditions for the RPS operation (1.19), (1.20). For a centralized determination of the optimal DEG modes and adjustment of the debugging parameters of the local ACS, an imitation of the "ideal" DEG modes is used.

The stability and efficiency of control is achieved by dividing the functions into centralized formation of the ACS debugging parameters and their local implementation according to locally measured parameters. The proposed control system was used to optimize the reactive power flows in the Vinnytsia city power grids 10 kV. It is shown that, despite the rapid changes in the reactive load during the day, with an appropriate adjustment of the ACS settings, it is possible to achieve a significant reduction in electricity losses (**Fig. 1.6**). The experiment showed that timely adjustment of the ACS settings in terms of time and power factor brings the schedule of reactive power output by a local source closer to the optimal one. This achieves an additional reduction in electricity losses for a fragment of the distribution grid of about 8 %.
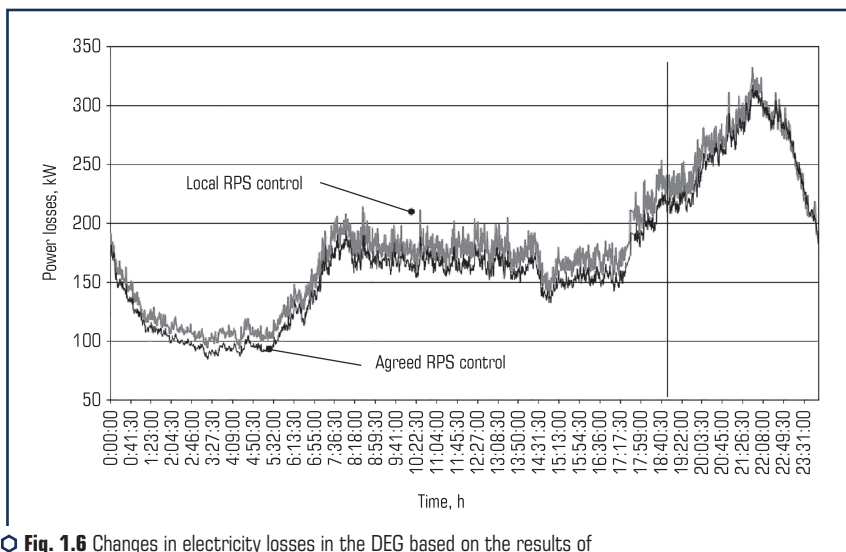
○ **Fig. 1.6** Changes in electricity losses in the DEG based on the results of the AUKRM-160 RPS operation at TS-557

1.3.2 ALGORITHM FOR OPTIMIZING THE REACTIVE POWER OF SOURCES BASED ON THE SIMULATION OF THE "IDEAL" MODE OF THE ELECTRICAL GRID

The process of determining the debugging parameters of local ACS for their coordination involves a significant number of calculations of optimal modes. For this, a module is used to simulate the "ideal" DEG modes (**Fig. 1.7**). This module is designed to solve the following problems: calculation of the DEG mode and its entry into the allowable area; optimization of the DEG mode in terms of reactive power. These tasks are functionally linked and use a number of collaborative processes.

The initial data for determining the optimal power of the RPS are the parameters of the DEG equipment, the parameters of the current mode, as well as the design parameters of the RPS used to optimize the reactive power flows. Information about the parameters of the equipment comes from the corporate databases of the distribution system operator, the archives of the line service, substations, and the dispatch service. Regime parameters are mainly calculated on the basis of technical monitoring data and commercial electricity metering and are placed in the database of the simulation model.

The optimal powers of the RPS according to the criterion of maximum profit from their operation are determined in the following sequence:

1. From the available information support, the initial data are formed for calculating the given DEG mode. The voltages at the nodes are determined. To do this, a nonlinear system of nodal voltage equations is resolved in the form of a power balance [31]. Active and reactive powers in the nodes (except for the base one), including the RPS powers and the DEG powers, are considered unchanged. Based on the results of the calculation, the currents in the nodes are determined. This provides a transition to a linearized model of the DEG mode.

2. A calculation model of the DEG is compiled to reproduce its "ideal" mode in terms of power losses. For the replacement circuit, the DEG is supplied only by active resistances (r-circuit). Available RPS with fixed powers is supplied by direct currents. Sources, for which the optimization of parameters is carried out, taking into account the restrictions on the voltage and power of the installation, are supplied by additional economic resistances. The latter are determined from **Table 1.1** based on the affiliation of the RPS and the conditions of their operation. Such sources can mainly be owned by the DEG. However, it can be a means of compensating the reactive power of active consumers providing a voltage regulation system service. These can be conventional and renewable energy sources, which can change generation at the request of the distribution system operator. Therefore, the economic pillars for them will be different. The nodes to which the RPS is connected receive a sign of balancing reactive power. This removes their cardinalities from the list of independent variables and allows to determine their extreme values.

3. According to the linearized model of the steady state mode of the RPS, using the Gauss method, the DEG mode is calculated with minimal power losses. Since economic resistances are introduced into the interceptor circuit, the reactive currents of the RPS will correspond to their powers, which ensure maximum profit from their operation.
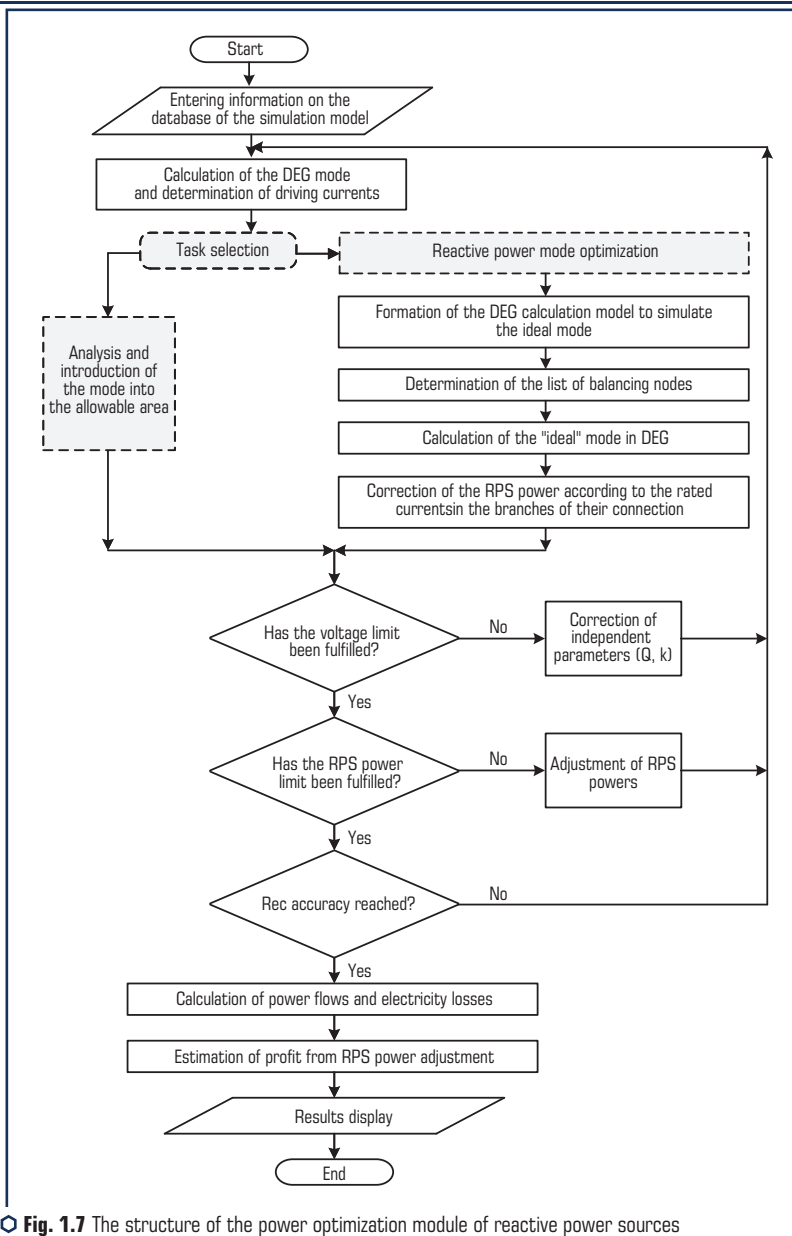
○ **Fig. 1.7** The structure of the power optimization module of reactive power sources based on the simulation of the "ideal" mode

4. Reactive currents in branches with economic resistances of the RPS are listed in the value of the reactive powers of the RPS, providing maximum profit from their operation.

5. Voltage limits are checked at the DEG nodes. For nodes where restrictions are not met, voltage regulation is simulated by changing the transformation ratios of power transformers within their regulation range.

6. If the specified measure does not give a result, the calculated powers of the RPS are adjusted based on the results of solving the auxiliary optimization problem (1.12). After that, the powers of the corresponding RPSs are derived from the list of optimized variables. Next, the calculation model is refined and the DEG mode is recalculated.

7. The calculated power of the RPS may differ from the degrees of regulation of real devices. Therefore, these values are rounded up. If the RPS power was previously reduced to meet the voltage limits, then the direction of rounding the power to the standard value will be in the direction of reduction. Since any deviation of the RPS power from the calculated value leads to a decrease in profit, it is necessary to round off the calculated powers to the nearest standard ones in the direction of increase or decrease.

8. After the restriction on the parameters is fulfilled, the current mode is considered conditionally optimal, but requires clarification. Since the economic resistances of the RPS depend on their powers, they must be listed. If the maximum deviation between the values at adjacent iterations exceeds the specified accuracy, the "ideal" mode is recalculated starting from step 2. Otherwise, the solution is considered optimal.

9. Taking into account the optimal powers of the RPS and the transformation ratios of transformers at substations, the power overflows in the DEG are specified and the losses are determined.

10. The results of the calculation are loaded into the database of the simulation model and are used to set up the RPS, in particular, to determine the settings of local ACS by power factors.

Thus, the problem of optimizing the RPS power, regardless of the conditions of their operation, can be reduced to the problem of minimizing losses in the substituting scheme of DEG with economic supports. This problem is fundamentally simpler, since it can be solved by calculating the steady-state mode of the DEG according to its interceptor r-scheme. Fulfillment of voltage restrictions requires adjustment of the transformation ratios and clarification of the RPS power. The optimal values of the RPS power and the transformation ratios are determined from the system of nodal equations. The latter is compiled based on the results of the calculation of the "ideal" DEG mode.

1.4 ENSURING THE EFFICIENCY OF THE AUTOMATED REACTIVE POWER FLOW CONTROL SYSTEM

The adequacy of the optimality conditions (1.19), (1.20) and the efficiency of the algorithms for setting the local ACS settings (**Fig. 1.5**) was tested using the example of the 10 kV Vinnytsia city power grids. The settings for the regulated RPS installed at the transformer substation 10/0.4 kV "TS-496" were determined. The substation receives power from the power grids of

the F-113 feeder of the Nova substation. At this substation, a 200 kvar AUKRM 0.4-200-10-5 RPS is installed.

The initial data for determining the optimal schedules for the RPS generation were measured by means of ASCAE. In particular, hourly consumption of active and reactive electricity was recorded on 0.4 kV buses of feeder transformer substations. For TS-496, the graphs of active and reactive consumption were measured with a discreteness of 15 s. **Fig. 1.8** shows a schedule for the release of reactive energy from the 0.4 kV buses of the transformer T-1 TS-496. It follows from the above that the reactive load changes significantly during the day. This leads to constant changes in the flow of reactive power in the feeder grid.
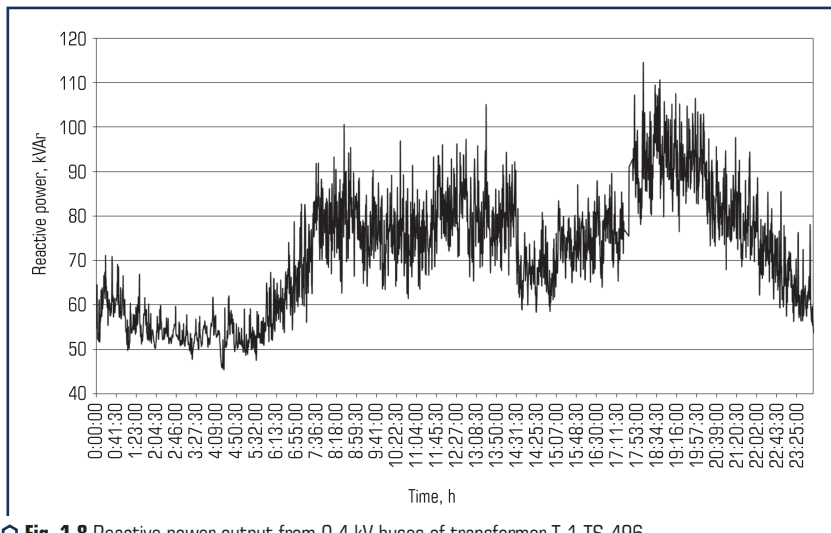
○ Fig. 1.8 Reactive power output from 0.4 kV buses of transformer T-1 TS-496

The power factor on the substation buses varies within 0.82–0.97 (**Fig. 1.9**). This indicates that the reactive power flows are not optimal. The graph of the optimal powers of the RPS to compensate for local consumption is shown in **Fig. 1.10**. The graph was obtained based on the results of the ACS operation with the settings: $cos\phi_{min} = 0.99$; $cos\phi_{max} = -0.99$; $\Delta t = 30$ s.

Using a simulation model, it is shown that such control contributed to a significant increase in the power factor on the TS-496 buses (**Fig. 1.11**) and a decrease in the reactive power flow by the F-113 feeder grids of the Nova substation.

Therefore, the local control system of the RPS with the selected settings ensures the generation of reactive power sufficient to compensate for local consumption. However, such a schedule for the generation of the RPS turns out to be not optimal for reducing electricity losses in the 10 kV grids of the F-113 feeder.
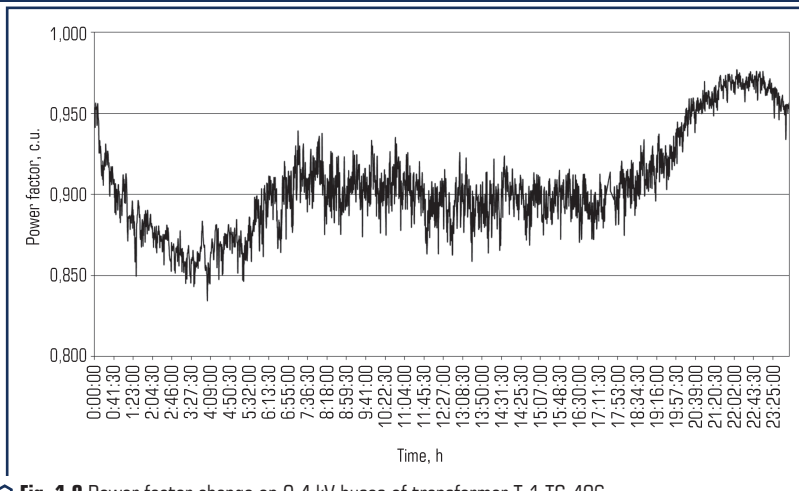
Fig. 1.9 Power factor change on 0.4 kV buses of transformer T-1 TS-496
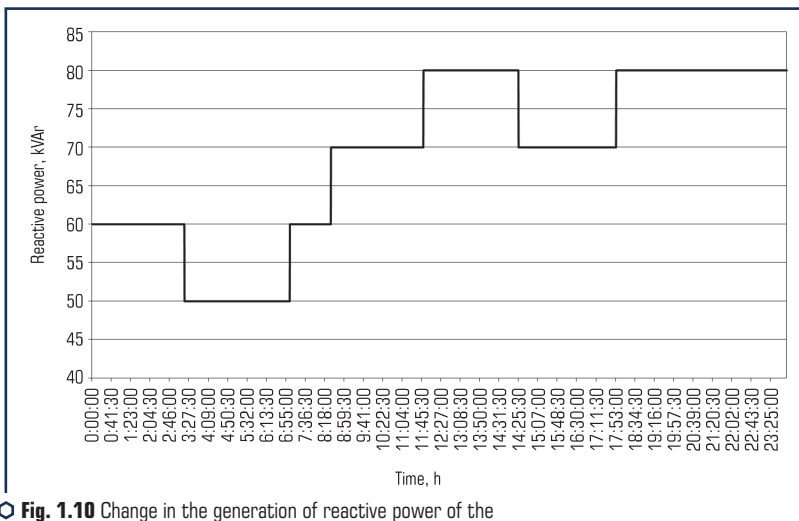
Fig. 1.10 Change in the generation of reactive power of the compensating plant installed at TS-496

Using the measurement results, the economic resistance of the RPS was determined. For each time slice, the "ideal" DEG mode was simulated and the optimal RPS power was calculated according to the criterion of maximum profit from its operation. The graph of the optimal generation power for the RPS, installed at the 0.4 kV input of the transformer T-1 TS-496, is shown

in **Fig. 1.12**. The implementation of such control made it possible to reduce the loss of electricity in the experimental grid by 9 %. But reactive power control according to such a schedule is impossible. After all, RPS provides stepwise adjustment with a degree of 10 kvar. In addition, this is impractical due to the operation of the RPS resource.
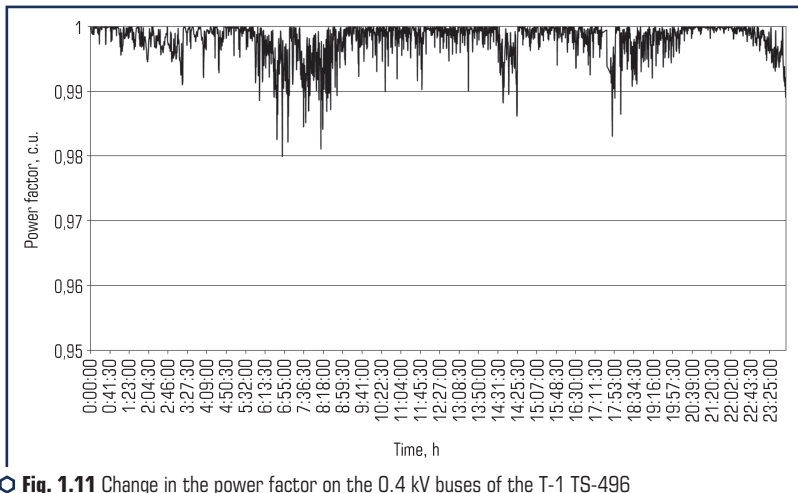
○ **Fig. 1.11** Change in the power factor on the 0.4 kV buses of the T-1 TS-496 transformer after installing the RPS
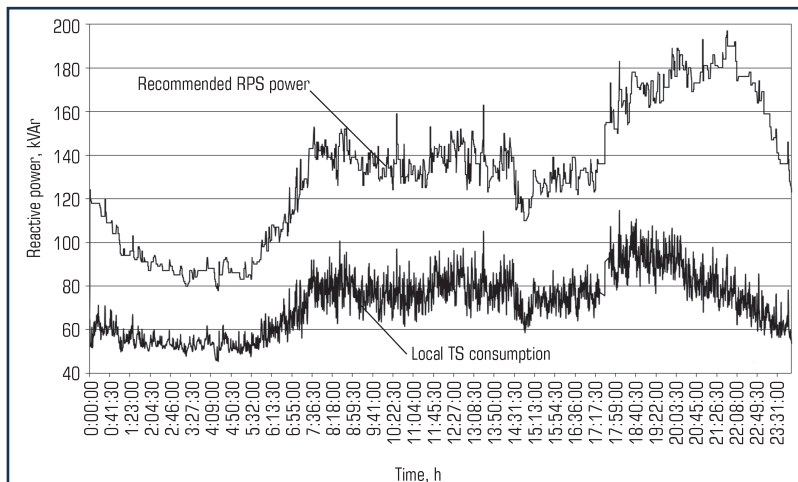
○ **Fig. 1.12** AUKRM 0.4-200-10 optimal RPS power at TS-496, determined by the results of simulating the "ideal" DEG mode

To automatically maintain the optimal schedule for changing the reactive power of the RPS using the local control system, several groups of inserts were defined for it.

The control system settings were determined in two stages. Initially, the necessary frequency of updating the settings was determined. And then the value of insertions for each update interval is calculated. At the first stage, using the square of the Pearson exponent, the correlation between the optimal RPS power Q_{opt} and the local reactive power consumption Q_{nav} was investigated (**Fig. 1.12**). For this, changes in the Q_{opt}/Q_{nav} ratio over time were determined (**Fig. 1.13**). For this function, gradually expanding the area of comparison of the Q_{opt}/Q_{nav} and Q_{nav} graphs, time intervals were determined within which it is possible to use the same settings for the RPS ACS (**Fig. 1.14**).
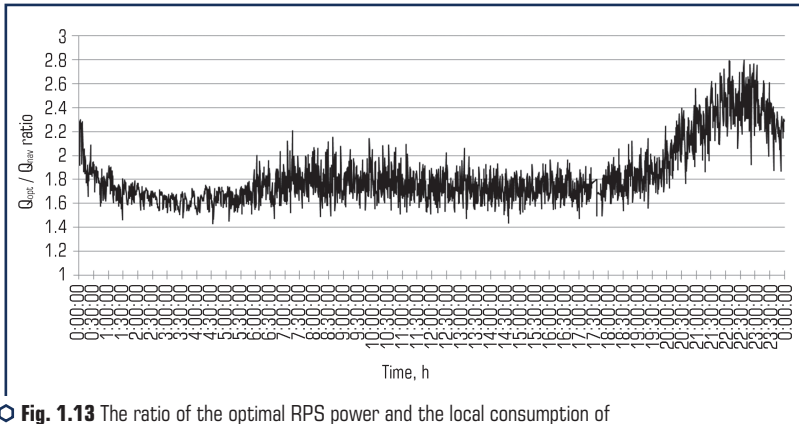
○ **Fig. 1.13** The ratio of the optimal RPS power and the local consumption of reactive power TS-496

The boundaries of the intervals for refining the settings were determined as the moments of time corresponding to the maximum values of the squared Pearson coefficient calculated for the set of Q_{opt}/Q_{nav} (function value) and the Q_{nav} (argument value) ratios. Thus, on the daily interval, five points of time were allocated for which it is necessary to update the ACS settings.

To determine the settings for each time interval, a block for simulating the ACS operation of the automated power flow control system in the distribution zone was used (**Fig. 1.5**). For each time interval (**Fig. 1.15**), the optimal power factors $cos\phi_{min}$ and $cos\phi_{max}$ were selected according to the criterion of minimum sum of squared deviations. The deviations between the optimal RPS powers and the powers that will be issued by the RPS under the action of the local ACS were analyzed. The time settings were determined taking into account the average rate of changes in the optimal RPS power and local consumption at a given interval.

So, for TS-496, five sets of inserts were preventively formed by the automated control system for the corresponding time periods (**Fig. 1.15**) [4, 27]:

— Set 1: $cos\phi_{min} = -0.97$, $cos\phi_{max} = -0.95$, $\Delta t = 10$ min;

– Set 2: $cos\phi_{min} = -0.97$, $cos\phi_{max} = -0.96$, $\Delta t = 10$ min;

– Set 3: $cos\phi_{min} = -0.99$, $cos\phi_{max} = -0.96$, $\Delta t = 5$ min;

– Set 4: $cos\phi_{min} = -0.96$, $cos\phi_{max} = -0.95$, $\Delta t = 10$ min;

– Set 5: $cos\phi_{min} = -0.96$, $cos\phi_{max} = -0.93$, $\Delta t = 5$ min.

The results of their implementation by local ACS are shown in **Fig. 1.15**.
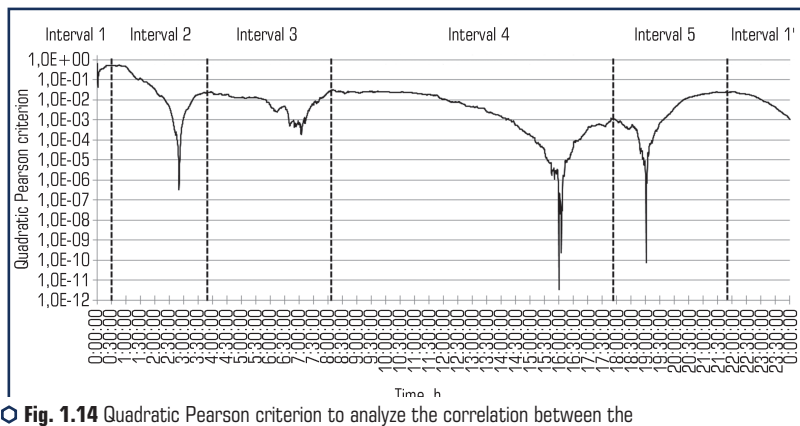
○ **Fig. 1.14** Quadratic Pearson criterion to analyze the correlation between the sets Q_{opt}/Q_{nav} and Q_{nav} (logarithmic scale)
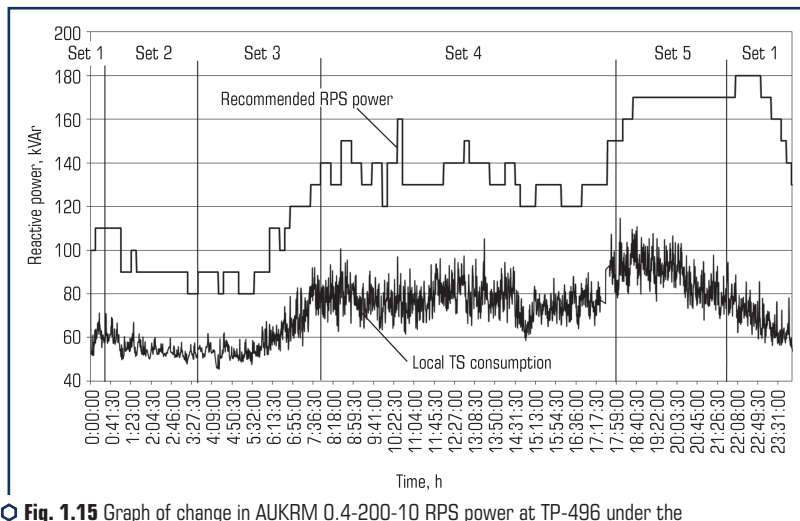
○ **Fig. 1.15** Graph of change in AUKRM 0.4-200-10 RPS power at TP-496 under the influence of local ACS after optimization of its debugging parameters

It can be seen from the graphs that the number of RPS power configurations has been significantly reduced. At the same time, the RPS generation schedule corresponds to the optimal generation schedule. Automatic control of the RPS according to the specified settings ensures the value of the power factors for the investigated TS is not lower than 0.93 (**Fig. 1.16, *a***). In addition, the implementation of such a power distribution schedule for the RPS made it possible to reduce the loss of electricity in the investigated DEG by about 8 % (**Fig. 1.16, *b***).
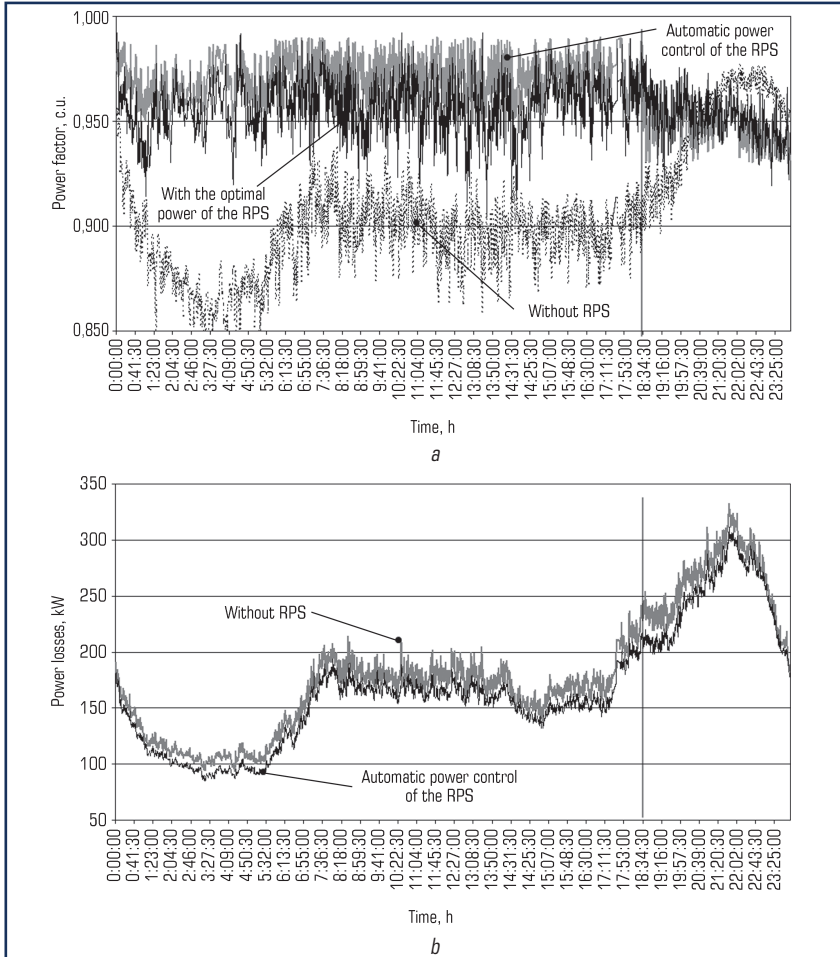
○ **Fig. 1.16** The results of the simulation of the operation of the RPS AUKRM 0.4-200-10 RPS at TS-496: *a* – graphs of changes in the power factor on the TS buses; *b* – electricity losses in DEG

CHAPTER 1

To determine the settings within the period of relevance, it is advisable to use the simulation model of the RPS ACS. It is advisable to select the power factors $cos\phi_{min}$ and $cos\phi_{max}$ by the method of least square deviations between the optimal and simulated powers of the RPS. It is advisable to determine the ACS time delays by the average rate of change of the optimal RPS powers and local consumption within the period of relevance.

CONCLUSIONS

1. In the work, a new solution to the actual scientific problem of increasing the efficiency of automated control of reactive power flows in distribution grids was obtained. It consists in the development of methods and algorithms for coordinating the RPS operation with automatic control according to local parameters. Coordination is carried out by proactively determining the debugging parameters that ensure the sharing of the RPS to ensure maximum profit from the optimization of reactive power flows in grids. Their implementation makes it possible to increase the efficiency of the RPS use in the grids of distribution system operators and active consumers.

2. The expediency of using the model of the "ideal" DEG mode for optimizing the RPS power according to the technical and economic criterion is substantiated. This made it possible to reduce the specified problem of nonlinear optimization to the problem of finding an extremal current distribution in the interceptor r-circuit of the grid, which is fundamentally simpler. To take into account the economic factors of the optimization problem, the replacement r-scheme is supplemented with fictitious resistances. Their values are calculated in such a way as to ensure that the cost of operating the RPS and the cost of electricity losses in these towers. Expressions for calculating economic resistances are obtained for different types of RPS and the conditions for their operation in electrical grids.

3. A feature of the problem of optimizing the RPS power is a significant dependence of the voltage levels in the grids on these powers. To take into account the restrictions on the voltage deviation in the nodes of distribution grids, it is proposed to solve an auxiliary problem of minimizing the deviation of the optimality criterion from the extreme value. The use of power loss distribution coefficients made it possible to reduce the last problem to linear programming.

4. To improve the efficiency of operation of local reactive power optimization systems, a criterion is proposed and analytical conditions for the optimality of the RPS modes are obtained, taking into account the costs of their operation and the quality of electricity.

5. For a complex of spatially distributed RPSs that jointly perform the functions of optimizing reactive power flows in electrical grids, it is necessary to ensure coordinated control. The paper proposes a two-level block diagram of an automated proactive control system with a simulation model and local ACS. To reduce the time spent on determining the debugging parameters of local ACS, an algorithm is proposed for identifying their update periods according to typical or predicted load and generation schedules.

CONFLICT OF INTEREST

The authors declare that they have no conflict of interest in relation to this research, whether financial, personal, authorship or otherwise, that could affect the research and its results presented in this paper.

REFERENCES

1. Ramsami, P., Ah King, R. T. F. (2021). Dynamic Distribution Network Reconfiguration for Distributed Generation Integration: A Systematic Review. 2021 IEEE 2nd China International Youth Conference on Electrical Engineering (CIYCEE). doi: https://doi.org/10.1109/ciycee53554.2021.9676972

2. Sahay, S., Samal, S., Nayak, S., Barik, P. K., Soni, R. K., Pradhan, A. (2022). Risks in an Active Distribution Network: A Review of the Literature. 2022 4th International Conference on Smart Systems and Inventive Technology (ICSSIT). doi: https://doi.org/10.1109/icssit53264.2022.9716295

3. Ibrahim, I. A., Hossain, M. J. (2021). Low Voltage Distribution Networks Modeling and Unbalanced (Optimal) Power Flow: A Comprehensive Review. IEEE Access, 9, 143026–143084. doi: https://doi.org/10.1109/access.2021.3120803

4. Kulyk, V., Burykin, O., Pirnyak, V. (2017). Optimization of the placement of reactive power sources in the electric grid based on modeling of its ideal modes. Technology Audit and Production Reserves, 2 (1 (40)), 59–65. doi: https://doi.org/10.15587/2312-8372.2018.129237

5. Becker, W., Hable, M., Malsch, M., Stieger, T., Sommerwerk, F. (2017). Reactive power management by distribution system operators concept and experience. CIRED – Open Access Proceedings Journal, 2017 (1), 2509–2512. doi: https://doi.org/10.1049/oap-cired.2017.0347

6. Hinz, F., Most, D. (2018). Techno-Economic Evaluation of 110 kV Grid Reactive Power Support for the Transmission Grid. IEEE Transactions on Power Systems, 33 (5), 4809–4818. doi: https://doi.org/10.1109/tpwrs.2018.2816899

7. Zecchino, A., Marinelli, M., Træholt, C., Korpås, M. (2017). Guidelines for distribution system operators on reactive power provision by electric vehicles in low-voltage grids. CIRED – Open Access Proceedings Journal, 2017 (1), 1787–1791. doi: https://doi.org/10.1049/oap-cired.2017.0377

8. Narayan, S. R. (2003). Solved Nonlinear Optimization Problems in Optimization Principles: Practical Applications to the Operation and Markets of the Electric Power Industry. New-York: Wiley-IEEE Press, 245–295.

9. Wang, L., Yang, J., Zhang, Q., Zhang, D., Huang, Y., Li, W., Shi, B. (2022). Research on Coordinated Reactive Power and Voltage Control Strategy for Regional Power Grids with High

CHAPTER 1

Penetration of Renewable Energy. 2022 IEEE/IAS Industrial and Commercial Power System Asia (I&CPS Asia), 1160–1165. doi: https://doi.org/10.1109/icpsasia55496.2022.9949876

10. Singh, P., Purey, P., Titare, L. S., Choube, S. C. (2017). Optimal reactive power dispatch for enhancement of static voltage stability using jaya algorithm. 2017 International Conference on Information, Communication, Instrumentation and Control (ICICIC). doi: https://doi.org/10.1109/icomicon.2017.8279044

11. Wong, K. P., Li, A., Law, T. M. Y. (1999). Advanced, constrained, genetic algorithm load flow method. IEE Proceedings – Generation, Transmission and Distribution, 146 (6), 609–618. doi: https://doi.org/10.1049/ip-gtd:19990638

12. Yin, S., Wu, L., Song, W., Wang, X. (2017). Multi-objective reactive power optimisation approach for the isolated grid of new energy clusters connected to VSC-HVDC. The Journal of Engineering, 2017 (13), 1024–1028. doi: https://doi.org/10.1049/joe.2017.0484

13. Khan, S., Bahadoorsingh, S., Rampersad, R., Sharma, C., Powell, C. (2018). Reactive power planning combining the reduced jacobian V-Q and voltage sensitivity indices on the sub-transmission network of a caribbean island power system. Proceedings of the 2018 IEEE Texas Power and Energy Conference (TPEC). doi: https://doi.org/10.1109/tpec.2018.8312097

14. Kyrylenko, O. V., Seheda, M. S., Butkevych, O. F., Mazur, T. A. (2010). Matematychne modeliuvannia v elektroenerhetytsi. Lviv: Natsionalnyi universytet "Lvivska politekhnika", 608.

15. Idehen, I., Abraham, S., Gregory, Murphy, V. (2018). Reactive power and voltage control in a power grid: A game-theoretic approach. 2018 IEEE Texas Power and Energy Conference (TPEC). doi: https://doi.org/10.1109/tpec.2018.8312103

16. Liang, C. H., Chung, C. Y., Wong, K. P., Duan, X. Z. (2007). Parallel Optimal Reactive Power Flow Based on Cooperative Co-Evolutionary Differential Evolution and Power System Decomposition. IEEE Transactions on Power Systems, 22 (1), 249–257. doi: https://doi.org/10.1109/tpwrs.2006.887889

17. Dehkordi, B. M. (2006). Optimal Voltage and Reactive Power Control Based on Multi-Objective Genetic Algorithm. 2006 International Conference on Power Electronic, Drives and Energy Systems. doi: https://doi.org/10.1109/pedes.2006.344226

18. Choi, J., Lee, K. Y. (2022). Genetic Algorithm for Generation Expansion Planning and Reactive Power Planning. Probabilistic Power System Expansion Planning with Renewable Energy Resources and Energy Storage Systems, 177–202. doi: https://doi.org/10.1002/9781119819042.ch10

19. Dai, C., Chen, W., Zhu, Y., Zhang, X. (2009). Seeker Optimization Algorithm for Optimal Reactive Power Dispatch. IEEE Transactions on Power Systems, 24 (3), 1218–1231. doi: https://doi.org/10.1109/tpwrs.2009.2021226

20. Saebi, J., Ghasemi, H., Afsharnia, S., Rajabi Mashhadi, H. (2012). Imperialist Competitive Algorithm for reactive power dispatch problem in electricity markets. 20th Iranian Conference on Electrical Engineering (ICEE2012), 433–437. doi: https://doi.org/10.1109/iraniancee.2012.6292397

21. Mahesh, V., Deepeeha, J. R., Kamaraj, N. (2013). Reactive power dispatch and its pricing in re-structured electricity markets. 2013 International Conference on Power, Energy and Control (ICPEC), 377–381. doi: https://doi.org/10.1109/icpec.2013.6527685

22. Qingfu Zhang, Hui Li. (2007). MOEA/D: A Multiobjective Evolutionary Algorithm Based on Decomposition. IEEE Transactions on Evolutionary Computation, 11 (6), 712–731. doi: https://doi.org/10.1109/tevc.2007.892759

23. Zhou, B., Chan, K. W., Yu, T., Wei, H., Tang, J. (2014). Strength Pareto Multigroup Search Optimizer for Multiobjective Optimal Reactive Power Dispatch. IEEE Transactions on Industrial Informatics, 10 (2), 1012–1022. doi: https://doi.org/10.1109/tii.2014.2310634

24. Etehad, M. M., Siahkali, H. (2017). Multi-objective optimization of reactive power dispatch in power systems via SPMGSO algorithm. 2017 Smart Grid Conference (SGC). doi: https://doi.org/10.1109/sgc.2017.8308868

25. Bhattacharjee, T., Chakraborty, A. K. (2012). Congestion management in a deregulated power system using NSGAII. 2012 IEEE Fifth Power India Conference. doi: https://doi.org/10.1109/poweri.2012.6479529

26. Man-Im, A., Ongsakul, W., Singh, J. G., Boonchuay, C. (2015). Multi-objective optimal power flow using stochastic weight trade-off chaotic NSPSO. 2015 IEEE Innovative Smart Grid Technologies – Asia (ISGT ASIA). doi: https://doi.org/10.1109/isgt-asia.2015.7387120

27. Kulyk, V., Burykin, O., Juliya, M., Viktor, P. (2018). Optimization of Reactive Energy Flows in the Electric Grid Taking Into Account Allowable Voltage Fluctuations. 2018 IEEE 3rd International Conference on Intelligent Energy and Power Systems (IEPS). Kharkiv, 265–270. doi: https://doi.org/10.1109/ieps.2018.8559542

28. Procopiou, A. T., Ochoa, L. F. (2017). Voltage Control in PV-Rich LV Networks Without Remote Monitoring. IEEE Transactions on Power Systems, 32 (2), 1224–1236. doi: https://doi.org/10.1109/tpwrs.2016.2591063

29. Liu, Y., Xia, W. B., Zheng, S., Wang, K., Wu, P., Fang, S. (2017). A semi-definite programming approach for solving optimal reactive power reserve dispatch. 2017 IEEE PES Asia-Pacific Power and Energy Engineering Conference (APPEEC). doi: https://doi.org/10.1109/appeec.2017.8309019

30. Poliak, D. (2022). Review of Least Action Principle in Electromagnetics Part I: Derivation of Continuity Equation and Lorentz Force. 2022 International Conference on Software, Telecommunications and Computer Networks (SoftCOM). doi: https://doi.org/10.23919/softcom55329.2022.9911297

31. Lezhniuk, P. D., Kulyk, V. V., Netrebskyi, V. V., Teptia, V. V. (2014). Pryntsyp naimenshoi dii v elektrotekhnitsi ta elektroenerhetytsi. Vinnytsia: UNIVERSUM-Vinnytsia, 212.

32. Ibrahim, S., Cramer, A., Liu, X., Liao, Y. (2018). PV inverter reactive power control for chance-constrained distribution system performance optimisation. IET Generation, Transmission & Distribution, 12 (5), 1089–1098. doi: https://doi.org/10.1049/iet-gtd.2017.0484

CHAPTER 1

33. Zhibing, W., Yang, X., Xitian, W. (2017). Coordinated control strategy of reactive power for large-scale wind power transmission by LCC-HVDC links. The Journal of Engineering, 2017 (13), 1082–1086. doi: https://doi.org/10.1049/joe.2017.0496

34. Jizhong, Z. (2009). Reactive Power Optimization. Optimization of Power System Operation. New-York: Wiley-IEEE Press, 409–454. doi: https://doi.org/10.1002/9780470466971.ch10

35. Hu, Y., Xiang, J., Peng, Y., Yang, P., Wei, W. (2018). Decentralised control for reactive power sharing using adaptive virtual impedance. IET Generation, Transmission & Distribution, 12 (5), 1198–1205. doi: https://doi.org/10.1049/iet-gtd.2017.1036

36. Wen, S., Wang, Y., Tang, Y., Xu, Y., Li, P. (2019). Proactive frequency control based on ultra-short-term power fluctuation forecasting for high renewables penetrated power systems. IET Renewable Power Generation, 13 (12), 2166–2173. doi: https://doi.org/10.1049/iet-rpg.2019.0234

37. Ghiasi, M., Niknam, T., Dehghani, M., Baghaee, H. R., Wang, Z., Ghanbarian, M. M., Blaabjerg, F., Dragicevic, T. (2022). Multipurpose FCS Model Predictive Control of VSC-Based Microgrids for Islanded and Grid-Connected Operation Modes. IEEE Systems Journal, 1–12. doi: https://doi.org/10.1109/jsyst.2022.3215437

38. Kulyk, V., Burykin, O., Malogulko, J., Hrynyk, V. (2020). Anticipatory control of transit power flows from the renewable energy sources in electric power system. 2020 IEEE 7th International Conference on Energy Smart Systems (ESS), 123–127. doi: https://doi.org/10.1109/ess50319.2020.9160115

39. Pham, H. V., Ahmed, S. N. (2018). Multi-Agent based Approach for Intelligent Control of Reactive Power Injection in Transmission Systems. Dynamic Vulnerability Assessment and Intelligent Control for Sustainable Power Systems. New-York: Wiley-IEEE Press, 269–282. doi: https://doi.org/10.1002/9781119214984.ch13

40. Zhu, Y., Fan, Q., Liu, B., Wang, T. (2018). An Enhanced Virtual Impedance Optimization Method for Reactive Power Sharing in Microgrids. IEEE Transactions on Power Electronics, 33 (12), 10390–10402. doi: https://doi.org/10.1109/tpel.2018.2810249

41. Aquino-Lugo, A. A., Overbye, T. (2010). Agent Technologies for Control Applications in the Power Grid. 2010 43rd Hawaii International Conference on System Sciences. doi: https://doi.org/10.1109/hicss.2010.43

42. Adhikari, S., Li, F., Li, H. (2015). P-Q and P-V Control of Photovoltaic Generators in Distribution Systems. IEEE Transactions on Smart Grid, 6 (6), 2929–2941. doi: https://doi.org/10.1109/tsg.2015.2429597

43. Aly, M. M., Abdel-Akher, M., Ziadi, Z., Senjyu, T. (2014). Assessment of reactive power contribution of photovoltaic energy systems on voltage profile and stability of distribution systems. International Journal of Electrical Power & Energy Systems, 61, 665–672. doi: https://doi.org/10.1016/j.ijepes.2014.02.040

44. Eid, A., Abdel-Akher, M. (2016). Voltage/var control of unbalanced distribution systems equipped with distributed single-phase PV generators. 2016 Eighteenth Interna-

tional Middle East Power Systems Conference (MEPCON). doi: https://doi.org/10.1109/mepcon.2016.7836930

45. Li, H., Huang, Y., Lu, J. (2016). Reactive power compensation and DC link voltage control using Fuzzy-PI on grid-connected PV system with d-STATCOM. 2016 IEEE PES Asia-Pacific Power and Energy Engineering Conference (APPEEC), 1240–1244. doi: https://doi.org/10.1109/appeec.2016.7779691

46. Kulyk, V. V., Hrytsiuk, I. V., Hrytsiuk, Yu. V. (2013). Optymalne keruvannia po-tokamy reaktyvnoi potuzhnosti v rozpodilnykh elektromerezhakh z rozo-seredzhenym heneruvanniam. Pratsi Instytutu elektrodynamiky NANU, 151–158.

47. Burykin, O. B., Lezhniuk, P. D., Kulyk, V. V. (2008). Vzaiemovplyv elektrychnykh merezh i system v protsesi optymalnoho keruvannia yikh rezhymamy. Vinnytsia: UNIVERSUM–Vinnytsia.

48. Gryniewicz-Jaworska, M., Lezhniuk, P. D., Kulyk, V. V., Netrebskiy, V. V., Duchkov, Y. V. (2018). Adaptive optimal control of electric power system operation mode on the base of least action principle. Advances in Science and Technology Research Journal, 12 (3), 61–65. doi: https://doi.org/10.12913/22998624/94922

49. Lezhniuk, P., Bondarchuk, A., Shullie, I. (2019). Investigation and implementation of the fractal properties of electric load on civilian objects in order to efficiently predict and control electrical consumption. Eastern-European Journal of Enterprise Technologies, 3 (8 (99)), 6–12. doi: https://doi.org/10.15587/1729-4061.2019.168182

50. Lezhniuk, P., Kravchuk, S., Netrebskiy, V., Komar, V., Lesko, V. (2019). Forecasting Hourly Photovoltaic Generation On Day Ahead. 2019 IEEE 6th International Conference on Energy Smart Systems (ESS). doi: https://doi.org/10.1109/ess.2019.8764245

CHAPTER 1

Viacheslav Komar, Petro Lezhniuk, Vladyslav Lesko,
Yuliya Malogulko, Volodymyr Netrebskyi, Olena Sikorska

CHAPTER 2

CHAPTER 2

ELECTRICITY CONSUMPTION AND RENEWABLE ENERGY SOURCES GENERATION SCHEDULES COORDINATION IN ELECTRIC NETWORKS FOR BALANCE RELIABILITY INCREASING

ABSTRACT

The chapter analyzes the schedules of electricity consumption and generation in the electricity network with renewable energy sources (RES) as an opportunity to improve the electricity balance in it. It is shown that in order to achieve a positive effect from the introduction of RES into the electric grid, a balance of electricity generation and consumption must be ensured in it. To do this, first of all, the values of the optimal installed power of RES are determined to coordinate the generation and electricity consumption schedules, and the principles of consumption management in the electric network are formed. In order to increase the stability of power supply systems, it is proposed to use electric power accumulators, which, if there is a certain energy reserve in the accumulator, can be used in case of an insufficient amount of RES generation. An algorithm for the method of matching the generation schedules of the PV power plants and the electric load of the network has been developed. At the same time, the cost of displacement of consumption power is estimated, for which a corresponding indicator has been developed. Since the quality of power supply depends not only on the balance of active power, but also reactive power, RES with inverter energy conversion devices are considered as a means of regulating reactive power in the electrical network in order to maintain the voltage within acceptable limits.

KEYWORDS

Electric network, renewable energy sources, electric energy balance, generation and consumption schedules, coordination.

Determining the priority of solving problems in local electric networks (LEN), we determine balance reliability, when its calculation model is determined by the balance of consumption and own generation of electricity, taking into account external income. How other tasks are successfully solved depends on how and by what means balance reliability is ensured [1–3]. Its technical

and economic indicators depend on the balance of active and reactive power in LEN [4, 5]. The process of power balancing in LEN is significantly affected by the instability of the generation of renewable energy sources (RES), in particular, photovoltaic and wind power plants (PV and wind power plants).

The instability of RES generation is compensated by the power supplied to LEN from the power system. Because of that, the balancing conditions of the LEN mode also affect the modes of the electric power system (EPS). A number of works [6–9] have been devoted to the optimization of the joint operation of LEN and EPS. In today's conditions, ensuring the balance is entrusted purely to the centralized power supply system. However, changes are gradually taking place in the energy market functioning mechanisms, which encourage RES owners to work according to a given schedule, in particular, the introduction of fines for non-compliance with the stated daily generation schedule.

Increasing RES generation in distribution networks by reducing the load on the centralized power supply system allows for a number of positive effects. They are manifested in the reduction of power and electricity losses in power transmission lines, which are used to transport power, the improvement of the quality of electricity, and the unloading of electrical networks [10]. However, this applies only to cases where the RES generation schedule is consistent with the local electricity consumption schedule. Therefore, the task of artificial coordination of RES generation and electric load schedules arises. It should also be taken into account that the schedule of electrical loads is also non-uniform. For example, the daily dip in the load schedule falls on the peak of generation of the PV power plant, which thereby increases such unevenness. There is a need to motivate consumers to shift their daily schedule of electric loads to the hours of peak generation of PV power plant.

In order to successfully solve the problem of coordinating the schedules of electricity consumption and its generation by renewable energy sources in electric networks as a means of increasing balance reliability, it is first necessary to first of all determine the value of the optimal installed power of RES and form the principles of consumption management in LEN to coordinate the schedules of generation and electricity consumption.

2.1 DETERMINATION OF THE OPTIMAL INSTALLED RES CAPACITY

The RES generation schedule depends on the natural conditions of the region in which the source is located. The value of the installed capacity of the RES should be chosen under the condition of maximum compliance of the generation schedule with the consumption schedule. Given the stochastic nature of both graphs, the method is based on probability analysis.

The starting information for starting the calculation is: statistical data (minimum for the previous year) and a forecast of natural conditions (solar radiation, wind currents); graphs of power consumption of feeder nodes; diagram and parameters of replacement of electrical network elements [11].

Step 1. An annual base of daily insolation (wind flow) schedules is formed to a dimensionless form by dividing by the maximum value. An annual base of total daily schedules for the feeder is formed and reduced to a dimensionless form.

Step 2. Annual schedules are formed by duration, respectively, for RES and consumers.

Step 3. The coefficient of energy security is estimated

$$k_{es} = \frac{M(E_{cons})}{M(E_{RES})},$$

where $M(E_{cons})$ – mathematical expectation of annual consumption; $M(E_{RES})$ – mathematical expectation of annual RES generation.

Step 4. If necessary, the RES schedules obtained in Step 1 are refined in order to obtain an energy security factor equal to 1.

Step 5. For refined schedules, let's determine the probabilities of ensuring the balance:

$$k_{stab} = \sum_{i=1}^{24} \left[p_{daily\,i} \sum_{j \in D} \left(p_{RES\_year_j} \sum_{l \in F} p_{Aons\_year_l} \right) \right],$$

where p_{daily} – the probability of the appearance of the degree of the daily schedule $\left(p_{daily} = 1/24\right)$; p_{RES_year} – the probability of the occurrence of a degree of generation during the year; D – set of non-zero powers; p_{Aons_year} – the probability of the degree of consumption occurring during the year; F – set of levels of consumption that are below the generation level of the corresponding period of the day.

Step 6. Let's determine the coefficients of current distribution according to the equation:

$$\mathbf{C}_r = \mathbf{R}^{-1}\mathbf{M}^T \left(\mathbf{M}\mathbf{R}^{-1}\mathbf{M}^T \right)^{-1},$$

where $\mathbf{R}$ – the matrix of resistances of the branches of the electric network; $\mathbf{M}$ – the matrix of connections of the branches of the circuit in the nodes (T is the transformation symbol).

The coefficients of current distribution depend on the installation point of the RES, so let's choose the line of the matrix $\mathbf{C}_r$ corresponding to the line through which the generated power of the RES flows into the network. All possible (according to technical conditions) connection points are considered.

Step 7. By analyzing the received vectors $\mathbf{C}_r$, for each of the nodes, the one with the largest sum of coefficients is selected.

Step 8. Based on the original daily consumption schedules, let's calculate the mathematical expectation of the power consumed by each node of the feeder.

Step 9. Let's determine the mathematical expectation of generation power

$$M\left(P_{RES}\right) = M\left(P_{cons}\right)^{T} C_{r}^{T}.$$

Step 10. Let's determine the installed capacity of RES as

$$P_{RES} = k_{stab} k_{es} M\left(P_{RES}\right).$$

The use of the coefficient of energy security and the probability of ensuring the balance in the algorithm allows not only to take into account the features of the generation and consumption schedules, but also to determine the RES capacity, which will ensure that the generation schedule is as close as possible to the consumption schedule [12].

The effectiveness of the proposed method can be shown by an example. Let's consider the feeder, the diagram of which is shown in **Fig. 2.1**.

CHAPTER 2
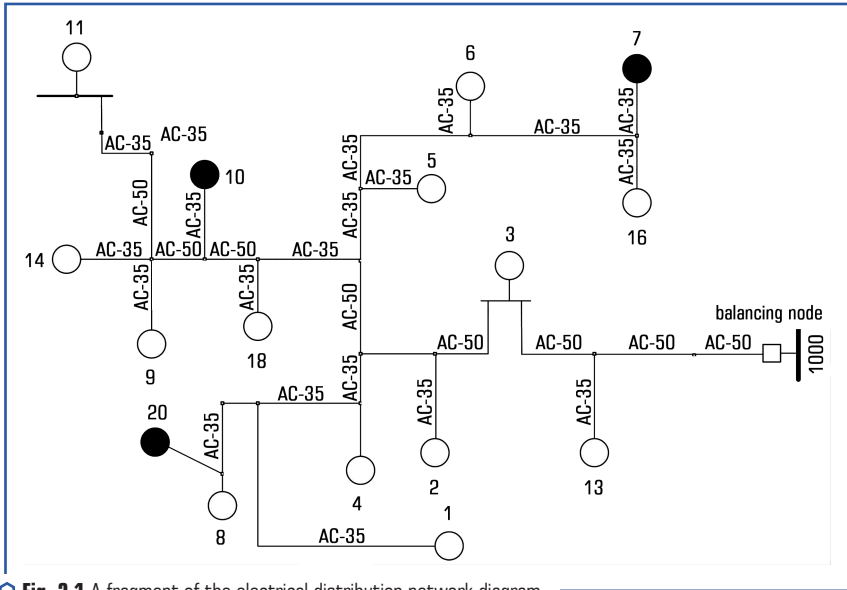
○ **Fig. 2.1** A fragment of the electrical distribution network diagram

Let's consider how nodes for connecting RES 20, 10 and 7 are possible according to the technical conditions. To choose the best of them according to the criterion of electrical energy losses,

let's determine the current distribution coefficients for each of the options. Let's summarize the values of the coefficients **C$_r$** in the **Table 2.1**. Since the total value of the coefficients is greater for node 10, this node is the best node for connecting RES. This is confirmed by the results of calculations. From **Fig. 2.2, 2.3** (for node 20), **Fig. 2.4** (for node 10) and **Fig. 2.5** (for node 7), it can be concluded about a greater unloading effect when the PV power plant is installed in node 10.

For comparison, the calculation of losses of active power in the EN with the selection of PV power plant capacities for the studied schedule of generation and consumption was carried out. Graphical interpretation of the results is shown in **Fig. 2.2–2.5**.

● **Table 2.1** Results of vector analysis of current distribution coefficients

The total value of current distribution coefficients

in relation to node 20	in relation to node 10	in relation to node 7
9.914	11.805	9.041

In **Fig. 2.2** shows the results of calculating daily electricity losses during the year. Accordingly, three cases were considered:

– without taking into account PV power plant generation (curve 1);

– with PV power plant generation at its optimal (according to the proposed method) installed capacity (81.5 kW) (curve 2);

– with PV power plant generation with an installed capacity of 200 kW (curve 3).
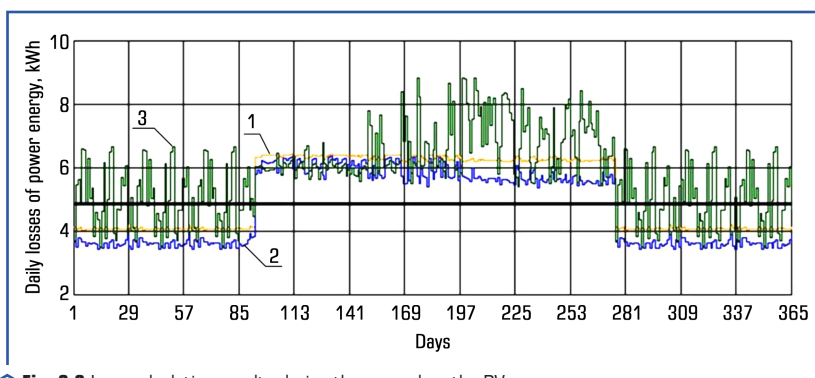
○ **Fig. 2.2** Loss calculation results during the year when the PV power plant is installed at node 20

From the analysis of the obtained graphs, it is possible to ascertain the adequacy of the results obtained by the proposed method.
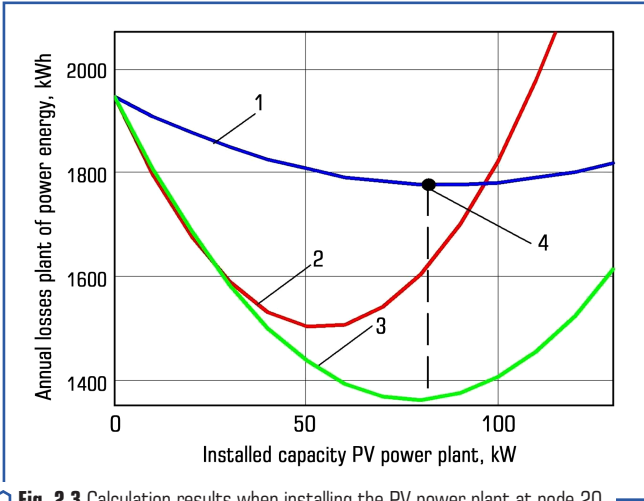
Fig. 2.3 Calculation results when installing the PV power plant at node 20
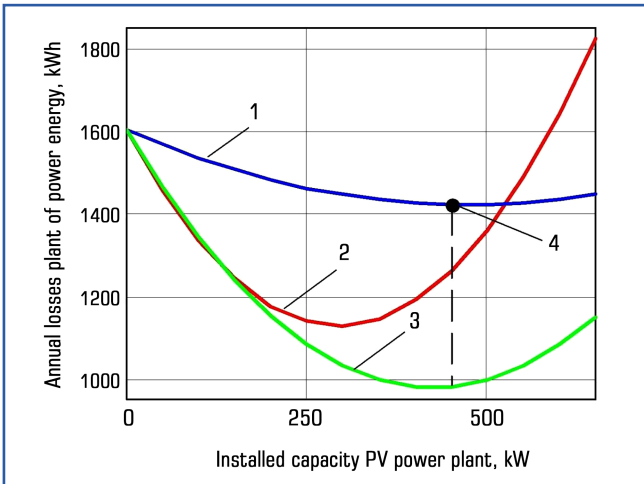
Fig. 2.4 Calculation results when installing the PV power plant at node 10

In **Fig. 2.3–2.5**, curve 1 — change in losses of active power during the year, obtained by counting the installed capacities of the PV power plant; curve 2 — the change in losses of active power during the year, obtained by searching the installed capacities of the PV power plant, provided that the installed capacity of the source is selected from the analysis of the most likely level of

CHAPTER 2

47

electricity consumption; curve 3 – the change in losses of active power during the year, obtained by overestimating the installed capacities of the PV power plant, provided that the mode of operation of the station is dictated not only by natural conditions, but also by the electricity consumption schedule; point 4 is the result of calculation according to the proposed method.
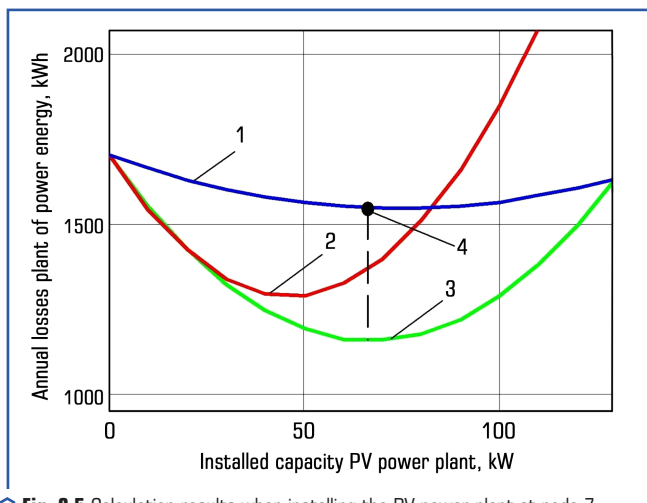
⭘ **Fig. 2.5** Calculation results when installing the PV power plant at node 7

The results are obtained under the condition that the power consumption schedules match, that is, the coefficient of stability of the coverage of the schedules is the same for each of the consumers. It is clear that this is a certain idealization of the real course of things, but this assumption is made in order to show the effectiveness of the established principle. To take into account real electricity consumption schedules, it is necessary to specify the current distribution coefficients by multiplying by the corresponding probability of ensuring the balance.

The proposed method allows to choose the optimal connection location and installed capacity of RES [13]. Based on the obtained results, it is possible to carry out a comprehensive analysis to assess the ensured quality of the operation of the electric network.

The result of the dependence of the quality of LEN operation for the most probable state depending on the installed generating capacity of the PV power plants is shown in **Fig. 2.6**.

The value of the PV power plant generation capacity is presented in relative units of the actual installed capacity of $P_{inst.PV} = 1.431$ MW (the calculation was made for the second stage of PV power plant input). The results of the calculation show that to ensure a high-quality power supply, the power of the PV power plant would be optimal in the range of 47 % – 80 % of the actually installed. Namely, the recommended capacity of the PV power plant should be 0.95 MW. The indicator of the quality of functioning for the optimal capacity of the PV power plant will be $E_{q\_opt.PV} = 0.41$.

CHAPTER 2
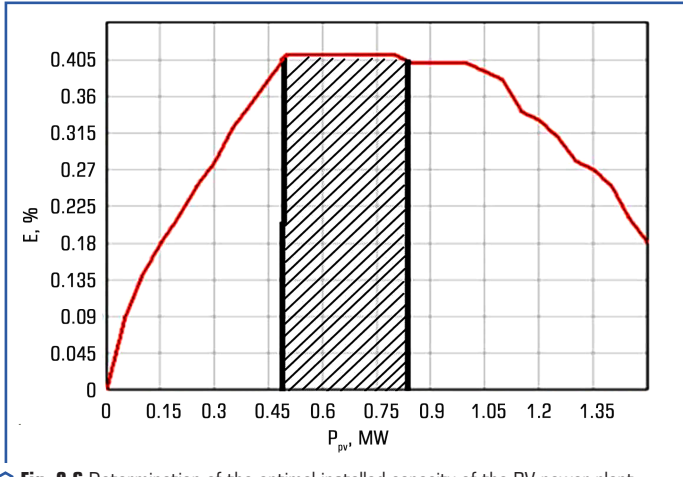
Fig. 2.6 Determination of the optimal installed capacity of the PV power plant

The selection of the optimal generation power of the PV power plant allows to improve the voltage levels in the nodes and increase the probability of ensuring the economy of the regime in the LEN [14]. Coordination of generation and consumption schedules within the framework of the consumption regulation program is also effective [15–17].

The proposed method is implemented as a separate module in PC "Losses". The window of the software module for forming optimal RES connection schemes has the following form (**Fig. 2.7**).

The main window is intended for the user to initialize the corresponding modes of the automated system:

1. Entering information on potential connection locations and existing distributed generation facilities. In this mode, the structure of the distribution network, the number and names of fragments (feeders) and objects (TS) are entered into the "Objects" table.

2. Entering information on 10(6) kV feeders. In this mode, information about the number and names of the corresponding 10(6) kV feeders is entered in the "Equipment" table.

3. Selection of potential sites for RES connection to power grids. This mode is implemented in the main window of the module by selecting fragments and objects from the structural tree (**Fig. 2.7**).

4. Selection of a set of optimization criteria. In this mode, the user selects the criteria by which a multi-criteria analysis of the distribution network objects will be conducted to determine the feasibility of connecting RES (**Fig. 2.7**).

5. Output of results is carried out after performing computational procedures at the operator's initiative. At the same time, a report is created in Microsoft Excel format, an example of which is shown in **Fig. 2.8**.

The results of optimization calculations are shown in **Fig. 2.9**, which are obtained for a real example of the connection of RES, consisting of three stages of photovoltaic generation (500 kW,

CHAPTER 2

570 kW, 630 kW) and a small hydropower plant with a capacity of 250 kW. According to the results of the research, a RES connection scheme was formed, which was implemented in practice and showed sufficient technical and economic efficiency.

○ **Fig. 2.7** The window of the software module for forming optimal RES connection schemes

○ **Fig. 2.8** An example of a report on multi-criteria evaluation and ranking of RES connection points to power grids
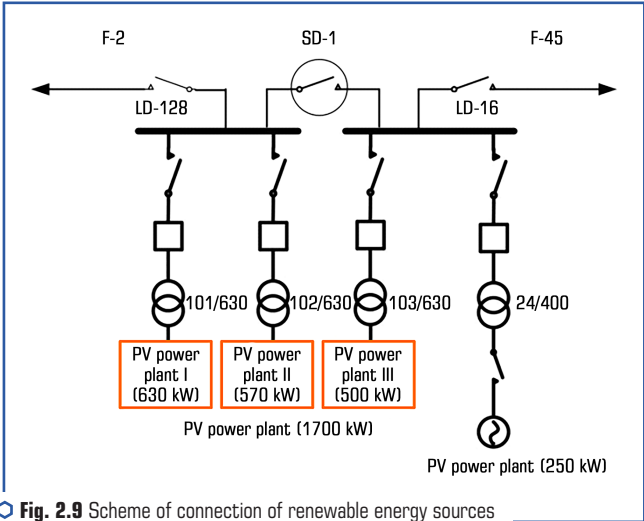
○ **Fig. 2.9** Scheme of connection of renewable energy sources to distribution grids

The integral quality indicator was determined before the introduction of the PV power plant ($E = 0.876$) and after the introduction of the PV power plant ($E = 0.78$) (**Fig. 2.10**). The decrease in the quality indicator is explained by the overload of the feeder. After the introduction of the 1,700 kW power plant, the electricity and voltage losses in the feeder nodes, where a small 250 kW power plant is already operating, increased. It is possible to unload the feeder if part of the power will be distributed to the substation of the neighboring district electric network. Due to the reduction of electricity and voltage losses and improvement of reliability, the overall technical and economic efficiency of electric networks and renewable energy sources increases. Transferring part of the PV power plant electricity to another substation allows to increase the effect on the feeder ($E = 0.93$).
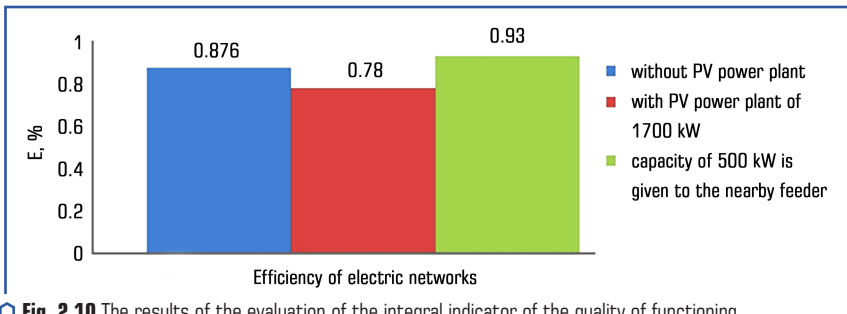
○ **Fig. 2.10** The results of the evaluation of the integral indicator of the quality of functioning

CHAPTER 2

2.2 CONSUMPTION MANAGEMENT TO COORDINATE GENERATION AND ELECTRICITY CONSUMP-
TION SCHEDULES

As noted in [15–17], consumption management is a fairly effective means of increasing the efficiency of power supply systems. The implementation models of such regulation are different in each state. However, the underlying principles are similar. A generalized diagram of the principles of implementing demand management is shown in **Fig. 2.11**.

According to this scheme, every consumer who has a certain freedom in the amount of electricity consumption, the so-called "active consumer", (due to the flexibility of the technological process, the ability to minimize its consumption in certain periods at the expense of its own sources or energy storage devices, etc.) can independently or through the aggregator to provide paid services in changing your consumption at the request of the system. Each country develops the financing mechanism for such services individually.

In conditions of RES development, demand management can improve the quality of operation of electrical networks.
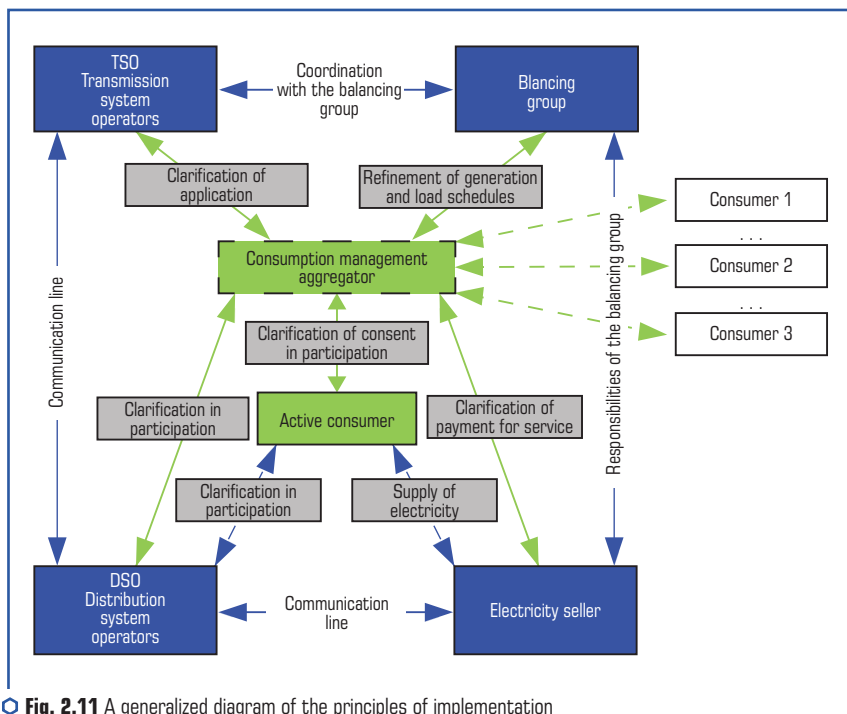
⚪ **Fig. 2.11** A generalized diagram of the principles of implementation of demand management

The analysis of the overall schedule of the feeder load shows that there are hours during the day when the generation of the PV power plant is greater than the local consumption. Such an extension increases the loss of electricity in the LEN, has a negative effect on the voltage deviation and increases the total unevenness of the daily generation.

The principle of the "ideal" regime, which is the basis for evaluating the quality of the operation of electrical networks, allows to evaluate the efficiency of each consumer in the task of coordinating the schedules of RES generation and consumption. The choice of consumers whose consumption schedule change will have the maximum efficiency for LEN (**Fig. 2.1**) is proposed to be made on the basis of the analysis of the coefficients of the current distribution matrix for r the scheme in relation to the generating unit. The row of the matrix $\mathbf{C}_r$ corresponding to the line that connects the PV power plant to the distribution electrical network feeder is given in the **Table 2.2**.

● **Table 2.2** Fragment of the matrix of current distribution coefficients of the feeder of distribution electric networks

No. node	14	9	18	11	5	6	7	4
The value of the current distribution coefficient	0.998	0.997	0.853	0.75	0.74	0.79	0.61	0.75
No. node	8	20	2	1	3	13	16	–
The value of the current distribution coefficient	0.689	0.66	0.68	0.71	0.64	0.59	0.6	–

It is obvious that it is advisable to level the schedule by changing the load of nodes located near the generation source and with a relatively large power consumption, that is, with the largest current distribution coefficients. Losses of active power in power transmission lines will be reduced by reducing the distance of electric energy transportation from the PV power plant. Such nodes are nodes 14, 9, 18.

The method is based on the application of the transport problem algorithm and is solved in tabular form [18]. The result of matching the schedules depends on the coefficients of the cost of displacement of the consumption capacity.

Estimation of the cost of displacement of consumption capacity in the conditions of a multizone tariff for electric energy can be carried out according to the expression [19]:

$$B_{ij} = P_{sh} \cdot C_t \left(K_{Tj} - K_{Ti} \right) + \beta - \Delta P \cdot C_t, \tag{2.1}$$

where K_{Tj} – coefficient of the cost of electricity according to the zone tariff of the level of the schedule from which the capacity is planned to be transferred, in the central office; K_{Ti} – coefficient of the cost of electricity according to the zone tariff of the stage of the schedule to which the power is planned to be transferred, in the central office; P_{sh} – the power that the consumer

CHAPTER 2

must shift to level the LEN load schedule, kW; C_t – tariff for electricity according to the energy supply company, hryvnias/kWh; β – the cost of the technological shift in production, which must be compensated by the power system, hryvnias; ΔP – reduction of power losses due to adjustment of the consumer's load schedule, kW.

The indicator of the cost of transferring the load B_{ij} from one stage of generation to another is expedient to use in the task of matching the RES generation schedules to the load. Application of this approach, in the problem of equalization of daily generation, will allow not only to reduce the unevenness of the latter, but also to reduce the loss of electricity in the LEN.

To reduce the unevenness of the total daily generation of distribution electrical network and to minimize losses of active power, it is suggested to adjust the schedule by each node in turn according to the current distribution coefficient.

In **Table 2.3**, in which it is conditionally possible to highlight m the hours in which the actual consumption of the node is greater than the generation of the PV power plant, $A_i,...,A_m$, and n the hours in which PV power plant generation will exceed node consumption, $Z_i,...,Z_m$. For this purpose, node capacities are used, refined by multiplying by the current distribution coefficient. The relative cost B_{ij} of power transfer from one time interval of the schedule to another will be determined by (2.1).

It is obvious that the value of relative values B_{ij} will differ for each node.

● **Table 2.3** Distribution of consumption displacement values according to the transport problem

B_{11}	B_{12}	B_{13}	B_{14}	B_{15}	B_{16}	B_{17}	...	...	B_{1i}	Z_1
B_{21}	B_{22}	B_{23}	B_{24}	B_{25}	B_{26}	B_{27}	...	...	B_{2i}	Z_2
...	...	...	...	...	...	...	...	...	...	...
B_{j1}	B_{j2}	B_{j3}	B_{j4}	B_{j5}	B_{j6}	B_{j7}	...	...	B_{ji}	Z_n
A_1	A_2	A_3	A_4	A_5	A_6	A_7	...	...	A_m	...

In accordance with the given task, let's write down the objective function:

$$\sum_{i=1}^{m}\sum_{j=1}^{n} B_{ij} \cdot P_{ij} \to \min, \tag{2.2}$$

where P_{ij} – the power that needs to be shifted from the j-th stage of the load schedule to the i-th.

The first group of restrictions indicates that the power at any generation stage must be equal to the total power consumption of this generation stage:

$$\sum_{i=1}^{m} P_{ij} = A_i. \tag{2.3}$$

The second group of restrictions indicates that the total shift in consumption for a certain level of generation must fully compensate for the generation at this level:

$$\sum_{i=1}^{n} P_{ij} = Z_j. \tag{2.4}$$

There is also a restriction on the impossibility of shifting negative values of capacity consumption:

$$P_{ij} \geq 0, \, i = 1,2,\ldots,m, \, j = 1,2,\ldots,n. \tag{2.5}$$

The dependence of the mode of operation of renewable energy sources on natural conditions in most cases leads to the deterioration of the mode of operation of distribution electric networks. Therefore, it is necessary to carry out artificial coordination of load and RES schedules. This is especially true of photovoltaic plants.

According to the developed method, the transport matrix of the displacement values of the load capacities at node 14 is given in the **Table 2.4**. The results of optimizing the load schedule for node 96 are presented in the **Table 2.5**.

As mentioned earlier, leveling the load schedule of the local electrical system due to the selection of consumers based on the current distribution coefficient allows to reduce losses of active power in it. **Fig. 2.12** shows the change in active power losses depending on the time of day for all stages of optimization. A total reduction in electrical energy losses is also achieved – the result is shown in **Fig. 2.13**.
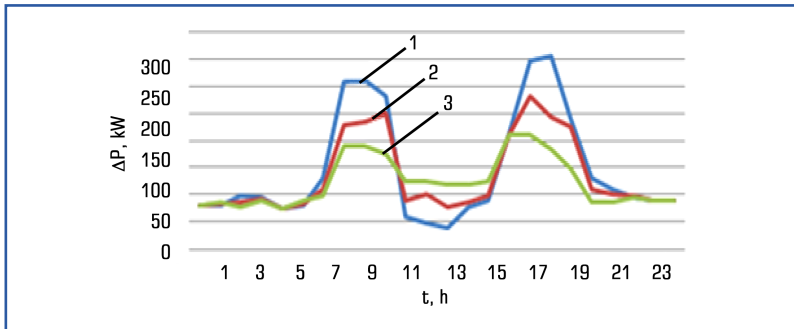
○ **Fig. 2.12** Change in losses of active power in LEN: 1 – taking into account PV power plant generation; 2 – after leveling the graph at node 14; 3 – after leveling the graph at node 9

The evaluation of the effect of coordinating the generation and load schedules of the PV power plant is carried out on the basis of the developed LEN functioning quality coefficient, which for the agreed generation and load schedules is $E_{q\_agreed} = 0.84$.

CHAPTER 2

● **Table 2.4** Transport matrix of power consumption of 14 nodes

Time intervals of generation	Z_m	Time intervals of generation															Fictitious node load
		0	1	2	3	4	5	6	7	17	18	19	20	21	22	23	
8	270	3.6	3.5	3.4	3.3	3.2	3.1	3	2.9	2.7	3.1	3.2	3.3	2.9	3	3.6	0
9	410	4.2	4.1	4	3.9	3.8	3.7	3.6	3.5	3.1	3.5	3.6	3.7	3.3	3.4	4	0
10	600	4.3	4.2	4.1	4	3.9	3.8	3.7	3.6	3	3.4	3.5	3.6	3.2	3.3	3.9	0
11	760	3.9	3.8	3.7	3.6	3.5	3.4	3.3	3.2	2	3	3	3	3	3	3	0
12	790	4	3.9	3.8	3.7	3.6	3.5	3.4	3.3	2.3	2.7	2.8	2.9	2.5	2.6	3.2	0
13	790	4.1	4	3.9	3.8	3.7	3.6	3.5	3.4	2.2	2.6	2.7	2.8	2.4	2.5	3.1	0
14	630	4.2	4.1	4	3.9	3.8	3.7	3.6	3.5	2.1	2.5	2.6	2.7	2.3	2.4	3	0
15	270	4.3	4.2	4.1	4	3.9	3.8	3.7	3.6	2	2.4	2.5	2.6	2.2	2.3	2.9	0
16	110	4.4	4.3	4.2	4.1	4	3.9	3.8	3.7	1.9	2.3	2.4	2.5	2.1	2.2	2.8	0
A_m		80	110	50	60	100	150	70	10	80	100	100	120	50	80	60	3410

● **Table 2.5** Optimization result for node 14

Time intervals of generation	Z_m	Time intervals of generation															Fictitious node load
		0	1	2	3	4	5	6	7	17	18	19	20	21	22	23	
8	270	0	0	0	0	0	0	0	0	0	0	0	0	0	0	0	270
9	410	0	0	0	0	0	0	0	0	0	0	0	0	0	0	0	410
10	600	0	0	0	0	0	0	0	0	0	0	0	0	0	0	0	600
11	760	26	32	0	0	11	27	3	0	5	13	10	16	0	13	5	599
12	790	27	35	20	22	32	43	25	6	27	31	32	37	19	25	21	386
13	790	27	35	19	23	32	44	25	4	28	32	33	37	19	25	21	387
14	630	0	8	11	15	24	36	17	0	20	24	25	30	11	17	13	379
15	270	0	0	0	0	0	0	0	0	0	0	0	0	0	0	0	270
16	110	0	0	0	0	0	0	0	0	0	0	0	0	0	0	0	110
A_m		80	110	50	60	100	150	70	10	80	100	100	120	50	80	60	3410
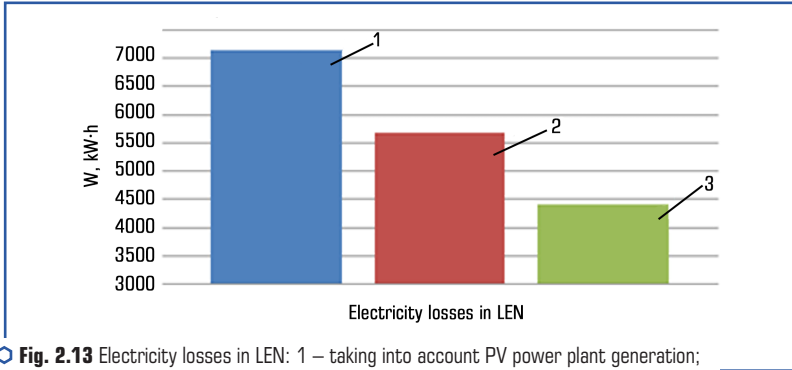
Fig. 2.13 Electricity losses in LEN: 1 – taking into account PV power plant generation;
2 – after leveling the schedule at node 14; 3 – after leveling the schedule at node 9

Coordination of generation and load schedules leads to improvement of technical and economic and mode parameters of LEN operation. But since the generation of PV power plant has the nature of generation dependent on variable weather parameters, even in the case of agreed schedules, the use of capacity reserve is mandatory.

2.3 ELECTRIC ENERGY ACCUMULATORS AS AN ELEMENT OF INCREASING THE BALANCE RELIABILITY OF LOCAL ELECTRIC SYSTEMS

One of the ways to increase the stability of power supply systems is the accumulation of excess energy, which is formed as a result of the imbalance between the energy produced by RES and consumed in the LES. The presence of a certain energy reserve in the accumulator can be used in case of an insufficient volume of RES generation. Control of the charge/discharge process is most often performed based on the presence/absence of a positive difference between the energy generated by RES and consumed by the load.

It is clear that in case of installation of the accumulator within the limits of the balance sheet ownership of the energy source, the calculation of its technical characteristics should be based on the assessment of the instability of the RES generation process [19, 20]. As an example, this can be shown by the results of calculations of excess and deficit capacity of the Galzhbiyiv PV power plant. **Fig. 2.14** illustrates the excesses and deficits of capacity in the form of a graph that displays the value of the possibility of accumulating a certain amount of capacity $Q(t)$ – provided that the initial capacity of the storage $Q_0(t) = 0$.

From **Fig. 2.14**, it can be seen that for this PV power plant, the mathematical expectation of surplus is greater than the mathematical expectation of deficit $M_{sup\,l\,t} > M_{def\,t}$ in the time interval from 10:30 to 13:30. Therefore, for the installed generating capacity of this PV power plant, the storage capacity will be equal to:

$$Q(t) = \frac{W_{\text{sup}}(t)}{U_{stor}} = \frac{2756.35}{12} = 230 \, kA \, h. \tag{2.6}$$

Due to the surplus that can be accumulated during the PV power plant generation hours from 10:30 a.m. to 1:30 p.m., it is possible to increase the number of hours in which the PV power plant will independently ensure the balance between the generation and electricity consumption of the PV power plant (**Fig. 2.15**). Another advantage of using accumulators is that excess generation will not lead to an increase in additional losses of active power and deterioration of the quality of electricity in the electrical network.
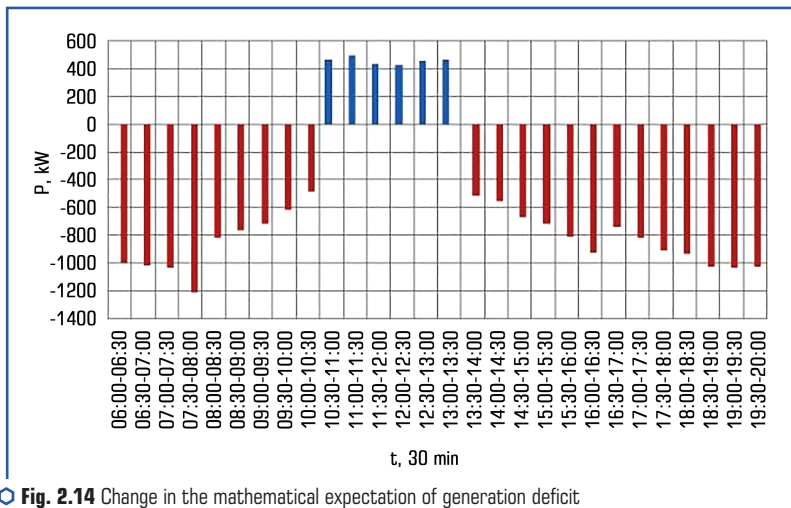
○ Fig. 2.14 Change in the mathematical expectation of generation deficit and surplus during the day

Taking into account the installed energy storage (SE), the quality of the LES operation will increase to $E_{q\_inst\_RES\,stor} = 0.583$.

Installation of a storage device of such capacity requires substantial capital investment. The amount of stored electricity depends directly on the capacity of the energy storage, as well as on the installed generating capacity of the PV power plant.

According to the Law of Ukraine on the electric energy market [21], renewable energy sources must announce the hourly schedule of electric energy production a day in advance. Taking into account the insufficient accuracy of the forecast of meteorological parameters, in order to ensure the accuracy [22, 23] of working out the declared generation schedule, it is necessary to use a system of accumulating excess energy, which can be used as an additional source in periods of insufficient generation.
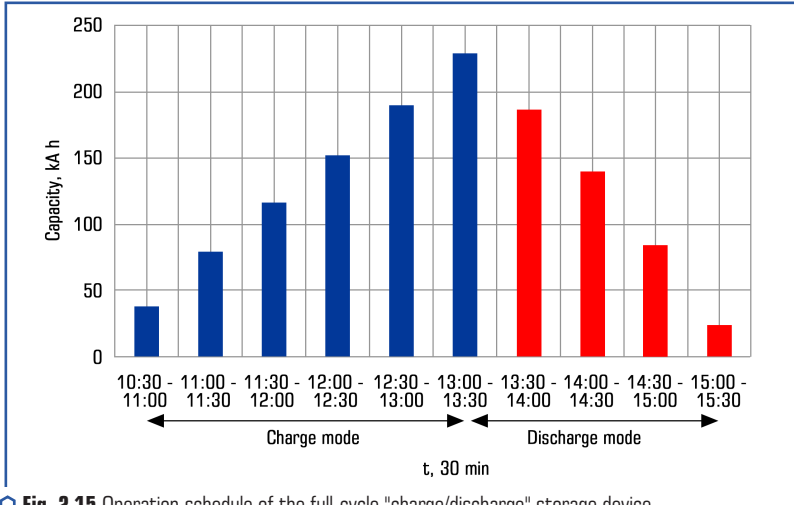
Fig. 2.15 Operation schedule of the full-cycle "charge/discharge" storage device

For this purpose, a mathematical model of such a system was developed in the work and simulation modeling of its operation was carried out.

Matlab/Simulink PC was used to develop the mathematical model. **Fig. 2.16** and **2.17** show the Simulink model of the PV power plant complex and the electrochemical storage. **Fig. 2.18** shows the operation logic of the storage management system in the mode of maintaining the declared generation schedule.
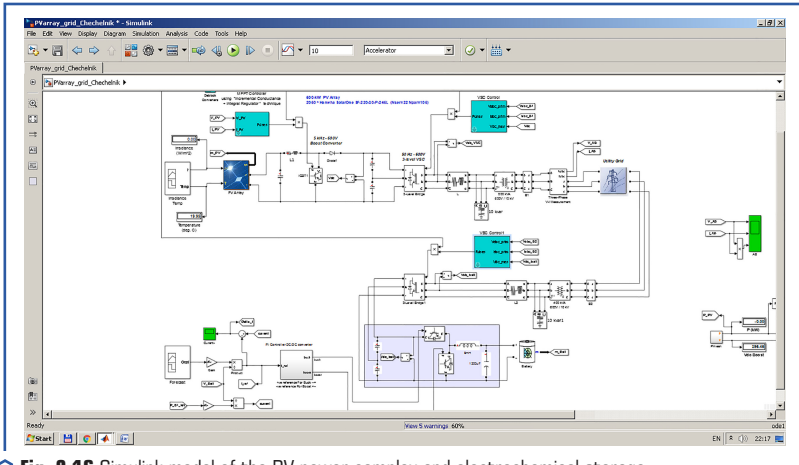
Fig. 2.16 Simulink model of the PV power complex and electrochemical storage

CHAPTER 2
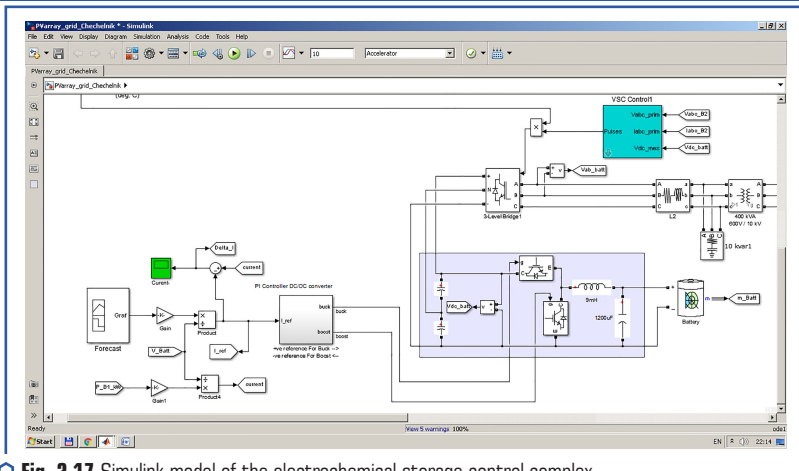
Fig. 2.17 Simulink model of the electrochemical storage control complex
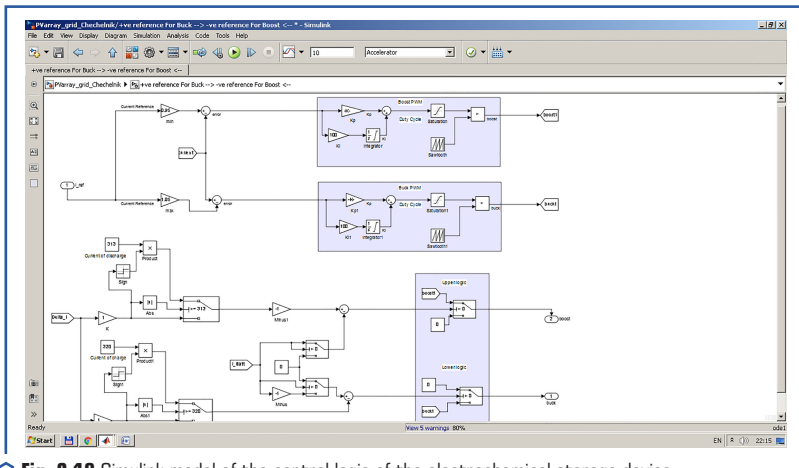
Fig. 2.18 Simulink model of the control logic of the electrochemical storage device

The Simulink model was used as a model of an electrochemical energy storage device. The characteristics correspond to a Li-Ion battery. The discharge and charge curves are shown in **Fig. 2.19**.

The results of simulation modeling of the operation of the energy storage system at various PV power plants are shown in **Fig. 2.20–2.22**.

For a day characterized by an average level of cloud cover, an hourly schedule was forecast (**Fig. 2.20–2.22**, the red curve takes into account the provision of the area of permissible devia-

tions of ±10 %). Taking into account the actual schedule of operation of the PV power plant (black curve), a simulation of the operation of the energy storage system was performed, taking into account 50 % battery charge (blue curve). The simulation was carried out for storage systems with batteries of different capacities. As a result, the smallest capacity was selected, at which the predicted generation schedule was provided as accurately as possible.
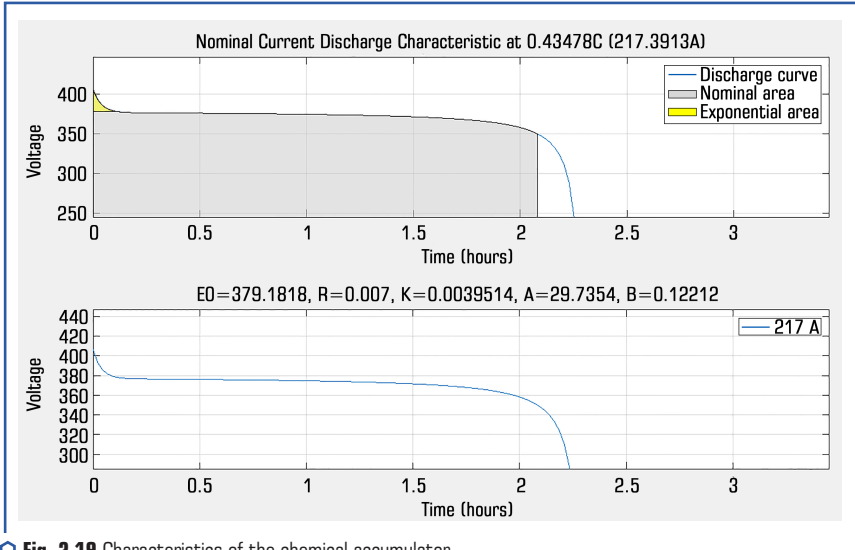
● **Fig. 2.19** Characteristics of the chemical accumulator
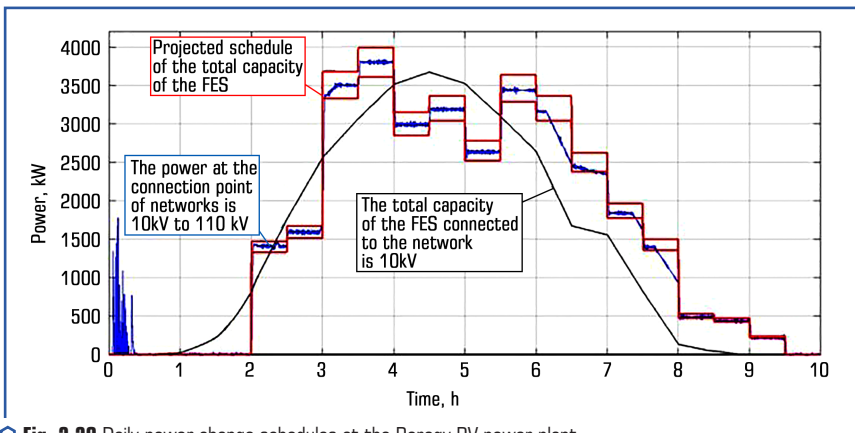
● **Fig. 2.20** Daily power change schedules at the Porogy PV power plant
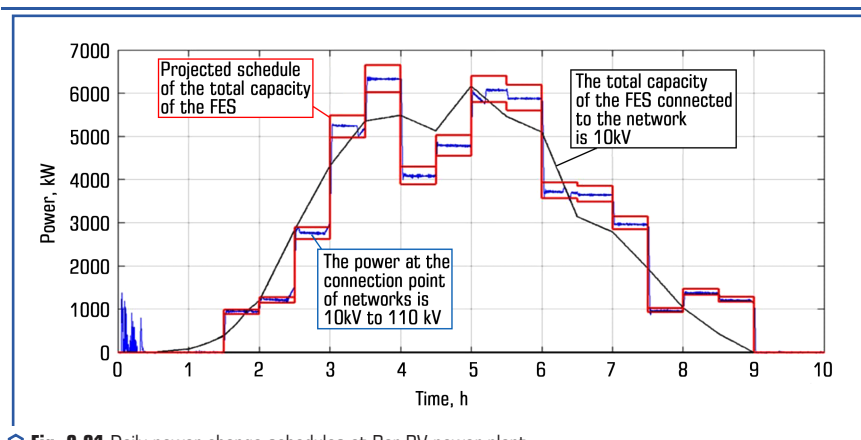
Fig. 2.21 Daily power change schedules at Bar PV power plant
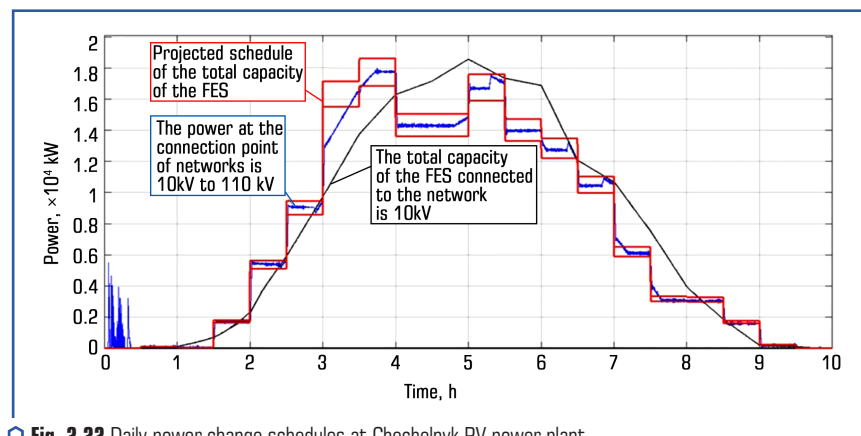
Fig. 2.22 Daily power change schedules at Chechelnyk PV power plant

The results of the simulation analysis are shown in **Fig. 2.23** and **2.24**. **Fig. 2.23** and **2.24** show the values of discharge and charge energy for storage systems installed at each station and at a group of stations. We can clearly conclude that it is economically feasible to install storage devices on a group of stations, as it allows reducing the total capacity of batteries. In addition, the group storage can be used when solving a number of other problems (balancing modes, providing system services for regulating mode parameters, etc.), which increases the profitability of invested funds.

Since it is practically impossible to ensure balance reliability purely by PV power plant generation, it is necessary to determine the capacity of the reserve, which should be provided by the power system to maintain the balance between consumed and generated electricity in the LES.
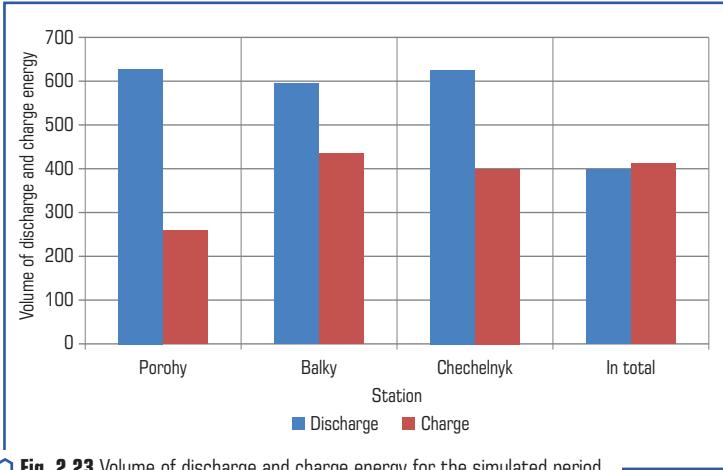
○ **Fig. 2.23** Volume of discharge and charge energy for the simulated period
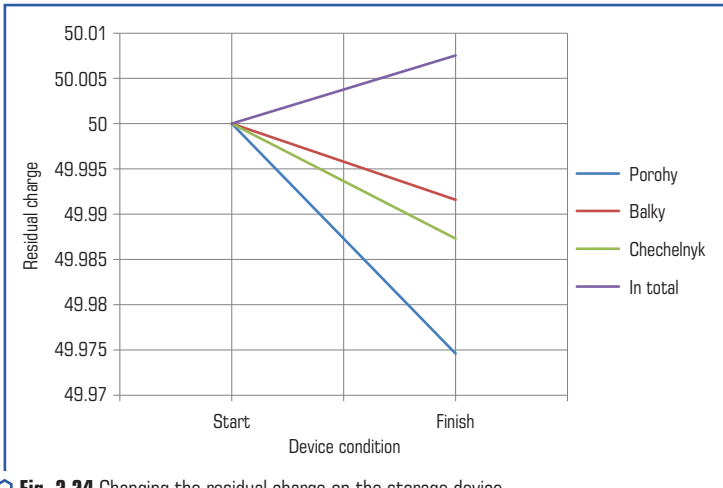
○ **Fig. 2.24** Changing the residual charge on the storage device

It is possible to get benefits from the generation of photovoltaic plants due to the introduction of additional means. The paper considers the possibility of using electric energy storage to coordinate the schedules of PV power plant generation and local electricity consumption, determine the optimal power of PV power plant generation, and determine the reserve capacity that should be provided by the energy supply company. All the means listed above have different effects on the quality of the operation of the LES. According to the proposed quality indicator, it is possible to

determine which of them is able to improve the quality of electricity supply to the LES to a greater extent (**Fig. 2.25**) [24].

Among the considered means, the highest coefficient of quality of functioning has an agreed schedule of generation of PV power plant with electricity consumption of LES with a defined reserve capacity $E_{q\_agr.with\_reser.} = 0.989$.

What is more, for the PV power plant generation schedule coordinated with local electricity consumption, the required reserve capacity will be the smallest (**Fig. 2.26**).
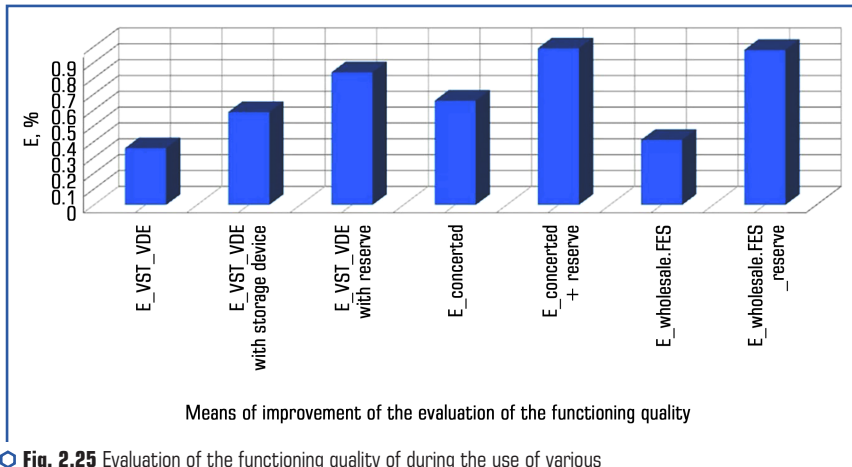
○ **Fig. 2.25** Evaluation of the functioning quality of during the use of various means of its improvement
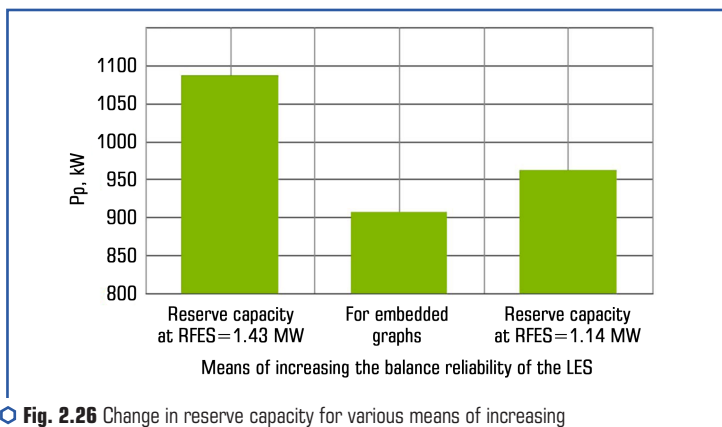
○ **Fig. 2.26** Change in reserve capacity for various means of increasing the balance reliability of the LES

2.4 ALGORITHM FOR MATCHING SCHEDULES OF PV POWER PLANT GENERATION AND ELECTRIC LOAD OF LES

The increase in the generation of photovoltaic power plants in distribution networks due to the reduction of the load on the centralized power supply system makes it possible to obtain a positive effect in the electric power system (EPS). They are manifested in the reduction of power and electricity losses in transmission lines and transformers, which are used to transport power, in the improvement of the quality of electricity, and the unloading of electrical networks. However, this applies only to cases when the generation schedules of the PV power plant are consistent with the level of local electricity consumption and the topology of electrical networks [25, 26]. That is, the positive effect on the PV power plant should also be taken into account in the algorithm for matching the generation schedules of the PV power plant and the electric load of the LES.

In order to develop a method of coordinating the generation schedules of the PV power plant and the load of the LES, it is necessary to evaluate the influence of the generation of distributed energy sources on the unevenness of the daily schedule of electric loads (SEL).

Among the existing methods of assessing the unevenness of the daily load schedule, the means of morphometric analysis should be noted [27, 28]. To analyze and evaluate the influence of renewable energy sources on the total load schedule of the electric network, it is possible and appropriate to use morphometric indicators of the unevenness of SEL. The advantage of such indicators when analyzing the unevenness of load schedules lies in their integrality. Taking into account the integral characteristics of morphometric indicators, it is possible to more accurately justify the alignment of SEL and coordination with the RES generation schedule.

Given that the schedule of electric loads is uneven, and the peak generation of the PV power plant falls on a daily dip in the load schedule, which increases such unevenness, there is a need to motivate consumers to shift the daily schedule of electric energy and loads up to the peak generation hours of the PV power plant. For this, the concept of virtual power plants and regulator consumers is used, which greatly simplifies such a task.

The main idea of this approach is not to generate electricity, but to create new or motivate existing electricity consumers to maneuver their own consumption. Currently, the main measure of motivation for electricity consumers is the zonal electricity tariff (**Table 2.6**), according to which the cost of electricity is differentiated by periods of the day. Thus, the consumer can reduce the electricity bill without reducing the amount of consumption. At the same time, the unevenness of electricity consumption schedules is reduced. A similar approach can be used to evaluate the effectiveness of coordination of schedules of generation and consumption of RES in the electric network.

In order to estimate the cost of shifting consumption power, it is necessary to develop an indicator that would take into account the change in the coefficient of the cost of electricity according to the zone tariff, the cost of compensatory costs to the consumer for shifting the electricity consumption schedule, the cost of reducing power losses due to the coordination of the total daily SEL with the generation schedule:

CHAPTER 2

$$B_{ij} = \left(K_{tj} - K_{ti}\right) \cdot C_t + \beta - \delta P \cdot C_t, \tag{2.7}$$

where K_{tj} – coefficient of the cost of electricity according to the zonal tariff of the stage of the schedule from which the capacity is planned to be transferred; K_{ti} – coefficient of the cost of electricity according to the zonal tariff of the stage of the schedule to which the power is planned to be transferred; C_t – electricity tariff according to the energy supply company; β – cost of the technological shift in production, which must be compensated by the energy system; δP – reduction of power losses due to adjustment of the consumer's load schedule.

● **Table 2.6** The zonal tariff for electricity is differentiated by time periods

Period of time	Night	Day	Peak
Two-zone tariffs, differentiated by time periods			
Tariff coefficients	0,5	1	–
Duration of the period	23:00 – 07:00	07:00 – 23:00	–
Three-zone tariffs, differentiated by time periods			
Tariff coefficients	0,4	1	1,5
Duration of the period	23:00 – 07:00	07:00 – 08:00 11:00 – 20:00 22:00 – 23:00	08:00 – 11:00 20:00 – 22:00

The indicator of the cost of transferring the load B_{ij} from one stage of SEL to another is expedient to use in the task of coordinating RES generation schedules for the load.

The appearance of sources of decentralized generation in distribution electric networks allows to consider them not as main-radial networks, but as networks with two-way power supply or local electric systems. Since the configuration of the electrical network can be considered relatively constant, using the coefficients of the current distribution matrix, it is possible to determine the consumers whose load schedule will have the greatest impact on the total unevenness of the daily electrical load schedule of the LES caused by the generation of the PV power plant.

The use of such an approach, in the task of equalizing the daily SEL, will allow not only to reduce the unevenness of the latter, but also to reduce the loss of electricity in the LES.

To reduce the unevenness of the total daily REL DEN and minimize losses of active power, it is suggested to adjust the schedule by each node in turn according to the current distribution coefficient. To solve this problem, let's use the classical transport problem (**Table 2.3**), in which it is possible to conditionally allocate m hours in which the actual consumption of the node is greater than the generation of SES, $A_i, \ldots, A_m$, and n hours in which the generation of SPP will prevail over the consumption of the node, $Z_i, \ldots, Z_m$. For this purpose, node capacities are used, refined by multiplying by the current distribution coefficient. The relative cost B_{ij} of power transfer from one-time interval of the schedule to another will be determined by (2.7).

The dependence of the mode of operation of renewable energy sources on natural conditions in most cases leads to the deterioration of the mode of operation of distribution electric networks. Therefore, it is necessary to carry out artificial coordination of load and RES schedules. This is especially true of photovoltaic power plants.

A method based on the application of morphometric analysis of consumption schedules, optimal coefficients of current distribution and transport problem is proposed to solve the problem of equalizing the total schedule of electric power consumption of DEN and reducing electricity losses in distribution electric networks.

The algorithm for matching the generation schedules of the PV power plant and the load of the LES is shown in **Fig. 2.27**. Having information about these schedules and information about the number of consumers in the LES, the initial data for the operation of the algorithm are formed. Taking into account the topology of the electrical network and the value of the load and generation capacities, the matrix of current distribution coefficients is determined for each consumer in relation to the PV power plant. It should be noted that this matrix has the dimension of the number of nodes per the number of branches in the network. To determine the current distribution coefficients of the PV power plant, only the row corresponding to the node in which the plant is installed is selected from the matrix.

To determine the power that can be maneuvered by the consumer, the technological minimum is determined for each consumer. Based on this, the power that can be displaced by the consumer will be equal to the difference between the actual consumption power P_{Hi} and the technological minimum $P_{min\,i}$ and at a certain hour of the load schedule. Next, consumers are ranked according to their current distribution ratio.

The hours in which the actual consumption of the node is less than the generating capacity of the PV power plant are conditionally referred to as "generation" hours. That is, the hours for which consumption capacity will need to be shifted.

The hours in which the load is greater than the generation capacity and the condition $P_{load_{it}} - P_{min_{it}} > 0$ is fulfilled are the hours from which the power can be transferred. It is this difference that determines the amount of excess power $P_{sup\,l_{it}}$ that can be shifted at a certain cost and $P_{def_{it}}$ – the power that is not enough at a certain hour of the day to balance the daily schedule. Taking into account the identified deficit and surplus capacities, a transport matrix of capacity transfer from surplus hours to deficit hours is formed to equalize the daily load schedule. In the event that the total generation power will exceed the power that can be shifted to equalize the electric load schedule, let's introduce an additional fictitious load source $P_{FLS} = \sum_t P_{SEL_{it}} - \sum_t P_{sup\,l_{it}}$ (FLS) to obtain a balanced transport problem. In the case when the own generation of the PV power plant is not enough to meet the electricity needs of consumers, let's introduce a conditional source of centralized power.

The solution to the transport problem is a recommendation to shift the schedule of electric loads of consumers, which have the greatest impact on the unevenness of the total load schedule of the LES.
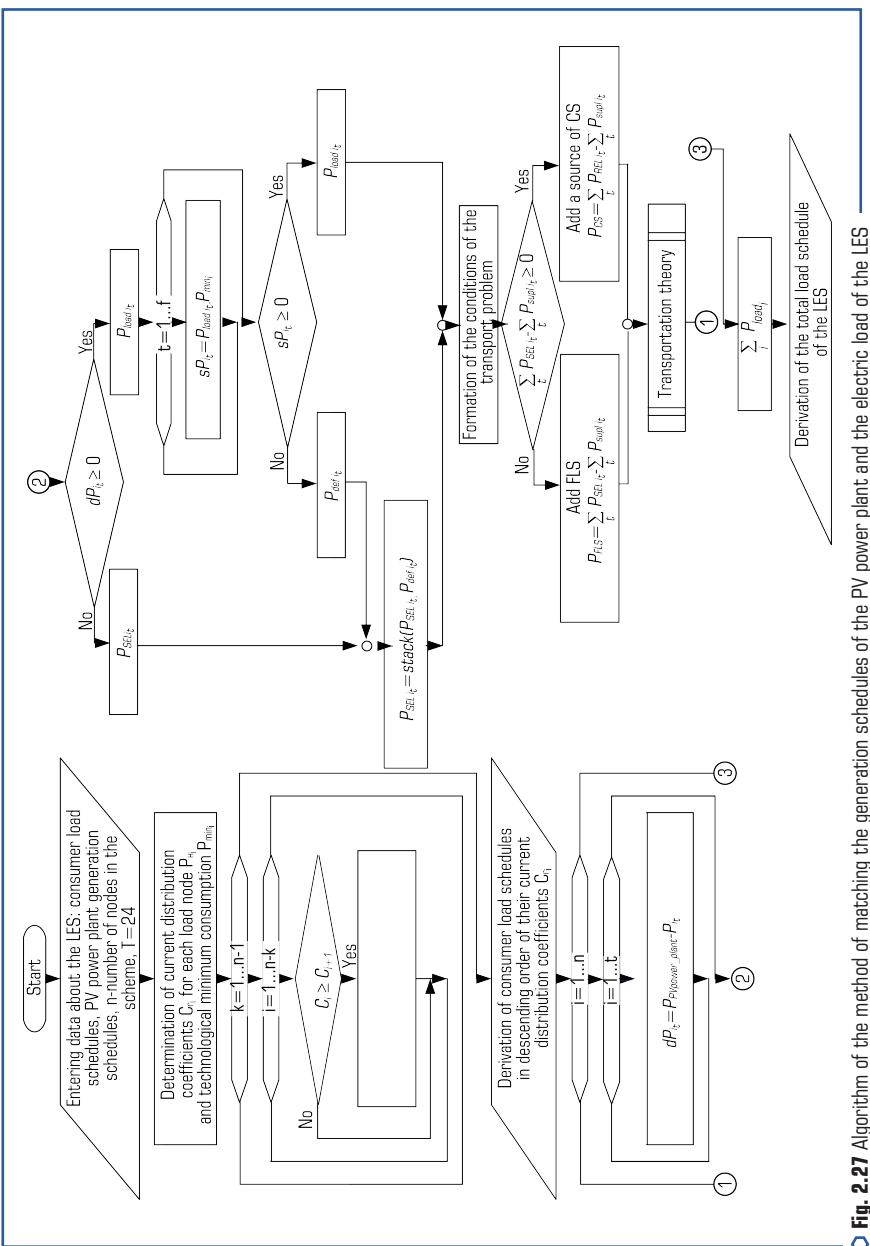
○ **Fig. 2.27** Algorithm of the method of matching the generation schedules of the PV power plant and the electric load of the LES

2.5 RENEWABLE ENERGY SOURCES WITH INVERTER ENERGY CONVERSION DEVICES AS A MEANS OF REGULATING REACTIVE POWER IN THE ELECTRICAL NETWORK

The impact of RES on the quality of electrical energy has an ambiguous result, especially with regard to the non-sinusoidal nature of voltages and currents and voltage deviations [29].

Ensuring the quality of electricity directly depends on ensuring the balance of active and reactive power in the electrical system. As a source of electrical energy, RES is an element capable of influencing the quality of electricity supply. As for the balance of active capacity, the necessity of forecasting the daily schedule of active capacity for a day ahead is foreseen at the legislative level. As for the reactive power balance, since RES such as PV power plant are not its source, we cannot talk about the impact on the balance. However, the technical ability of the inverter to influence the angle between the current and the voltage at its output allows it to influence the flows of reactive power in the electrical network.

Since one of the main elements of a photovoltaic plant is an inverter, we will consider its possible modes. **Fig. 2.28** shows a fragment of an electrical circuit with an inverter with PWM control and a vector diagram for it.
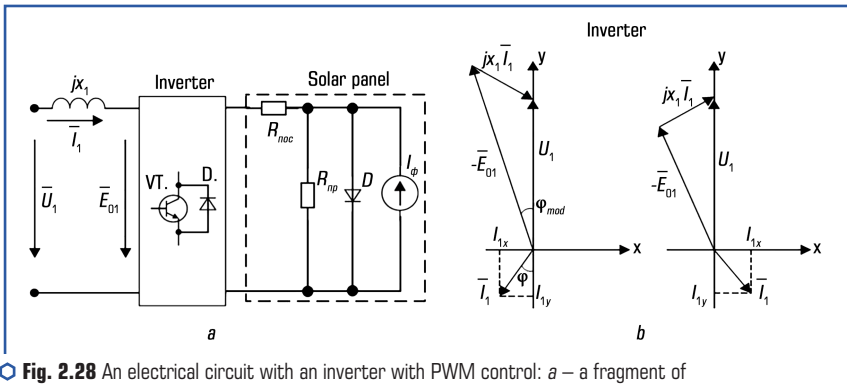
○ **Fig. 2.28** An electrical circuit with an inverter with PWM control: *a* – a fragment of the electrical circuit; *b* – vector diagrams

The equation compiled according to Kirchhoff's second law for the circuit (**Fig. 2.28, *a***) will be written as follows:

$$\overline{U}_1 = \overline{E}_0 + jx_1\overline{I}_1, \tag{2.8}$$

where $\overline{E}_0$, $\overline{U}_1$, $\overline{I}_1$ – the resulting vectors of the EMS at the output of the inverter, the network voltage and current:

$$\overline{E_0} = \mu U_0 e^{i\varphi_{mod}},$$ (2.9)

where μ – modulation coefficient, φ_{mod} – the phase of the modulation voltage in relation to the mains voltage.

In the supply network, an increase $\overline{E_0}$ compared to $\overline{U_1}$ leads to an effect corresponding to the appearance of capacitive currents at the point of connection of the PV power plant to the electric network. So, it is possible to say that by changing the opening angle of the thyristors of the inverter, it is possible to achieve different angles between current and voltage, which will cause a change in reactive power flows in the electrical network.

To confirm these conclusions, mathematical modeling was performed in the Simulink Matlab R2015a environment. It is based on the model presented in the Matlab example base (**Fig. 2.29**) – 'power_PVarray_grid_det' [30]. Since this model worked out only one of the possible modes implemented by modern inverters, the model of the inverter control system was improved for the possibility of implementing the active power output mode with a power factor equal to unity. The model also allows maintaining a given value of it other than unity and maintaining a given level of reactive power at the connection point of the PV power plant. In addition, the parameters of the model were changed in accordance with the parameters of the real PV power plant to check the adequacy of the model (data on solar insolation and temperature of solar panels are taken for an average day without precipitation, significant cloudiness and wind).
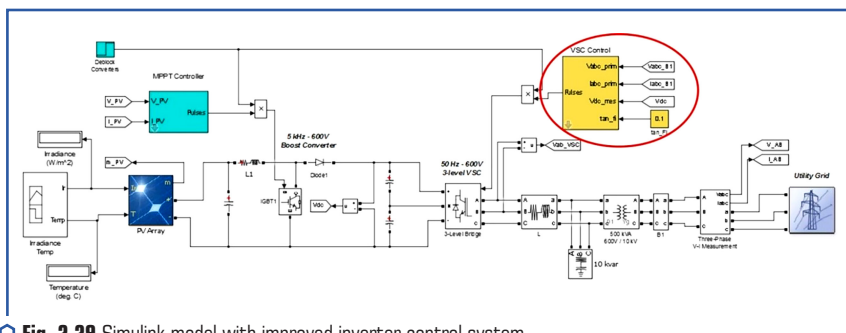
○ **Fig. 2.29** Simulink model with improved inverter control system

Fig. 2.30 shows the results of modeling the graph of active power generation for different reactive power modes. Curve 1 corresponds to the change in the generated active power in the DC network.

Curve 2 corresponds to the graph of active power generation in the alternating current network at the point of connection of the PV power plant to the 10 kV network, in the mode when the inverter is set to $cos\varphi = 1$. Curve 3 corresponds to the generated active power at the point of

connection of the PV power plant to the 10 kV network in the mode when the inverter is adjusted to maintain the specified voltage level by influencing the reactive power balance. All curves shown in **Fig. 2.30**, obtained under the same conditions.

Therefore, photovoltaic stations have the technical ability to influence the flows of reactive power in the electrical system. Depending on the power and voltage class of the electrical network to which the PV power plant is connected, it is possible to provide different modes of influence on reactive power flows. In **Fig. 2.31** schematically shows the area of possible impacts.

The change in reactive power flows affects the losses of active power in the network, that is, photovoltaic stations can be used to increase the efficiency of electrical systems [31].

CHAPTER 2
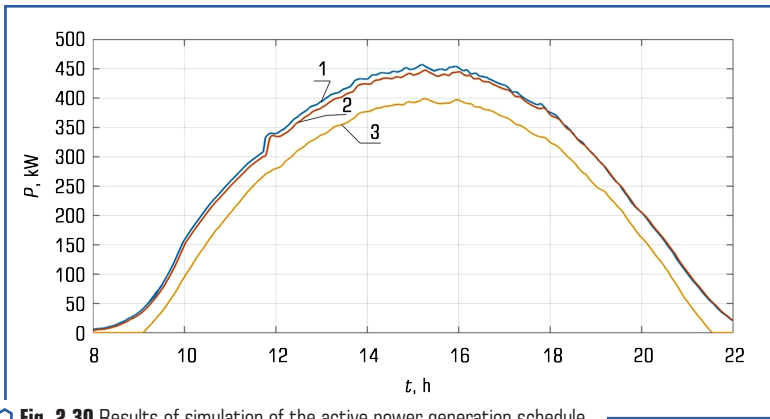
Fig. 2.30 Results of simulation of the active power generation schedule
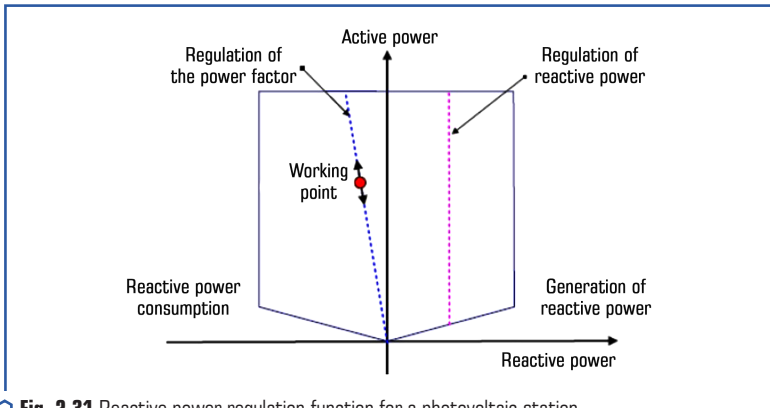
Fig. 2.31 Reactive power regulation function for a photovoltaic station

Therefore, it is possible to draw a conclusion about the technical possibility of using sources of electrical energy such as PV power plant to maintain the necessary level of power supply quality by using inverters in modes that allow influencing the flows of reactive power in the electrical network. As a result, it is possible to influence not only voltage deviations in network nodes, but also their cost-effectiveness.

CONCLUSIONS

Renewable energy sources can be used as a means of improving the quality of electricity supply. However, due to the dependence of their generation mode on natural conditions, it requires the development of methods to determine the conditions for their appropriate development. The results of the conducted research confirm the positive influence of distributed generation sources on the balance reliability of distribution electric networks. However, this positive effect is obtained only if a detailed analysis of the connection point and the power of the electrical energy source is performed. The methods of estimating the probabilistic characteristics of RES proposed in the work allow to improve the methods of determining the value of the installed capacity, which should be connected to a certain point of the electric network. At the same time, the configuration of the network and the features of the connected load, which is fed from it, are taken into account.

Taking into account the possibilities that open up during the development of "smart" networks, a method of coordinating the schedules of RES generation and consumption is proposed. This approach allows obtaining conditions for the effective use of renewable energy sources and improving the quality of electricity supply. This approach is especially effective if electricity storage is provided in the electrical network. In this case, it is possible to regulate not only the schedule of electricity consumption, but also to actively influence the balance of electricity in the electrical network, using the charge/discharge of accumulators. In addition, the use of electrical energy storage systems in networks would allow to reduce the reserve volume in the electric power system.

The availability of inverter equipment on a number of sources of renewable energy expands their use also for regulating reactive power flows in electrical networks. Modeling of different modes of inverters and studies of modes of electrical networks carried out on their basis confirmed the technical feasibility and effectiveness of such use of RES.

CONFLICT OF INTEREST

The authors declare that they have no conflict of interest in relation to this research, whether financial, personal, authorship or otherwise, that could affect the research and its results presented in this paper.

REFERENCES

1. Yue, X., Tu, M., Li, Y., Chang, G., Li, C. (2022). Stability and Cementation of the Surrounding Rock in Roof-Cutting and Pressure-Relief Entry under Mining Influence. Energies, 15 (3), 951. doi: https://doi.org/10.3390/en15030951

2. Hai, W., Kai, L., Cheng, Z., Yongcan, L. (2021). Research on Line Loss Improvement of Station Area in Distribution Network by Modular Photovoltaic Energy Storage System. 2021 IEEE/IAS Industrial and Commercial Power System Asia (I&CPS Asia), 1285–1289. doi: https://doi.org/10.1109/icpsasia52756.2021.9621597

3. Bondarenko, R., Dovgalyuk, O., Omelyanenko, G., Pirotti, O., Syromyatnikova, T. (2018). Increasing the reliability of the functioning of distribution electric networks. Bulletin of the Petro Vasylenko Kharkiv National Technical University of Agriculture, 195, 69–71.

4. Lezhniuk, P., Komar, V., Sobchuk, D. (2014). Determination of the optimal installed power of renewable energy sources in the distribution network by the criterion of minimum losses of active power. Scientific works of the Donetsk National Technical University. Series: Electrical engineering and energy, 1 (16), 130–136.

5. Ma, Y., Zhao, L., Zhang, Y., Zhou, Q., Zhang, M., Yang, S. (2020). Multi-objective Optimal Scheduling of Power Systems Based on Complementary Characteristics of Heterogeneous Energy Sources. 2020 IEEE 4th Conference on Energy Internet and Energy System Integration (EI2), 1533–1538. doi: https://doi.org/10.1109/ei250167.2020.9347052

6. Lezhniuk, P., Kotylko, I., Kravchuk, S. (2019). Increasing Electric Network Reliability by Dispersed Generation. 2019 IEEE 20th International Conference on Computational Problems of Electrical Engineering (CPEE). doi: https://doi.org/10.1109/cpee47179.2019.8949124

7. Lakshmi, G. S., Rubanenko, O., Hunko, I. (2021). Control of the Sectioned Electrical Network Modes with Renewable Energy Sources. 2021 International Conference on Sustainable Energy and Future Electric Transportation (SEFET). doi: https://doi.org/10.1109/sefet48154.2021.9375781

8. Faraji, J., Ketabi, A., Hashemi-Dezaki, H., Shafie-Khah, M., Catalao, J. P. S. (2020). Optimal Day-Ahead Self-Scheduling and Operation of Prosumer Microgrids Using Hybrid Machine Learning-Based Weather and Load Forecasting. IEEE Access, 8, 157284–157305. doi: https://doi.org/10.1109/access.2020.3019562

9. Grigorieva, N., Shabaykovich, V., Gumeniuk, L., Humeniuk, P., Dobrovolska, L., Sobchuk, D. (2020). Odnawialna energia elektryczna z dwutlenku węgla. Informatyka, Automatyka, Pomiary w Gospodarce i Ochronie Środowiska, 10 (1), 72–76. doi: https://doi.org/10.35784/iapgos.934

10. Lezhniuk, P., Rubanenko, O. (2021). Optimal solutions sensitivity analysis in complex systems in relative units. Scientific Research of the XXI Century. Vol. 2. California, 111–118. doi: https://doi.org/10.51587/9781-7364-13302-2021-002-111-118

11. Komar, V., Ostra, N., Kuzmyk, O., Hutsol, S. (2013). Evaluation of Dispersed Generation to Mode of Distributive Electric Networks.. Scientific works of the Donetsk National Technical University, 1 (14), 104–107.

CHAPTER 2

12. Lezhnyuk, P., Komar, V., Sobchuk, D. (2014). Determining the optimal installed power of renewable energy sources in the distribution network by the criterion of minimum losses of active power. Scientific works of the Donetsk National Technical University Series: "Electrical engineering and energy", 1 (16), 130–135.

13. Lezhniuk, P. D., Komar, V. A., Sobchuk, D. S. (2014). Method for Determination of Optimal Installed Capacity of Renewable Sources of Energy by the Criterion of Minimum Losses of Active Power in Distribution System. Energy and Power Engineering, 6 (3), 37–46. doi: https://doi.org/10.4236/epe.2014.63005

14. Lezhnyuk, P., Komar, V., Buslavets, O. (2016). Impact of renewable sources of energy on the level of active power losses in distribution networks. 2016 2nd International Conference on Intelligent Energy and Power Systems (IEPS), 73–78. doi: https://doi.org/10.1109/ieps.2016.7521856

15. Commission Regulation (EU) 2016/1719 of 26 September 2016 establishing a guideline on forward capacity allocation (2016). European Commission. Official Journal of the European Union.

16. Electricity Balancing Guideline (2017). European Commission. Official Journal of the European Union, 312/6-312/53.

17. Demand Side Response. Policy paper (2014). ENTSOE. Available at: https://www.entsoe.eu/2014/09/23/demand_side_response_policy_paper/

18. Lezhniuk, P., Komar, V., Kravchuk, S. (2016). Coordination of schedules of generation of renewable energy sources and electric load in the local electric system. Bulletin of Kharkiv National Technical University of Rural Economy named after Pyotr Vasylenko. Technical sciences. Problems of energy supply and energy saving in the agricultural sector of Ukraine, 2, 30–37.

19. Lezhniuk, P., Komar, V., Kravchuk, S. (2016). Determination of optimal power reserves for carrying balance reliability of local electric system. Bulletin of the National Technical University "KhPI" Series: New Solutions in Modern Technologies, 42 (1214), 69–75. doi: https://doi.org/10.20998/2413-4295.2016.42.11

20. Varetsky, Y., Hanzelka, Z. (2016). Stochastic modelling of a hybrid renewable energy system. Tekhnichna Elektrodynamika, 2016 (2), 58–62. doi: https://doi.org/10.15407/techned2016.02.058

21. On Electricity Market (2017). Law of Ukraine No. 2019-VIII. 11.04.2017. Available at: http://zakon.rada.gov.ua/laws/show/2019-19

22. Kuznetsov, M. P. (2010). Methods of forecasting electricity generation by wind power plants. Renewable energy, 3, 42–47.

23. Kuznetsov, M. P., Lysenko, O. V. (2017). Possibilities of short-term forecasting of solar energy. Renewable energy, 1, 25–33.

24. Komar, V. O., Lesko, V. O. (2017). Balance reliability of electrical systems and the influence of renewable energy sources on it. Environmental safety and renewable energy sources, 98–101.

25. Kudrin, B. I. (2009). Elektrosnabzhenie promyshlennykh predpriiatii. Moscow: Teplotechnik, 698.

26. Chatterjee, S., Firat, A. (2007). Generating Data with Identical Statistics but Dissimilar Graphics. The American Statistician, 61 (3), 248–254. doi: https://doi.org/10.1198/000313007x220057

27. Komenda, N. V. (2011). Morphometric evaluation and criterion of uniformity of the schedule of electric loads. Bulletin of the National University "Lviv Polytechnic", 66, 42–46.

28. Komenda, N. V., Komenda, T. I., Demov, O. D. (2010). Search for consumers – regulators based on the morphometric approach in managing the daily load of an industrial enterprise. Proceedings of the Institute of Electrodynamics of the National Academy of Sciences of Ukraine, 27, 22–26.

29. Kyrylenko, O. V., Pavlovsky, V. V., Lukyanenko, L. M. (2011). Technical aspects of the implementation of distributed generation sources in electric networks. Technical electrodynamics, 1, 46-53.

30. Detailed Model of a 100-kW Grid-Connected PV Array (2017). Mathworks. Available at: https://www.mathworks.com/help/physmod/sps/examples/detailed-model-of-a-100-kw-grid-connected-pv-array.html?requestedDomain=true

31. Lezhniuk, P. D., Kovalchuk, O. A., Komar, V. O., Kravchuk, S. V. (2018). Mathematical modeling of reactive power regulation by photovoltaic stations. Renewable energy for energy efficiency of the 21st century, 273–277.

CHAPTER 2

Volodymyr Khomenko, Oksana Chernysh, Viacheslav Barsukov,
Viktor Tverdokhlib, Arkadij Berezovskij, Volodymyr Slobodianyk

CHAPTER 3

COMPOSITE MATERIALS BASED ON WATER-SOLUBLE BINDERS FOR ELECTROCHEMICAL CAPACITORS

ABSTRACT

Today, more and more attention is paid to non-traditional rechargeable sources of electric current, which are able to quickly charge and discharge (in a few seconds or minutes), have high power (kW/kg) and a long service life (tens of thousands of charge-discharge cycles). Such current sources include electrochemical capacitors (EC), which in the special literature are called supercapacitors, ultracapacitors, ionistors, or molecular storage devices.

The principle of operation of such current sources is based on their ability to store and release electrical energy at a given time through the internal redistribution of electrolyte ions in a double electric layer (DEL). The rate of redistribution of ions in the DEL is several orders of magnitude higher than the rate of ion transfer through the "electrode-electrolyte" phase boundary during classical redox transformations in batteries. That is why ECs are non-traditional current sources, they have significant advantages over batteries in terms of their specific power, the rate of charge-discharge processes and service life, although they are inferior to batteries in terms of their capacity and energy density. Particular attention has been paid to EC in connection with the start of production in many countries of the world of environmentally friendly cars and buses with electric motors that require high power at the time of engine start. In addition to being used in transport, ECs are widely used in military and space technology, in energy storage systems at peak loads, for regulating wind generator turbines, etc.

The production of electrochemical capacitors requires fairly large capital investments. This is due to the requirements for the environmental friendliness of the production itself, where a significant amount of costs is spent on ensuring safe working conditions for personnel, on capturing harmful substances and their disposal. That is why the issue of developing EC to reduce the cost of production through the use of new materials and the improvement of technological processes becomes especially relevant.

The main scientific research in recent years in the field of EC has been associated with the study of new electrochemical systems, electrode materials and electrolytes. To a certain, but insufficient extent, attention was also paid to the improvement of the technology of combining the active material and the current collector. Even less research work is related to the development of

environmentally friendly technologies for the production of composite active materials for capacitors, although the development of these components can potentially provide high electrical performance of capacitors and significantly reduce the cost of their production. These circumstances put forward the research and development of environmentally friendly methods for obtaining composite materials for electrochemical capacitors into the category of complex, but relevant scientific and technical problems.

KEYWORDS

Electrochemical capacitor, cellular carbonaceous material, activated carbon, graphite, polymer-carbon composite, water-based polymers.

Electrochemical capacitors (EC), compared to traditional primary and secondary current sources and electrolytic capacitors, are a relatively young type of current sources that are at the beginning of their wide practical implementation. A significant difference between the operating principle of EC and traditional CCS systems is that charge accumulation occurs in a double electric layer (**Fig. 3.1**). This makes it possible to distinguish EC into a separate class of current sources.
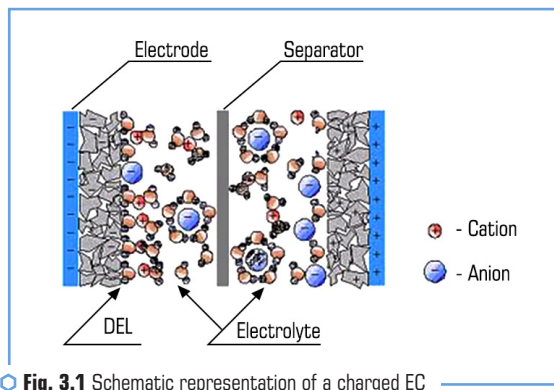
○ **Fig. 3.1** Schematic representation of a charged EC

However, the basic principle on which the operation of EC is based remains the same as for traditional systems: a positive charge is collected mainly on one electrode, and a negative charge is collected on another, which is located nearby, but electrically separated from the first by an insulating layer. That is, the accumulation of electrical energy occurs in a static form, as in traditional capacitor systems. For EC, three main factors determining the possibility of energy storage are

CHAPTER 3

decisive: the surface area of the electrodes, the distance between them, and the dielectric properties of the insulating layer between the electrodes. The entire path of development of capacitor engineering was associated with the improvement of these three factors: an increase in the area of the electrodes, a decrease in the distance between them, and an improvement in the properties of the insulating layer. EC is no exception to this rule. That is, the EC capacitance is also described by the classical formula for a flat capacitor:

$$C \approx \varepsilon S / d, \tag{3.1}$$

C – EC capacitance; ε – dielectric constant of the insulating layer; S – area of the electrode; d – distance between the electrodes.

The difference is that the EC in the case of identical electrodes consists of two capacitors connected in series through the resistance of the electrolyte, where the total capacitance of the EC is described as:

$$1 / C = 1 / C_1 + 1 / C_2, \tag{3.2}$$

and if $C_1 = C_2$, then

$$C = C_1/2. \tag{3.3}$$

According to formula (3.1), an increase in the specific area of the electrodes leads to an increase in the specific capacitance. Therefore, EC developers pay great attention to electrode materials with a large specific surface area [1].

Taking into account that the EC is actually two capacitors connected in series through the resistance of the electrolyte, the calculation of the specific capacity of the material was carried out according to the formula:

$$C_{spec} = \frac{2C_m}{T_1}, \tag{3.4}$$

where C_{spec} – specific capacity of the material; C_m – measured capacitance during discharge; T_1 – mass of the active material of one electrode.

In EC, the accumulation of electrical energy occurs directly along the electrical double layer. In this case, there is no charge transfer along the phase interface, that is, a true capacitance is observed. The surface charge generation mechanism includes surface dissociation of the electrolyte, adsorption of ions from solution in pores and defects in the electrode crystal lattice. In this case, an excess (or deficit) of charge appears on the electrode surface, and ions with the opposite charge flow around the electrode/electrolyte interface to maintain electrical neutrality [2].

The DEL thickness depends on the electrolyte concentration and ion size (**Fig. 3.2**) and is about 5–10 Å for concentrated electrolytes. The DEL capacitance varies from 10 to 20 μF/cm^2 for smooth electrodes in concentrated electrolyte solutions.

○ **Fig. 3.2** Schematic representation of the electrical double layer
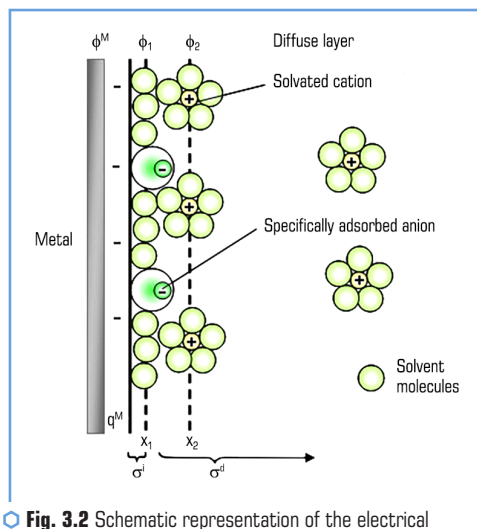
The main difference between EC and traditional electrolytic capacitors is as follows: instead of developing a microstructure (for example, increasing the surface of aluminum foil by electrochemical etching, followed by the formation of a dielectric oxide layer on it [3] with a thickness of about several micrometers), in EC, for the manufacture of electrodes, mainly carbon nanostructured materials. That is, ECs accumulate charge in carbon nanotubes or nanosized pores of activated carbon. Carbon nanofibers are used less frequently, and relatively recently information has appeared on the use of graphenes as electrode materials [4, 5].

Various names are used in the technical literature for electrochemical capacitors: ionists, supercapacitors, ultracapacitors, asymmetric capacitors, hybrid capacitors, etc. Unlike the well-known conventional capacitor, the EC does not have a dielectric layer. The technical implementation of EC began with the Baker patent (USA, 1957) [6], and its use began in the 1980s (NEC, Japan), although the basic principle was discovered at the end of the 19th century by Helmholtz [7].

Unfortunately, there is no mass production of EC in Ukraine yet. Limited Liability Company "UNASCO Ukraine", the successful scientific management of which is carried out by Corresponding Member of NAS of Ukraine, Doctor of Chemical Sciences, Yuriy Maletin, powerful ECs based on organic electrolytes were developed, which were tested in 2006 at the Institute of Transportation

CHAPTER 3

Studies (Davis, CA, USA), recognized as the best among the EC prototypes of world manufacturers [8] and are now mass-produced for specific customers. It should be noted that in Ukraine there are no state programs for financing developments in the field of EC, and therefore developments are carried out through the sale of finished products. For comparison, Maxwell received 3 million USD in 2005 under the Clean Transportation Development Program in the United States for the development of EC for a hybrid bus [9].

Currently, the manufacturers mentioned above offer different types of EC, so it becomes necessary to classify them. There are different approaches to the classification of EC. The classification adopted in the USA (Miller, J., JME Inc.) [10] is generally recognized, according to which all ECs are divided into 4 classes, conventionally called generations. Each class also displays the sequence in which the given CI type appears. In accordance with the proposed classification, the following types of ECs can be distinguished:

I. *First generation ECs* contain the same positive and negative activated carbon electrodes and an aqueous electrolyte solution (mainly KOH or H_2SO_4).

II. *Second-generation ECs* are electrochemical systems similar to first-generation ECs that use an organic electrolyte based on aprotic solvents (mainly acetonitrile).

III. *Third-generation ECs* are created by combining electrodes with a fundamentally different mechanism for the occurrence of electrode reactions (charge-discharge DEL and redox process) and using an aqueous electrolyte solution. An example of such an EC is an electrochemical system in which one of the electrodes is made of activated carbon, and the second is a redox electrode made of CCS such as a nickel-cadmium or lead-acid battery.

IV. *Fourth-generation ECs* are also built using fundamentally different types of electrodes and an organic electrolyte. An example of such an EC can be electrochemical systems in which one of the electrodes is made of activated carbon, the other is made of intercalation-type materials that work inversely in aprotic electrolytes (for example, graphite or $Li_4Ti_5O_{12}$).

Third and fourth generation ECs are often referred to as "asymmetric" or "hybrid". Electrochemical capacitors can be divided into groups according to the mechanism of electrode reactions, namely:

a) EC of the electrical double layer (EC of the 1st and 2nd generation);

b) pseudocapacitive EC (3rd and 4th generations).

Accordingly, the type of electrochemical process and electrolyte are divided by the above ECs in terms of power and energy. So, ECs of the 1st, 3rd and partially 2nd generations are more powerful ECs compared to ECs of the 4th generation. The most powerful are ECs of the 1st generation (up to 15 kW/kg per pulse), but their energy does not exceed 1 Wh/kg. The most energy-intensive are ECs of the 4th generation (more than 10 Wh/kg), but their power is <1 kW/kg.

The characteristics of the above electrochemical systems depend on the method of manufacturing the electrodes. The most widely known method of manufacturing electrodes for EC is the rolling method using an aqueous suspension of polytetrafluoroethylene (PTFE) as a binder [11]. The binding mechanism is that the PTFE particles undergo fibrilization as a result of mechanical agitation and form long, thin fibers. Due to the formed fibers (fibrils), a strong electrode grid is

formed. Elasticity and electrochemical stability of PTFE in a wide temperature range from −70 to +270 ^{0}C gives certain preferences to this polymeric material. In general, the rolling method has its advantages and disadvantages. The advantages of the method include the high density of the electrode and the absence of toxic organic solvents. The disadvantages of the method are the complexity of manufacturing thin electrodes (thickness less than 30 μm) and the need to preliminarily apply an adhesive sublayer to the metal current collector (most often aluminum foil), since PTFE has practically no adhesion to aluminum [12].

Carbon particles from a high electrical conductivity material are first applied to the surface of an aluminum current collector to form a carbon discrete layer. After that, an electrically conductive adhesive film is applied to the surface of the aluminum current collector formed by carbon particles, and the carbon particles are partially pressed into the surface of the polarization electrode and the aluminum current collector [13].

When carbon particles are pressed into the surface of an aluminum current collector, the oxide film on the aluminum surface is destroyed, exposing pure aluminum, while a tight mechanical contact is formed between the carbon particle and aluminum, which prevents the interaction of aluminum with oxygen in the air and the capacitor electrolyte, i.e. this ensures low resistance and stability of the electrical contact between the aluminum current collector and the particles of the carbon material pressed into its surface. The adhesive conductive film has two functions. First, it fixes the position of the polarizing electrode relative to the aluminum current collector with an embedded carbon layer, which stabilizes the operation of the electrode. Secondly, due to the electrically conductive component of the electrically conductive adhesive film, an additional electrical contact is created between the polarization electrode and the aluminum current collector, which reduces the contact resistance. Thus, the electrodes of the double electric layer capacitor, made by rolling, have a low contact resistance and high stability [14].

One of the well-known methods of manufacturing electrodes is the pressing of the active material. This method is widely used in laboratory research. For the manufacture of electrodes, activated carbon is mixed with electrically conductive additives and a polymer, followed by the formation of a mixture by pressing and heat treatment to the softening temperature of the polymer and the connection of the base with the current collector [15].

This method of manufacturing an electrode material requires the addition of a large amount of a binder material. An increase in the amount of binder leads to a decrease in the amount of activated carbon material, which significantly worsens the electrical characteristics of the capacitor. It should also be noted that this method is acceptable for the production of small-sized electrochemical capacitors with a capacity of up to 10 F [16].

The smear method [17] is well known and tested in the battery industry and makes it possible to obtain electrodes of different thicknesses – from 2 μm with an accuracy of ±1 μm [18]. The essence of the method lies in the fact that the prepared mixture of the active material with the binder solution is applied to the metal current collector, followed by drying and compaction (rolling) of the obtained active material layer. The difference in the mechanism of binding dry components in

this method in comparison with the rolling method is that the binding polymers are in the state of solution, which makes it possible to more evenly distribute the polymer over the electrode volume. In addition, the range of polymers that can be used in the manufacture of electrodes is greatly expanded. Among them, the following polymeric materials should be distinguished: polyvinylidene fluoride, sodium carboxymethyl cellulose, styrene-butadiene rubber, and others [19].

Certain requirements are imposed on the polymer binder:
– inertness to electrolyte;
– high physicochemical and electrical resistance and stability;
– high adhesion to the metal down conductor;
– stability at elevated temperatures during the manufacture and operation of EC;
– high mechanical strength and elasticity of the electrode with a minimum amount of polymer in it.

All of the above requirements are met by the polymer polyvinylidene fluoride (PVDF), which is widely used in the production of chemical current sources.

The sodium salt of carboxymethyl cellulose (Na-carboxymethyl cellulose, NaCMC) is of the greatest practical importance. It is an amorphous colorless substance with a bulk density of 400–800 kg/m^3 and a density of 1.59 g/cm^3. NaCMC is an anionic polyelectrolyte, highly soluble in water. The viscosity of the NaCMC solution is practically independent of pH; it also binds water well.

Dry NaCMC salt has a weak corrosive effect. It is biologically inactive and resistant to biodegradation; however, its aqueous solutions undergo enzymatic hydrolysis during long-term storage in air (**Fig. 3.3**).
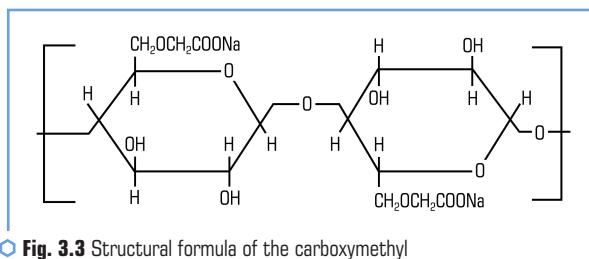
○ **Fig. 3.3** Structural formula of the carboxymethyl cellulose sodium salt molecule

The main property of carboxymethyl cellulose is the ability to form a viscous colloidal solution that does not lose its properties for a long time [20].

It should be noted that an aqueous suspension of styrene-butadiene rubber (SBR) is used as a binder polymer, which is a completely amorphous polymer with a density of 0.91–0.99 g/cm^3 [21]. The properties of the polymer differ depending on the content of bound styrene (**Fig. 3.4**).

With an increase in the content of the attached styrene in the polymer, the density, glass transition temperature, and dielectric characteristics increase. Rubber is soluble in aliphatic and aromatic hydrocarbons, chloroform, carbon tetrachloride, carbon disulfide.
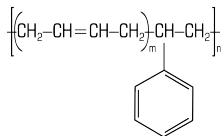
○ **Fig. 3.4** Structural formula of styrene-butadiene rubber

3.1 RESEARCH METHODS, MATERIALS AND THEIR CHARACTERIZATION

Viscometric method

In this work, solutions of N-methylpyrrolidone with different contents of PVDF were studied. The studies were carried out using a ВПЖ-4 glass viscometer at a temperature of 30 °C, which was maintained with a thermostat.

To determine the dynamic viscosity of the studied solutions, a calibration graph (**Fig. 3.5**) was constructed based on the viscosity of glycerol solutions of different concentrations (**Table 3.1**).

● **Table 3.1** Viscosity and leakage time of glycerol* from the ВПЖ-4 viscometer at different temperatures

Glycerol, %	t, °C	Viscosity, cPs	Time, s
100	20	1495	7286
100	25	942	4667
100	30	622	3130
95	30	248	1295
90	30	115.3	756
85	30	60	345

Viscosity of glycerin solutions is taken from the handbook [22]

The relative viscosity of the studied solutions was determined by the formula:

$$\eta_{spec} = \eta_{sol} \cdot \left(d_x \cdot \tau_x \right) / \left(d_{sol} \cdot \tau_{sol} \right), \qquad (3.5)$$

where η_{sol} and d_{sol} — the viscosity and density of the solvent; τ_x and τ_{sol} — the outflow times of the solution and solvent, respectively; d_x — density of the solution.

The density of the solution was determined by the pycnometric method, maintaining the temperature at 30 °C.

CHAPTER 3
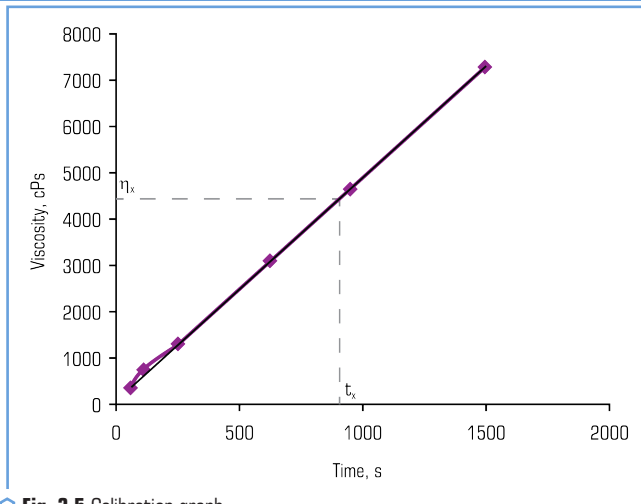
○ **Fig. 3.5** Calibration graph

Specific viscosity reflects the increase in relative viscosity compared to unity. To take into account the influence of the concentration of the solution, it is necessary to estimate how high the specific viscosity per unit concentration of the solute is.

According to formula (3.6), the specific viscosity η_{spec} was determined:

$$\left(\eta_{spec} = \left(\eta_s - \eta_{sol} \right) / \eta_{sol} \right), \tag{3.6}$$

where η_s – viscosity of the solution; η_{sol} – viscosity of the solvent.

Formula (3.7) was used to calculate the reduced viscosity:

$$\left(\eta_{red} = \eta_{spec} / c \right), \tag{3.7}$$

where η_{spec} – specific viscosity; c – concentration of the solution.

Having plotted the graphs of the dependence of the induced viscosity on the concentration (**Fig. 3.6**), let's determine the intrinsic viscosity [η] of the solutions of the studied polymers.

For this purpose, the experimental curves were extrapolated up to their intersection with the y-axis and the numerical values of the intrinsic viscosity of PVDF solutions were determined. The characteristic viscosity does not depend on the concentration of the solution and the conformational state of the macromolecules. The dependence of intrinsic viscosity on molecular weight is described by the Mark-Kuhn-Houwink equation [23]:

$$\left[\eta \right] = k \cdot M^{\alpha}, \tag{3.8}$$

CHAPTER 3

where k – constant for the homologous series of polymers; α – parameter characterizing the shape of a macromolecule in solution. Its values vary within 0.55–0.85 and characterize the elasticity of macromolecule chains in solution.

The coefficients k and α are determined experimentally. From the intrinsic viscosity data, the average molecular weight of the HMC can be calculated:

$$M = \sqrt[\alpha]{\frac{[\eta]}{k}}. \tag{3.9}$$
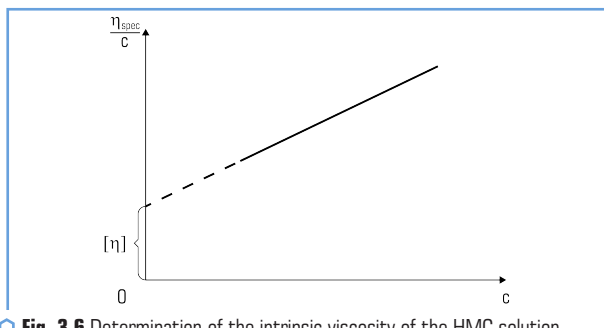
Fig. 3.6 Determination of the intrinsic viscosity of the HMC solution

Determination of viscosity by rotational method

The viscosity of the active masses during their manufacture was measured by the rotational method using the Fungilab Alpha series instrument.

Thanks to a set of rotary cylinders of different diameters, the device allows measurements in a wide range of viscosities for viscous systems, temperature range from 25 to 40 °C.

Calibration of the Fungilab Alpha series instrument was performed using silicone oil with a viscosity of 200 cSt (PMS-200, GOST 13032-77).

X-ray fluorescence analysis

To determine the chemical composition of the active masses of the electrodes, an X-Supreme 8000 X-ray fluorescence analyzer from Oxford Instruments (Great Britain) was used.

Using a spectrometer, various elements can be found from sodium to uranium. This device uses an X-ray tube with a palladium anode as a radiation source. The detector resolution is 123 eV. X-Supreme 8000 complies with international test standards such as ASTM D4294, ISO8754, ISO20847 and ISO13032.

Determination of the surface area and porosity of active masses of EC electrodes

The surface area and porosity were measured by the nitrogen capillary condensation method. Adsorption isotherms were obtained using Quantachrome Instruments version 3.0. For a detailed

analysis of the porous structure of the active material of the electrode (calculation of the proportion of pores of different diameters in the total porous structure) using adsorption isotherms, the BET method proposed by Brunauer, Emmett and Taylor was used. The BET method is a method of mathematical description of physical adsorption based on the theory of polymolecular (multilayer) adsorption. The linear form of the adsorption isotherm (BET equation) has the form:

$$\frac{\rho / \rho_0}{a\left(1 - \rho / \rho_0\right)} = \frac{1}{a_m C} + \frac{(C-1)\rho / \rho_0}{a_m C},$$ (3.10)

where ρ/ρ_0 – ratio of the pressure in the system to the condensation pressure; a – the adsorption value; a_m – monolayer volume on the adsorbent surface; C – ratio of the adsorption equilibrium constants in the first layer and the condensation constants.

The BET method can be used to determine the surface area with an accuracy of 5–10 % in the range of relative pressure values (ρ/ρ_0) 0.05–0.35. For a more detailed analysis of the cellular structure of a solid (calculation of the proportion of pores of different diameters in the total cellular structure), additional computational models were also used from adsorption isotherms.

Infrared spectroscopy

Infrared spectroscopy was used to determine the presence of certain functional groups in polyvinylidene fluoride molecules.

IR spectra were obtained using a Termo scientific IR spectrometer, the operating range of which is within (400 cm^{-1}–4000 cm^{-1}).

In this work, we used the most common method for preparing samples for infrared spectroscopy, namely, pressing a polymer sample into a tablet with KBr.

Optical microscopy

The size and shape of particles, as well as the structure of polymers and active masses of the electrodes, were studied in direct and reflected light using microscopes MSt 30 (minor magnifications) and MB-15U42 (large magnifications, studies in penetrating and reflected light), MIN-8 (study in polarized light). The image was captured using a DCM 520 digital camera (USB 2.0). The dimensions of the structural elements were determined using an object micrometer.

Scanning electron microscopy

An electron microscope, due to its high resolution (more than two orders of magnitude higher than a light microscope), makes it possible to observe subtle features and details of the structure of micro-objects at the atomic-molecular level. The technique of scanning electron microscopy and energy dispersive elemental analysis (EDEA) was used in the work. The study was carried out on a scanning electron microscope REM-130. The EDAX EDEA detector was used to determine the elemental composition.

Method for determining the factor of structure formation

One of the most common methods for determining the structure formation factor is the "oil absorption" method. The factor is characterized by the amount of milliliters of linseed oil that is absorbed by 1 gram of soot [24].

The structure of carbon materials is understood as the type and method of combining individual particles into aggregates of larger and smaller sizes (the latter are more stable) in the form of a chain or clusters. High structure carbon materials are used to make electrically conductive plastics. Low structure – characterized by good dispersion and a slight tendency to concentrate.

On the one hand, oil claying depends on the specific surface of the particles of carbon materials, which increases with decreasing particle size; on the other hand, with the same specific surface area (and dispersion), oil absorption increases with increasing product structure. The oil absorption of different brands of carbon materials highlights the differences in their structure. Oil absorption is determined by finding the so-called points of fat content and the beginning of the flow. In the latter case, the final stage of oil absorption is reached when the so-called standing paste is formed (**Fig. 3.7, *a***), which bends to the glass plate (**Fig. 3.7, *b***) on which it was rubbed from a light push.

a   *b*
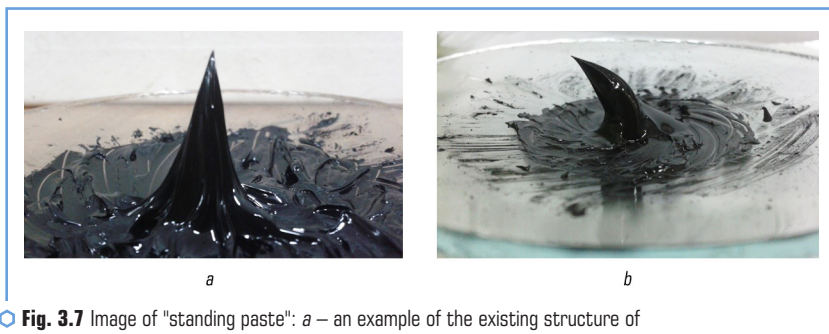
⭕ **Fig. 3.7** Image of "standing paste": *a* – an example of the existing structure of the paste; *b* – deformation of the paste during a push

The procedure itself is as follows: a 0.5 g sample of carbon material was transferred to a glass plate, to which 2 ml of linseed oil was gradually added dropwise. After each stage of adding oil, thoroughly mix the mass with a metal spatula. The final stage of oil absorption will be considered the concentration at which, after removing the spatula, the paste will be extracted into a pointed cone (**Fig. 3.7**) hence the name "standing paste".

pH determination

In the manufacture of electrodes, one has to pay attention to the interaction of the adhesive with the substrate. Not only physical interaction occurs between them, but hydrogen and even chemical bonds can form. To assess the possibility of formation of such bonds, the pH value of a

solution of a polymeric aqueous extract from the corresponding carbon material is used. To do this, the investigated carbon material was boiled for several minutes, and after cooling it was filtered through filter paper. The pH value of the resulting filtrate was measured using an 801 Stirrer "Metrohm" pH meter.

Methods for determining adhesive strength
Uniform breakaway method

Particular attention was paid to the adhesion of the electrode composition to the current collector, which primarily affects the operation of electrochemical current sources. Adhesion was evaluated by the method of uniform separation of the electrode composition from the metal current collector. This method measures the amount of force applied over the entire contact area required to separate the composite polymer material from the substrate. The force is applied perpendicular to the plane of the connecting seam, and the adhesion value is characterized by the force applied per unit contact area (N/m^2) (**Fig. 3.8**).

a   *b*

○ **Fig. 3.8** Laboratory unit for measuring the amount of force applied to detach the sample from the surface of the base: *a* — a device for measuring the adhesion of a composite material to a substrate; *b* — a steel plate with glued samples and a metal nickel of the same diameter, for peeling off with a load

The device consisted of a fixed platform, to which the test sample was fixed with a double-sided adhesive tape from the metal side, as well as a movable cylinder connected to an electronic dynamometer.

This movable cylinder was connected to the surface of the active layer of the electrode also by means of double-sided adhesive tape. During the study, the dynamometer together with the cylinder was slowly lifted up and the force of separation of the electrode mass from the metal current collector was recorded.

Adhesion test method using adhesive tape according to ASTM D 3359

This test procedure describes a procedure for evaluating the adhesion of coatings to metal substrates by applying and peeling off adhesive tape to slots made in the coating. A cross-shaped incision of 6 blades is made on the surface of the coating, on which the adhesive tape is glued and then torn off. Adhesion is assessed excellently on a scale from 0 to 5 (**Fig. 3.9**).
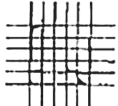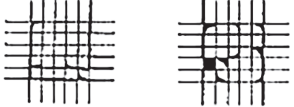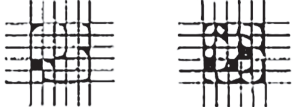
Classification	% of the removed area	Turning over sections of the grating after peeling off the tape
5B	0 % absent	
4B	< 5 %	
3B	5–15 %	
2B	15–35 %	
1B	35–65 %	
0B 0B	> 65 % > 65 %	

Fig. 3.9 Classification of adhesion test results according to ASTM D 3359

CHAPTER 3

However, for our coating, the qualitative assessment method was reduced to three criteria (**Fig. 3.10**):

1) good adhesion and cohesion;
2) poor adhesion, good cohesion;
3) good adhesion, poor cohesion.
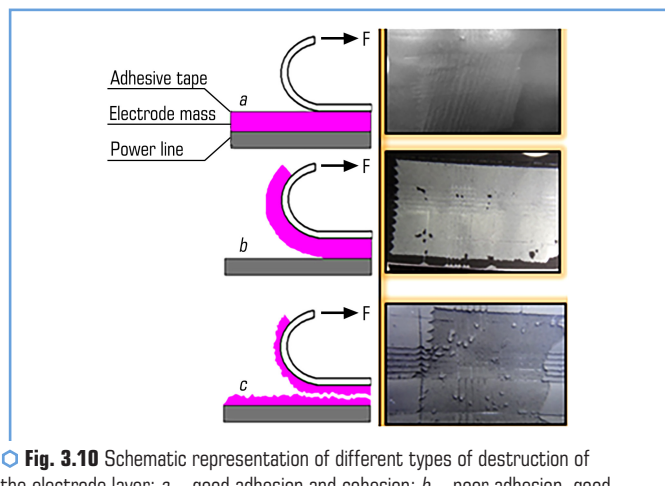
○ **Fig. 3.10** Schematic representation of different types of destruction of the electrode layer: *a* – good adhesion and cohesion; *b* – poor adhesion, good cohesion; *c* – good adhesion, poor cohesion

Composite mixing methods

By means of an electromagnetic stirrer, mechanical mixing of the electrode mass was carried out; in some cases, heating was also used simultaneously.

A compact vacuum mixer GN-SFM-7 was also used. The mixer is designed for vacuum mixing of the components of electrode materials and obtaining homogeneous suspensions without gas bubbles.

Characteristics:

– rotation speed: not less than 320 rpm;
– ultimate vacuum: –0.8…0.9 MPa;
– vibrating platform vibration frequency: not less than 1000 Hz.

By means of ultrasonic stirring, additional dispersion of the components of the electrode mass was carried out. In addition, with the help of ultrasound, air was removed from the pores of carbonaceous materials. This method is quite effective and should not be neglected.

Method of manufacturing electrodes for EC

In the production of EC electrodes, dry substances are prepared in advance and stored in hermetically sealed containers.

Preparation of the electrode suspension is carried out by mixing the dry mixture with a certain amount of a binder solution. Preparation of the electrode mass was carried out in special mixers. Let's use the doctor blade method of applying the electrode mixture to a metal current collector (foil 20 μm thick). When applying an electrode coating on the current collector, the electrode suspension must have a certain density and viscosity, which is determined separately for each electrode composition. The electrode coating by the doctor blade method was carried out on specialized equipment such as Doctor Blade. The main instrument of this equipment was an adjustable applicator (squeegee) – a thin steel plate pointed at the end for removing the excess layer of the electrode composition. When applying the coating by the squeegee method, the electrode suspension is loaded into the applicator, which, when pulled, doses the suspension on the surface of the metal foil. The thickness of the coating layer depends on the speed of the squeegee and its distance from the surface of the foil. The quality of the coating depends to a large extent on the parameters of the application process (applicator gap distance, application speed, slurry and foil temperature) and the composition of the electrode slurry. All these parameters were optimized for each composition of the EC electrode.

After coating, the electrodes are dried in air for 20–30 min at a temperature of 60–100 °C to remove the binder polymer solvent. The final drying of the electrodes is carried out in a special vacuum cabinet at a temperature of 100–120 °C for 8–12 hours. After that, the electrodes are subjected to rolling and cutting to the standard size of the test cell.

After assembling the EC mock-ups, they were tested using electrochemical methods of analysis.

Electrochemical research methods

For various electrochemical studies, computerized potentials MSTAT 32 (Arbin Corporation, USA) and VMP3 (Princeton Applied Researcher, UK) were used.

The characteristics of electrodes and electrochemical capacitors were determined by standard methods, and the results of research and modeling were performed using specialized software for personal computers, namely:

– software for multichannel potentiostats – ARBIN (MITS Pro Software MSTAT 32, Arbin Corporation, USA) and UMP3 (EC-LAB software U9.42, Bio-Logic-Science Instruments, France);

– software for analysis and modeling of impedance spectroscopy data – ZSimpWin (Princeton Applied Researcher, UK).

Models of supercapacitors were fabricated using a sandwich cell (**Fig. 3.11**, **3.12**).

The appearance of EC layouts is shown in **Fig. 3.12**.

The EC charge/discharge characteristics at DC are produced to determine charge/discharge capacity over a specific voltage range, energy efficiency, and to calculate equivalent series resistance values.

Since the studied EC can have a wide range of capacitance values, it is necessary to set the value of the cycle current. The test current at the beginning of testing was C/1 or C/3 (where C is the rated capacitance of the EC).
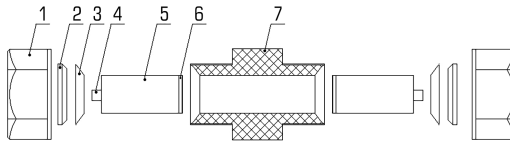
Fig. 3.11 Design of the two-electrode cell of the laboratory model of the EC:
1 – nut; 2, 3 – sealing rings; 4, 6 – down conductor; 5 – electrode; 7 – body
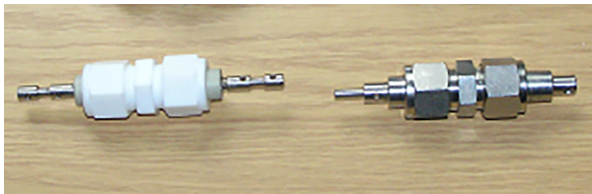
Fig. 3.12 Two-electrode laboratory mock-ups of EC

At the beginning of the test, the actual capacitance of the capacitor is unknown. Therefore, the value of the discharge current corresponding to the nominal capacity of the EC is calculated as follows. The theoretical value of the charge for the capacitor is found from the classical relation $Q=C \cdot U$ according to the equation:

$$Q = \frac{C\left(U_{max} - U_{min}\right)}{3600},$$ (3.11)

where C – capacitance in farads; U_{max}–U_{min} – operating voltage range used in the study; Q – final charge in ampere-hours.

This Q value divided by 3 is the C/3 current rate. But the magnitude of the current is used only for the initial determination of the nominal capacity. After the test is completed and a stable capacitance is determined, the current strength is specified for subsequent testing.

Capacitor capacitance determination

The nominal capacitance was determined in a certain voltage range (from U_{max} to U_{min}) at a constant current of 5C. This value is considered more suitable for possible use in EC than C/1 or C/3 used at the beginning of testing. The nominal capacity is determined from the discharge data from U_{max} to U_{min} in 12 minutes at room temperature. The capacity of the EC is determined by the results of the discharge, which were carried out at least 3 times. The capacitance value is calculated according to the equation:

$$C_I = \frac{Q_I}{U_{max} - U_{min}}, \tag{3.12}$$

where C_I – actual capacitance at current I; Q_I – charge transferred at current I (in the range between U_{max} and U_{min}).

The change in nominal capacitance (ΔC) during long-term cycling was recorded as a relative value of the decrease in capacitance, expressed as a percentage of the initial capacitance C_0. Calculations are made according to the equation:

$$\Delta C(\%) = 100 \times (1 - C_t / C_0). \tag{3.13}$$

For cycling capacitors, the power loss (ΔP) and energy loss (ΔW) is calculated as a percentage of the nominal values according to equations (3.10) and (3.11):

$$\Delta P(\%) = 100 \times (1 - P_n^0 / P_n), \tag{3.14}$$

where $P_N = U^2 / 4R$;

$$\Delta W(\%) = 100 \times (1 - W_n^0 / W_n), \tag{3.15}$$

where $W_N = CU^2 / 2$.

Determination of equivalent EC resistance

The determination of the equivalent resistance RESR is made by a fixed change in the current value. The equivalent resistance is calculated according to the equation:

$$R_{ESR} = \frac{\Delta U}{\Delta I}, \tag{3.16}$$

where ΔU – change in voltage due to a change in the current value.

R_{ESR} was also determined from the data of impedance spectroscopy at a frequency of 1000 Hz.

Impedance spectroscopy

Impedance spectroscopy (IS) is used to study the metal, metal oxide or semiconductor electrode/electrolyte interface, dielectric and transport properties of materials, establish the mechanism of electrochemical reactions, study the properties of porous electrodes, passive surfaces and fuel cells, assess the state of electrochemical batteries and the integrity of poly [25–34]. The essence of the method (IS) is to apply an exciting sinusoidal signal of small amplitude to the system under study and study the signal-response caused by it at the output (**Fig. 3.13**) [35].
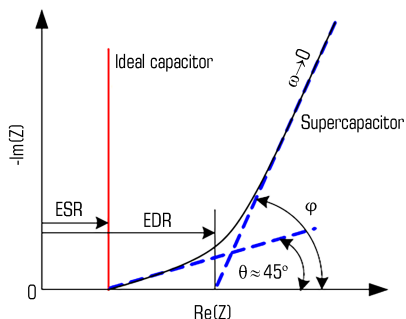
○ **Fig. 3.13** Diffuse system resistance: (ESR) equivalent resistance – the resistance of all components of the capacitor; (EDR) equivalent diffuse resistance includes ESR and additional resistance to the process of charge redistribution in the electrode

Active materials used in the manufacture of electrodes

After preliminary studies, our attention was focused on the following carbon materials, with which the study continued (**Table 3.2**).

● **Table 3.2** Carbon materials with which studies were carried out
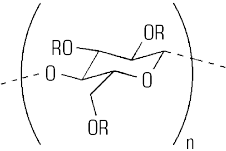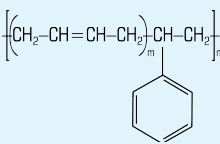
Brand	Manufacturer	General information
Supra 30	Norit (USA)	Activated carbon
Super 30	Norit (USA)	Activated carbon
Supra 50	Norit (USA)	Activated carbon
Super 30	Norit (USA)	Activated carbon
YP-50F	Kuraray Co. (Japan)	Activated carbon
Super C65	Timical (Switzerland)	Conductive additive
Pure Blake	Superior Graphite Co. (USA)	Conductive additive
Acetylene soot	MTI Co. (Korea)	Conductive additive
Carbon black-001	Superior Graphite Co. (USA)	Conductive additive
Carbon black-003	Superior Graphite Co. (USA)	Conductive additive
ABG-1000	Superior Graphite Co. (USA)	Conductive additive

Polymer binders

Among the many varieties of polymer binders, attention has been focused on N-MP-soluble polymers of polyvinylidene fluoride, as well as on its aqueous suspensions. Other water-based

polymers such as polytetrafluoroethylene, styrene-butadiene rubber, and water-soluble sodium carboxymethyl cellulose were also investigated (**Table 3.3**).

● **Table 3.3** Characteristics of the polymeric materials used in the research

Material	Formula	Molecular weight, g/mol	Density, kg/m^3	Melting point, °C
Polyvinylidene fluoride	$[-CH_2-CF_2-]_n$	90000–300000	1680–1760	171–180
Polytetra-fluoroethylene	$[-CF_2-CF_2-]_n$	140000–500000	2000–2200	326.8
Carboxymethyl cellulose sodium salt	R=H or CH_2CO_2H	76000–130000	1348–1590	150–170
Styrene butadiene rubber		150000–400000	910–990	120–130

Materials for a metal down conductor

Since one of the important parameters of an electrochemical capacitor is the reduction of the transition resistance between the active mass and the metal current collector, various types of aluminum foil were considered (**Table 3.4**).

● **Table 3.4** Different types of metal down conductors

Manufacturer	Metal	Thickness, μm	Surface condition
Hohsen Co	Aluminum	20	Smooth
Kawatake Electronics Co	Aluminum	20	Etched
MTI	Aluminum	30	Applied electrically conductive carbon polymer layer
Henkel	Aluminum	30	Aqueous dispersion of LOCTITE DAG 1050 E&C graphite applied

CHAPTER 3

3.2 STUDY OF POLYMERIC BINDERS

Study of physico-chemical binding properties

Today, the creation of new composite materials for EC has gained special weight, since they determine the electrical characteristics of EC. To develop modern technologies for the production of EC electrodes, it becomes necessary to choose a good polymer binder. There are certain requirements for a polymer binder that it must meet when used in chemical current sources.

One of the polymers that meets most requirements is PVDF. PVDF samples may differ in molecular weight, supramolecular structure, the introduction of another monomer units into the chain, the presence of surfactants or plasticizers. Undoubtedly, the chemical nature of the polymer binder affects its adhesion to the substrate and thus also affects the electrochemical properties of the electrode [36–39].

As part of the EU Energy Caps international collaborative project, we were tasked with researching and selecting modified PVDF polymers from Solvay's range of synthesized polymers that can be used in the manufacture of EC, and comparing their properties with some commercially available types of PVDF produced in Japan and the USA.

To evaluate the properties of PVDF, which were studied, model samples of electrodes were made containing composites based on various types of PVDF and Norit activated carbon, for which the values of the fracture force were determined by the direct separation method, as well as the surface area by the BET method. In addition, the electrodes were used to make EC mock-ups and determine internal resistances. The results obtained are presented in **Table 3.5**.

● **Table 3.5** Destruction strength of electrodes with different types of PVDF

Polymer code	Without PVDF	Solef 0001	Solef 0004	Solef 5130	Solef 5320	Solef 6020	KF 1100	KF 9306	Flex 2801
Breakaway force, N/m^2	–	680	335	860	75	225	15	1950	Peeled off
EC diffusion resistance, Ohm	–	7.6	6.7	7.8	4.1	3.9	4.4	9.2	3.7
BET surface, m^2/g	1430	830	956	850	1100	920	985	780	1150

Results in the **Table 3.5** indicate a decrease in the active surface of activated carbon when using samples of PVDF containing functional groups. Such polymer samples lead to a significant increase in the internal resistance of the EC and, accordingly, to a decrease in its power. Therefore, it is necessary to carefully optimize the content of the polymer binder in the electrode.

To establish differences in the chemical composition of PVDF samples, their IR – spectroscopic studies were carried out. **Fig. 3.14** shows the spectra of polymers Solef 6020 (curve 1) and Solef 5130 (curve 2).

The obtained IR absorption spectra indicate that the Solef 5130 polymer contains oxygen-containing functional groups. Thus, in the case of Solef 5130, intense absorption peaks appear at 1724 cm^{-1} and 1750 cm^{-1}, which can correspond to the carboxyl and carbonyl groups, respectively.
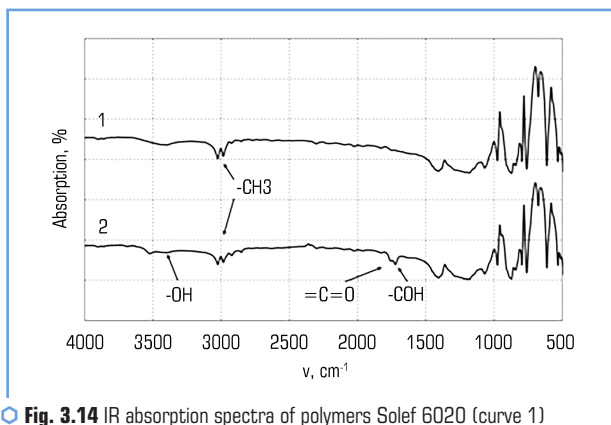
○ **Fig. 3.14** IR absorption spectra of polymers Solef 6020 (curve 1) and Solef 5130 (curve 2)

The presence of a hydroxyl group was also established, which is confirmed by the presence of an extended peak at frequencies of 3650–3200 s^{-1}.

In this work, all selected samples of PVDF were analyzed for the presence of oxygen-containing functional groups in them. The results of IR spectroscopy are presented in **Table 3.6**.

Based on the IR spectroscopy data, all the studied samples can be divided into two groups. Solef 6020, KF 1100 and Flex 2801 polymers are functional group free. On the contrary, all other samples of PVDF (Solef 001, Solef 004, Solef 5320, Solef 5130 and KF 9306) contain functional groups in the macromolecule. It is the presence of oxygen-containing functional groups that can explain the increase in the viscosity of the polymer solution and the improvement in the adhesive properties of the metal current collector.

Reducing the amount of polymer binder leads to a decrease in adhesive properties, but increases the mass fraction of the active material. The given data indicate that different samples of PVDF provide different adhesion of the composite to the metal current collector. It can be assumed that this is primarily due to the different molecular weights of these polymers. In order to determine the molecular weight, rheological studies were carried out, the kinetic, relative, specific and intrinsic viscosities were determined, and based on the data obtained, relative viscosity versus concentration dependences were plotted. The studied solutions of PVDF with N-MP solvent were conditionally divided into low-viscosity (up to 20 Pa) (**Fig. 3.15**) and high-viscosity (up to 120 Pa) (**Fig. 3.16**).

Based on the data obtained, the intrinsic viscosity values were determined, which made it possible to determine the molecular weight of the studied PVDF using the Mark-Houwink formula (**Table 3.7**).

CHAPTER 3

Table 3.6 Presence of oxygen-containing functional groups in different types of PVDF

PVDF code	Functional group		
	Hydroxyl (3650–3200 cm^{-1})	Carbonyl (1750–1705 cm^{-1})	Carboxyl (1725–1700 cm^{-1})
Solef 001	+	+	+
Solef 004	+	+	+
Solef 5320	+	+	–
Solef 5130	+	+	+
Solef 6020	–	–	–
KF 1100	–	–	–
KF 9306	+	+	–
Flex 2801	–	–	–

Fig. 3.15 Dependence of relative viscosity (up to 20 Pa) on the concentration of polymer binders
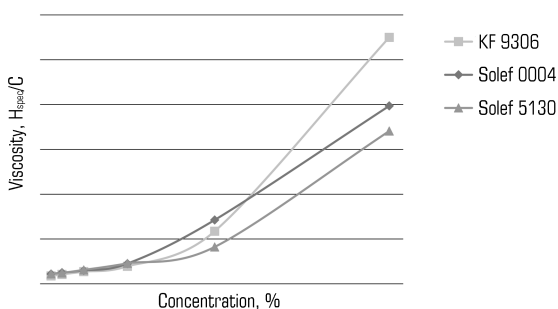
Fig. 3.16 Dependence of relative viscosity (up to 120 Pa) on the concentration of polymer binders

● **Table 3.7** Intrinsic viscosity and molecular weight of different types of PVDF

PVDF code	[η] Pa·s	M
Solef 001	0.710	37052
Solef 004	3.904	422727
Solef 5320	1.921	153554
Solef 5130	3.177	314944
Solef 6020	2.772	259258
KF 1100	1.067	66250
KF 9306	2.954	283938
Flex 2801	1.490	106750

Drawing an analogy between the intrinsic viscosity and the molecular weight of polymers, it can be assumed that for uniform dispersion of the active mass of the electrode and ensuring optimal physico-chemical characteristics, the best option is a viscosity within 3 Pa·s. This value corresponds to the polymers Solef 5130, Solef 6020 and KF 9306, which molecular weights are quite close in value. However, the latest KF 9306 is characterized by the fact that its working solution (5 %) has a fairly large increase in viscosity.

According to the nature of the curves in the graphs, it can be assumed that low-viscosity polymers crystallize with the formation of a spherulitic structure, while high-viscosity polymers remain with an amorphous structure. It is known that the adhesion of amorphous polymers to the substrate is preferable compared to crystallizable polymers. The best adhesion performance in our studies was demonstrated by the Kureha KF 9306 polymer. However, if we take into account the value of the useful surface area for electrodes according to the BET analysis results, then the Kureha KF 9306 polymer blocks it to the maximum. In addition, EC samples, the electrodes of which are made using this binder, have the highest resistance.

In terms of adhesive properties and molecular weight, Solef 5130 is the closest to KF 9306. Based on the results obtained, Solef 5130 and Solef 6020 were selected for further studies. Based on the dependence of viscosity on binder concentration, it can be concluded that polymers with low viscosity. (**Fig. 3.14**) refer to polymers with linear macromolecules capable of crystallization. The degree of crystallinity of the PVDF homopolymer is 60 %. While high-viscosity polymers (**Fig. 3.16**) can be attributed to typical amorphous ones by the nature of the curves. To determine the super-molecular structure of these polymers, films were formed from solutions; micrographs of their structures are shown in **Fig. 3.17**.

In **Fig. 3.17, *a*** is a micrograph of a film with Solef 6020 polymer, which crystallizes to form a typical supramolecular spherulitic structure. A micrograph for a Solef 5130 film in **Fig 3.17, *b*** indicates that the supramolecular structure is globular, characteristic of amorphous polymers.

CHAPTER 3

a   *b*
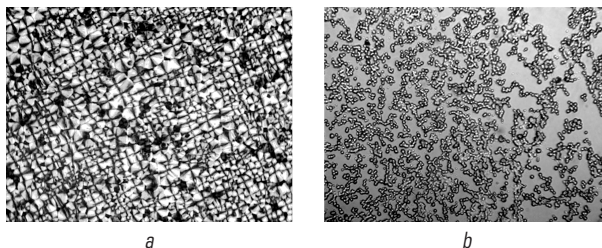
○ **Fig. 3.17** Supermolecular structure of PVDF films: *a* – Solef 6020, magnification (x20); *b* – Solef 5130, magnification (x80)

Based on the theory of polymer adhesion, our results well confirm the fact that amorphous polymers always have preferable adhesion characteristics than crystalline ones. It is known from the literature that with an increase in the viscosity of the polymer solution, its adhesive properties decrease. But in our case, high adhesion with Solef 5130, in theory, is facilitated by the functional groups present in the macromolecule, which are capable of forming hydrogen, and possibly chemical bonds with oxygen groups on the metal surface.

Analyzing the results of the experiments, we can conclude that the nature of the interaction of the studied polymers with the carbon filler segments is different. If the Solef 5130 macromolecules interact better with the filler lobules, which promotes adhesion to them, then they are limited by the ability to move one relative to the other. Also, a polymer containing various functional groups can interact more strongly with the surface of the carbon material. Such an interaction can manifest itself in blocking the active surface of the electrode material, which is undesirable for EC electrodes. This conclusion was confirmed experimentally. According to (**Fig. 3.18**), it can be argued that the Solef 5130 polymer with functional groups blocks the activated carbon surface more strongly, increasing the EC diffuse resistance in the Nyquist diagram by almost a factor of two.
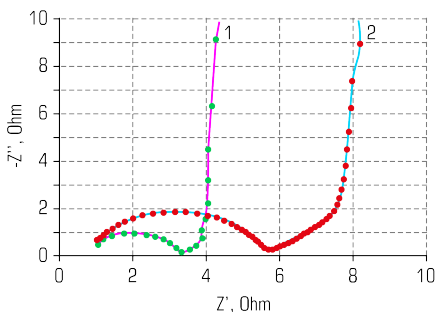
○ **Fig. 3.18** Nyquist diagram obtained for EC with electrodes with various polymer binders: 1 – Solef 6020; 2 – Solef 5130

CHAPTER 3

Effect of polymer binder concentration on electrode properties

It should be noted that the mechanical properties of electrodes largely depend on the conditions of their manufacture, as well as the ratio of components. In this paper, the physical and mechanical properties of various EC electrodes based on the use of Solef 5130 and Solef 6020 as a binder were studied. Particular attention was paid to the adhesion of the electrode composition to the current collector, since it primarily affects the operation by affecting the contact of the electrode mass with the current collector, thereby changing the contact resistance of the system. To evaluate the adhesive properties of the studied PVDF samples, electrode samples were made. Adhesion was evaluated by the method of uniform separation of the electrode composition from the metal current collector. This method measures the amount of force applied over the entire contact area, which is necessary to separate the composite polymer material from the substrate (**Table 3.8**).

● **Table 3.8** Dependence of the force to destruction of the carbon composite layer on the binder concentration. (Electrode composition: Solef 6020 – 4–8 %, graphite – 89–93 % and carbon filler (graphitized carbon soot) – 3 %)

Polymer code	Binder content, %	Thickness of the wet active layer, μm	Thickness of the active layer after drying, μm	Breaking force, N/m²
PVDF – 5130	4	100	92	2073
PVDF – 5130	6	100	81	2994
PVDF – 5130	8	100	78	3651

A decrease in the concentration of the binder in the composite material reduces its adhesion to the metal, worsens the cohesive properties of the electrode mass, brittleness appears, but the density and electrical conductivity of the electrodes increase and the content of the active material increases.

One of the main requirements for a polymer binder is to ensure sufficient mechanical strength of the electrode composite itself with its minimum amount. An increase in the polymer content in the electrode not only reduces the usable mass of the electrode, but also increases its resistance [40]. In most cases, the content of dry polymer content in the electrode should not exceed 10 %.

The influence of the binder concentration (by dry residue) on the adhesion of a composite material to an aluminum current collector was studied in this work. As can be seen from the results given in **Table 3.9**, with an increase in the content of Solef 5130 in the original composition from 4 to 8 wt. % adhesion of composites increases by 80 %.

The same pattern is observed in Solef 6020, where adhesion increased by 70 %. This is obviously caused by changes in both the composition and structure of the electrodes.

Taking into account the different viscosities of the working solutions of the studied polymers, it is obvious that the density of the electrode compositions prepared under the same conditions will be different. Samples prepared on the basis of a less viscous 5 % solution in N-MP Solef 6020 have a noticeably higher density (**Table 3.9**).

CHAPTER 3

● **Table 3.9** Effect of PVDF content on the adhesion of electrode active material

PVDF concentration, %	PVDF concentration, %	Graphite content, %	Conductive additive, 3 %	Density ρ, kg/m³	Breaking force, N/m²
5130	8	89	Pure Black	946	1774
5130	6	91	Pure Black	1275	520
5130	4	93	Pure Black	1539	353
5130	8	89	C65	1414	1970
5130	6	91	C65	1688	764
5130	4	93	C65	–	412
6020	8	89	Pure Black	1235	916
6020	6	91	Pure Black	–	539
6020	4	93	Pure Black	1780	221

This is probably due to the greater mobility of the particles of the dispersed phase in the solution of this polymer in the process of applying the composite material to the current collector using the Doctor Blade device. Analyzing the results of the research, it can be concluded that with a decrease in the concentration of the binder, the density of the electrode material increases, on which the electric capacitance of the electrode depends.

3.3 EFFECT OF EC ELECTRODE MANUFACTURING CONDITIONS ON THEIR CHARACTERISTICS

We have studied the influence of such factors on the characteristics of EC electrodes:
– suspension mixing time;
– mechanical mixing and ultrasonic dispersion;
– influence of drying and rolling temperature.

Temperature-time modes of preparation of EC electrodes

The distribution of the binding volume of the composite material is undoubtedly affected by the technological parameters of their manufacture. There is a significant improvement in the adhesion of the composite (**Fig. 3.19**) to the substrate with an increase in the mixing time of the suspension used to obtain it. The combination of mechanical mixing with the use of ultrasonic dispersion of the system components improves the characteristics of the electrodes and reduces the mixing time of the suspension by 2–3 times.

Mechanical mixing with the additional action of ultrasound, in our opinion, is not only a mechanical process, since the viscosity of the system decreases with time. Composite material of long mixing is able to deform more easily under load. This can be explained by the partial destruction of

macromolecules under the action of the bias voltage and the fixation of the formed radicals on the unpaired electrons of the carbon segments. Of course, the capacitance of the electrode depends on the amount of active material in it. But the existing technology practically does not allow increasing the thickness of the composite layer. With a thickness of more than 200–250 microns, when the composite dries, a system of cracks appears on its surface. This is primarily noticeable when the binder has insufficient adhesion to the filler. **Fig. 3.20** shows a photograph of the surface of a composite based on Solef 6020.
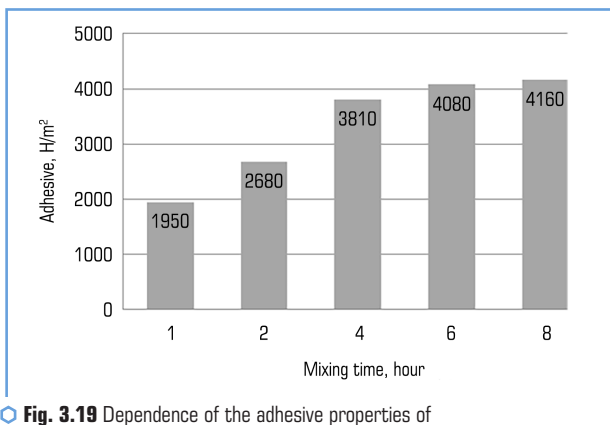
○ **Fig. 3.19** Dependence of the adhesive properties of the composite material on the mixing time
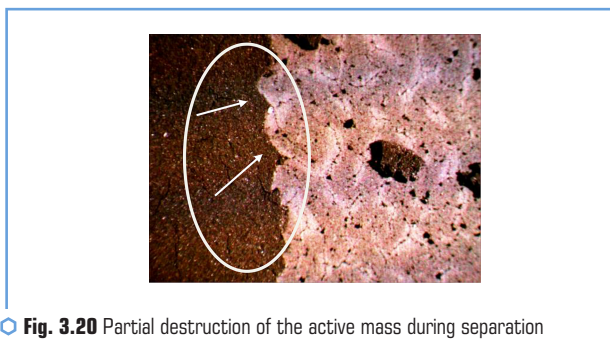
○ **Fig. 3.20** Partial destruction of the active mass during separation (layer thickness 250 μm, magnification 5x)

CHAPTER 3

The formation of these cracks is facilitated by the compression of the polymer during drying. Model samples of films obtained from a solution of PVDF in N-MP showed that their shrinkage upon drying was approximately 10 % (**Fig. 3.21**) [41].

○ **Fig. 3.21** Shrinkage of the polymer after drying

In our opinion, with high adhesion of the polymer, the active mass adjacent to the metal is not able to contract when the solvent evaporates. With distance from the adhesive layer, its influence on the counteraction of the sealing forces gradually decreases and, at a certain distance, the cohesive forces in some places are not able to withstand the stresses that arise during drying.

The effect of the adhesive layer on the mechanical properties of the electrodes is also evidenced by the results of the studies given in **Table 3.10**. With an increase in the thickness of the active mass, its mechanical properties decrease.

● **Table 3.10** Dependence of breakaway force on coating thickness

Thickness of the wet active layer, μm	50	100	120	140	160	180
Breakaway force, N/m^2	4700	4425	4380	4290	3985	2980

An important parameter in the manufacture of electrodes are temperature-time conditions. To assess the effect of temperature on the properties of Solef 6020 films, model samples were made from its solutions in N-MP under normal conditions. The polymer was applied to copper tapes 0.5×7 cm in size; their thickness after drying was 0.5 mm. They are elastic, easily stretched with the formation of a neck, in which the original structures turned into fibrillar. Their elongation before failure is 50–70 %. After heating the films to 150 °C (the crystallization temperature of polyvinylidene fluoride is 140–150 °C), the films become rigid and insoluble in N-MP in a short time. After a series of experiments, the drying temperature of the samples was chosen at 120 °C. The effect of the film heating time at this temperature on the adhesive properties of the polymer is shown in **Fig. 3.22**.

At the studied temperature, to relieve stress, the macromolecules gradually begin to occupy the most favorable position on the surface of the substrate over time, which contributes to an increase in adhesion.

As seen in **Fig. 3.22**, already after 120 min of warming up, the value of the load force almost does not change with time. In addition, according to the previously obtained results, it was shown

CHAPTER 3

that already after 180 min of heating, the density of the polymer begins to increase significantly. The results obtained showed that the maximum reverse deformations are observed in the region up to 180 min and heating at a temperature of 120 °C. The nature of residual deformation changes during heating. Vacuum-dried samples are deformed uniformly and the main type of plastic deformation is due to the movement of macromolecules relative to each other. But already in the process of heating, when the samples are stretched, "necks" appear on the material, associated with the transition of the initial globular to the oriented fibrillar structure, the reverse deformation of which does not exceed 1 % (**Fig. 3.23**).
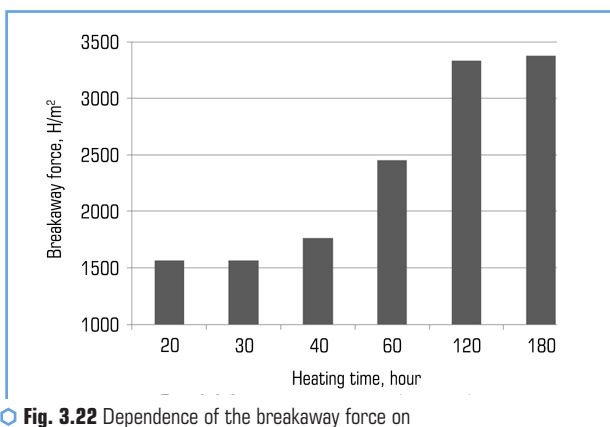
⬡ **Fig. 3.22** Dependence of the breakaway force on the heating time at 120 °C
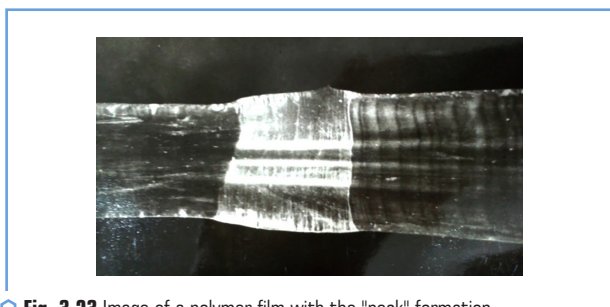
⬡ **Fig. 3.23** Image of a polymer film with the "neck" formation

Thus, it can be seen from the results obtained that the main processes at the molecular level occur when PVDF is heated at 120 °C for up to 180 minutes. Further heating not only reduces the reverse deformation, but also stiffens the structure.

Electrode rolling

The specific energy consumption of EC depends on the specific mass of the active substance on the surface of the current collector. During the evaporation of the solvent, the composite material is compacted on the surface of the current collector (**Fig. 3.24**), but the lobules of the solid filler interfere with obtaining the active mass of the desired density.

It should be taken into account that the technique for the production of electrodes implies the compaction of the dried composite material using rollers at an elevated temperature (100 °C). An increase in temperature reduces the internal stress that occurs during the evaporation of the solvent, and thus increases the adhesive properties of the polymer (**Table 3.11**). It has been established that the compaction of the electrode composition improves the adhesive properties by 8–12 %.
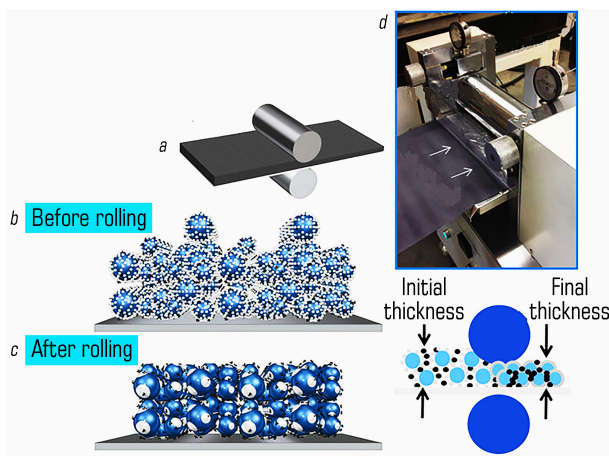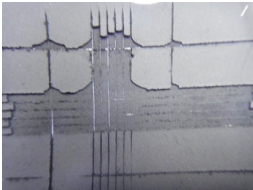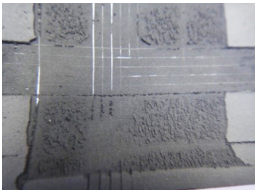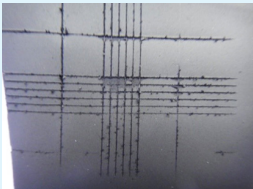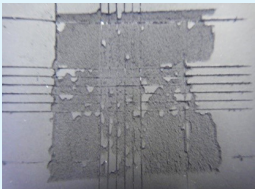
Fig. 3.24 Scheme of rolling electrodes and the device itself: *a* – rolls for rolling; *b* – electrode for rolling; *c* – electrode after rolling; *d* – device

Table 3.11 Density and breakaway force of the active layer of electrodes before and after their rolling (composite composition: graphite – 89–91 %, conductive admixture Pure Black – 3 %, binding Solef 5130 – 6–8 %)

Nº	PVDF, %	Before rolling		After rolling	
		ρ, kg/m³	P, N/m²	ρ, kg/m³	P, N/m²
1	8	873	2484	995	2822
2	6	977	2185	1147	2372

By means of rolling, all components of the electrode mass are compacted. This, in turn, promotes better contact between the active material and the conductive additives. Also in the work, the influence of the temperature of the rollers was studied. It has been established that heating the electrodes during rolling reduces the tension of the material itself and contributes to a more uniform and compact arrangement of the components of the electrode mass. The heating of the electrodes during compaction of the active material reduces the internal resistance of the electrode and thereby improves the electrical conductivity of the system as a whole. As can be seen from **Table 3.12**, the appearance of the surface of the electrodes without rolling and with rolling at a temperature of 100 °C differs significantly after cutting through the electrodes.

● **Table 3.12** Image of the surface of the electrodes after applying the method with cutting into segments. Electrode composition: activated carbon YP-5F – 89 %, conductive additive C65 – 5 %, polymer binder Solef 6020 – 6 %

Rolling	After cutting	After peeling off the tape
Without rolling		
Rolling at temperature (100 °C)		

<div style="text-align:right">CHAPTER 3</div>

The active mass of the electrode without rolling already after cutting peels off quite easily and disappears, however, such a result is no longer observed after the application of rolling. The second stage of this experiment after peeling off the adhesive tape is characterized by better adhesion of the sample with rolling compared to the sample without rolling.

There is a direct relationship between rolling force and internal resistance - the greater the compaction, the lower the resistance. But there are reasonable limits to rolling beyond which further compaction is inappropriate. After a series of experiments, it was determined that compaction of 20–30 % of the electrode mass is optimal. With further compaction of the active layer of the electrodes, a shear stress arises (**Fig. 3.25**), which can adversely affect the structure of the composite and even deform the metal current collector (**Fig. 3.26**).
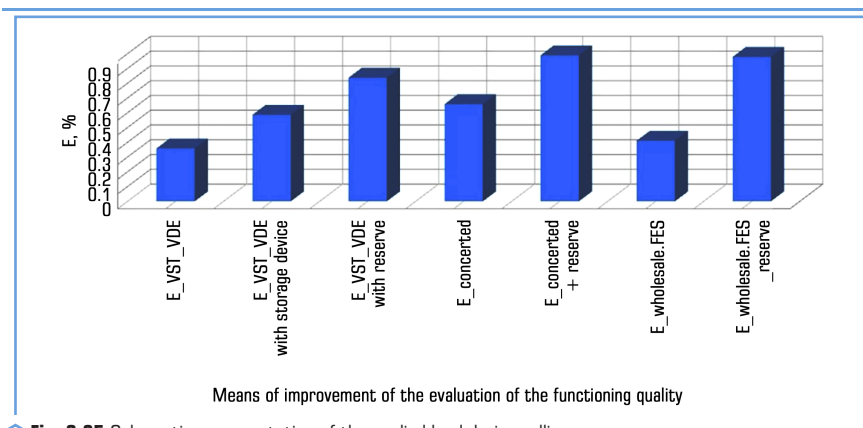
Fig. 3.25 Schematic representation of the applied load during rolling
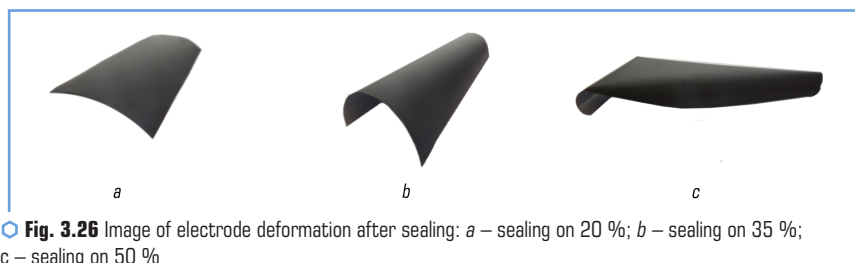
Fig. 3.26 Image of electrode deformation after sealing: *a* – sealing on 20 %; *b* – sealing on 35 %; *c* – sealing on 50 %
Note: Electrode composition: activated carbon (YP-50F) – 88 %, conductive additive C65 – 5 %, polymer binder Solef 6020 – 7 %

Under the action of pressure, the interlayers of the polymeric binder between the lobules of the active material decrease and the area of contacts between them increases, which, of course, contributes to a decrease in the electrical resistance of the electrodes.

Table 3.13 shows the values of the internal resistance of EC, assembled with electrodes before and after compaction.

● **Table 3.13** Change in the internal resistance of the EC depending on the compaction modes

PVDF type	PVDF content, %	Electrode processing	R_{ESR}, Ohm	R_{EDR}, Ohm
Solef 6020	8	Without rolling	0.28	4.85
		Rolling without heating (20–25 °C)	0.28	1.72
		Rolling at heating (100 °C)	0.27	0.59

*EC assembled on the basis of activated carbon Norit Supra 50 and electrolyte -1.5 M TEABF4 in acetonitrile, electrode area 2 cm²

Selection of a metal down conductor for EC

An essential component of the total resistance of the electrode is the resistance between the active mass and the metal current collector.

In this work, electrodes were fabricated using commercial samples of aluminum foil recommended for use in lithium-ion batteries (LIA) and EC. To compare adhesive and electrical characteristics, four types of aluminum current leads were selected (**Table 3.14**), namely, foils manufactured by Hohsen Co. (*a*), Kawatake Electronics Co. (*b*) LIB foil pre-coated with an electrically conductive carbon-polymer layer obtained from MTI Co. (*c*), as well as an analogue of such a composite current collector, made by applying a hydrogen dispersion of LOCTITE DAG 1050 E&C graphite to aluminum foil from Henkel (*d*). The selection of graphite dispersion LOCTITE DAG 1050 E&C is based on Henkel's recommendation of this product for the production of lithium-ion battery electrodes and electrochemical capacitors.

As can be seen from **Table 3.14**, the foil sample from Kawatake Electronics Co. has the best adhesion (breakaway force) (Japan) and a sample with a carbon-polymer layer from MTI Co. (USA), although the latter demonstrates a rather high resistance as part of the finished EC.

● **Table 3.14** Commercial samples of aluminum foils for use in LIB and EC*

Code	Aluminum foil (manufacturer)	Breakaway force, N/m²	EC Resistance R_{EDR}, Ohm
(*a*)	Foil from Hohsen Co. (Japan)	3381	1.43
(*b*)	Foil from Kawatake Electronics Co. (Japan)	4704	1.15
(*c*)	Foil from MTI Co. with carbon-polymer layer (USA)	4116	4.31
(*d*)	Foil from Henkel with graphite layer LOCTITE DAG1050 E&C	1744	5.12

*EC assembled on the basis of activated carbon Norit Supra 50 and electrolyte -1.5 M TEABF4 in acetonitrile, electrode area 2 cm²

A sample with a carbon layer based on LOCTITE DAG1050 E&C demonstrates both sufficiently low adhesion and the highest resistance in the EC composition. This indicates that the polymer used by LOCTITE DAG1050 E&C has poorer adhesion to the Henkel foil.

We have found that the main criteria affecting the adhesion force are the surface and the shape of the aluminum foil surface relief. The more developed the surface and the inhomogeneous relief, the better the contact of the active mass of the electrode with the metal surface. This profile is achieved by targeted surface treatment of the aluminum foil by the manufacturer.

Fig. 3.27 shows the change in the EC impedance in the case of using foil from Hohsen Co. as a current collector. and Kawatake Electronics Co.

As can be seen from **Fig. 3.27**, the modification and increase in the specific surface area of the current collector (foil from Kawatake Electronics Co.) significantly reduces the internal resistance of the capacitor compared to the EC based on untreated (smooth) foil from Hohsen Co.
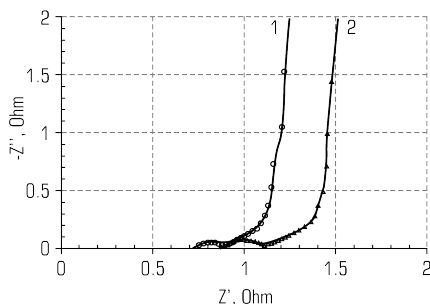
○ **Fig. 3.27** Change in EC impedance depending on the type of current collector: curve 1 – foil from Kawatake Electronics Co.; curve 2 – foil from Hohsen Co.

Also, according to the studies, it was shown that the preliminary application of an electrically conductive polymer-carbon layer does not always improve the electrical characteristics of the EC. As can be seen from **Table 3.14**, the electrically conductive polymer-carbon layer in options (*c*), (*d*), deposited on the aluminum current collector, on the contrary, significantly increases the internal resistance of the capacitor compared to modified foil electrodes from Kawatake Electronics Co., which do not have such a layer. This can be explained by the presence of a large amount of polymer in the pre-applied layer (*c*) and insufficient adhesion in option (*d*), which leads to blocking of the charge-discharge kinetics of the EC active material.

The selection of an aluminum current collector with a fine-grained relief (for example, grass foil from Kawatake Electronics Co.) can significantly (approximately 40 %) improve the adhesion of the electrode layer by increasing the effective contact surface, as well as reduce the internal resistance of the electrochemical capacitor by 20 % to a down conductor from Hohsen Co., which is often considered "standard").

Unlike the unmodified surface of the Japanese-made foil, the surface of the Kawatake Electronics Co. foil has been artificially modified. In our opinion, this fact can be explained by photographs of the foil surfaces (**Fig. 3.28**).

Fig. 3.28, *a* shows the surface of a Japanese Hohsen foil with machining marks. The foil surface of Kawatake Electronics Co. is modified by electrochemical digestion, which greatly increases the effective surface area.

An original technique for reducing contact resistance is proposed in patents [13]. According to this technique, slices of graphite or soot are fused into the aluminum surface using electrospark technology (**Fig. 3.28**). In this case, the aluminum oxide surface layer is destroyed and is not restored further on the graphite/aluminum interface. According to this technique, the specific contact resistance decreases by two orders of magnitude.

a   *b*
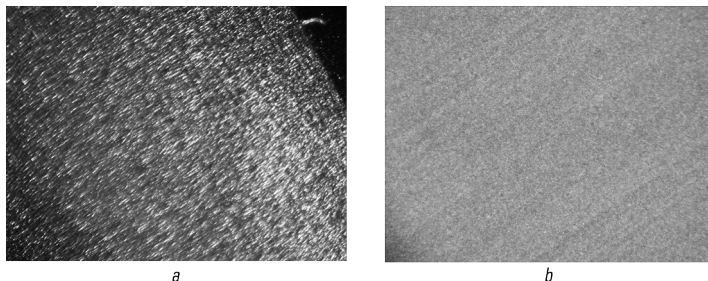
Fig. 3.28 Surface of Al foil of the company: *a* – Hohsen; *b* – Kawatake Electronics Co.

Microscopic studies confirm the fusion of graphite particles into aluminum (**Fig. 3.29**).
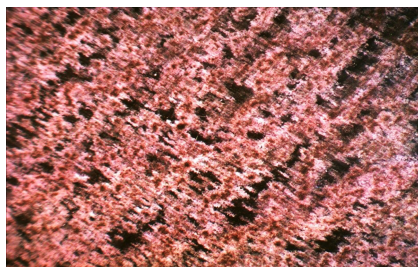
Fig. 3.29 Modified surface of aluminum foil by spark discharge

Electrospark processing leads to point deformation of the foil, which increases its specific surface.

Using the uniform breakaway method, it was determined that the adhesion of such a foil is 30 % higher compared to the adhesion of a smooth foil from Hohsen and amounted to 5580 N/m^2. However, obtaining such a foil on an industrial scale is a rather complicated process and leads to significant costs for electricity.

Thus, grass foil from Kawatake Electronics Co. shows the best results. (Japan), which has sufficiently high adhesion rates and, accordingly, a low contact resistance, which positively affects the electrochemical characteristics of EC. It was this foil that was chosen for further use in the manufacture of EC.

As a result of the studies performed, in the third chapter it can be concluded that it is the Solef 6020 polymer in N-MP that meets most of the electrochemical characteristics and requirements for a polymer binder.

The combination of mechanical mixing and ultrasonic dispersion significantly improves the homogeneity of the electrode mass suspension, which affects the uniformity of application to the metal current collector.

By many experiments, the appropriate concentrations of binder polymers, the composition of the components of the electrode mass, the thickness of the deposition, and the temperature-time modes of drying the electrodes were selected. Also, after drying the electrodes, they were additionally rolled at a temperature of 100 rolls °C for compaction. After rolling, the number of useful contacts in the electrode partially increases and, in turn, the internal resistance decreases (by 80 %). Thus, the rolling of the electrode layer improves the electrochemical and physical characteristics of the EC electrodes.

3.4 APPLICATION OF WATER-SOLUBLE POLYMER BINDERS

In further studies, the possibility of replacing the organic solvents of PVDF with water was considered. This is possible when using aqueous solutions (suspensions, emulsions) of polymers. In particular, electrodes were fabricated using mixtures of sodium carboxymethyl cellulose (NaCMC) solution with industrial acrylate (BM-12), polyurethane, and styrene-butadiene (SBR) suspensions. The active masses with these binders showed high adhesive properties of the aluminum current collector, which are not inferior to the properties of the composite based on PVDF [42].

Carboxymethyl cellulose is a simple ester of cellulose and glycolic acid [43]. It is a colorless substance, insoluble in water, low molecular weight alcohols and ketones. As a rule, not the polymer itself is used, but its sodium salt, which is also often called carboxymethyl cellulose.

NaCMC is also an amorphous colorless substance with a softening point of 170 °C and a density of 1.59 g/cm^3, soluble in water. The most common for the use of NaCMC are polymers with a degree of polymerization of 200–1500. The degree of substitution of hydroxyl groups for sodium ions in the macromolecule unit is from 0.4 to 1.2. Polymers with a degree of substitution of more than 0.4 dissolve well. Transparent solutions are characterized by high viscosity, so that the viscosity of a 2 % solution is 10–25 10^3 mPa s. NaCMC is well compatible in aqueous solutions with other water-soluble natural and synthetic polymers. In aqueous solutions, it has the properties of weak surface-active substances (surfactants). From aqueous solutions, transparent films are obtained with a breaking load of 4900–9114 N/m^2 and a relative elongation at failure of 8–14 %. Possesses weak acidic properties.

The rheological and adhesive properties of solutions of this artificial polymer depend on many factors, including the nature of the initial cellulose (cotton, wood species, and other plants), molecular weight, the degree of substitution of hydroxyl groups in the macromolecule unit, and the purity of the finished product. We had three samples of NaCMC at our disposal: technical, food (Holland), and electrolyte (Dow Chemical, Germany). In the solid state, they are in the form of a fine white powder, but their solutions are transparent. In this work, thin films formed during the drying of

solutions of these polymers were carefully studied. Careful examination of these films at the optical level revealed the presence of foreign solid particles in them (**Fig. 3.30**).
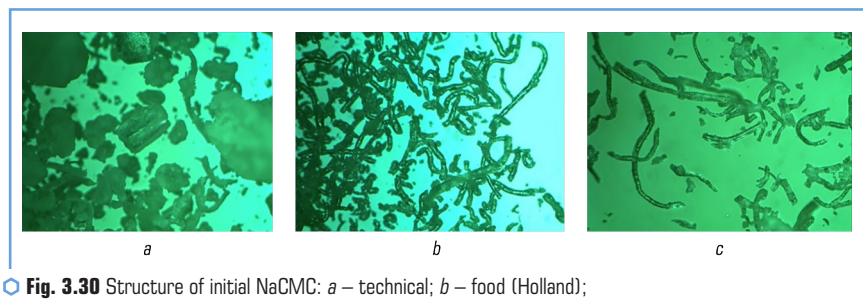
⬭ **Fig. 3.30** Structure of initial NaCMC: *a* — technical; *b* — food (Holland); *c* — electrolyte (Dow Chemical, Germany)

In our opinion, wood was used as the starting material for the preparation of technical NaCMC, while residues of cotton fibers were found in the food and electrolyte samples. The conducted studies unequivocally indicate that the electrolyte NaCMC is the purest of those studied. It was this polymer that was selected for further work.

As mentioned earlier, the polymeric EC electrode binder [44] should have good adhesion to the metal current collector. Typically, in the technology of manufacturing electrodes, solutions are used, the concentrations of which are 5–8 %. It was interesting to compare the adhesive properties of 5 % solutions of PVDF and NaCMC. Thin films were fabricated from such solutions on copper foil, and after drying they were examined by the detachment method. The results show that the adhesion of PVDF (breakaway force 4537 N/m^2) is much greater (by 97 %) compared to NaCMC (breakaway force 118 N/m^2). In our opinion, this difference can be explained by a significant difference in the viscosities of the solutions studied in this experiment. Even when applying the solution to the copper base, it was clear that due to the low mobility of macromolecules in a rather viscous solution of NaCMC, the polymer wets the substrate much worse. In addition, the NaCMC viscous solution formed a thicker film compared to PVDF, which, according to theory, also weakens adhesion. To reduce the viscosity, a 1 % solution of NaCMC was prepared. The adhesion properties of such a film have increased significantly (breaking load 3676 N/m2). Considering that aqueous solutions of NaCMC are well compatible with solutions of water-soluble polymers, it was interesting to modify NaCMC with aqueous suspensions of polymers with high adhesion to metals.

Synthetic latexes are aqueous dispersions of synthetic polymers stabilized with surfactants [45]. In latex macromolecules are in the form of balls (globules). The size of the globule significantly affects the viscosity of the latex, as well as its stability. The smaller the globule size, the higher its stability. The average diameter of globules of different polymer emulsions is

CHAPTER 3

from 80 to 300 nm. When water-soluble polymers are added to the latex, the globules grow in size [46].

The most common are polyurethane, polybutadiene-styrene, polyacrylate synthetic latexes. An example of the globular structure of latex suspensions is shown in **Fig. 3.31**.

○ **Fig. 3.31** Surface of ultrathin film of BM-12 acrylate suspension (x13000, electron microscopy)

Linear polyurethanes have the general formula $[-OCHN-R-NHCO-OR'O-]_n$.

The presence of strongly polar groups (urethane, complex and ether bonds) in the chain of the macromolecule promotes the formation of hydrogen bonds. Reactive isocyanate groups may remain at the ends of the macromolecule. There are many varieties of polyurethanes, since there are a large number of starting monomers. The disadvantage is the low resistance to thermal and thermal-oxidative degradation. Macromolecules of some polyurethanes begin to decompose at a temperature of 120 °C.

Styrene-butadiene latexes are amorphous polymers. They have a density of 0.91–0.99 g/cm^3. Soluble in aromatic and aliphatic hydrocarbons.

Polyacrylate latexes are obtained by emulsion polymerization of esters of acrylic and metaacrylic acids with different numbers of carbon atoms in the radicals [45, 46].

General formula: $(-CH_2-CR'(COOR-)_n$.

Physico-mechanical characteristics significantly depend on the length of the radicals. Under normal conditions, polyacrylate latexes are resistant to dilute acids and alkalis, but at temperatures above 80 °C they can be hydrolyzed by solutions of polyacrylic acid and alkalis. At temperatures above 150 °C, thermal destruction of macromolecules begins, accompanied by cross-linking of macromolecules. In this case, a slight release of monomers may occur. When the aqueous dispersion dries, polyacrylates form a stable transparent film.

Some doubts are caused by polyurethane and polyacrylate suspensions, the macromolecules of which contain active functional groups, which can later react with the components of the electrode system. Signs of the onset of coagulation were noticed when the polyacrylate suspension was added to the NaCMC solution.

CHAPTER 3

For further work, preference was given to a suspension of styrene-butadiene rubber (SBR) (**Fig. 3.32**).
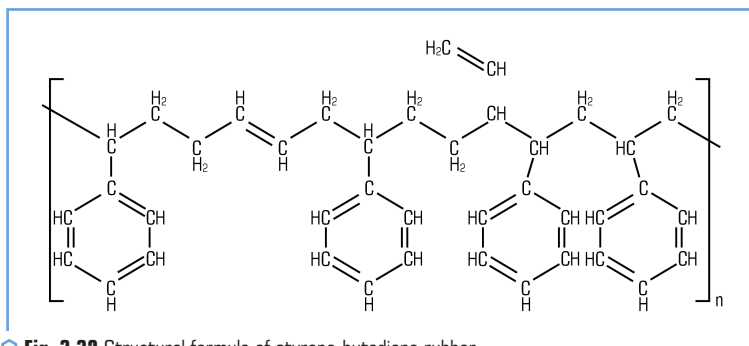
○ **Fig. 3.32** Structural formula of styrene-butadiene rubber

First, there are no active groups in the macromolecule of this polymer that could interact with the electrolyte; the polymer is resistant to acids and bases. Secondly, the polymer has flexible chains with good adhesive properties. Thirdly, π-bonds in macromolecules and free bonds on carbon particles, under certain conditions, can lead to the formation of a cross-linked structure and, thus, strengthen the composite material. Aqueous suspension of SBR is technologically advanced, sedimentation-resistant for a long time of storage.

Thus, for further studies, a suspension of SBR was chosen for comparison and characterization.

On the basis of a mixture of NaCMC and SBR, EC electrodes were fabricated and studied. The composition of the electrode: activated carbon – 89 %, conductive additive – 5 %, polymer binder – 6 %. Table 15 shows the internal resistance values of EC based on electrodes made from these polymer binders and electrodes made from solutions of Solef 6020 in N-MP.

● **Table 3.15** EC internal resistance

Polymer bonding electrodes	R_{ESR}, Ohm	R_{EDR}, Ohm
NaCMC / SBR in a ratio of 1:1	1.1	2.7
Solef 6020	0.71	1.15

Electrochemical studies of electrodes based on NaCMC/SBR composites indicate their poorer stability compared to PVDF. **Fig. 3.33** shows the anodic polarization curve of an aluminum current collector, on the surface of which various polymers were deposited.

According to the results obtained, SBR can be oxidized at potentials of more than 3.7 V relative to the lithium reference electrode, which is almost 1 V less than in the case of PVDF.

CHAPTER 3
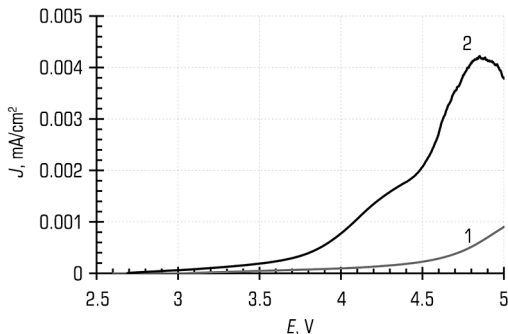
○ **Fig. 3.33** Linear voltammetry of an aluminum current collector with a polymer film: 1 — PVDF; 2 — SBR. The potential sweep rate is 1 mV/s. Electrolyte: 1M LiPF$_6$ solution in EC/DMC (1:1)

Use of water-based polyvinylidene fluoride suspensions

Solef® PVDF aqueous suspensions (XPH-859 and XPH-884) were used to develop highly stable EC electrodes, which were started to be produced by the Belgian company Solvay. Within the framework of the joint international project of the EU Energy Caps, we were tasked to investigate the possibilities of using these binders to obtain EC electrodes.

Aqueous suspensions contained amorphous polymers with a molecular weight of about 90,000; they are elastic in the solid state and have a globular structure (**Fig. 3.34**).
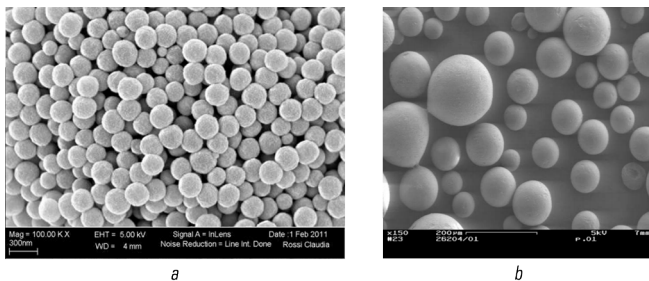
○ **Fig. 3.34** Scanning electron microscopy of the Solef KhRN-884 structure with different magnifications of PVDF particles: *a* — 300 nm/cm; *b* — 100 nm/cm

The concentration of Solef XPH-884 is 22 %, and Solef XPH-859 is 27 %. The polymers have different sedimentation resistance, which is low in Solef PVDF XPH-859. After some time, about 6 months, the Solef XPH-859 polymer precipitates and polymerizes to form an insoluble precipitate.

In addition, the surfactant in the Solef XPH-884 suspension has a pronounced foaming ability. Films obtained from these suspensions differ significantly in structure and their physical and mechanical properties (**Fig. 3.35**).

Thus, homogeneous, transparent, elastic films are formed from the Solef XPH-859 suspension, while films from Solef XPH-884 retain a clear globular structure, are quite fragile and opaque.
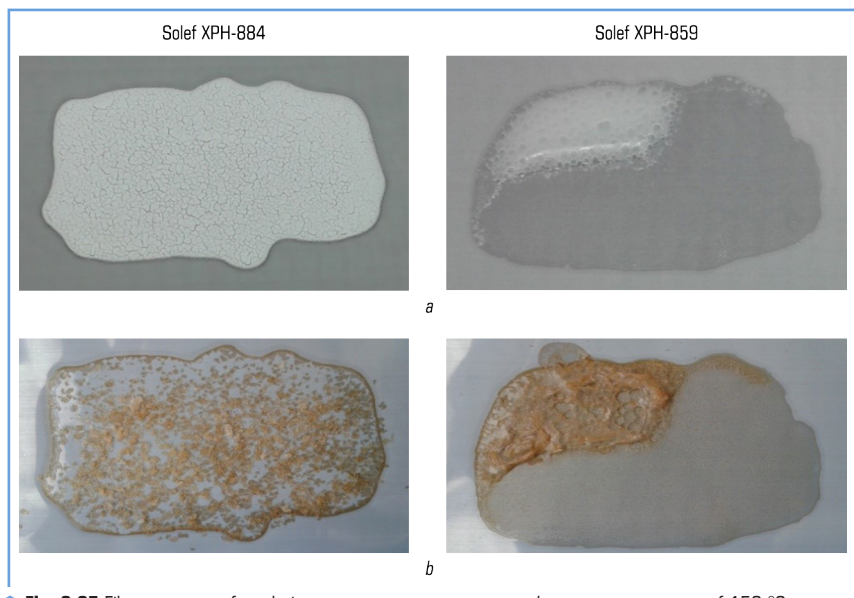
Fig. 3.35 Film structure after drying: *a* – at room temperature; *b* – at a temperature of 150 °C

CHAPTER 3

The polymers feature stabilizing surface agents (Solef XPH-859 suspensions have a pH of approximately 4.5 and Solef XPH-884 $\approx$2.5), and Solvay limits information on polymer composition for confidentiality reasons. The joint between these suspensions is very low viscosity. This makes it impossible to produce a stable suspension for applying the active material to the current collector of the electrode. To increase the viscosity of the suspension, we proposed the use of NaCMC.

This polymer belongs to the rigid-chain ones, due to which it forms a slightly deformed structure. The rigidity of NaCMC macromolecules and the presence of active groups in them have a significant effect on the physical and mechanical properties of the active material of EC, the components of which are activated carbon and a conductive additive. On the particles of these components there are always active centers in the form of oxygen-containing groups, edges and corners of crystallites, other atoms. Naturally, their number depends on different methods of obtaining these materials and affects the formation of conductive structures in the composite. When preparing the mixture, it should be taken into account that the maximum viscosity of the NaCMC

solution is achieved at a pH of about 7–9, and the used aqueous PVDF suspensions are acidic, which helps to reduce the viscosity of the working binder solution. The results showed that the use of these suspensions in combination with NaCMC has rather high electrochemical parameters compared to the classical PVDF polymer soluble in N-MP (**Table 3.16**) [47, 48].

● **Table 3.16** Internal resistance of EC* with electrodes made with different polymers

Polymer binders	R_{ESR}, Ohm	R_{EDR}, Ohm
Solef 6020 (from N-MP solution)	0.71	1.15
NaCMC/SBR (ratio 1/2)	1.10	2.70
NaCMC/XPH 859 (ratio 1/2)	0.37	1.43
NaCMC/XPH 884 (ratio 1/2)	0.44	1.15

*EC was assembled on the basis of Norit Supra 50 activated carbon and -1.5 M TEABF4 electrolyte in acetonitrile. The polymer content in the electrode was 10 %

As for the adhesion strength of electrodes made using water-based polymer suspensions, it is higher than that of electrodes made using the standard method based on solutions of PVDF in N-MP (**Table 3.17**).

● **Table 3.17** The value of the internal resistance of EC based on electrodes made of various polymeric binders

Polymer binders	P, N/m^2	Score at ASTM D 3359
NaCMC/XPH 859 (ratio 1/2)	2420	3B
NaCMC /XPH 884 (ratio 1/2)	2519	3B
Solef PVDF 6020 (from N-MP solution)	2201	2B

Thus, the replacement of N-MP-based technology with a mixture of suspension PVDF and water-soluble NaCMC makes it possible to simplify the technology for manufacturing EC electrodes and obtain better results (by 38 %) in reducing the internal resistance of EC.

3.5 MANUFACTURING AND TESTING OF MODELS OF AN ELECTROCHEMICAL CAPACITOR

Selection of activated carbon for the production of EC electrodes

Carbon materials are widely used in various branches of technology and are used as adsorbents, carriers for catalysts, and catalysts themselves [49–55]. They are most widely used in adsorption processes. There are many different activated carbon materials that differ in origin and

method of activation, for example, according to [56], more than 150 types of activated carbon (AC) are presented. The entire range of presented materials is characterized by narrowly specific areas of application, and so far the specific area of application of each new material is selected only empirically, and there is no single approach to predict the properties and behavior of AB in specific systems.

For example, it is known [56] that activated carbon selectively absorbs hydrocarbons and their derivatives, aromatic compounds, dyes, and, to a lesser extent, lower alcohols, carboxylic acids, and esters, and the chemical structure of the surface of the carbon material has a great influence on water adsorption [57]. For example, water adsorption does not occur on an unoxidized carbonaceous surface, and when the surface is oxidized, significant H_2O adsorption is noted, which can be increased by introducing alkaline earth metal ions and increases by a factor of 4–5 for alkali metal ions. Functional groups can be aliphatic radicals, hydrogen atoms, and various oxygen-containing compounds (hydroxyl, carboxyl, carbonyl, lactone, quinoid, etc.).

Each of the functional groups is attached to one carbon atom, the lactone group is already closed on two adjacent carbon atoms, and the quinoid group changes the electronic structure of the carbon atom associated with it.

The presence of such features leads to many options for implementing surface properties for the same initial structure [58]. Depending on the direction and method of surface transformation, various functional groups are formed and, accordingly, the surface can acquire directed specificity upon adsorption of certain molecules [59].

Since the capacitance of an electrochemical capacitor directly depends on the available surface area of the carbon material on which a double electric layer is formed, part of the work was focused on the selection of carbon material [60–63]. Samples of activated carbon brand Norit DLC (Netherlands) and YP-50F Kuraray Chemical Co (Japan) were selected for research [64]. The main characteristics of the samples are given in **Table 3.18**.

As can be seen from **Table 3.18**, activated carbon of the Supra 30 and Supra 50 brand has the largest surface area and micropore volume.

The EC characteristics are greatly affected by the pore size distribution. Supra 30 and Supra 50 activated carbons have very small pores, which are not available for $TEABF_4$ electrolyte.

The electrodes made from these samples of activated carbon were of poor quality. Due to the sufficiently high internal stress, the active layer of the electrode cracked and was characterized by low adhesion to the current collector. **Fig. 3.36** shows ASTM D 3359 test results for Supra 30 and Supra 50 activated carbon electrodes.

The active layer is completely detached when the adhesive tape is peeled off from the Kawatake Electrics Co. Grass Aluminum Foil.

Fig. 3.37 shows the results of the ASTM D 3359 test for the YP-50F activated carbon electrode.

Activated carbon of the YP-50F brand differed from previous brands in that the active layer has good adhesion to the metal current collector (**Fig. 3.37**) even with a lower content of polymer binder (6 % versus 10 %). High adhesion has a positive effect on the electrical characteristics of

CHAPTER 3

the electrode. It was found that EC based on YP-50F has a significantly lower internal resistance compared to EC based on Supra 50 activated carbon (**Table 3.19**). According to **Table 3.19** Internal resistance of Supra 50 based EC is 63 % higher than that of YP-50F activated carbon based EC.

● **Table 3.18** General characteristics of various types of activated carbon

General indicator	Brands of activated carbon				
	Super 30	Supra 30	Super 50	Supra 50	YP-50F
Total surface area (BET), m^2/h	1850	2100	1850	2100	1660
Imaginary density, kg/m^3	350	275	400	325	370
Micropore volume, cm^3/g	0.68	0.85	0.68	0.85	0.74
Mesopore volume, cm^3/h	0.07	0.1	0.07	0.1	0.21
Particle size D10, μm	2–4	2–4	3–5	3–5	5–20
Particle size D50, μm	5–10	5–10	9–13	9–13	
Particle size D90, μm	13–20	13–20	21–31	21–31	
Particle size D100, μm	30	30	50	50	
Ash content, %	2	2	2	2	0.3
Solvent components of ash, %	0.02	0.02	0.02	0.02	–
Chlorides, g/100g	0.04	0.04	0.04	0.04	–
Iron, ppm	40	40	40	40	–
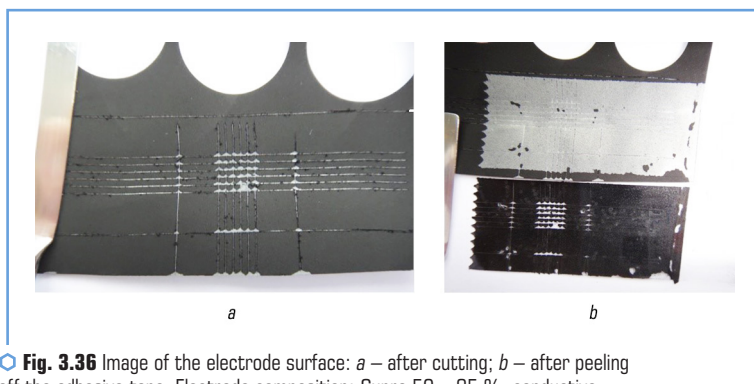
○ **Fig. 3.36** Image of the electrode surface: *a* – after cutting; *b* – after peeling off the adhesive tape. Electrode composition: Supra 50 – 85 %, conductive additive – 5 %, polymer binder Solef-6020 – 10 %

CHAPTER 3
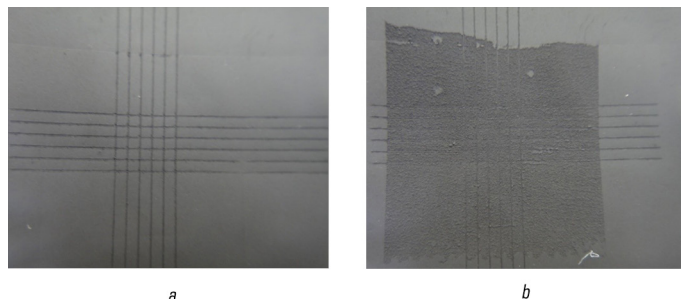
○ **Fig. 3.37** Image of the electrode surface: *a* — after cutting; *b* — and peeling off the adhesive tape. Electrode composition: YP-50F — 89 %, conductive additive — 5 %, polymer binder Solef-6020 — 6 %

● **Table 3.19** EC internal resistance based on different brands of activated carbon

Activated carbon	R_{ESR}, Ohm	R_{EDR}, Ohm
Supra 50	1.2	3.9
YP-50F	0.89	1.43

In order to establish the reasons for the different characteristics of electrodes based on activated carbon samples with fairly similar physical and chemical characteristics (**Table 3.18**), microscopic studies of the structure of the samples were carried out. Activated carbon Norit Supra 50 after soft dispersion has a fine structure (**Fig. 3.38, *a***) with a small amount of soot chains, unlike YP-50F carbon (**Fig. 3.38, *b***).
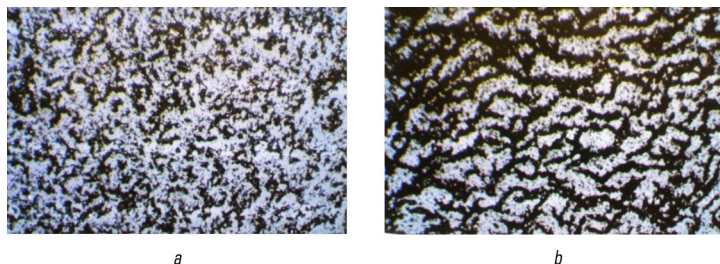
○ **Fig. 3.38** Microstructure of activated carbon film: *a* — Norit Supra 50; *b* — YP-50F at 7x magnification

CHAPTER 3

Thus, the YP-50F activated carbon covers the metal foil more compactly. This is due to the secondary structure of the particles of said sample of activated carbon. **Fig. 3.39** shows the results of electron microscopic studies of YP-50F coal.

20.0 μm

a   b
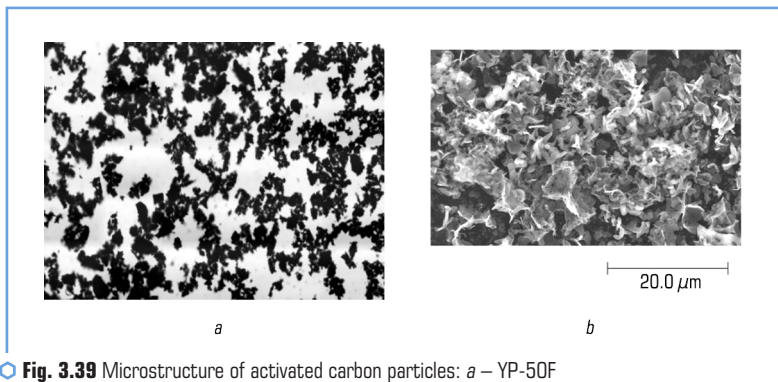
○ **Fig. 3.39** Microstructure of activated carbon particles: *a* – YP-50F magnification; *b* – magnification by 200 times

From **Fig. 3.39** it follows that activated carbon particles up to 20 μm form a secondary structure in the form of compact chains. It is possible that such a structure makes it possible to obtain a compact coating on the current collector.

The structure formation of finely dispersed carbon materials can be assessed by oil absorption. To this end, the oil absorption of various carbon materials was established. The results of the study are given in **Table 3.20**.

● **Table 3.20** Oil absorption value of different carbon materials

Carbon material	Oil absorption, ml/g
Norit Supra 50	1.6
Norit Super 50	1.9
Norit Supra 30	1.7
Norit Super 30	1.8
YP-50F	2.2
Graphite soot (Pure Black-205)	3.8
Graphite carbon soot (Super C65)	9.4
Acetylene soot	2.8
Acetylene soot (Shawinigan)	7.9

Selection of conductive additive

The specific characteristics of the activated carbon particles and the conductive additive can affect their interaction with the polymer macromolecules. Such characteristics can be considered the chemical nature, size, shape, granulometric composition, specific surface area (geometric, total), real and bulk density, porosity, particle packing, surface pH.

The hydrogen index of the water extract from carbon materials makes it possible to speak about their wetting, selective adsorption, and the ability to aggregate particles.

Nevertheless, the nature of surface active centers has the main influence on the intermolecular interactions of the polymer-filler and filler-filler [65]. Such active centers on carbon particles can be unpaired electrons, foreign atoms and groups of atoms (primarily oxygen), and crystallite lattice defects. In turn, the nature and number of active centers depend on the technology for obtaining carbon particles.

The primary structure of carbon black (soot) is chaotically arranged packets of planar molecular layers [66]. These fine layers have a structure similar to graphite, but are irregularly arranged. Such crystallites are linked by valence bonds and form two- or three-dimensional racemose aggregates. Considering all this, one of the important components of electrode masses is a conductive additive, which provides reliable contact between the system components and promotes better wetting with electrolyte [67–70]. Among these additives, we chose Super C65 carbon black with a density of 160 kg/m^3, which differed from others in its good dispersion and ensured reliable contact between active material lobules [71].

Fig. 3.40 shows a schematic model of the arrangement of particles of a carbonaceous conductive additive in an EC electrode. Using this model, it is possible to explain how exactly the conductive additive works and according to what scheme the charge is transferred to the current collector [72].

CHAPTER 3

○ **Fig. 3.40** Schematic representation of the location of the particles of the conductive additive C65
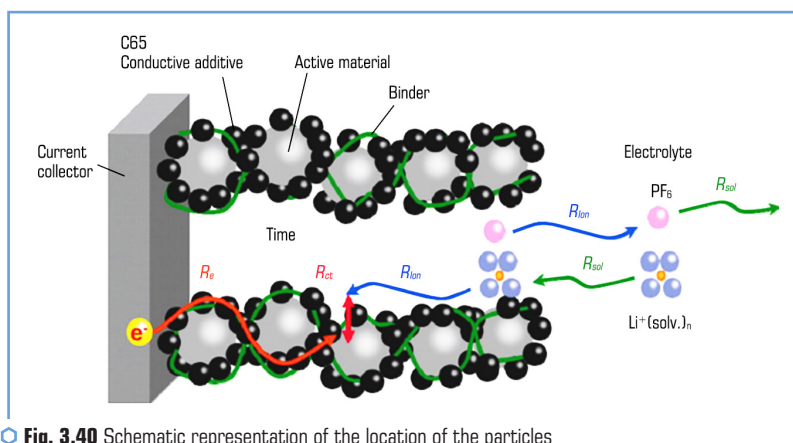
As can be seen from **Table 3.20**, graphitized carbon black Super C65 demonstrates maximum oil absorption, which is characterized by a good structure formation factor and, accordingly, the ability to form chains of soot lobules for reliable electrical contact of all components (**Fig. 3.41**).

The ability to structure increases with an increase in the degree of dispersion of particles and a decrease in the amount of volatile impurities in them.

The specificity of the electrode mass is that it should have maximum electrical conductivity with a minimum amount of polymer binder, which ensures the mechanical strength of the electrode. It is known that a small content of a solid dispersed filler in a polymer can increase the strength of the composite, since cracks growing under the action of a load are stopped by filler particles. However, an excessive concentration of filler increases the brittleness of the material.

In our case, the maximum oil absorption provides the greatest value of structure formation on the one hand, but also has the greatest shrinkage after drying on the other (**Fig. 3.42**).

The samples were prepared in the ratio of carbon material – 90 %, polymer binder (sodium salt of carboxymethyl cellulose) – 10 %. As can be seen from **Fig. 3.42**, the greatest shrinkage was observed precisely in Super C65, which had the maximum oil absorption value of all carbon materials, which indicates a fairly strong intermolecular interaction between carbon segments. In addition, Super C65 is sufficiently well dispersed and wetted by electrolyte, which has a positive effect on the electrochemical characteristics of EC.

a   *b*

c   *d*
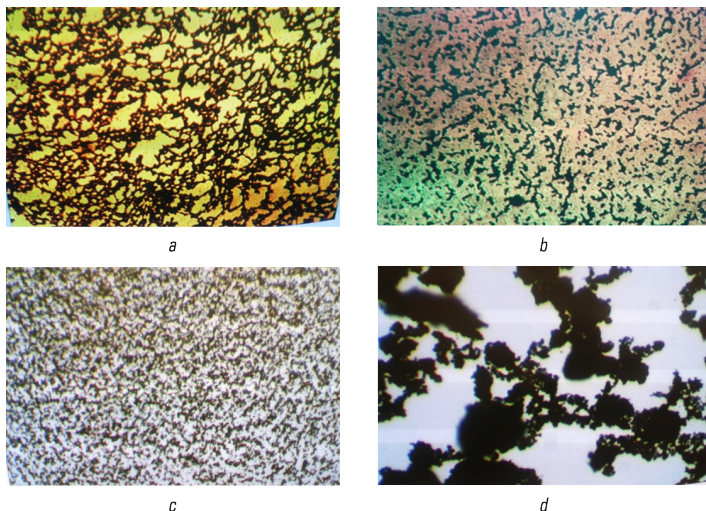
○ **Fig. 3.41** Micrographs of structures of various electrically conductive materials at 7x magnification: *a* – Super C65; *b* – acetylene soot; *c* – acetylene soot (Shawinigan); *d* – graphitized carbon soot (PureBlack-205)
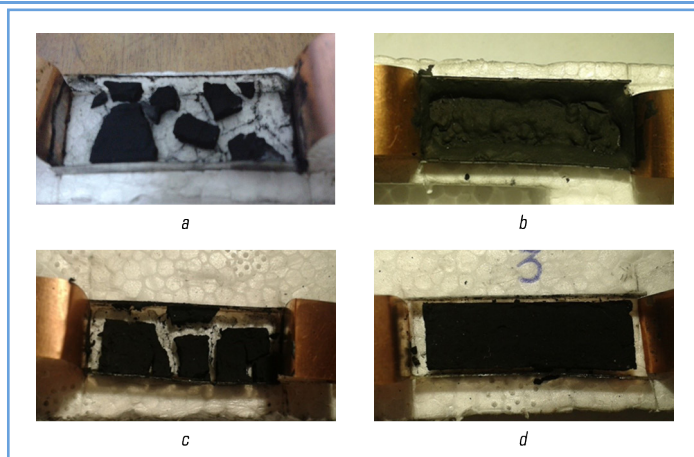
○ **Fig. 3.42** Image of shrinkage of a composite material based on various types of conductive additives after drying of the polymer binder: *a* – Super C65; *b* – acetylene soot; *c* – carbon Black 001; *d* – Pure Black

Optimization of the composition of the EC electrode

As was shown earlier, the state of the surface of the current collector of the electrode has a significant effect on the adhesion of the polymer [73, 74]. Therefore, surface-modified aluminum foil from Kawatake Electronics Co. was preferred as the metal current collector (Japan). As shown in **Fig. 3.43**, the contact surface of the active material and the metal is significantly increased due to the high porosity of the surface layer of the foil. Therefore, the production of EC electrodes was realized on the basis of aluminum foil from Kawatake Electronics Co. (Japan).

5 μm
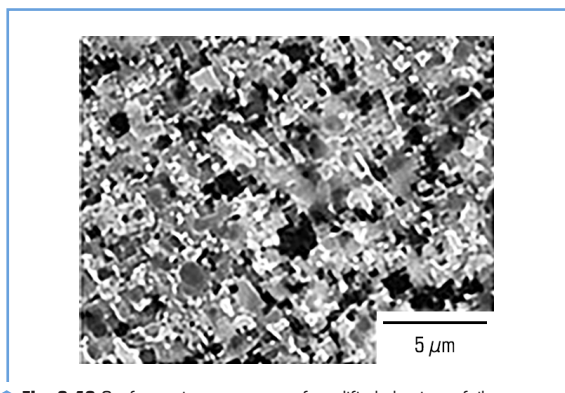
○ **Fig. 3.43** Surface microstructure of modified aluminum foil

CHAPTER 3

In this work, nitrogen sorption isotherms were obtained for electrode material samples based on selected YP-50F activated carbon and various polymeric materials. **Fig. 3.44** shows isotherms of sorption and desorption of nitrogen.
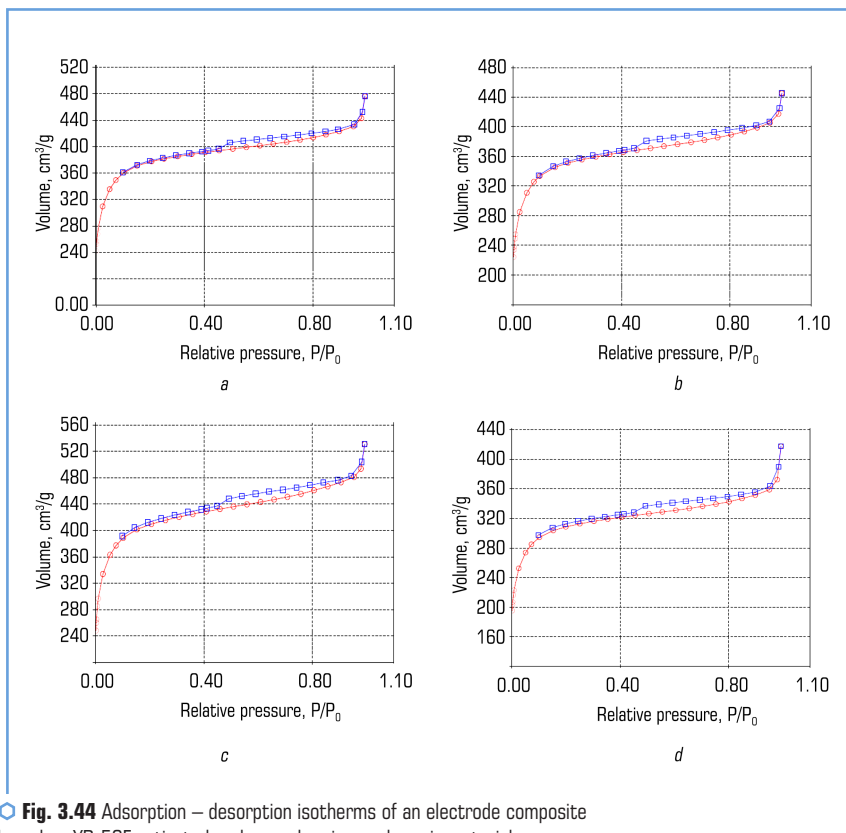
Fig. 3.44 Adsorption – desorption isotherms of an electrode composite based on YP-50F activated carbon and various polymeric materials: *a* — SBR; *b* — Solef XPH-859; *c* — Solef XPH-884; *d* — Solef 6020

The obtained isotherms are typical for polymolecular adsorption in micro and mesopores of cellular materials. For all samples, the isotherms show a hysteresis loop, which is associated with capillary condensation in mesopores. The parameters of the porous structure of the electrode compositions were determined based on the analysis of nitrogen adsorption/desorption isotherms.

As can be seen from **Fig. 3.45** and **3.46**, the introduction of a polymeric binder leads to a decrease in the specific surface area and total pore volume of the electrode composite.
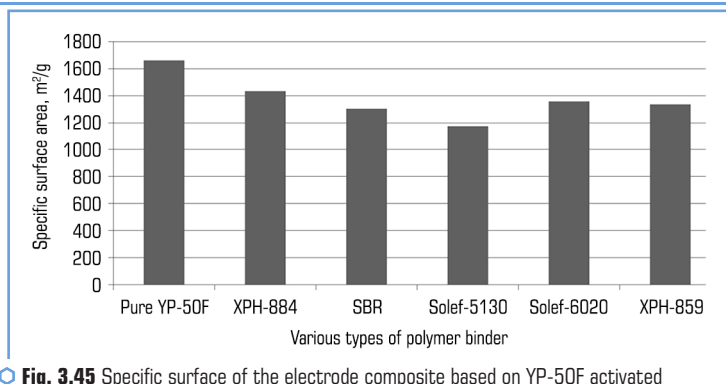
◯ **Fig. 3.45** Specific surface of the electrode composite based on YP-50F activated carbon and various polymeric materials (dry binder content — 10 %)
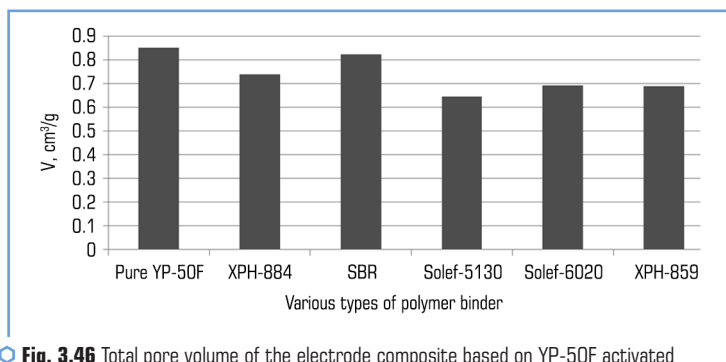
◯ **Fig. 3.46** Total pore volume of the electrode composite based on YP-50F activated carbon and various polymeric materials (10 % of the binder by dry residue)

According to the results of the study, the use of an aqueous suspension of Solef XPH-884 and SBR as a polymer for the electrode mass, in combination with a soluble sodium salt of CMC, makes it possible to obtain composites with the maximum specific surface area and the largest total pore volume. It should be noted that this binder fully met all the requirements for a polymer binder in the manufacture of electrochemical current sources [75–77]. The electrode composite had good adhesion to the metal current collector, ensured reliable connection of all components of the system, and left the surface of the active material as accessible as possible, which was confirmed by analysis.

Considering all the results obtained, a combination of an aqueous suspension of Solef XPH-884 with NaCMC in a ratio of 2:1 was proposed as a binder polymer. The latter served as a polymeric thickener and provided the necessary viscosity of the suspension for applying it to the metal current collector by the doctor blade method (**Fig. 3.47**).

CHAPTER 3

The first step in the manufacture of electrodes was to obtain a working solution of polymers containing a dispersed electrically conductive additive. To do this, a weighed portion of the Super C65 conductive additive was added to a solution of Solef XPH-884 with NaCMC in a ratio of 2:1 in three stages. Each introduction of carbon material into the solution was accompanied by mechanical stirring for 15 min and 10 min. The electrode mass was subjected to the action of ultrasound. Activated carbon YP-50F was also added to the prepared solution in three stages. To achieve a homogeneous mass, a combination of mechanical mixing and ultrasonic dispersion was also carried out. The second stage was the direct application of the electrode mass to the current collector. After the final drying, the electrodes were compacted by rolling at a temperature of 100 °C.

The microstructure of the obtained electrode is shown in **Fig. 3.48**.
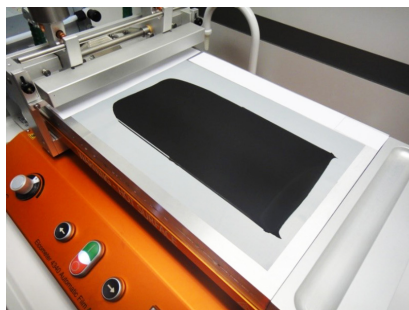
○ **Fig. 3.47** Image of the electrode on the device Dr. Blade after applying the YP-50F activated carbon suspension and the combination of Solef XPH-884 aqueous emulsion with NaCMC in a ratio of 2:1
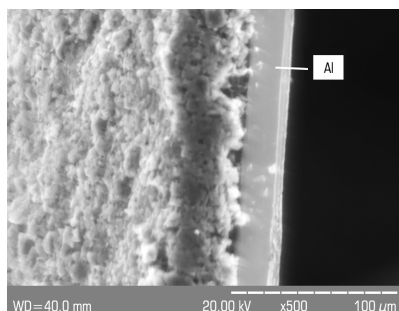
○ **Fig. 3.48** Photomicrograph of the surface and side cut of an electrode based on activated carbon YP-50F and a combination of an aqueous suspension of Solef XPH-884 with NaCMC in a ratio of 2:1

The active material layer has high strength and adheres tightly to the metal current collector. Also, the conductive additive is evenly distributed in the active layer. According to **Fig. 3.48**, the correct selection of technological parameters for applying an electrode suspension makes it possible to avoid the well-known defects of the electrode layer, which are typical for the manufacture of electrodes based on aqueous suspensions of polymers. In particular, there are no formations of agglomerates and holes in the electrode layer of the electrode.

Electrical characteristics of EC laboratory prototypes

In this work, compact ECs with an organic electrolyte were fabricated. EC mock-ups were made using body parts of primary lithium CDM of CR2016 size (**Fig. 3.49**).
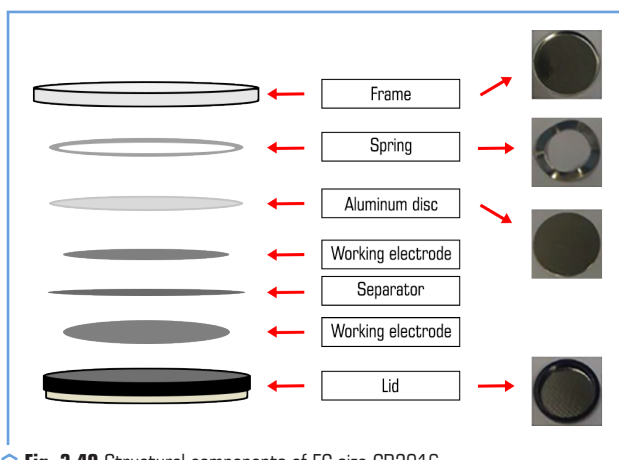
○ **Fig. 3.49** Structural components of EC size CR2016

Various organic electrolytes have been studied in this work. A solution of $TEABF_4$ in acetonitrile has the best electrical conductivity. For example, 1.5 M $TEABF_4$ in acetonitrile has the highest electrical conductivity (over 60 mS/cm) of organic electrolytes and allows the operation of electrochemical systems down to −40 °C.

However, such solutions have high chemical activity with respect to stainless steel-based EC body parts. Corrosion of body parts complicates the development of the EC design based on them. An aluminum disk 0.5 mm thick is used to protect the body parts. The electrolytes of lithium current sources allow the use of stainless steel body parts, which simplifies the selection and design of the EC, but they are significantly lower in electrical conductivity (13–15 mS/cm).

In the work, models of electrochemical capacitors based on manufactured electrodes with different electrolytes were compiled and tested. The CVs of capacitors with electrodes based on various electrolytes are shown in **Fig. 3.50**. The curves are rectangular, which is typical for an ideal

capacitor. On the CV of a capacitor with an electrolyte composition of 1.2 M LiTFSI in acetonitrile, a sharp increase in current is observed at a voltage above 2.5 V.

This may indicate the passage of corrosion processes in such EC.

Fig. 3.51 shows the impedance spectra of a symmetrical capacitor based on different electrolytes.
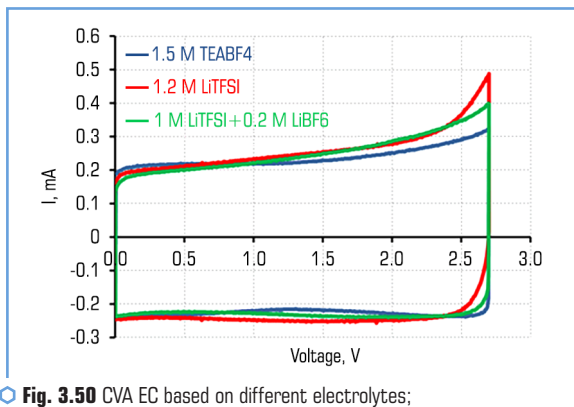
Fig. 3.50 CVA EC based on different electrolytes; EC voltage sweep rate – 10 mV/s
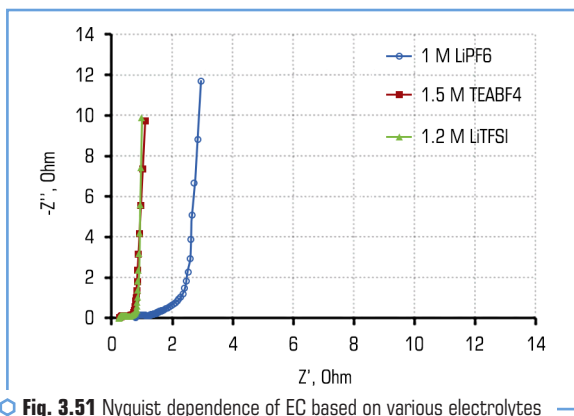
Fig. 3.51 Nyquist dependence of EC based on various electrolytes

The internal resistance of capacitors made with lithium battery electrolytes (1M $LiPF_6$ in EC:DMC) is three times higher than EC.

Therefore, we fabricated and studied ECs based on YP-50F activated carbon with the proposed combined composite binder: NaCMC Solef XPH-884 and electrolyte 1.5 M $TEABF_4$ in acetonitrile.

For comparison, ECs were also studied with electrodes made from binding PVDF according to the standard method (using solutions of PVDF in N-MP). The electrical characteristics of the developed EC are given in **Table 3.21**.

● **Table 3.21** Specific characteristics of laboratory models of EC

Electrode material		Characteristics*			
Activated carbon	Bonding material	Voltage, V	W, W·h/kg	Resistance, Ohm·cm	Pмах, kW/kg
YP-50F	Solef-6020	3.0	29	0.88	47
YP-50F	Solef-5130	3.0	26	1.43	34
YP-50F	Solef XPH-884 with NaCMC	3.0	33	0.67	73

* electrical characteristics are calculated without taking into account the mass of the EC body

In terms of electrical characteristics, the ECs based on a mixture of suspension PVDF and water-soluble NaCMC are not inferior to analogs manufactured by the standard method. One of the main advantages of the developed ECs is the avoidance of using the toxic organic solvent N-MP [78, 79]. This made it possible to ensure a low cost of EC production and improve the environmental situation in the manufacture of EC electrodes.

Laboratory studies of EC based on the proposed electrode composite showed that there is no significant change in their electrical characteristics after cycling. Experimental data obtained during the first 100 cycles show that the total capacitance loss of the capacitor is 3 %. The drop in capacity after a cycle for 10,000 charge/discharge cycles was less than 5 %.

CHAPTER 3

CONCLUSIONS

1. A technology has been developed for producing electrodes based on a mixture of an aqueous suspension of PVDF (Solef XPH-884) and a water-soluble sodium salt of CMC. These electrodes are not inferior in electrochemical characteristics to electrodes made using PVDF solutions, and in some cases even surpass them (for example, they provide a decrease in internal resistance up to 40 %). Due to the use of water-based components, the production of EC becomes cheaper and more environmentally friendly.

2. Taking into account the results of a comparative analysis of a series of PVDF samples of various modifications synthesized by Solvay, PVDF-6020 homopolymer and PVDF-5130 copolymer brands were chosen as a binder in electrode compositions. Of these, PVDF-5130 has the best adhesive properties (by 40÷75 %). However, this polymer significantly blocks the surface of activated carbon, thereby doubling the internal resistance of the EC, so its concentration in the electrode should not exceed 4 %.

3. The possibility of replacing the N-MP solvent for the PVDF polymer with a safer DMSO solvent for the manufacture of EC electrodes has been proven. The technological process of applying a suspension of the active material based on DMSO should be carried out at a temperature of 40–60 °C. The presence of functional groups in the polymer (for example, as in PVDF Solef-5130) leads to an increase in the content of sulfur-containing products (up to 400–600 g) in the active layer of the electrode. The source of sulfur-containing compounds are the decomposition products of DMSO. Getting into the electrolyte EC, they cause side reactions leading to self-discharge of the EC and limiting its operating voltage to 1.5 V, as well as a drop in capacity during cycling. However, the replacement of the toxic solvent by DMSO becomes possible with additional washing of the EC electrodes with ethyl alcohol.

4. Comprehensive studies have been carried out on the process of formation of EC strip electrodes with an active layer thickness of up to 100 μm. Technological parameters of the process of formation of EC electrodes and their operational characteristics are established. A technological scheme for the production of electrodes is proposed.

5. It is shown that the highest capacity of electrodes based on an aqueous suspension of PVDF and water-soluble NaCMC corresponds to a polymer content of 6 %; drying of the electrodes should be carried out in two stages — at 60 °C for 15…20 minutes, then at 120 °C in a vacuum; the density of the active layer of electrodes should be 0.6…0.8 g/cm^3; Increasing the temperature of the rollers during rolling up to 100 °C makes it possible to increase the density and strength of the electrodes up to 2 times.

6. Prototypes of stable ECs have been developed, where for the first time new composite materials based on a mixture of water-soluble suspensions of PVDF (Solef XPH-884) and NaCMC are used. The specific energy of laboratory prototypes of ECs is 33 Wh/kg, which is almost an order of magnitude higher than the energy of traditional ECs with electrodes made using PVDF solutions in N-MP.

CONFLICT OF INTEREST

The authors declare that they have no conflict of interest in relation to this research, whether financial, personal, authorship or otherwise, that could affect the research and its results presented in this paper.

REFERENCES

1. Wang, Y., Song, Y., Xia, Y. (2016). Electrochemical capacitors: mechanism, materials, systems, characterization and applications. Chemical Society Reviews, 45 (21), 5925–5950. doi: https://doi.org/10.1039/c5cs00580a

CHAPTER 3

2. Ali, A., Andriyana, A. (2020). Properties of multifunctional composite materials based on nanomaterials: a review. RSC Advances, 10 (28), 16390–16403. doi: https://doi.org/10.1039/c9ra10594h

3. Malietin, Yu., Stryzhakova, N., Zelinskyi, S. et al. (2011). Cuperkondensatory – nakopychuvachi elektrychnoi enerhii z vykorystanniam nanorozmirnykh vuhletsevykh materialiv. Visnyk NAN Ukrainy, 12, 23–29.

4. Vivekchand, S. R. C., Rout, C. S., Subrahmanyam, K. S., Govindaraj, A., Rao, C. N. R. (2008). Graphene-based electrochemical supercapacitors. Journal of Chemical Sciences, 120 (1), 9–13. doi: https://doi.org/10.1007/s12039-008-0002-7

5. Stoller, M., Zhu, Y., Ruoff, R. (2008). Graphene-based ultracapacitors. Proc. 18th Intern. Seminar on Double Layer Capacitors and Hybrid Energy Storage Devices, 4–7.

6. Burke, A. (2007). R&D considerations for the performance and application of electrochemical capacitors. Electrochimica Acta, 53 (3), 1083–1091. doi: https://doi.org/10.1016/j.electacta.2007.01.011

7. Kurzweil, P. (2009). HISTORY | Electrochemical Capacitors. Encyclopedia of Electrochemical Power Sources, 596–606. doi: https://doi.org/10.1016/b978-044452745-5.00006-x

8. Noori, A., El-Kady, M. F., Rahmanifar, M. S., Kaner, R. B., Mousavi, M. F. (2019). Towards establishing standard performance metrics for batteries, supercapacitors and beyond. Chemical Society Reviews, 48 (5), 1272–1341. doi: https://doi.org/10.1039/c8cs00581h

9. Murphy, T. C., Wright, R. B., Sutula, R. A. (1997). Electrochemical Capacitors II, Proceedings. The Electrochemical Society. Pennington, 96, 258.

10. Miller, J. R., Burke, A. (2008). Electrochemical Capacitors: Challenges and Opportunities for Real-World Applications. The Electrochemical Society Interface, 17 (1), 53–57. doi: https://doi.org/10.1149/2.f08081if

11. Delhaes, P. (2019). Graphite and Precursors. CRC Press, 312.

12. Drobnyi, D. M., Tychyna, S. O., Stryzhakova, N. H., Malietin, Yu. A. (2015). Polimerni materialy dlia kompozytnykh elektrodiv superkondensatoriv. Perspektyvni polimerni materialy ta tekhnolohii. Kyiv, 19–23.

13. Malietin, Yu. A., Shembel, O. M., Novak, P., Podmohilnyi, S. M., Stryzhakova, N. H., Izotov, V. Yu. et al. (2010). Pat. Ukrainy No. 90448 UA. Metod vyhotovlennia elektrodiv z nyzkym kontaktnym oporom dlia batarei ta kondensatoriv podviinoho sharu. MPK: H01G 9/00, H01G 9/155 (2006.01). No. a200506296. declareted: 25.06.2005; published: 11.15.2010.

14. Izotov, V. Yu., Biriukova, Yu. V. (2008). Pat. No. 35069U. Elektrod dlia kondensatoriv podviinoho elektrychnoho sharu. MPK: H01G 9/00. No. u200805440. declareted: 25.04.2008; published: 26.08.2008.

15. Baklan, V. Yu., Korolenko, S. D. (2010). Stan ta perspektyvy rozvytku khimichnykh dzherel strumu. Visnyk KNUTD, 5, 227–232.

16. Merena, R. I., Budzuliak, I. M., Hryhorchak, I. I. et al. (2004). Doslidzhennia kharakterystyk elektrokhimichnykh kondensatoriv, sformovanykh na osnovi aktyvovanoho vuhletsiu, modyfikovanoho vysokotemperaturnoiu obrobkoiu. Fizyka i khimiia tverdoho tila, 5 (4), 836–839.

CHAPTER 3

17. Béguin, F., Presser, V., Balducci, A., Frackowiak, E. (2014). Carbons and Electrolytes for Advanced Supercapacitors. Advanced Materials, 26 (14), 2219–2251. doi: https://doi.org/10.1002/adma.201304137

18. Conway, B. E. (1999). Electrochemical supercapacitors. Scientific fundamentals and technological applications. New York, 698.

19. Drobnyi, D. (2017). Pat. No. WO2017025792 A1. Sposob izgotovleniia elektroda dlia elektrokhimicheskogo kondensatora dvoinogo sloia. MPK: H01G11/86; declareted: 09.08.2016; published: 16.02.2017.

20. Pashkevich, K., Yezhova, O., Kolosnichenko, M., Ostapenko, N., Kolosnichenko, E. (2018). Designing of the complex forms of women's clothing, considering the former properties of the materials. Man-Made Textiles in India, 46 (11), 372–380.

21. Ellis, B., Smith, R. (2020). Polymers A Property Database. CRC Press, 1052.

22. Horonovskyi, Y. T., Nazarenko, Yu. P., Nekreh, E. F. (1974). Kratkyi spravochnyk po khymyy. Kyiv: Naukova dumka, 830.

23. Barzic, A. I., Rawat, N. K., Haghi, A. K. (Eds.) (2021). Imidic Polymers and Green Polymer Chemistry. New York: Apple Academic Press, 380. doi: https://doi.org/10.1201/9781003057918

24. Schwartz, M. (2008). Smart Materials. CRC Press, 554.

25. Marphy, R., Krehl, P., Liang, C. (1981). Technologies for the Transition. 16th Intersociety Energy Conversion Engineering Conference. New York, 1, 97.

26. Perelmuter, V. (2017). Electrotechnical Systems. Simulation with Simulink® and SimPowerSystems™. CRC Press, 450.

27. Gür, T. M. (2018). Review of electrical energy storage technologies, materials and systems: challenges and prospects for large-scale grid storage. Energy & Environmental Science, 11 (10), 2696–2767. doi: https://doi.org/10.1039/c8ee01419a

28. Broussely, M., Bodet, J. M., Staniewicz, R. J. (1994). Proceedings of the Symposium on Rechargeable Lithium and Litium-ion Batteries. Extended Abstracts of Fall Meeting of the Electrochemical Society. Maimi Beach, 224.

29. Pat. No. 2249455 FR. Kondensator pereminnoi yemnosti (1975). Kl. NO1 m 13/06, declareted: 29.10.73, published: 23.05.75.

30. Haghi, A. K., Ribeiro, A. C. F., Pogliani, L., Balköse, D., Torrens, F., Mukbaniani, O. V. (2021). Applied Chemistry and Chemical Engineering, Research Methodologies in Modern Chemistry and Applied Science. Apple Academic Press, 390.

31. Moore, J. H., Spencer, N. D. (2001). Encyclopedia of Chemical Physics and Physical Chemistry. CRC Press, 2814.

32. Uendland, U. (1978). Termicheskie metody analiza. Moscow, 279.

33. Song, M.-K., Cairns, E. J., Zhang, Y. (2013). Lithium/sulfur batteries with high specific energy: old challenges and new opportunities. Nanoscale, 5 (6), 2186–2204. doi: https://doi.org/10.1039/c2nr33044j

CHAPTER 3

34. Kolosnichenko, O., Yakovlev, M., Prykhodko-Kononenko, I., Tretyakova, L., Ostapenko, N., Pashkevich, K., Ripka, G. (2020). Study of dominant quality indicators of materials and designs of railroad conductors' uniforms. Vlákna a textile, 3 (27), 90–96.

35. Shlaiker, C., Young, C. (1980). Batteries for implantable biomedical devices. 29th Power Sources Symposium, 129.

36. Borshch, A. V., Chernysh, O. V. (2016). Porivniannia kharakterystyk polivinilidenftorydiv 6020 ta 5130 v elektrodnykh kompozytnykh materialakh. Naukovi rozrobky molodi na suchasnomu etapi, 1, 297.

37. Zaiets, O. V., Tverdokhlib, V. S. (2004). Vlastyvosti polimernoho zv'iazuiuchoho aktyvnykh mas litii-ionnykh dzherel strumu. Naukovi rozrobky molodi na suchasnomu etapi, 1, 159.

38. Zaiets, O. V., Tverdokhlib, V. S. (2005). Vyvchennia vlastyvostei polimernoho zv'iazuiuchoho PVDF u yon-litiievykh dzherelakh strumu. Naukovi rozrobky molodi na suchasnomu etapi, 1, 184.

39. Chernysh, O. V., Khomenko, V. H., Barsukov, V. Z., Borshch, A. V. (2016). Vplyv tekhnolohichnykh modyfikatsii polivinilidenftorydu na fizyko-mekhanichni vlastyvosti elektrodiv khimichnykh dzherel strumu. Visnyk KNUTD, 5, 141–148.

40. Wang, F., Wu, X., Yuan, X., Liu, Z., Zhang, Y., Fu, L., Zhu, Y., Zhou, Q., Wu, Y., Huang, W. (2017). Latest advances in supercapacitors: from new electrode materials to novel device designs. Chemical Society Reviews, 46 (22), 6816–6854. doi: https://doi.org/10.1039/c7cs00205j

41. Zaiets, O. V., Kolodii, I. O., Mykoliuk, S. V. (2006). Optymizatsiia umov vysushuvannia aktyvnykh mas litii-ionnykh KhDS. Naukovi rozrobky molodi na suchasnomu etapi, 1, 232.

42. Veres, A. R., Drahan, D. R., Chernysh, O. V. (2014). Mozhlyvosti vykorystannia vodorozchynnykh zv'iazuiuchykh v kompozytnykh elektrodnykh materialakh. Naukovi rozrobky molodi na suchasnomu etapi, 1, 367–368.

43. Zhao, W. (2020). Handbook for Chemical Process Research and Development. CRC Press, 858.

44. Simon, P., Gogotsi, Y. (2020). Perspectives for electrochemical capacitors and related devices. Nature Materials, 19 (11), 1151–1163. doi: https://doi.org/10.1038/s41563-020-0747-z

45. Wypych, G. (2016). Handbook of Polymers. ChemTec Publishing, 706. doi: https://doi.org/10.1016/c2015-0-01462-9

46. Namsheer, K., Rout, C. S. (2021). Conducting polymers: a comprehensive review on recent advances in synthesis, properties and applications. RSC Advances, 11 (10), 5659–5697. doi: https://doi.org/10.1039/d0ra07800j

47. Barsukov, V. Z., Khomenko, V. G., Chernysh, O. V. et al. (2016). Perspektivnye materialy i tekhnologii dlia sovremennykh KhIT i elektronnoi tekhniki. Sovremennye elektrokhimicheskie tekhnologii i oborudovanie. Minsk, 147–148.

48. Barsukov, V., Khomenko, V., Chernysh, O., Makyeyeva, I. (2016). Modern materials for lithium-ion batteries and supercapacitors. 11th International conference on physics of advanced materials. Cluj-Napoca, 122.

CHAPTER 3

49. Hank Ellison, D. (2022). Handbook of Chemical and Biological Warfare Agents. CRC Press, 838. doi: https://doi.org/10.4324/9781003230564

50. Saldívar-Guerra, E., Vivaldo-Lima, E. (Eds.) (2013). Handbook of Polymer Synthesis, Characterization, and Processing. John Wiley & Sons, Inc., 622. doi: https://doi.org/10.1002/9781118480793

51. Lendlein, A., Sisson, A. (Eds.) (2001). Handbook of Biodegradable Polymers: Synthesis, Characterization and Applications. WILEY-VCH, 426.

52. Balköse, D., Horak, D., Šoltés, L. (2021). Key Engineering Materials, Current State-of-the-Art on Novel Materials. Apple Academic Press, 584.

53. Roy Crompton, T. (2017). Organic Compounds in Natural Waters Analysis and Determination. CRC Press, 306.

54. Peebles, L. H. (1995). Carbon Fibers Formation, Structure, and Properties. CRC Press, 218.

55. Dragan, E. S. (2021). Advanced Separations by Specialized Sorbents. CRC Press, 358.

56. Webster, G. K., Kott, L. (Eds.) (2019). Chromatographic Methods Development. Jenny Stanford Publishing, 566. doi: https://doi.org/10.1201/9780429201721

57. Uwamariya, V. (2014). Adsorptive Removal of Heavy Metals from Groundwater by Iron Oxide Based Adsorbents. CRC Press, 160.

58. Barsukov, V. Z., Il'in, E. A., Likhnitskii, K. V., Zayats, O. V., Tverdokhleb, V. S., Kryukov, V. V. et al. (2008). Graphites from the Zavalie deposit as active materials for lithium-ion batteries. Russian Journal of Electrochemistry, 44 (5), 579–584. doi: https://doi.org/10.1134/s1023193508050121

59. Lynch, C. T. (2021). CRC Handbook of Materials Science. Material Composites and Refractory Materials. CRC Press, 654.

60. Barsukov, V. Z., Chernysh, O. V., Plavan, V. P. (2013). Stiikist do okyslennia zvychainoho i modyfikovanoho rozshyrenoho hrafitu. Tekhnolohii ta dyzain. Khimichni tekhnolohii ta ekolohichna bezpeka, 3, 1–8.

61. Khomenko, V. H., Barsukov, V. Z., Makieieva, I. S., Chernysh, O. V. (2016). Vplyv hrafitovykh materialiv na elektrychni kharakterystyky litii-ionnykh kondensatoriv. Perspektyvni materialy ta protsesy v tekhnichnii elektrokhimii. Kyiv, 22–26.

62. Zaiets, O. V., Shkromyda, R. V., Davydov, O. S. (2006). Vplyv dyspersnosti chastochok na vlastyvosti pryrodnoho hrafitu. Naukovi rozrobky molodi na suchasnomu etapi, 1, 233.

63. Barsukov, V., Langouche, F., Khomenko, V., Makyeyeva, I., Chernysh, O., Gauthy, F. (2015). Modeling of porous graphite electrodes of hybride electrochemical capacitors and lithium-ion batteries. Journal of Solid State Electrochemistry, 19 (9), 2723–2732. doi: https://doi.org/10.1007/s10008-015-2835-6

64. Kim, J.-A., Park, I.-S., Seo, J.-H., Lee, J.-J. (2014). A Development of High Power Activated Carbon Using the KOH Activation of Soft Carbon Series Cokes. Transactions on Electrical and Electronic Materials, 15 (2), 81–86. doi: https://doi.org/10.4313/teem.2014.15.2.81

CHAPTER 3

65. Chernysh, S. I., Chernysh, I. H., Nikitin, Yu. O., Loboda, P. I. (2008). Pro vplyv metodiv dysperhuvannia na mikrostrukturu i morfolohiiu dyspersnykh chastynok pryrodnoho hrafitu ta termohrafenitu. Naukovi visti NTUU "KPI", 1, 76–80.

66. Wang, G., Yu, M., Feng, X. (2021). Carbon materials for ion-intercalation involved rechargeable battery technologies. Chemical Society Reviews, 50 (4), 2388–2443. doi: https://doi.org/10.1039/d0cs00187b

67. Struminska, T. V., Kolosnichenko, S. I., Chuprina, E. V., Ostapenko, N. V. (2019). Designing of special clothing based on experimental researches of material properties. Fibres and Textiles, 26 (4), 84–95.

68. Khomenko, V., Raymundo-Piñero, E., Béguin, F. (2008). High-energy density graphite/AC capacitor in organic electrolyte. Journal of Power Sources, 177 (2), 643–651. doi: https://doi.org/10.1016/j.jpowsour.2007.11.101

69. Cao, W. J., Zheng, J. P. (2012). Li-ion capacitors with carbon cathode and hard carbon/stabilized lithium metal powder anode electrodes. Journal of Power Sources, 213, 180–185. doi: https://doi.org/10.1016/j.jpowsour.2012.04.033

70. Schroeder, M., Winter, M., Passerini, S., Balducci, A. (2012). On the Use of Soft Carbon and Propylene Carbonate-Based Electrolytes in Lithium-Ion Capacitors. Journal of The Electrochemical Society, 159 (8), A1240–A1245. doi: https://doi.org/10.1149/2.050208jes

71. Rezqita, A., Hamid, R., Schwarz, S., Kronberger, H., Trifonova, A. (2015). Conductive Additive for Si/Mesoporous Carbon Anode for Li-Ion Batteries: Commercial Graphite vs Carbon Black C65. ECS Transactions, 66 (9), 17–27. doi: https://doi.org/10.1149/06609.0017ecst

72. Schütter, C., Ramirez-Castro, C., Oljaca, M., Passerini, S., Winter, M., Balducci, A. (2014). Activated Carbon, Carbon Blacks and Graphene Based Nanoplatelets as Active Materials for Electrochemical Double Layer Capacitors: A Comparative Study. Journal of The Electrochemical Society, 162 (1), A44–A51. doi: https://doi.org/10.1149/2.0381501jes

73. Chernysh, O. V., Khomenko, V. H., Barsukov, V. Z. (2016). Vplyv morfolohii poverkhni aliuminiievoho strumovidvodu na adheziiu elektrodnoho materialu i opir elektrokhimichnoho kondensatora. Visnyk KNUTD, 6, 188–194.

74. Borshch, A. V., Chernysh, O. V. (2015). Doslidzhennia nadiinosti kontaktu robochoi masy superkondensatora do metalevoho strumovidvodu. Naukovi rozrobky molodi na suchasnomu etapi, 1, 316.

75. Khomenko, V., Barsukov, V., Chernysh, O., Makyeyeva, I., Isikli, S., Gauthy, F. (2016). Green Alternative binders for high-voltage electrochemical capacitors. IOP Conference Series: Materials Science and Engineering, 111, 012025. doi: https://doi.org/10.1088/1757-899x/111/1/012025

76. Chernysh, O. V., Khomenko, V. H., Makieieva, I. S., Barsukov, V. Z. (2015). Vodorozchynni polimerni kompozytsii dlia khimichnykh dzherel strumu. Perspektyvni polimerni materialy ta tekhnolohii. Kyiv, 101–106.

CHAPTER 3

77. Barsukov, V., Khomenko, V., Chernysh, O. et al. (2015). Green alternative binders for high voltage electrochemical capacitors and lithium-ion batteries. Baltic Polymer Symposium. Sigulda, 35.

78. Barsukov, V. Z., Khomenko, V. G., Senik, I. V., Chernysh, O. V. (2013). Litievye batarei dlia primeneniia na transporte: sovremennye problemy i perspektivy. Voprosy khimii i khimicheskoi tekhnologi, 4, 127–131.

79. Khomenko, V., Barsukov, V., Chernysh, O. et al. (2015). Development of Advanced Lithium-Ion Capacitors. 6th International Conference on Carbon for Energy Storage, Conversion and Environment Protection "CESEP' 2015". Poznan, 64.

Natalia Minska, Roman Shevchenko, Vasyl Servatyuk,
Valery Strelets, Victoria Lukashenko, Yaroslav Kalchenko

CHAPTER 4

STRUCTURAL AND TECHNOLOGICAL SOLUTIONS FOR FILM SOLAR CELLS BASED ON CDS/CDTE FOR RESERVE POWER SUPPLY OF EMERGENCY PREVENTION SYSTEMS

ABSTRACT

Investigations of solar cells based on CdS/CdTe, designed for reserve power supply of security systems and control of objects in conditions of damage to the power supply system, have been carried out. An analysis is made of losses in the initial parameters of solar cells based on cadmium telluride, which are due to the design features of the device structure and photoelectric processes occurring in their volume upon absorption of light. Implemented approaches to increasing the efficiency of a photocell based on CdS/CdTe and their effectiveness are studied. Ways are proposed to increase the efficiency of such film solar cells by improving the method of obtaining a rear contact. Design and technological solutions for SC ITO/CdS/CdTe/Cu/Au have been developed, which make it possible to obtain laboratory samples with an efficiency factor of more than 10 %. Laboratory samples of ITO/CdS/CdTe/Cu/ITO CEs have been fabricated, the two-sided illumination of which makes it possible to increase the electric power by 30 %. The research of Cu/ITO transparent rear contacts for CdTe-based solar cells intended for use in tandem and bilaterally sensitive device structures have been studied. The study of the light Current-voltage characteristics of SnO_2:F/CdS/CdTe/Cu/ITO solar cells under illumination from both sides made it possible to establish significant differences in the initial parameters and light diode characteristics under illumination from the side of the glass substrate and from the side of the transparent rear electrode. Testing of laboratory samples of ITO/CdS/CdTe/Cu/ITO solar cells as part of tandem photovoltaic converters has been carried out. Research has been carried out on methods for obtaining CdTe base layers for creating efficient solar cells on a flexible substrate. With a series connection of ITO/CdS/CdTe/Cu/Au SC, experimental samples of micromodules with an efficiency of 5.4 % have been obtained.

KEYWORDS

Film solar cell, cadmium telluride, rear contact, transparent rear contact, tandem structure, two-sided sensitive solar cell, flexible substrate, micromodule.

CHAPTER 4

An analysis of emergency situations shows that one of the problems of localization and elimination of consequences is power outages due to damage to power lines. Therefore, it is necessary to provide emergency power supplies or the tools used must work autonomously.

Modern security and control systems consume only a small part of the total energy consumption of the facility, their uninterrupted operation is ensured by the presence of electricity in the network. As a rule, such security systems have a backup power source in case of an emergency power outage in the network, but in most cases, its charge lasts no more than 24 hours. In this case, the use of solar cells becomes relevant. In general, the scope of solar panels is expanding every day. Sometimes the most unexpected branches of industry and the national economy turn to solar cells for help [1–3]. Solar cells are out of competition in places where there is no conventional power grid, but there is enough sun, or in the event of long-term damage to the grid supply of electricity.

Photovoltaic technology is one of the most important renewable energy sources, for which, since its first recognition in 1839, many studies have been carried out to improve their efficiency. But improving the efficiency and reducing the cost of photovoltaic technology still requires a lot of effort. Crystalline silicon (c-Si) solar cells are known as materials in first generation solar cells. In terms of cost, performance and manufacturability, the application of new advanced materials such as amorphous silicon (a-Si), cadmium telluride (CdTe) and indium gallium copper diselenide (CIGS) is achieved in the second and third generations of solar cells. The typical conversion efficiency of first generation technologies is currently between 15 % and 24 %, while that of second generation technologies is currently between 7 % and 16 %. The unique physical characteristics of CdTe make it possible to use the material to create a number of microelectronic devices. Cadmium chalcogenide films are increasingly being used as the base layers of various devices. The main goal of many scientific studies of cadmium telluride should be considered the development of a technology for obtaining thin films of the compound with certain electrical parameters.

Therefore, an urgent topic is the development of approaches to the use of CdTe-based photovoltaic cells for redundant security and control systems in the event of a long-term power outage from utility networks.

4.1 STUDY OF FILM SOLAR CELLS BASED ON CDS/CDTE

4.1.1 IMPROVING THE EFFICIENCY OF FILM SOLAR CELLS BASED ON CDS/CDTE

Solar cells based on crystalline silicon and thin films are the most common commercial technologies in the field of photovoltaics. However, the dominant position in the market is occupied by solar cells based on crystalline silicon, the serial production of which is 85 % of the world production of all photovoltaic converters [4]. In the manufacture of this type of SC, high-quality raw materials are used, the production of which is currently energy-intensive. In addition, SC based on single-crystal

and polycrystalline silicon are indirect-gap conductors and, accordingly, have a low absorption co-efficient. Therefore, for the effective use of solar radiation, the thickness of the base layers should not be less than 200 microns. Also, in such device structures, a significant decrease in efficiency with increasing temperature is observed.

Promising technologies for terrestrial application are solar cells based on CdTe [5].

The formation of such instrumental structures is carried out with less energy consumption for their manufacture. In addition, the technology for producing CdS/CdTe films is rapidly reproducible and makes it possible to form uniform thin films with an area of more than 1 m^2, which have the highest theoretical efficiency among single-junction photovoltaic converters, 29 % [6]. However, the maximum experimental efficiency is 16.5 % and was recorded for SC based on the CdS/CdTe heterosystem when implementing the back-barrier structure of the devices [7], shown in **Fig. 4.1**.
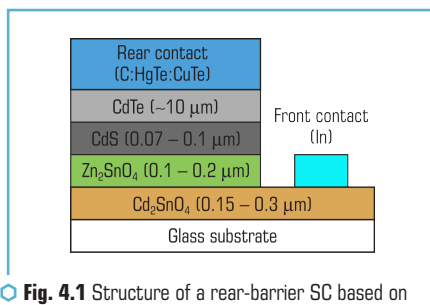
○ **Fig. 4.1** Structure of a rear-barrier SC based on CdS/CdTe with an efficiency of −16.5 %

To achieve such high values of the efficiency of creation, shown in **Fig. 4.1**, SC was carried out on borosilicate glass [7], which is more valuable than traditional SiO$_2$. The TCO (In$_2$O$_3$SnO$_2$) layer was replaced with a TCO (Cd$_2$SnO) layer [7] because the leading oxide Cd$_2$SnO$_4$ has a better combination of optical and electrical properties and has a higher transparency (over 90 %). Thin CdS films were deposited using an aqueous solution of Cd(C$_2$H$_3$O$_2$)$_2$, C$_2$H$_3$O$_2$NH$_4$ CS(NH$_2$)$_2$ NH$_4$OH and according to the technology described in [8]. The deposition of CdTe was carried out by sublimation in a closed space. After CdTe deposition, the samples were subjected to chloride treatment, which is a mandatory procedure for the formation of efficient CdTe-based SCs [9, 10]. Without chloride treatment, the efficiency of CdTe-based SC is typically <5 %. The chloride treatment is believed to increase the grain size of CdTe, passivate their grain boundaries, and promote efficient adhesion of CdS and CdTe. To form a rear contact, HgTe:CuTe graphite paste was applied, followed by the deposition of silver paste and an antireflection MgF$_2$ layer.

However, despite the implemented technologies, the efficiency of the obtained samples is far from the theoretical value. Since the formation of stable low-resistance rear contacts is another important step in the fabrication of high-performance CEs based on CdTe/CdS [11].

CHAPTER 4

The main technological approach implemented by many authors when creating low-resistance contacts to SCs based on CdS/CdTe is the formation of tunnel contacts [12]. The formation of an ohmic contact to the p-CdTe base layer under industrial production conditions is not economical, since only platinum has the electron work function necessary for the formation of an ohmic transition. Therefore, tunneling contacts are traditionally formed to p-CdTe layers using thin films containing copper or copper chalcogenide [12]. However, the diffusion of copper into the base layer leads to degradation of the initial parameters of film CEs based on CdS/CdTe. Therefore, comprehensive studies are needed to develop rear contacts in CdTe base layers to create highly efficient, degradation-resistant solar cells.

4.1.2 ANALYSIS OF LOSSES IN THE INITIAL PARAMETERS OF SOLAR CELLS BASED ON CDS/CDTE

The main characteristic of any solar cell is the coefficient of performance (COP). The value of the efficiency of any solar cell is calculated by the formula [13]:

$$\eta = \left(P_{HM} / P_u \right) \times 100\ \% = \left[P_{HM} / \left(P_{r^*} S_{ce} \right) \right] \times 100\ \%, \tag{4.1}$$

where P_{r^*} – the specific radiation power on the photoreceiving surface of the solar cell; S_{ce} – the area of the photoreceiving surface of the solar cell.

The power P_{HM} depends on three experimentally determined initial parameters of the SC as follows:

$$P_{HM} = I_{sc} V_{nl} FF, \tag{4.2}$$

where I_{sc} – the short-circuit current; V_{nl} – the no-load voltage; FF – the filling factor of the light current-voltage characteristic.

Therefore, to calculate the efficiency of a photoelectric converter, along with formula (4.1), the following relation is used:

$$\eta = \left[I_{sc} V_{nl} FF / \left(P_{r^*} S_{ce} \right) \right] \times 100\ \%. \tag{4.3}$$

As can be seen from expression (4.3), the efficiency increases with an increase in each of the three key initial SC parameters – I_{sc}, V_{nl} and FF, and therefore it is necessary to analyze the losses of these quantities.

Short-circuit current density losses (J_{sc}) in the SC are due to the following processes:
– reflection of solar radiation from the surface of the instrumental structure;
– absorption of solar radiation in photoelectrically inactive layers;
– absorption of light in the area of contacts.

The short circuit current density is determined by the following analytical expression:

$$J_{sc} = \int_{\lambda_{min}}^{\lambda_{max}} Q_E(\lambda) J_{sol}(\lambda) d\lambda, \qquad (4.4)$$

where $Q_E(\lambda)$ – the quantum efficiency coefficient, J_{sol} – the intensity of solar radiation. The losses corresponding to each of the actions described above can be calculated using the following expression:

$$J_{loss} = \int_{\lambda_{min}}^{\lambda_{max}} F(\lambda) J_{sol} d\lambda, \qquad (4.5)$$

where $F(\lambda)$ – the partial reflection or absorption of each wavelength.

The sum of losses and quantum efficiency (Q_E) values should be equal to units for all wavelengths.

The main physical mechanisms that cause losses in the value of the open-circuit voltage have not been sufficiently studied at present. It is believed that Vnl is limited by the dominant current flow mechanism. The current-voltage characteristics of a typical solar cell is described as follows [13]:

$$J \approx J_0 \exp\left[\frac{q(V - V_{p-n})}{AkT}\right] - J_p, \qquad (4.6)$$

where J_p – the photocurrent density; J_0 – the saturation diode current density; V – the voltage drop across the SC; V_{p-n} – the potential barrier height; q – the electron charge; k – the Boltzmann constant; T – the temperature of the solar cell; A – the diode ideality factor. Saturation diode current density (J_0) depends on the specific operating mechanism that dominates the forward current flow. Let's assume that the processes in CdTe solar cells are mainly controlled by volume recombination and, therefore, J_0 can be expressed as:

$$J_0 = qpv_r, \qquad (4.7)$$

where p – the hole concentration; v_r – the recombination rate. Thus, V_{nl} can be represented as:

$$V_{nl} = V_{p-n} - \frac{AkT}{q}\ln\left(\frac{qpv_r}{J_p}\right). \qquad (4.8)$$

The expression relating the height of the potential barrier and the band gap (E_g) looks like this:

$$V_{p-n} = \frac{E_g}{q} - \frac{kT}{q}\ln\left(\frac{N_v}{p}\right), \qquad (4.9)$$

where N_v – the effective density of states in the valence band.

CHAPTER 4

143

So for $A = 2$:

$$V_{nl} = \frac{E_g}{q} - \frac{kT}{q}\ln\left(\frac{q^2 N_v p v_r^2}{J_p^2}\right).$$ (4.10)

Regardless of the details, V_{nl} decreases with increasing recombination rate. Thus, a decrease in recombination should contribute to an increase in V_{nl}. The ratio of recombination rate to thermal rate is expressed as (v_r/v_t), where v_t is 107 cm/s, and is used as the primary recombination parameter for voltage loss analysis.

To analyze the losses in the value of the replenishment factor of the light current-voltage characteristic (*FF*), an empirical expression is used that determines the dependence of *FF* on the open-circuit voltage (V_{nl}), diode ideality factor (A), series resistance (R_p) and shunt conductivity (G).

In the absence of series resistance and shunt conductance, the expression for FF can be represented as [14]:

$$FF_0 = \frac{v_{nl} - \ln(v_{nl} + 0.72)}{v_{nl} + 1},$$ (4.11)

where

$$v_{nl} = \frac{qV_{nl}}{AkT}.$$ (4.12)

In the presence of a series resistance (R_s), the expression for the filling factor of the light current-voltage characteristic (FF_s) becomes:

$$FF_s = FF_0\left(1 - R_s / R_E\right),$$ (4.13)

where $R_x = V_{nl}/J_{sc}$ – characteristic impedance. When the series resistance (R_s) and shunt conductance (G) are significant, the expression for the duty factor of the light current-voltage characteristic (FF_{s+w}) is:

$$FF_{s+w} = FF_s\left[1 - \frac{(v_{nl} + 0.72)FF_s}{v_{nl} / (R_E G)}\right].$$ (4.14)

According to expression (4.14), it is obvious that an increase in the value of FF_{s+w} will contribute to a decrease in R_s and G.

4.1.3 ANALYSIS OF IMPLEMENTED APPROACHES TO REDUCE LOSSES IN THE INITIAL PARAMETERS OF A SOLAR CELL BASED ON CDS/CDTE

To reduce the reflection of solar radiation from the surface of the device structure, in the design of modern CdS/CdTe film SCs, SnO_2 layers are usually used, which, with a surface resistance of about 10 Ohm/□, have a transmittance of 80 %. An alternative to the traditional SnO_2 layer was the use of Cd_2SnO_4 oxide as a front, transparent electrode, which has the best combination of optical and electrical properties. Cd_2SnO_4 layers have a higher transparency (over 90 %), which is achieved by reducing their thickness to 0.1 μm, since their surface resistance is about 3 Ohm/□, which is several times lower than that of traditional SnO_2 electrodes [15–17]. Thus, the use of Cd_2SnO_4 contributes to the reduction of losses Jsc to the level of 0.62 mA/cm^2 due to absorption in the spectral range (300–800) nm, while for traditional SnO_2 layers such losses are (2.8–1.3) mA/cm^2 [18].

The recombination of nonequilibrium charge carriers generated under the action of photons in the spectral range (300–520) nm in the CdS layer also has a significant negative effect on the J_{sc} value. Reducing the recombination level can be achieved by reducing the thickness of the CdS layer, however, this leads to a decrease in the values of V_{nl} and FF. In [19], it was proposed to use a ZTO buffer layer, which ensures mutual diffusion with the CdS layer during structure formation. During interdiffusion, which occurs at an annealing temperature of 600 °C in the presence of Ar or He, penetration of approximately 3–5 % Cd in the ZTO layer and approximately 2–3 % Zn in the CdS layer is observed. Diffusion at a lower annealing temperature of 420 °C for 15 minutes in the presence of $CdCl_2$ also indicates a significant amount of abundant Cd and Zn in the ZTO and CdS layers, respectively.

Thus, the consumption of the CdS layer during interdiffusion contributes to a decrease in the absorption of photons with energies exceeding the band gap of CdS, an increase in the quantum efficiency of >75 % for photons with a wavelength of more than 400 nm, and a decrease in losses Jsc due to absorption 1.0–1.3 mA/cm^2 in the layer, while maintaining high V_{nl} and FF values. At present, an obligatory technological operation in the manufacture of high-efficiency film solar cells based on CdS/CdTe is chloride heat treatment [20]. The processes occurring as a result of Cd-Te-CdCl$_2$ interfacial interaction cause an increase in the grain size of cadmium telluride and cadmium sulfide, as well as an increase in the lifetime of nonequilibrium charge carriers [21]. However, the stresses at the TCO/CdS interface arising as a result of grain growth can significantly impair the adhesion of these layers and contribute to the formation of a bulge. The use of a buffer layer ZTO (Zn_2SnO_4) reduces the stress that has arisen in the crystal lattice, providing better adhesion [22]. The use of optimal "chloride" heat treatment and the use of the ZTO buffer layer makes it possible to reduce the diode saturation current density J_0 to 10–11–10^{-9} /cm^2 and the diode ideality factor A to 1.6–2, while for traditional film solar cells based on CdS/CdTe $J_0 > 10^{-9}$ and $A > 2$. The application of this approach makes it possible to reduce losses J_{sc} due to recombination within grains. There are two theoretical approaches to increase open circuit voltage. The first approach is to increase the concentration of holes (acceptors) in the CdTe layer up to 2×10^{17} cm^{-3}. It should be

CHAPTER 4

noted that at present, for a typical SC based on CdTe, the concentration of acceptors in the base layer is three orders of magnitude lower, 2×10^{14} cm^{-3}. In this case, a decrease in the width of the depletion region at an increased concentration of charge carriers contributes to an increase in the diffusion length of minority charge carriers, and, therefore, provides an increase in the lifetime, which will increase V_{sc}. In addition, an increase in the concentration of charge carriers leads to an increase in the height of the potential barrier, the value of which limits the maximum possible value of the open circuit voltage. However, with an increase in the charge carrier concentration, the rate of surface recombination at the CdS/CdTe heterojunction can limit the increase in open circuit voltages due to the intensification of the removal of nonequilibrium charge carriers generated under the action of light in the base layer. In addition, it is impossible to actually achieve the required charge carrier concentrations with existing approaches to reducing resistivity. At present, the decrease in resistivity is carried out with the "chloride" treatment, as a result of which shallow acceptor levels are generated that have defective ClTe – VCd complexes. With an increase in the chlorine concentration, the energy structure of the base layer evolves; as a result of an increase in the concentration, there are no defective complexes described above, but isoelectronic traps 2ClTe – VCd are formed, which contribute to an increase in the resistivity of the base layer [23]. The second approach is to form a p–i–n structure with a hole concentration in the CdTe layer of 2×10^{13}. In this case, the internal field propagates over the entire thickness of CdTe, and the resulting barrier, which is called the "electronic reflector", limits the recombination rate on the rear surface. Without an increase in the conduction band barrier, the voltage is lower than the voltage at a typical charge carrier concentration of 2×10^{14} cm^3 in CdTe, but even with a modest electronic reflector (0.2 eV), the V_{sc} voltage should increase significantly. One possibility to create such a barrier is to add a layer of ZnTe [13] or other material with an extended discontinuity in the conduction band. A potential difficulty, however, is that any recombination in CdTe/ZnTe or contact with a reflector is fraught with the positive effect of an "electronic" reflector [24].

To increase the filling factor of the light current-voltage charsteristics (*FF*), it is necessary to provide a decrease in R_s and an increase in R_w. One way to reduce R_s is to replace the traditional doped SnO$_2$ layer with a Cd$_2$SnO$_4$ layer, which has a lower resistivity value caused by a high mobility value ($\mu = 54.5$ cm^2/(Vs)) and a high level of charge carrier concentration n$=8$, 94×10^{20} cm^{-3} while maintaining its transparency, which is twice as much as in the SnO$_2$ layer.

An increase in R_w can be realized by introducing an undoped ZTO (Zn$_2$SnO$_4$) layer about 0.1–0.2 μm thick into the TCO/CdS contact region. With a decrease in the thickness of the CdS layer in order to increase J_{sc}, small windows appear in it, through which the TCO contacts p-CdTe and the p-n junction is shunted. A high-resistance ZTO layer with an optical band gap ($\sim$3.6 eV) prevents the appearance of a defective TCO/CdTe heterojunction. By implementing the approaches described above, the authors of [25] managed to increase the *FF* value to the level of 77.34 %.

The analysis performed shows that many directions for increasing the efficiency of SCs based on cadmium telluride have already been practically implemented. At the same time, insufficient attention is currently paid to the problems of increasing the efficiency by optimizing the rear contacts.

4.1.4 FORMATION OF LOW-RESISTANCE REAR CONTACTS IN SC BASE LAYERS BASED ON CDS/CDTE

The efficiency of operation, as well as the resistance to degradation of SC based on CdS/CdTe, depends on the material and method of obtaining the rear contact. When a metal film is deposited on the surface of the CdTe layer, a Schottky barrier is formed. Because the electronic affinity of CdTe is so great, only metals with a work function >5.7 eV form ohmic contacts. Platinum has the highest work function (5.5 eV). But such a material is not economically feasible to use [25].

Therefore, a tunnel junction is usually used as a rear contact. To do this, CdTe is digested on the back surface to form an excess of elemental Te [26]. The next step is to deposit CdTe or a semimetal with a low bandgap on the surface of a semiconductor in the form of a thin buffer layer (~10 nm), followed by the deposition of a metallization layer.

Base film CdS/CdTe heterosystems were deposited by thermal vacuum evaporation in a single technological cycle. The formation of film back contacts, which are Cu/Au film heterostructures of nanosized thickness, was also carried out by this method. The back contacts of the ITO films (indium and tin oxides) were deposited by non-reactive DC magnetron sputtering using an original material-saving magnetron. Before applying the rear contacts, the cadmium telluride surface was etched in a 5 % solution of bromine in methanol for 10 seconds. Then, copper layers 12 nm thick and a gold film 50 nm thick were deposited on the surface of the base layer by thermal condensation without heating the substrate. After that, annealing was carried out in air at a temperature of 200 °C for 30 minutes. In this case, during the previous 10 minutes, the laboratory sample was heated up to annealing. In addition to laboratory samples with standard technological operations during the formation of rear contacts, let's analyze SCs in the design of the rear contacts of which there was no copper layer and which, after obtaining the Cu/Au film heterosystem, were not annealed.

To study the effect of a nanosized copper layer in the back contact design on the efficiency of photovoltaic processes in ITO/CdS/CdTe film SCs, let's measure the light current-voltage characteristics of a series of samples with different back contact design solutions at an illumination power of 10 mW/cm^2 to 10 (100 mW/cm^2 corresponds to the standard mode lighting AM1) [27].

Thus, in the process of studying SCs based on CdS/CdTe with a back contact consisting of a copper interlayer 12 nm thick and a layer of gold 50 nm thick, as well as SCs whose back contact does not include copper, it was found that the SC efficiency at power illumination of 1000 W/m^2 with the Cu/Au rear contact approaches 10 %, and with the Au rear contact it approaches 3.1 %, which is primarily due to the high value of the open circuit voltage and the filling factor of the light CVC. The dependence of the short circuit current density on the level of illumination of both types of contacts is traditionally linear (**Fig. 4.2, *a***). In this case, for a SC with a rear contact containing copper, at a radiation power of 70 mW/cm^2, the maximum efficiency is observed, and for device structures with a rear contact of Au, the efficiency somewhat increases with increasing illumination. The light current-voltage characteristics of the SC at different illumination powers are shown in **Fig. 4.2**.

CHAPTER 4
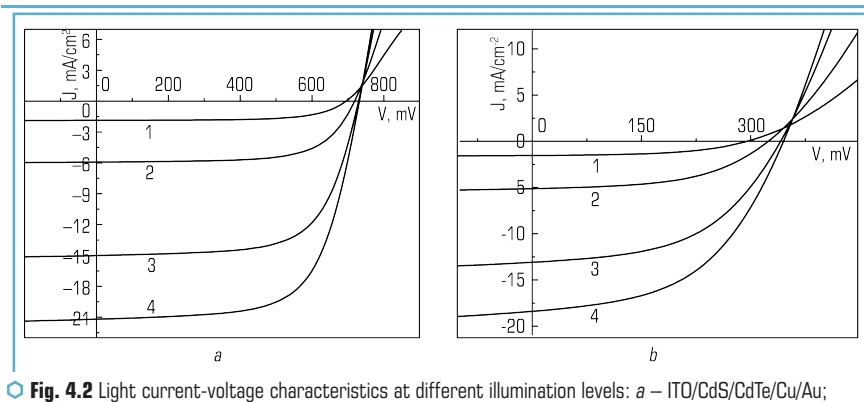
○ **Fig. 4.2** Light current-voltage characteristics at different illumination levels: a – ITO/CdS/CdTe/Cu/Au; b – ITO/CdS/CdTe/Au; 1 – 10 mW/cm^2; 2 – 30 mW/cm^2; 3 – 70 mW/cm^2; 4 – 100 mW/cm^2

An analysis of the light diode characteristics shows that for a SC with a Cu/Au back contact, with increasing illumination, a traditional increase in the photocurrent density is observed (**Table 4.1**), which is due to an increase in the concentration of nonequilibrium charge carriers with an increase in the incident photon flux density. With an increase in illumination, the shunt resistance decreases, which is due to an increase in the specific conductivity of the base layer. The size of the series resistance does not depend enough on the illumination. This indicates that the predominant contribution to the value of the series resistance of the device structure is made by the resistance of the back and front contacts.

● **Table 4.1** Effect of illumination level on initial parameters and light diode characteristics of ITO/CdS/CdTe/Cu/Au

Parameters and characteristics	P_c, mW/cm^2									
	10	20	30	40	50	60	70	80	90	100
J_{SC}, mA/cm^2	1.9	3.8	5.94	8.3	10.3	12.8	15.0	17.0	19.5	21.2
V_{nl}, mV	697	711	719	720	728	727	729	731	727	731
FF, c.u.	0.66	0.67	0.67	0.67	0.67	0.663	0.66	0.66	0.66	0.66
Efficiency, %	8.7	9.1	9.49	10	10	10.29	10.37	10.23	10.36	10.19
J_p, mA/cm^2	1.87	3.8	5.95	8.4	10.3	12.8	15.1	17.0	19.5	21.3
R_s, Ohm·cm^2	<1	<1	<1	<1	<1	1.3	1.3	1.4	1.6	1.6
R_w, Ohm·cm^2	8250	4420	2390	2400	1280	1010	894	741	694	623
A, c.u.	2.9	2.9	2.8	2.8	2.7	2.6	2.6	2.5	2.5	2.5
J_0, 10^{-7} A/cm^2	1.3	2.2	2.7	2.7	2.6	2.2	2.6	2.1	1.8	1.9

CHAPTER 4

The effect of annealing at a temperature of 200 °C for 30 minutes on the initial characteristics of a SC with a Cu/Au back contact was also studied.

● **Table 4.2** Effect of rear contact annealing on the initial parameters of the ITO/CdS/CdTe/Cu/Au

Output parameters	V_{nl}, mV	J_{sc}, mA/cm^2	FF	Efficiency, %
Before annealing	322	20.2	0.41	1.6
After annealing in air	723	22.2	0.54	8.8

It has been established that the efficiency is limited to 2 % after annealing in device structures. The decisive contribution to the limitation of efficiency is made by low values of the no-load voltage. The results obtained indicate that only annealing in a SC with a Cu/Au back contact leads to the formation of an effective tunnel contact. According to the literature data [28], this is due to the interfacial interaction of the copper film and the surface layer of tellurium, which leads to the formation of a degenerate $Cu_{2-x}Te$ semiconductor. Without a degenerate semiconductor layer, in device structures with a Cu/Au back contact, as well as for a SC with an Au back contact, the through diode mode is implemented, which limits the value of the open-circuit voltage.

4.2 STUDY OF TANDEM AND BILATERALLY SENSITIVE SOLAR CELLS BASED ON CDS/CDTE

4.2.1 RESULTS OF INVESTIGATION OF TRANSPARENT REAR CONTACTS CU/ITO FOR DOUBLE-SIDED SENSITIVE SNO$_2$:F/CDS/CDTE/CU/ITO SOLAR CELLS

A promising direction for increasing the efficiency of photoelectric conversion of solar energy and the ability to work stably for a long period of time is the development of tandem and bilaterally sensitive photoelectric converters (PECs). The development of multilayer tandem structures involves the use of several base layers with different band gaps. This makes it possible to efficiently convert solar radiation in a wide spectral range. Thus, high-energy photons are absorbed in the first base layer, the rest of the radiation enters the PEC located below with a base layer having a smaller band gap. The main requirements for the creation of tandem structures are the small thickness and transparent rear contact of the PEC with the wide-gap base layer [29]. This is necessary for the passage of the long-wavelength part of the spectrum through the base layer with minimal losses. For bilaterally sensitive photovoltaic converters, the main requirement is efficient conversion of solar radiation when illuminated from both sides. Given the high radiation resistance of cadmium telluride, it is promising to use bilaterally sensitive solar cells based on it for power supply of spacecraft. Since the back of the solar battery of the spacecraft is illuminated by solar radiation reflected from the body. Therefore, it is necessary to conduct research on the conditions for creating transparent rear electrodes for pho-

CHAPTER 4

toelectric converters based on CdTe, intended for use in both tandem and bilaterally sensitive device structures.

The use of PV film PEC with CdTe and CuInSe$_2$ [30] base layers is promising for creating tandem structures. It is known that the band gap of CdTe is 1.46 eV [6], and the band gap of CuInSe$_2$ is 1.10 eV [31]. The combination of the energy structure of such PECs is able to provide efficient conversion of solar radiation, both in terrestrial and atmospheric conditions. However, the use of PEC based on CdTe in tandem structures is constrained by the difficulty of creating back contacts suitable for industrial production. This is due to the fact that only platinum has the electron work function necessary for the formation of an ohmic transition. Other metals with cadmium telluride form a Schottky barrier, which affects the efficiency of photovoltaic processes in solar cells based on it [32]. Therefore, the main approach to the creation of low-resistance electrodes is the formation of tunnel electrodes containing copper. However, the diffusion of copper into the base layer leads to degradation of the initial parameters of film solar cells based on CdS/CdTe. The authors of [33] proposed the creation of a rear contact without the use of copper. However, the efficiency of the studied samples did not exceed 6.2 %, and their degradation resistance was studied only for one year, which is not enough for operation in terrestrial and atmospheric conditions. The work [34] presents studies devoted to the creation of ohmic back contacts using an organic layer of the leading PEDOT-PSS polymer, which also does not contain copper. However, the efficiency of the obtained samples did not exceed 2 %. As shown by the authors, the low efficiency of experimental samples is due to the operation of the device structure in the mode of a through diode. The authors of [35] studied several types of metal oxides as a buffer layer for creating a high-quality rear contact for solar cells based on CdTe. But this approach complicates the adaptation to mass industrial production.

Thus, at present, the problem of creating efficient and transparent rear contacts with solar cells based on CdTe without the use of copper remains unresolved. Therefore, it is necessary to carry out research aimed at optimizing the design and technological solution for creating transparent rear electrodes.

4.2.2 MATERIALS AND EQUIPMENT USED TO OBTAIN SNO$_2$:F/CDS/CDTE/CU/ITO PHOTOVOLTAIC CONVERTERS

The studied device structures with a photoreceiving surface area of up to 2 cm^2 were obtained by thermal vacuum evaporation using a UVN67 vacuum unit with modified internal equipment [36–38]. The thickness of the CdTe base layer was 2.5 μm. The view of the internal equipment of the installation is shown in **Fig. 4.3**.

ITO films (indium and tin oxides) were deposited by nonreactive DC magnetron sputtering in a VUP-5M vacuum unit (**Fig. 4.4**). It should be noted that magnetron sputtering is one of the most promising methods for obtaining all transparent electrodes [15, 16]. This is due to the high degree

CHAPTER 4

of accuracy in transferring the target composition to the substrate and the reproducibility and controllability of the magnetron sputtering process [39, 40].
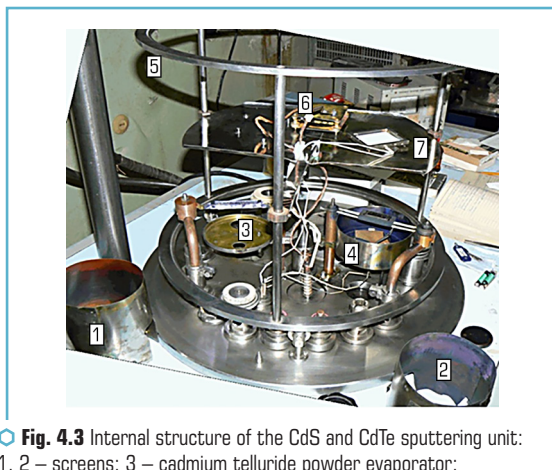
○ **Fig. 4.3** Internal structure of the CdS and CdTe sputtering unit:
1, 2 – screens; 3 – cadmium telluride powder evaporator;
4 – cadmium sulfide powder evaporator; 5 – carousel;
6 – substrate heater; 7 – substrate holder

a   *b*
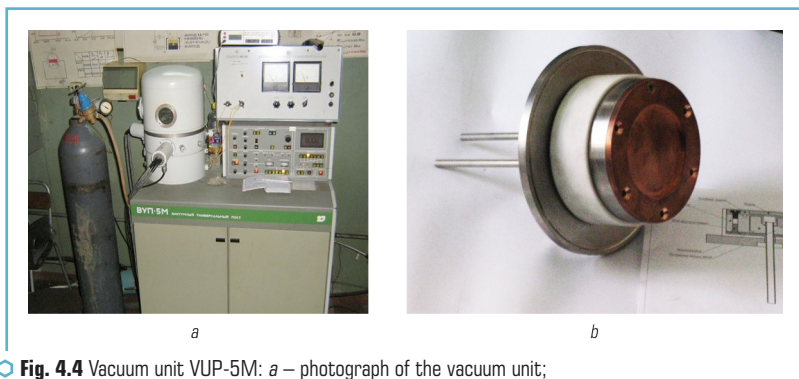
○ **Fig. 4.4** Vacuum unit VUP-5M: *a* – photograph of the vacuum unit;
b – photograph of the material-saving magnetron

Since it is not possible to obtain efficient device structures without a copper interlayer, a nano-sized copper layer 2 nm thick was deposited on the surface of cadmium telluride before ITO was deposited. The minimization of the copper layer thickness was aimed at increasing the degradation resistance of the device structure.

According to [27], the technology of forming tunneling electrodes provides for chemical digestion before applying the electrode, during which a Te layer is formed, and the final stage is annealing, leading to the formation of the $Cu_{2-x}Te$ phase, which is an innate conductor.

4.2.3 MEASUREMENT TECHNIQUE AND ANALYTICAL PROCESSING OF LIGHT CURRENT-VOLTAGE CHARACTERISTICS

The measurement of light current-voltage characteristics (hereinafter – CVC) was carried out according to the method described in [41]. Imitation of solar radiation, close to the standard mode AM1.5, was carried out using a system of LEDs.

To measure the compensation method in the stationary mode of irradiation, close to the standard AM1.5, of the light current-voltage characteristics of SC samples.

Determination of the output parameters and light diode characteristics of photoelectric converters based on cadmium telluride was carried out according to the experimental light current-voltage characteristics. Analytical processing of the light CVCs of the studied PECs was carried out using a PC.

The relationship between the PEC efficiency and the light diode characteristics is implicitly described theoretically by the light CVC of the PEC:

$$J_l = J_p + J_0 \left\{ exp\left[e\left(V_l - J_l R_s\right)/\left(AkT\right)\right] - 1\right\} + \left(V_l - J_l R_s\right)/R_w, \tag{4.15}$$

where J_l – the current density flowing through the load; e – the electron charge; k – the Boltzmann constant; T – the temperature of the solar cell; V_l – voltage drop across the load.

According to the program, the analytical expression (4.15) for the light CVC turns into expressions having the form:

$$I_l = A_0 - A_1 V_l - A_2 exp\left(A_3 V_l + A_4 I_l\right), \tag{4.16}$$

$$A_0 = \left(I_p + I_0\right)R_w / \left(R_s + R_w\right), \tag{4.17}$$

$$A_1 = 1/\left(R_s + R_w\right), \tag{4.18}$$

$$A_2 = I_0 R_w / \left(R_s + R_w\right), \tag{4.19}$$

$$A_3 = e/\left(AkT\right), \tag{4.20}$$

$$A_4 = eR_s / \left(AkT\right). \tag{4.21}$$

Using expression (4.16) and the experimentally obtained values of I_l and V_l, by varying the values of the above coefficients A_0, A_1, A_2, A_3, A_4 the best approximation of the experimental data $I_l = I_l(V_l)$ of the curve described by the transformed theoretical expression (4.16) is achieved. Usually, during analytical processing, the standard deviation does not exceed 10^{-8}, which corresponds to a relative error in determining the initial parameters and light diode characteristics at a level of no more than 1 %. After finding the indicated coefficients, which provide the best approximation, the initial parameters of the PEC are determined: I_{sc}, V_{nl}, FF, R_w, efficiency. The light diode characteristics R_s, R_w, A and I_0 are calculated from the found coefficients A_0, A_1, A_2, A_3, A_4, using relations (4.17)–(4.21) [42–44]. The error in determining the initial parameters and light diode characteristics is determined not only by the value of the standard deviation, but also by the error in the light CVC measurement.

4.2.4 RESULTS OF THE STUDY OF LIGHT CURRENT-VOLTAGE CHARACTERISTICS OF SNO$_2$:F/CDS/CDTE/CU/ITO PHOTOELECTRIC CONVERTERS

By analytical processing of the light CVCs (**Fig. 4.5**), the initial and light diode properties of the made solar cells were analyzed.
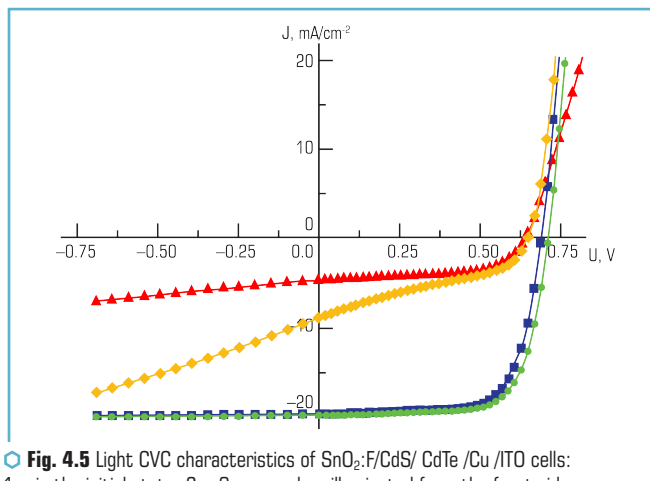
Fig. 4.5 Light CVC characteristics of SnO$_2$:F/CdS/ CdTe /Cu /ITO cells:
1 – in the initial state; 2 – 8 years when illuminated from the front side;
3 – in the initial state; 4 – ~ 8 years when illuminated from the back side

After taking the initial light CVCs under illumination from the front and back sides, the standards were kept at a constant light flux in a special chamber in the idle mode. Lighting was provided

by a 500 W incandescent lamp, the sample temperature was 80 °C. It was shown in [42] that such illumination regimes increase the degradation rate by a factor of 100. At certain intervals, conditionally corresponding to: 0; 0.5; 1.4; 3.6; 4.2; 5.4; 6.02 and 8 years, repeated measurements of light CVCs were made. **Table 4.1** presents the results of analytical processing of light CVC characteristics under illumination from the front side are shown in **Table 4.3**.

● **Table 4.3** Output parameters and light diode characteristics of ITO/CdS/CdTe/Cu/ITO PV cells when illuminated from the front side

t, h	0	0.5	1.4	3.6	4.2	5.4
J_{SC}, mA/cm^2	19.4	19.4	19.4	19.4	19.5	19.4
V_{nl}, mV	740	720	710	710	710	710
FF, c.u.	0.68	0.73	0.75	0.74	0.73	0.73
Efficiency, %	9.8	10.2	10.3	10.1	10.2	10.1
J_p, mA/cm^2	19.5	19.0	19.5	19.4	19.5	19.4
R_s, Ohm·cm^2	1.6	1.2	0.5	0.3	0.7	0.4
R_w, Ohm·cm^2	1031	911	882	965	821	922
A, c.u.	2.28	1.68	1.65	1.77	1.76	1.91
J_0, 10^{-7}A/cm^2	6.2×10^{-8}	1×10^{-9}	$9,7 \times 10^{-10}$	$3,3 \times 10^{-9}$	$2,5 \times 10^{-9}$	9×10^{-9}

Table 4.3 shows that at the beginning of the PEC operation and up to 1.4 years, there is an increase in efficiency from 9.9 % to 10.3 %, which is due to an increase in the filling factor of the light CVC from $FF=0.68$ to $FF=0.75$ against the background of an insignificant lowering the open circuit voltage from $V_{nl}=740$ V to $V_{nl}=710$ V and the short circuit current density from $J_{sc}=19.5$ mA/cm^2 to $J_{sc}=19.4$ mA/cm^2. With a further increase in the operating time to 6 years, the efficiency slowly decreases to 10 %. Then the decrease in efficiency occurs faster and with an increase in operating time up to 8 years, a decrease in efficiency to 9.7 % is observed. The reduction in efficiency occurs as a result of a decrease in the filling factor of the light CVC from $FF=0.75$ to $FF=0.71$, and the open-circuit voltage also continues to decrease slightly to 700 mV. The short circuit current density practically does not change. It should be noted that after 8 years of operation, the efficiency of the SnO$_2$:F/CdS/CdTe/Cu/ITO PEC practically coincides with the initial value, which indicates a high degradation resistance of the resulting heterosystems [45, 46].

An analysis of the worldwide diode characteristics of SnO$_2$:F/CdS/CdTe/Cu/ITO solar cells shows that initially, with an increase in operating time up to 1 year, the saturation diode current density decreases from $J_0=1.6 \times 10^{-8}$ A/cm^2 to $J_0=9.7 \times 10^{-10}$ A/cm^2, At the same time, the diode ideality coefficient also decreases. With a further increase in the operating time to 7.5 years, the diode saturation current density increases by almost two orders of magnitude up to $J_0=2.4 \times 10^{-8}$ A/cm^2,

the ideality factor also increases. This may be due to the fact that copper atoms, diffusing into the base layer at the grain boundary, reach the p-n transition region and partially shunt it. At the same time, the series resistance during almost the entire period of operation decreases from $R_s=2.2$ Ohm·cm^2 to $R_s=0.3$ Ohm·cm^2, and only after 7 years of operation is its reverse increase to $R_s=0.6$ Ohm·cm^2. The shunt resistance first increases from $R_w=850$ Ohm·cm^2 to $R_w=960$ Ohm·cm^2, and after four years it decreases to $R_w=880$ Ohm·cm^2 with a subsequent return to the level $R_w=960$ Ohm·cm^2.

The light diode characteristics of SnO$_2$:F/CdS/CdTe/Cu/ITO solar cells improve at the beginning of operation, and after 7–8 years they deteriorate and return almost to their initial values. This behavior of the diode characteristics is responsible for the observed high degradation resistance.

Thus, the use of a copper layer 2 nm thick makes it possible to create a rear Cu/ITO tunnel contact without lowering the degradation resistance of the device structure. Since thin-film PECs are traditionally guaranteed stable efficiency for 5 years, it becomes obvious that the use of the proposed transparent rear electrodes in the conditions of industrial production of film PECs based on cadmium telluride becomes obvious [47].

The results of analytical processing of the experimental CVC under illumination from the back are presented in **Table 4.4**.

● **Table 4.4** Output parameters and light diode characteristics of ITO/CdS/CdTe/Cu/ITO PV cells under illumination from the back side

t, h	0	1.4	3.6	5.4	6.0	8
J_{SC}, mA/cm^2	4.7	7.5	6.7	6.7	6.9	7.0
V_{nl}, mV	650	660	660	650	650	630
FF, c.u.	0.55	0.42	0.39	0,39	0.36	0.32
Efficiency, %	1.7	2.1	1.8	1.7	1.6	1.4
J_p, mA/cm^2	4.7	7.7	6.9	6.8	7.1	7.2
R_s, Ohm·cm^2	3.2	4.3	4.6	1.5	3.8	3.1
R_w, Ohm·cm^2	438	146	155	150	132	112
A, c.u.	1.9	1.2	1.3	1.3	1.1	1.1
J_0, 10^{-7}A/cm^2	6.9×10^{-9}	3.1×10^{-13}	3.8×10^{-12}	1.2×10^{-11}	3.6×10^{-13}	3.6×10^{-13}

CHAPTER 4

As can be seen from **Table 4.4**, the PEC efficiency when illuminated from the back side is significantly less than when illuminated from the front side. The ratio between the efficiency during the entire period of operation remains in the range from 5 to 7, reaching a minimum difference when the efficiency when illuminated from the front and rear sides reaches maximum values. Moreover,

the relative increase in efficiency at the beginning of operation with illumination from the back side is greater (23 % compared with the initial value) than with illumination from the front side (4 % compared with the initial value). The lower values of efficiency are primarily due to the lower values of the filling factor of the light CVC and the lower short-circuit current density. When illuminated from the back side in the initial state, the filling factor of the light CVC is $FF=0.56$, and after 7.5 years it decreases to $FF=0.32$. It should be noted that when illuminated from the front side, the fill factor decreases slightly. The short-circuit current density in the initial state when illuminated from the back side is 4 times less than when illuminated from the front side. After a year of operation, the ratio of these currents becomes approximately equal to 2.6 and remains unchanged further. The open-circuit voltage, both when illuminated from the front side and when illuminated from the back side, changes slightly and differs from the value for front illumination by (0.05–0.1) V.

Thus, the study of the light current–voltage characteristics of the SnO_2:F/CdS/CdTe/Cu/ITO PEC showed that a decrease in the thickness of the copper layer deposited on the CdTe surface to ~2 nm made it possible to create degradation-resistant solar cells with a transparent rear contact.

The fixed evolution of the output parameters with a change in the direction of illumination is due to a change in the light diode characteristics. The decrease in the short circuit current density is due to the corresponding decrease in the photocurrent density. The fixed decrease in J_p when the direction of illumination changes is due to the fact that when illuminated from the front side, active generation of nonequilibrium charge carriers occurs near the p-n junction or inside its depletion region. As a result, most of it is generated under the action of light from nonequilibrium charge carriers and falls into the region of the built-in electric field of the p-n junction, where, after separation, a photocurrent is formed. When the device structure is illuminated from the rear, the nonequilibrium carrier generation region is separated from the p-n transition region. Therefore, a significant part of the generated nonequilibrium charge carriers as a result of volume and surface recombination do not contribute to the creation of a photocurrent.

When illuminated from the back, the series resistance is several times higher than when illuminated from the front, and does not decrease with increasing operating time. The density of the diode saturation current when illuminated from the rear side decreases by almost three orders of magnitude and practically does not change with an increase in the operating time. When changing the direction of illumination from the front to the back, the shunt resistance decreases several times. In addition, with an increase in the operating time, a decrease in the shunt resistance is observed. So, in the initial state, the ratio of the shunt resistance in front lighting to the shunting resistance in back lighting was 2 times, and by the end of operation it quickly increased to 8 times.

When analyzing the world-class diode characteristics, it is necessary to take into account the possibility of realizing the inverted diode regime presented in [48] in the structure under study, when the rear contact is a diode connected in series with respect to the main diode. The energy structure of the diodes is affected by the direction of illumination, which causes a change in the series and shunt resistance, as well as a change in the diode saturation current density. If the main contribution to the value of J_0 is made by the energy structure of the main separating barrier,

the decrease in J_0 when the direction of illumination changes from front to rear is due to an exponential decrease in the intensity of its illumination.

This, in turn, reduces the concentration of nonequilibrium charge carriers near the p-n junction. If the main contribution to the shunt resistance is made by the barrier properties of the back contact, it becomes obvious that this diode characteristic decreases when the direction of illumination changes from front to back. When the rear barrier is illuminated in the space charge region, the concentration of nonequilibrium charge carriers increases, which leads to a decrease in the shunt resistance as a result of a decrease in the thickness of the depletion layer. The series resistance is higher when illuminated from the rear, since in this case a significant amount of nonequilibrium charge carriers is not generated near the main p–n junction, and the depletion region increases, which leads to an increase in series resistance.

The evolution of the global diode characteristics with an increase in the operating time is due to the diffusion of copper from the nanosized interlayer into the volume of the base layer, which can occur according to the grain boundary and volume mechanisms.

Since copper is an acceptor impurity for cadmium telluride, its diffusion in the volume of the base layer of cadmium telluride leads to a decrease in the resistivity of the base layer and, accordingly, to a decrease in the PEC series resistance [49]. Diffusion of the acceptor into the grain boundary surface leads to the formation of a p-p + transition between the boundary and the bulk of the grain. Such potential barriers push nonequilibrium electrons into the bulk of the grain, generated under the action of light, by their built-in electric field, which reduces the negative effect of the grain boundary surface as a region with a high concentration of recombination centers. This approach makes it possible to expand the range of materials for creating rear contact with CdTe-based solar cells.

The obtained low efficiency values of the SnO_2:F/CdS/CdTe/Cu/ITO PEC under illumination from the side of the transparent rear contact require a more detailed analysis and further studies aimed at optimizing the thickness of the base layer.

4.2.5 THE RESULTS OF THE STUDY OF THE INITIAL PARAMETERS OF THE ITO/CDS/CDTE/CU/ITO SC UNDER BILATERAL IRRADIATION

To quantify the effect of bilateral irradiation on the efficiency of electric power generation, comparative studies of the CdS/CdTe/Cu/ITO light CVC were carried out under irradiation from the back and front sides and simultaneous irradiation (**Fig. 4.6**).

By analytical processing of the light CVCs of the studied samples, the initial parameters were obtained for various types of irradiation, which are given in **Table 4.5**.

As can be seen from **Table 4.5**, when irradiated from the rear side, a significant decrease in the values of J_{sc} and V_{nl} is observed and, accordingly, is accompanied by a significant decrease in efficiency. However, simultaneous irradiation on both sides shows high results of the initial parameters.

CHAPTER 4
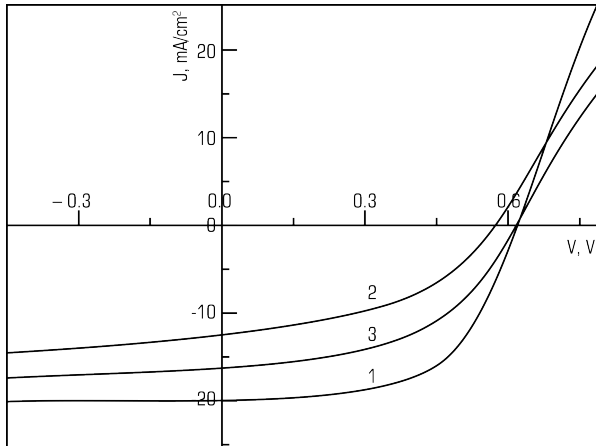
○ **Fig. 4.6** Light CVC of CdS/CdTe/Cu/ITO SCs: 1 – when irradiation from the rear side; 2 – when irradiated from the front side; 3 – when simultaneous irradiation from the back and front sides

● **Table 4.5** Initial parameters of the ITO/CdS/CdTe/Cu/ITO SCs under various irradiation options

SC initial parameters	Irradiation direction			
	from the front side	from the back side	on both sides at the same time	
J_{sc}, (mA/cm^2)	19.6	12.5	32.4	32.1*
V_{nl}, (mV)	620	570	610	–
FF, c.u.	0.59	0.44	0.50	–
Efficiency, %	7.17	3.13	9.88	–

*Note: * are the initial parameters of the theoretical light CVC obtained by adding two experimental light CVC under illumination from the back*

4.2.6 RESULTS OF STUDYING THE SPECTRAL DEPENDENCES OF THE ASSEMBLY FACTOR OF ITO/CDS/CDTE/CU/ITO SCS AT VARIOUS BIAS VOLTAGES

To analyze the possibility of using the developed SC based on ITO/CdS/CdTe/Cu/ITO in tandem device structures, let's study the spectral dependences of the removal factor at various bias voltages and various irradiation directions. On the basis of the obtained spectral dependences, the effect of the space-charge region of the rear contact on the efficiency of photoelectric processes in the base layer of a SC based on ITO/CdS/CdTe/Cu/ITO was analyzed (**Fig. 4.7**).
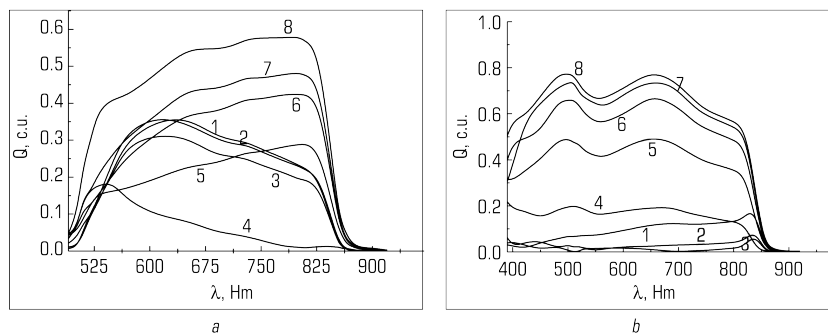
Fig. 4.7 Spectral dependences of the assembly factor of CdS/CdTe/Cu/ITO SCs with
a base layer thickness of 1 μm at various bias voltages (1 – 0 V, 2 – 0.5 V, 3 – 0.6 V,
4 – 0.7 V , 5 – 0.8 V, 6 – 0.9 V, 7 – 1.1 V, 8 – 1.2 V): a – when irradiated from the
front side; b – when irradiated from the back side

To quantify the contribution of incomplete absorption to a decrease in the photocurrent density,
let's study the CdS/CdTe/Cu/ITO light CVCs with a base layer thickness of 1 μm under illumination
from the rear side (**Fig. 4.8**).
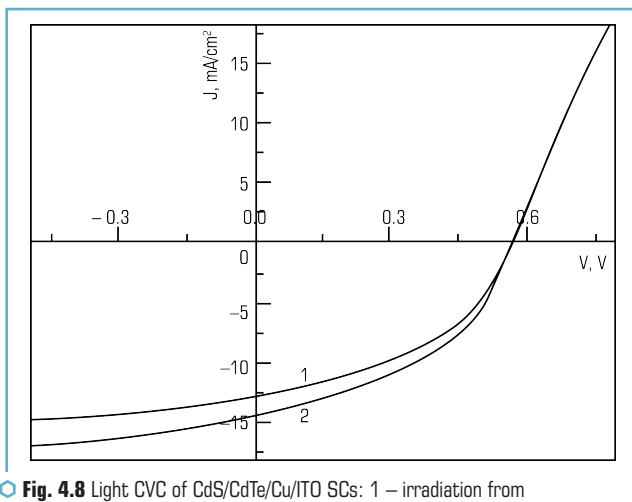
Fig. 4.8 Light CVC of CdS/CdTe/Cu/ITO SCs: 1 – irradiation from
the rear side; 2 – rear-front irradiation

The initial parameters of the SC during the analytical processing of light CVC are presented
in **Table 4.6**.

CHAPTER 4

● **Table 4.6** Initial parameters of the CdS/CdTe/Cu/ITO SCs with a base layer thickness of 1 μm for various irradiation options

SC initial parameters	Irradiation direction		
	Rear side	**rear-front**	**front**
J_{sc}, (mA/cm^2)	12.5	14.1	19.7
V_{nl}, (mV)	570	571	666
FF, c.u.	0.44	0.43	0.60
Efficiency, %	3.1	3.4	7.8

When conducting such studies, a mirror was installed on the front side under illumination from the back side, which allowed the radiation transmitted through the SC to be directed again to the base layer from the front side. Thus, the loss of electric power generated by the SC due to incomplete absorption of light when illuminated from the back was analyzed experimentally.

4.2.7 THE RESULTS OF THE STUDY OF THE INITIAL PARAMETERS OF THE ITO/CDS/CDTE/CU/ITO SCS AS PART OF TANDEM SCS

The developed ITO/CdS/CdTe/Cu/ITO SCs were tested as part of tandem SCs with a narrow-gap layer based on copper and indium diselenide. Such solar cells were made at the Swiss Institute of Technology. Mo/CuInSe$_2$/CdS/ZnO/ZnO:Al/Ni SCs were produced on glass substrates and had a front configuration. Illumination of such device structures is carried out from the side of Ni comb contact. The light CVCs of such device structures were studied when the ITO/CdS/CdTe/Cu/ITO SCs with a base layer thickness of 1 μm and an efficiency of 7.8 % was located on the illuminated surface (**Fig. 4.9**).

The initial parameters of characteristic samples of Mo/CuInSe$_2$/CdS/ZnO/ZnO: Al/Ni SCs and the ITO/CdS/CdTe/Cu/ITO – Mo/CuInSe$_2$/CdS/ZnO/ZnO: Al/Ni tandem photovoltaic converter are presented in **Table 4.7**.

As can be seen from **Table 4.7**, placing an ITO/CdS/CdTe/Cu/ITO SC on a Mo/CuInSe$_2$/CdS/ZnO/ZnO:Al/Ni surface leads to a significant decrease in the efficiency of the latter.

Thus, we have analyzed the parameters and efficiency of the device structure of the ITO/CdS/CdTe/Cu/ITO SC, which were obtained by analytical processing of light CVC. It has been established that the resulting light CVC of the SC when illuminated from both sides is the sum of the light CVC when illuminated from the rear and front sides.

However, double-sided lighting allows to increase the generated electrical power by 43 %. This reduces the area of the corresponding one-sided SC, which makes it possible to expand the possibilities of their use in the prevention of emergencies in the case of a limited deployment area.

CHAPTER 4
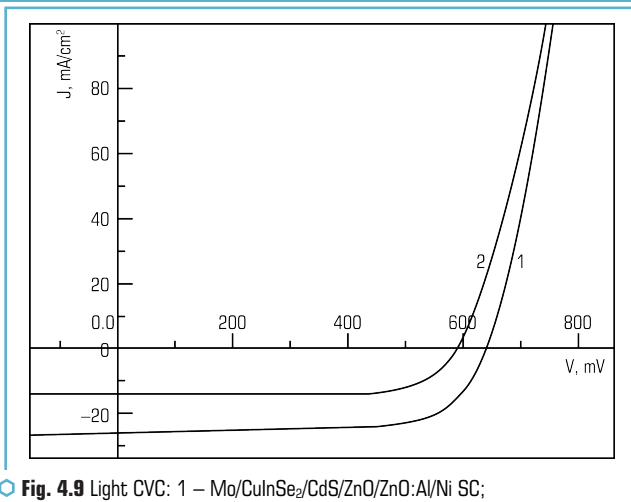
Fig. 4.9 Light CVC: 1 – $Mo/CuInSe_2/CdS/ZnO/ZnO:Al/Ni$ SC;
2 – when ITO/CdS/CdTe/Cu/ITO is located on its front surface

● **Table 4.7** Initial characteristics of the solar parts of the tandem structure

SC parameters	$CuInSe_2$	$CuInSe_2/CdTe$	CdTe
J_{sc}, (mA/cm^2)	25,9	13,8	19,7
V_{nl}, (mV)	634	590	666
FF, c.u.	0,68	0,74	0,60
Efficiency, %	11,2	6,0	7,8

An analysis of the spectral dependences of the ITO/CdS/CdTe/Cu/ITO SC collection coefficient at various bias voltages has been carried out. It was found that in the absence of a shear stress, the maximum in the spectral dependence is observed at a wavelength of 0.65 μm, then a decrease in the photoresponse is observed, so that the area under the spectral dependence decreases by 20 %.

Since the area under the spectral dependence of the quantum efficiency coefficient is proportional to the short-circuit current density, the efficiency of the device structure also decreased by 20 rel. %. Such a significant decrease in the efficiency of photoelectric processes can probably be due either to the negative effect of surface recombination at the rear contact or to incomplete absorption in the base layer due to the small thickness of the base layer.

Analysis of the **Table 4.6** shows that if the radiation transmitted through the solar cell, when illuminated from the back side, is again directed to the front surface with the help of a mirror,

CHAPTER 4

161

this leads to an increase in electric power by 0.3 mW/cm². The increase in efficiency is due to an increase in the short-circuit current density by 1.6 mA/cm² at constant values of the open-circuit voltage and the filling factor of the light CVC. Relative to the value of the short-circuit current density during irradiation from the front side, the increase in this initial parameter is 8 %. Thus, it has been experimentally shown that, in reducing the efficiency of photoelectric processes, the contribution of incomplete light absorption in the base layer to its photosensitivity practically coincides with the negative contribution of the rear contact.

With an increase in the forward bias, the area of the space charge of the main separating barrier, where there is a built-in electric field that accelerates the movement of electrons, decreases. This leads to a decrease in the assembly efficiency of nonequilibrium charge carriers generated under the action of light due to a decrease in the region of the semiconductor where they drift in an electric field. A decrease in efficiency is experimentally observed in the analysis of spectral dependences. With increasing voltage, a decrease in $Q(\lambda)$ is observed in the entire spectral range of the photosensitivity. In this case, the largest decrease is observed for nonequilibrium charge carriers generated under the action of photons from the long-wavelength part of the spectrum. With an increase in the wavelength, the depth of light absorption increases, which leads to the removal of the active generation region from the region of the separating barrier. There is also an increase in the negative effect on the volume recombination collection coefficient during the diffusion of charge carriers from the generation region to the separation region.

At a voltage of 0.7 V, which corresponds to the open circuit voltage, the photosensitivity becomes equal to zero, since the external electric field becomes equal to the internal field of the separating barrier. Since these electric fields have the opposite content, the process of separation of nonequilibrium carriers stops. With a further increase in the bias voltage, its drop is carried out on the rear diode, connected in the opposite direction. Therefore, the rear diode begins to separate nonequilibrium charge carriers. As a result, the shape of the spectral dependence of the photorecall changes. Nonequilibrium charge carriers, generated under the action of photons from the long-wavelength part of the spectrum, begin to make the greatest contribution to the creation of photoresponse, since the region of their generation is located near the fission region. When illuminated from the rear side (**Fig. 4.7, *b***), the maximum in the spectral dependence is observed when photons are absorbed from the long-wavelength region of the spectrum, which indicates a high surface recombination at the rear contact. Indeed, nonequilibrium charge carriers, when illuminated from the back side, are generated near the back surface. If this surface is characterized by a high rate of surface recombination, then the contribution of charge carriers generated near the back to the photorecall is minimized, which is observed experimentally. With an increase in the bias voltage, the energy structure of the rear contact is optimized and the depletion region grows, which causes an increase in the photoresponse over the entire spectral range of the photosensitivity.

An analysis of the initial parameters of the ITO/CdS/CdTe/Cu/ITO – Mo/CuInSe₂/CdS/ZnO/ZnO: Al/Ni tandem structure shows that the absorption of a part of the incident radiation in the

ITO/CdS/CdTe/Cu/ITO SC leads to a decrease in the efficiency SC Mo/CuInSe$_2$/CdS/ZnO/ZnO:Al/Ni from 11.2 % to 6.0 %. This decrease in efficiency occurs due to a decrease in the short circuit current density from 25.9 mA/cm^2 to 13.8 mA/cm^2.

In this case, the open-circuit voltage decreases slightly, and the filling factor of the light CVC increases. The results obtained are in good agreement with those shown in **Fig. 4.2** by the spectral dependence of the transmittance of the ITO/CdS/CdTe/Cu/ITO SC. Since the short circuit current density linearly depends on the intensity of the incident radiation, and the open circuit voltage depends on it logarithmically.

It should be noted that, despite a significant decrease in the efficiency of the Mo/CuInSe$_2$/CdS/ZnO/ZnO:Al/Ni SC when it is darkened by the ITO/CdS/CdTe/Cu/ITO SC, the efficiency of the tandem structure is noticeably higher than that of such CEs separately and amounts to 13.8 %.

4.3 STUDY OF SOLAR CELLS BASED ON CDS/CDTE ON A FLEXIBLE SUBSTRATE AS PART OF A MODULE

4.3.1 DEVELOPMENT OF A METHOD FOR OBTAINING A CDS/CDTE/CU/AU MODULE ON A FLEXIBLE SUBSTRATE DESIGNED FOR BACKUP POWER SUPPLY OF EMERGENCY PREVENTION SYSTEMS

Thin film solar cells can generally be designed in two structures, known as superstrate and substrate, depending on the direction of light entry into the bulk of the device structure. In film solar cells of the "superstrate" type, light enters the cell from the side of the substrate on which the base layers are deposited and then passes into the volume of the device structure. For film solar cells of the "substrate" type, the light comes from the side opposite to the substrate. Thus, for superstrate SCs, the substrate must be transparent in order to transmit enough light into the volume of the device structure. Therefore, for the most part, it is the "superstrate" type that is used to create efficient solar cells based on CdTe [50]. While metal substrates can only be used for the "substrate" structure, polymer substrates are used in both cases depending on their transparency [51]. At present, the highest efficiency of film solar cells based on CdTe on a flexible substrate in the implementation of the "substrate" type reaches 13.8 % [52]. For film elements of the "substrate" type, 7.3 % when using a polymer and 7.8 % when using a metal foil, while the predicted theoretical maximum for CdTe-based SC is almost 30 % [53].

It is believed that with the superstrate configuration it is possible to obtain more efficient solar cells. This is due to the "chloride" treatment, which results in a decrease in the electrical resistivity of CdTe due to the generation of ClTe—VCd acceptors. In [45, 54], the use of "chloride" treatment made it possible to obtain experimental samples of solar cells with an efficiency of more than 10 %, but solar cells were fabricated on glass substrates. In the case of "substrate", "chloride" treatment can only be applied to CdS layers [34, 55]. In such a case,

CHAPTER 4

the crystallinity of CdTe is not optimized. To create flexible solar cells, several materials are used as substrates, each of which has advantages and disadvantages. Among metals, molybdenum, titanium and stainless steel are most widely used, and among polymers – polyamide, polyethylene terephthalate and polyethylene naphthalate. The author of [56] used molybdenum as a flexible substrate. However, the efficiency of the obtained samples did not exceed 5 %, which is due to the complexity of forming an ohmic contact of such device structures. In [57], molybdenum and stainless steel were used as flexible substrates. The resulting device structures were studied by X-ray diffractometry, which made it possible to establish that, in addition to the difficulty of forming a rear contact, a limiting factor is the presence of defects in the form of dislocations in the base layer. In [58], Upilex polyimide films were used as substrates, which can withstand high temperatures (450 °C). The obtained results of the study demonstrated low efficiency values, which, according to the authors, is associated with inefficient radiation absorption in the polyamide substrate.

Thus, in the case of creating film solar cells based on CdTe on flexible substrates, the efficiency of device structures is limited by two groups of factors: firstly, it is the difficulty in creating a high-quality back contact, and secondly, significant absorption of the visible part of the spectrum when passing through the substrate .

4.3.2 PREPARATION OF SAMPLES OF THE ITO/CDS/CDTE/CU/AU MODULE ON A POLYAMIDE SUBSTRATE

The tested solar module based on CdS/CdTe consisted of four micromodules connected in parallel. Each micromodule consisted of five solar cells connected in series (**Fig. 4.10**). A set of metal masks was used to manufacture the module (**Fig. 4.11**). This method is more economical than photolithography. The module was fabricated on polyamide substrates, Kapton brand, manufactured by DuPont, amber color, 50 μm thick, by magnetron sputtering of the target [59]. The target was a compressed mechanical mixture of In_2O_3 (90 wt. %) and SnO_2 (10 wt. %).

ITO films were formed at a deposition temperature of 300 °C. For the deposition of ITO films, a mask was used without separation into separate electrodes. The initial partial pressure was 104 Pa. The specific power of the magnetron was 1.5 W/cm^2, which corresponds to the range of values commonly used to obtain transparent and electrically conductive ITO films [60]. ITO sputtering was carried out in an argon-oxygen mixture at a pressure of 8×10^{-1} Pa. Under such conditions, layers were formed with a surface resistance of 10 Ohm/□ and an average transmittance in the visible spectral range of about 90 %, which is achieved by reducing their thickness to 0.1 μm [60].

The same mask was used to apply the cadmium sulfide and telluride layers. The deposition of these layers was carried out in a single technological cycle by thermal vacuum deposition from graphite evaporators at an initial vacuum of 104 Pa without its excitation.

CHAPTER 4

Fig. 4.10 Appearance of the solar cell module
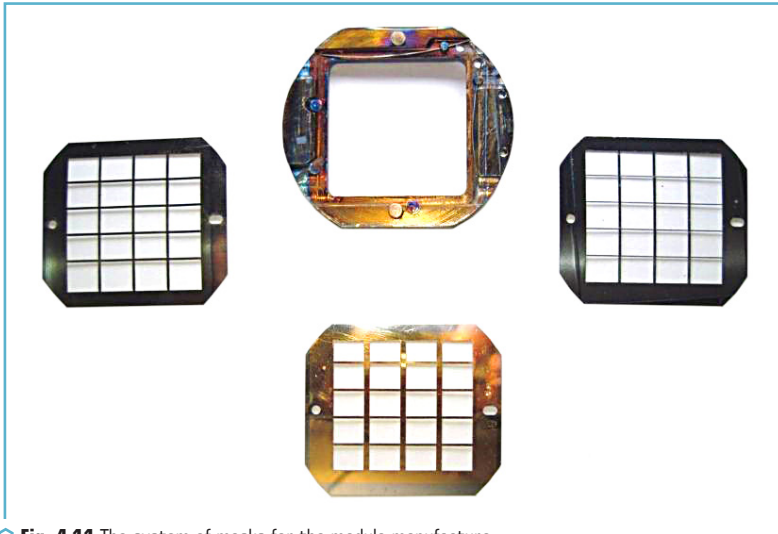
Fig. 4.11 The system of masks for the module manufacture

CHAPTER 4

The resulting instrumental heterosystems were subjected to the "chloride" treatment standard for this type of SC. In this case, smaller mask sizes were used. This is due to the fact that

cadmium telluride layers were used as dielectric layers separating the elements from each other, which are not affected by cadmium by the chloride layer and, therefore, were not subjected to "chloride" treatment, which reduces series resistance. To implement the "chloride" treatment, $CdCl_2$ films were deposited on the surface of the CdTe layers by thermal evaporation without heating the substrate. It is well known that "chloride" treatment [34] causes an increase in efficiency by several times. As a result of such treatment, the electrical resistivity of CdTe decreases due to the generation of ClTe–VCd acceptors with a concentration of about 10^{14} cm^{-3}, which reduces R_s. In addition, during such treatment, recrystallization of the base layer is observed, in which the CdTe columnar structure with a small grain size is transformed into a free orientation structure with large grain sizes. As a result, the probability of partial shunting of the separating barrier by the grain-boundary surface decreases, which causes an increase in R_w. Then the obtained multilayer film systems ITO/CdS/CdTe/CdCl$_2$ were annealed in air in a closed volume at a temperature of 430 °C for 25 min. To remove the reaction products, the annealed samples were subjected to digestion in a 5 % bromine solution in methanol.

To form the rear electrodes of the SC, two-layer Cu/Au electrical contacts were deposited on the etched surface of cadmium telluride in a vacuum setup by thermal evaporation. Since it is impossible to obtain effective device structures without a copper interlayer, a nanosized copper layer 2 nm thick was deposited on the surface of cadmium telluride. The minimization of the copper layer thickness was aimed at increasing the degradation resistance of the device structure.

4.3.3 RESULTS OF THE STUDY OF THE LIGHT CURRENT-VOLTAGE CHARACTERISTICS OF CDS/CDTE/CU/AU MICROMODULES ON A FLEXIBLE POLYAMIDE SUBSTRATE

The initial parameters of the micromodules included in the ITO/CdS/CdTe/Cu/Au module with serial connection of elements were obtained by analytical processing of the light CVCs (**Table 4.8**).

● **Table 4.8** Initial parameters of ITO/CdS/CdTe/Cu/Au micromodules with serial connection of solar cells

Micromodule	V_{nl}, mV	J_{sc}, mA/cm^2	FF	Efficiency, %
M5_1	2449	2.8	0.59	4.0
M5_2	3489	2.7	0.39	3.7
M5_3	3572	2.8	0.54	5.3
M5_4	3052	2.1	0.56	3.5

The light CVC of the micromodules, measured at a light flux power of 100 mW/cm^2 and with a series connection of solar cells, are shown in **Fig. 4.12, 4.13**.

CHAPTER 4
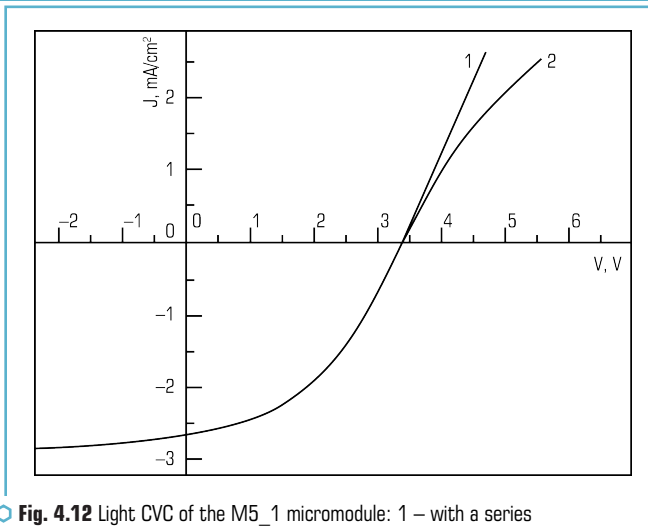
Fig. 4.12 Light CVC of the M5_1 micromodule: 1 – with a series connection of four SCs; 2 – with five solar cells are connected in series
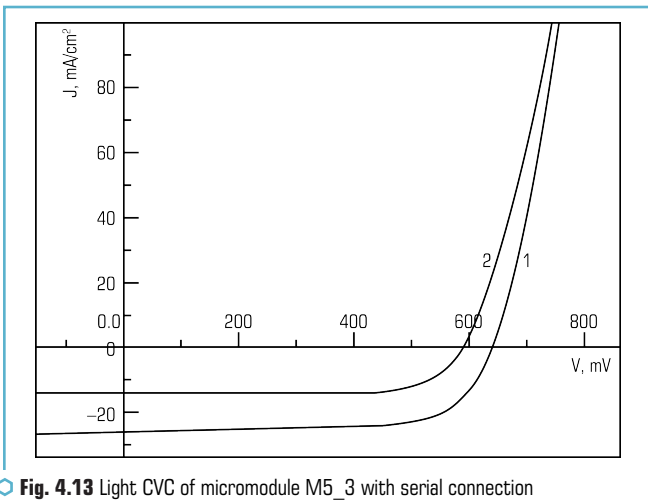
Fig. 4.13 Light CVC of micromodule M5_3 with serial connection of five solar cells

As can be seen from **Table 4.8**, when the elements in the micromodule are connected in series, the efficiency of the micromodules reaches the maximum efficiency at the level of 5.3 %.

CHAPTER 4

4.3.4 THE RESULTS OF THE STUDY OF THE EFFECT ON THE EFFICIENCY OF MICROMODULES ON A FLEXIBLE POLYAMIDE SUBSTRATE OF THE INITIAL PARAMETERS OF THE CONSTITUENT ELEMENTS AND CONDITIONS FOR OBTAINING EXPERIMENTAL SAMPLES

By analytical processing of light CVCs, the initial parameters and light diode characteristics of the studied solar cells were obtained separately and when they were connected in series as part of a micromodule.

The results obtained are presented in **Tables 4.9**, **4.10**, where C is a single SC, C2-C5 is a micromodule M5_1 when four SCs are connected in series, C1-C5 is a micromodule when five SCs are connected in series.

As can be seen from **Tables 4.9** and **4.10**, the solar cell in the micromodule M5_1 has the highest efficiency at the level of 8.4 %. However, the maximum efficiency of the entire micromodule is limited to 4.9 %.

● **Table 4.9** Output parameters and LED characteristics of micromodule SC M5_1

Sample	C1	C2	C3	C4	C5	C2-C5	C1-C5
V_{nl}, mV	97	748	755.5	133	752	2389	2486
J_{sc}, mA/cm^2	10.6	16.6	18.2	12.6	16.2	3.4	2.7
FF, c.u.	0.27	0.61	0.61	0.26	0.59	0.59	0.58
Efficiency, %	0.3	7.5	8.4	0.4	7.1	4.9	3.9
R_s, Ohm·cm^2	4.1	8.77	8.47	3.03	8.77	186	239
R_w, Ohm·cm^2	9.4	498	673	808	623	7×103	1×105
J_0, A/cm^2	9×10^{-4}	5×10^{-11}	4×10^{-11}	9×10^{-6}	6×10^{-9}	2×10^{-14}	2×10^{-14}
A, c.u.	1.8	1.5	1.5	1.1	2.0	3.7	3.8
J_p, mA/cm^2	18.4	16.7	18.4	17.3	16.5	3.5	2.8

The study of the initial parameters of micromodules in the composition of the module on a polyamide substrate showed that the maximum efficiency (**Table 4.8**) is observed for the M5_3 micromodule at the level of 5.3 %. Serial connection of solar cells in micromodules M5_1 made it possible to obtain an efficiency of 3.9 %. Such a low efficiency value for the micromodule M5_1 compared to the micromodule is due to M5_3 with a low value of Vnl. The presumably low V_{nl} value for the M5_1 micromodule is due to the shunting of the solar cells in the micromodule. This

assumption was confirmed by analyzing the initial parameters and light diode characteristics of individual solar cells of modules M5_1 and M5_3. An analysis of the initial parameters and light diode characteristics of individual solar cells of modules M5_1 and M5_3 showed that the first of the micromodules (M5_1) had two practically shunted solar cells. The second micro-module (M5_3) had one solar cell with a significantly lower efficiency.

● **Table 4.10** Output parameters and LED characteristics of micromodule SC M5_3

Sample	C1	C2	C3	C4	C5	C1-C5
V_{nl}, mV	752	762	552	758	741	3582
J_{sc}, mA/cm^2	15.2	16.7	16.9	17.8	16.9	2,7
FF, c.u.	0.54	0.61	0.28	0.60	0.55	0.55
Efficiency, %	6.2	7.7	2.6	8.1	6.8	5.3
R_s, Ohm·cm^2	5.6	5.7	12.8	6.3	10.1	243
R_w, Ohm·cm^2	238	476	24	520	400	15630
J_0, A/cm^2	3×10^{-7}	5×10^{-8}	6×10^{-8}	2×10^{-8}	7×10^{-9}	5×10^{-8}
A, c.u.	2.8	2.3	2.0	2.2	2.0	2.8
J_p, mA/cm^2	15.6	16.9	25.9	18.0	17.3	2.8

Analysis of the **Table 4.9** shows that for individual solar cells of the first micromodule, the light diode characteristics and initial parameters changed in the following intervals: $R_s=(3–9)$ Ohm·cm^2, $R_w=(9–620)$ Ohm·cm^2, $J_0=(4\times10^{-11}–9\times10^{-4})$ A/cm^2, $V_{nl}=(97–755)$ mV, $J_{sc}=(10.6–18.2)$ mA/cm^2, $FF=(0.26–0.61)$, efficiency$=(0.3–8.4)$ %, for the second micromodule – $R_s=(5.5–10)$ Ohm·cm^2, $R_w=(24–520)$ Ohm·cm^2, $J_0=(7\times10^{-9}–3.0\times10^{-7})$ A/cm^2, $V_{nl}=(550–760)$ mV, $J_{sc}=(15–17.8)$ mA/cm^2, $FF=(0,28–0.6)$, efficiency$=(2.6–8.1)$ %.

Thus, it can be argued that the low efficiency of micromodules in comparison with the efficiency of single solar cells in the micromodule is due to a decrease in all initial parameters. The creation of a Cu/Au tunnel back contact made it possible to obtain high Vnl values for individual solar cells, but as part of a micromodule it is limited to a shunted solar cell. The greatest role in reducing the efficiency of the entire micromodule is played by a significant decrease in Jsc, both for the first and second micromodules. This circumstance may be due to the inefficient absorption of radiation when passing through the dark yellow polyamide film. Therefore, for further research, it is necessary to focus on reducing the thickness of the polyamide film.

CHAPTER 4

CHAPTER 4

CONCLUSIONS

1. An analysis of losses in the initial parameters of solar cells based on CdS/CdTe showed that in order to increase the efficiency of the device structure, it is necessary to reduce the recombination rate of minority charge carriers in the volume of the photovoltaic converter, reduce the series resistance and conductivity of the shunt level.

The main directions for increasing the efficiency of CdS/CdTe based SCs by increasing V_{nl} and J_{sc} have already been implemented, but insufficient attention is paid to increasing the efficiency by increasing the FF of the light CVC by reducing the series resistance when creating low-tilt rear contacts.

It has been experimentally established that in the absence of a copper interlayer on the rear surface or the absence of an annealing process after the formation of a rear contact, the efficiency of ITO/CdS/CdTe/Cu/Au film SCs is limited at the level of 3–4 %, which is due to the operation of the device structure in the "through diode" mode. When a Cu/Au tunnel contact is formed, the SC efficiency increases to 10 %.

2. The study of transparent Cu/ITO rear contacts for CdTe-based solar cells intended for use in tandem and bilaterally sensitive device structures made it possible to establish that the preliminary deposition of a nanosized copper layer on the CdTe surface to form the back electrode makes it possible to form a high-quality tunnel contact. After 8 years of operation, the efficiency of the studied solar cells practically coincides with the initial one.

It has been established that changing the direction of illumination of the SnO_2:F/CdS/CdTe/Cu/ITO SCs leads to a significant decrease in the efficiency of the device structure. The differences in the initial parameters and light diode characteristics of SnO_2:F/CdS/CdTe/Cu/ITO SCs are due to the effect of the rear diode on the efficiency of photovoltaic processes in the base layer.

3. Using the DC magnetron sputtering method, experimental samples of a module based on cadmium telluride on a flexible polyamide substrate have been obtained, consisting of four micromodules with series-connected solar cells. Researches of initial parameters and light diode characteristics of the micromodules which are a part of the module havew been carried out.

It has been found that the maximum efficiency of the micromodule as part of the module reached 5.3 %. It has been established that the low efficiency values of micromodules are due to the partial shunting of solar cells in the composition of micromodules and inefficient absorption of the visible part of the radiation when passing through the polyamide substrate.

CONFLICT OF INTEREST

The authors declare that they have no conflict of interest in relation to this research, whether financial, personal, authorship or otherwise, that could affect the research and its results presented in this paper.

REFERENCES

1. Rashkevich, N., Shevchenko, R., Khmyrov, I., Soshinskiy, A. (2021). Investigation of the Influence of the Physical Properties of Landfill Soils on the Stability of Slopes in the Context of Solving Civil Security Problems. Materials Science Forum, 1038, 407–416. doi: https://doi.org/10.4028/www.scientific.net/msf.1038.407

2. Yeremenko, S., Sydorenko, V., Andrii, P., Shevchenko, R., Vlasenko, Y. (2021). Existing Risks of Forest Fires in Radiation Contaminated Areas: A Critical Review. Ecological Questions, 32 (3), 35–47. doi: https://doi.org/10.12775/eq.2021.022

3. Gurbanova, M., Loboichenko, V., Leonova, N., Strelets, V., Shevchenko, R. (2020). Comparative assessment of the ecological characteristics of auxiliary organic compounds in the composition of foaming agents used for fire fighting. Bulletin of the Georgian National Academy of Sciences, 14 (4), 58–66.

4. Kirichenko, M. V., Zaitsev, R. V., Deyneko, N. V., Kopach, V. R., Antonova, V. A., Listratenko, A. M. (2008). Influence of Constructive and Technological Solutions of Silicon Solar Cells on Minority Carrier Parameters of Base Crystals. Telecommunications and Radio Engineering, 67 (3), 227–240. doi: https://doi.org/10.1615/telecomradeng.v67.i3.40

5. Romeo, N., Bosio, A., Romeo, A. (2010). An innovative process suitable to produce high-efficiency CdTe/CdS thin-film modules. Solar Energy Materials and Solar Cells, 94 (1), 2–7. doi: https://doi.org/10.1016/j.solmat.2009.06.001

6. De Vos, A., Parrott, J., Baruch, P., Landsberg, P. (1994). Bandgap effects in thin-film heterojunction solar cells. Proceeding 12th European Photovoltaic Solar Energy Conference. Amsterdam, 1315–1319.

7. 16.5 %-Efficient CdS/CdTe polycrystalline thin-film solar cell (2001). 17th European Photovoltaic Solar Energy Conference. Munich, 995–1000.

8. Köntges, M., Reineke-Koch, R., Nollet, P., Beier, J., Schäffler, R., Parisi, J. (2002). Light induced changes in the electrical behavior of CdTe and Cu(In,Ga)Se2 solar cells. Thin Solid Films, 403-404, 280–286. doi: https://doi.org/10.1016/s0040-6090(01)01507-3

9. Zeng, G., Zhang, J., Li, B., Li, W., Wu, L., Wang, W., Feng, L. (2015). Effects of different CdCl2 annealing methods on the performance of CdS/CdTe polycrystalline thin film solar cells. Science China Technological Sciences, 58 (5), 876–880. doi: https://doi.org/10.1007/s11431-015-5787-2

10. Riech, I., Peña, J. L., Ares, O., Rios-Flores, A., Rejón-Moo, V., Rodríguez-Fragoso, P., Mendoza-Alvarez, J. G. (2012). Effect of annealing time of CdCl$_2$vapor treatment on CdTe/CdS interface properties. Semiconductor Science and Technology, 27 (4), 045015. doi: https://doi.org/10.1088/0268-1242/27/4/045015

11. Khrypunov, G. (2010). Development organic васk contact for thin-film CdS/CdTe solar cell. Physics and Chemistry of Solid State, 11 (1), 248–251.

CHAPTER 4

12. Wu, H. (2014). p-CdTe/n-CdS photovoltaic cells in the substrate configuration. University of Rochester.

13. Enzenroth, R. A., Barth, K. L., Sampath, W. S. (2005). Correlation of stability to varied CdCl2 treatment and related defects in CdS/CdTe PV devices as measured by thermal admittance spectroscopy. Journal of Physics and Chemistry of Solids, 66 (11), 1883–1886. doi: https://doi.org/10.1016/j.jpcs.2005.09.022

14. Bätzner, D. L., Romeo, A., Zogg, H., Wendt, R., Tiwari, A. N. (2001). Development of efficient and stable back contacts on CdTe/CdS solar cells. Thin Solid Films, 387 (1-2), 151–154. doi: https://doi.org/10.1016/s0040-6090(01)00792-1

15. Mamazza, R., Balasubramanian, U., More, D. L., Ferekides, C. S. (2002). Thin films of CdIn2O4 as transparent conducting oxides. Proceeding of the 29nd IEEE Photovoltaic Specialists Conference. Anaheim, 616–619. doi: https://doi.org/10.1109/pvsc.2002.1190640

16. Minami, T., Kakumu, T., Takeda, Y., Takata, S. (1996). Highly transparent and conductive ZnO In2O3 thin films prepared by d.c. magnetron sputtering. Thin Solid Films, 290-291, 1–5. doi: https://doi.org/10.1016/s0040-6090(96)09094-3

17. Effect of CdCl2 treatment on the interior of CdTe crystal (2001). Proceeding Materials Research Society Symposium. San Francisco, H1.6.1–H1.6.12.

18. Romeo, A., Bätzner, D. L., Zogg, H., Tiwari, A. N. (2000). Recrystallization in CdTe/CdS. Thin Solid Films, 361-362, 420–425. doi: https://doi.org/10.1016/s0040-6090(99)00753-1

19. Sandhu, A., Kobayashi, K., Okamoto, T., Yamada, A., Konagai, M. (2001). Effect of CdCl2 Treatment Conditions on the Deep Level Density, Carrier Lifetime and Conversion Efficiency of CdTe Thin Film Solar Cells. MRS Proceedings. San Francisco, 668, H8.13.1–H8.13.6. doi: https://doi.org/10.1557/proc-668-h8.13

20. High-efficiency Cd2SnO4/Zn2SnO4/ZnxCd1-xS/CdS/CdTe polycrystalline thin-film solar cells (2002). Proc. 29th IEEE Photovotaics Specialists Conf. New Orleans, 470–474.

21. Demtsu, S. H., Sites, J. R. (2005). Quantification of losses in thin-film CdS/CdTe solar cells. Conference Record of the Thirty-First IEEE Photovoltaic Specialists Conference, 347–350. doi: https://doi.org/10.1109/pvsc.2005.1488140

22. Schottky diode current (2002). Proc. 29th IEEE Photovotaics Specialists Conf. New Orleans, 535–538.

23. Terheggen, M., Heinrich, H., Kostorz, G., Baetzner, D., Romeo, A., Tiwari, A. N. (2004). Analysis of Bulk and Interface Phenomena in CdTe/CdS Thin-Film Solar Cells. Interface Science, 12 (2/3), 259–266. doi: https://doi.org/10.1023/b:ints.0000028655.11608.c7

24. Green, M. A. (1992). Solar cells: operating principles, technology and system applications. University of New South Wales. Kensington, 274.

25. Khrypunov, G., Meriuts, A., Klyui, N., Shelest, T., Deyneko, N., Kovtun, N. (2010). Development of back contact for CdS/CdTe thin-film solar cells. Functional materials, 17 (1), 114–119.

CHAPTER 4

26. Bätzner, D. L., Wendt, R., Romeo, A., Zogg, H., Tiwari, A. N. (2000). A study of the back contacts on CdTe/CdS solar cells. Thin Solid Films, 361-362, 463–467. doi: https://doi.org/10.1016/s0040-6090(99)00842-1

27. Meriuts, A. V., Khrypunov, G. S., Shelest, T. N., Deyneko, N. V. (2010). Features of the light current-voltage characteristics of bifacial solar cells based on thin CdTe layers. Semiconductors, 44 (6), 801–804. doi: https://doi.org/10.1134/s1063782610060187

28. Research, Solar Cell Production and Market Implementation of Photovoltaics (2004). European Commission, DG JRC, Institute for Environment and Sustainability Energies Unit Via Enrico Fermi 1; TP 450 I – 21020. Ispra, 95.

29. Mitchell, K., Fahrenbruch, A. L., Bube, R. H. (1977). Photovoltaic determination of optical-absorption coefficient in CdTe. Journal of Applied Physics, 48 (2), 829–830. doi: https://doi.org/10.1063/1.323636

30. Khripunov, G. S., Sokol, E. I., Iakimenko, Iu. I., Meriutc, A. V., Ivashchuk, A. V., Shelest, T. N. (2014). Conversion of solar energy by combination solar cells based on CdTe and CuInSe$_2$. Fizika i tekhnika poluprovodnikov, 48 (12), 1671–1675.

31. Jackson, P., Hariskos, D., Lotter, E., Paetel, S., Wuerz, R., Menner, R., Wischmann, W., Powalla, M. (2011). New world record efficiency for Cu(In,Ga)Se2 thin-film solar cells beyond 20 %. Progress in Photovoltaics: Research and Applications, 19 (7), 894–897. doi: https://doi.org/10.1002/pip.1078

32. Khrypunov, G., Vambol, S., Deyneko, N., Sychikova, Y. (2016). Increasing the efficiency of film solar cells based on cadmium telluride. Eastern-European Journal of Enterprise Technologies, 6 (5 (84)), 12–18. doi: https://doi.org/10.15587/1729-4061.2016.85617

33. Li, J., Zhang, Y., Gao, T., Hu, C., Yao, T., Yuan, Q. et al. (2017). Quantum dot-induced improved performance of cadmium telluride (CdTe) solar cells without a Cu buffer layer. Journal of Materials Chemistry A, 5 (10), 4904–4911. doi: https://doi.org/10.1039/c6ta10441j

34. Deyneko, N., Khrypunov, G., Semkiv, O. (2018). Photoelectric Processes in Thin-film Solar Cells Based on CdS/CdTe with Organic Back Contact. Journal of Nano- and Electronic Physics, 10 (2), 02029-1–02029-4. doi: https://doi.org/10.21272/jnep.10(2).02029

35. Alonzo, J., Kochemba, W. M., Pickel, D. L., Ramanathan, M., Sun, Z., Li, D. et al. (2013). Assembly and organization of poly(3-hexylthiophene) brushes and their potential use as novel anode buffer layers for organic photovoltaics. Nanoscale, 5 (19), 9357–9364. doi: https://doi.org/10.1039/c3nr02226a

36. Burmenko, A., Deyneko, N., Hrebtsova, I., Kryvulkin, I., Prokopenko, O., Shevchenko, R., Tarasenko, O. (2020). Investigating an alternative electricity supply system for preventing emergencies under conditions of limited capacity. Eastern-European Journal of Enterprise Technologies, 3 (12 (105)), 56–61. doi: https://doi.org/10.15587/1729-4061.2020.206395

CHAPTER 4

37. Deyneko, N., Zhuravel, A., Mikhailova, L., Naden, E., Onyshchenko, A., Savchenko, A., Strelets, V., Yurevych, Y. (2020). Devising a technique to improve the efficiency of CdS/CdTe/Cu/Au solar cells intended for use as a backup power source for the systems of safety and control of objects. Eastern-European Journal of Enterprise Technologies, 6 (5 (108)), 21–27. doi: https://doi.org/10.15587/1729-4061.2020.220489

38. Deyneko, N., Yeremenko, S., Kamyshentsev, G., Kryvulkin, I., Matiushenko, M., Myroshnyk, O. et al. (2021). Development of a method for obtaining a CdS/CdTe/Cu/Au module on a flexible substrate designed for backup supplying systems prevention of emergency situations. Eastern-European Journal of Enterprise Technologies, 1 (5 (109)), 31–36. doi: https://doi.org/10.15587/1729-4061.2021.225694

39. Venkatesan, M., McGee, S., Mitra, U. (1989). Indium tin oxide thin films for metallization in microelectronic devices. Thin Solid Films, 170 (2), 151–162. doi: https://doi.org/10.1016/0040-6090(89)90719-0

40. Jeong, W.-J., Park, G.-C. (2001). Electrical and optical properties of ZnO thin film as a function of deposition parameters. Solar Energy Materials and Solar Cells, 65 (1-4), 37–45. doi: https://doi.org/10.1016/s0927-0248(00)00075-1

41. Deyneko, N., Semkiv, O., Khmyrov, I., Khryapynskyy, A. (2018). Investigation of the combination of ITO/CdS/CdTe/Cu/Au solar cells in microassembly for electrical supply of field cables. Eastern-European Journal of Enterprise Technologies, 1 (12 (91)), 18–23. doi: https://doi.org/10.15587/1729-4061.2018.124575

42. Chernykh, E. P., Khripunov, G. C., Boiko, B. T. (2002). Otcenka stekhiometrii absorbernykh sloev CuGaSe2 i CuIn0,7Ga0,3Se2 plenochnykh fotoelektricheskikh preobrazovatelei. Visnik Sumskogo derzhavnogo universitetu, 13 (46), 133–140.

43. Boyko, B., Khrypunov, G., Kharchenko, M., Chernikov, A. (2001). Examination of thermal stability of ZnO:Al films obtained by RF-magnetron sputtering without preheating of substrate. Proceeding of 17th European Photovoltaic Solar Energy Conversion and Exhibition. Munich, 1128–1130.

44. Boiko, B. T., Chernykh, O. P., Khrypunov, H. S., Kopach, H. Y. (2001). Plivkovi fotoelektrychni peretvoriuvachi na osnovi CuGaSe2. Fizyka i khimiia tverdoho tila, 2 (4), 549–558.

45. Khrypunov, G. S., Kopach, V. R., Meriuts, A. V., Zaitsev, R. V., Kirichenko, M. V., Deyneko, N. V. (2011). The influence of prolonged storage and forward-polarity voltage on the efficiency of CdS/CdTe-based film solar cells. Semiconductors, 45 (11), 1505–1511. doi: https://doi.org/10.1134/s1063782611110133

46. Bolbas, O., Deyneko, N., Yeremenko, S., Kyryllova, O., Myrgorod, O., Soshinsky, O. et al. (2019). Degradation of CdTe SC during operation: modeling and experiment. Eastern-European Journal of Enterprise Technologies, 6 (12 (102)), 46–51. doi: https://doi.org/10.15587/1729-4061.2019.185628

47. Vambol, S., Vambol, V., Sychikova, Y., Deyneko, N. (2017). Analysis of the ways to provide ecological safety for the products of nanotechnologies throughout their life cycle.

CHAPTER 4

Eastern-European Journal of Enterprise Technologies, 1 (10 (85)), 27–36. doi: https://doi.org/10.15587/1729-4061.2017.85847

48. Romeo, A., Bätzner, D. L., Zogg, H., Tiwari, A. N. (2001). Influence of proton irradiation and development of flexible CdTe solar cells on polyimide. MRS Proceedings. San Francisco, 668, H3.3.1–H3.3.6. doi: https://doi.org/10.1557/proc-668-h3.3

49. Batzner, D. L., Romeo, A., Zogg, H., Tiwari, A. N., Wendt, R. (2003). Effect of back contact metallization on the stability of CdTe/CdS solar cells. 16 European Photovoltaic Solar Energy Conference: Proceeding of the conference. Glagow, 353–356.

50. Leterrier, Y., Médico, L., Demarco, F., Månson, J.-A. E., Betz, U., Escolà, M. F. et al. (2004). Mechanical integrity of transparent conductive oxide films for flexible polymer-based displays. Thin Solid Films, 460 (1-2), 156–166. doi: https://doi.org/10.1016/j.tsf.2004.01.052

51. Leterrier, Y., Pinyol, A., Gilliéron, D., Månson, J.-A. E., Timmermans, P. H. M., Bouten, P. C. P. et al. (2010). Mechanical failure analysis of thin film transistor devices on steel and polyimide substrates for flexible display applications. Engineering Fracture Mechanics, 77 (4), 660–670. doi: https://doi.org/10.1016/j.engfracmech.2009.12.016

52. Borysenko, I., Burmenko, O., Deyneko, N., Zobenko, O., Yivzhenko, Y., Kamyshentsev, G. et al. (2021). Development of a method for producing effective CdS/CdTe/Cu/Au solar elements on a flexible substrate designed for backup supplying systems prevention of emergency situations. Eastern-European Journal of Enterprise Technologies, 6 (5 (114)), 6–11. doi: https://doi.org/10.15587/1729-4061.2021.247720

53. McCandless, B. E. (2001). Thermochemical and Kinetic Aspects of Cadmium Telluride Solar Cell Processing. MRS Proceedings, 668, H1.6.1–H1.6.10. doi: https://doi.org/10.1557/proc-668-h1.6

54. Deyneko, N., Semkiv, O., Soshinsky, O., Streletc, V., Shevchenko, R. (2018). Results of studying the Cu/ITO transparent back contacts for solar cells SnO2:F/CdS/CdTe/Cu/ITO. Eastern-European Journal of Enterprise Technologies, 4 (5 (94)), 29–34. doi: https://doi.org/10.15587/1729-4061.2018.139867

55. Izu, M., Ellison, T. (2003). Roll-to-roll manufacturing of amorphous silicon alloy solar cells with in situ cell performance diagnostics. Solar Energy Materials and Solar Cells, 78 (1-4), 613–626. doi: https://doi.org/10.1016/s0927-0248(02)00454-3

56. Deyneko, N., Kovalev, P., Semkiv, O., Khmyrov, I., Shevchenko, R. (2019). Development of a technique for restoring the efficiency of film ITO/CdS/CdTe/Cu/Au SCs after degradation. Eastern-European Journal of Enterprise Technologies, 1 (5 (97)), 6–12. doi: https://doi.org/10.15587/1729-4061.2019.156565

57. Söderström, K., Escarré, J., Cubero, O., Haug, F.-J., Perregaux, S., Ballif, C. (2010). UV-nano-imprint lithography technique for the replication of back reflectors for n-i-p thin film silicon solar cells. Progress in Photovoltaics: Research and Applications, 19 (2), 202–210. doi: https://doi.org/10.1002/pip.1003

CHAPTER 4

58. Deyneko, N., Kryvulkin, I., Matiushenko, M., Tarasenko, O., Khmyrov, I., Khmyrova, A., Shevchenko, R. (2019). Investigation of photoelectric converters with a base cadmium telluride layer with a decrease in its thickness for tandem and two-sided sensitive instrument structures. EUREKA: Physics and Engineering, 5, 73–80. doi: https://doi.org/10.21303/2461-4262.2019.001002

59. Deyneko, N. (2020). Study of Methods for Producing Flexible Solar Cells for Energy Supply of Emergency Source Control. Materials Science Forum, 1006, 267–272. doi: https://doi.org/10.4028/www.scientific.net/msf.1006.267

60. First Solar sets world record for CdTe solar cell efficiency (2014). Solar First. Available at: https://investor.firstsolar.com/news/press-release-details/2014/First-Solar-Sets-World-Record-for-CdTe-Solar-Cell-Efficiency/default.aspx

CHAPTER 4

Ernst Kussul, Tetyana Baydyk,
Masuma Mammadova, Jorge Luis Rodriguez Mendoza

CHAPTER 5

SOLAR CONCENTRATOR APPLICATIONS IN AGRICULTURE

ABSTRACT

We have developed several prototypes of solar concentrators that are compact, light, and inexpensive. As an example of solar concentrators, we selected parabolic solar concentrators with plane mirrors that approximate the parabolic surface. A methodology is proposed for the evaluation of the impact of combinations of solar concentrators together with certain agricultural crops. The proposed mathematical model is simple and applicable for different cases of combination of solar concentrators and agricultural fields. This study is dedicated to renewable energy on the example of two countries, Mexico and Azerbaijan. The relief and climate of both countries have many common features, which are expressed particularly in the abundance of solar radiation, the predominance of mountainous regions with remote and hard-to-reach settlements that need to create autonomous life support systems. The main problem for proposed solar concentrators is the automatization of the assembly process of these solar concentrators. We proposed two methods of assembly that is, using a parabolic rule and using a robotic arm with a stereoscopic vision system. Both methods are described in this chapter.

KEYWORDS

Agricultural crops, mathematical model, solar concentrator, Micro Equipment Technology (MET), flat triangular mirrors, assembly, automatization.

The global climate change and its negative impact on the stable economic development of countries around the world have created a real danger to humanity in recent decades. It is well known that the active consumption of traditional energy sources (e.g., coal, oil, gas) is the main cause of environmental imbalance and climate change. This requires vigorous decisions and actions from the world community, scientists and politicians to hamper the global warming, reduce carbon dioxide emissions (CO_2) caused by anthropogenic factors. Scientists and experts on climate change estimate that even a 1.5 °C increase in temperature will lead to irreversible changes in the environment. Therefore, it is necessary to reduce greenhouse gas emissions (GHG) by 2030 by 45–60 %

CHAPTER 5

compared to 2010, and by 2050 it is necessary to achieve a zero balance allowing ecosystems to absorb all anthropogenic emissions [1].

To date, all UN member countries have ratified the Paris Agreement, which sets the goal of preventing global temperatures from rising by more than 2 °C [2]. Each country has committed to Nationally Determined Contributions (NDCs) to reduce greenhouse gas emissions. In this regard, the ever-growing demand for energy in the world is accelerating the gradual transition of nation-states to green energy. The implementation of NDCs includes commitments to reduce greenhouse gases in the energy, agriculture, transport, and other sectors.

Agriculture is a critical component of the economy and plays a vital role in food security [3]. This area also stimulates the employment of the able-bodied population living in rural settlements, and provides a certain contribution to the achievement of sustainable development goals [4].

Along with this, agriculture is the most vulnerable segment of the economy to climate change, which manifests itself in the amount and distribution of precipitation, drought, land pollution, reduced water supply, changing seasons, etc. [5–7].

One way to meet the growing demand for food is to increase agricultural productivity and reduce the cost of agricultural production. Addressing this issue is of particular importance given the demographic trends that contribute to some extent to increased emissions and lead to an increase in per capita consumption of agricultural products. According to the new UN forecasts, by mid-November 2022, the world's population is estimated to increase to 8 billion people, and humanity to reach 8.5 billion people by 2035, 9.7 billion people by 2050, and 10.4 billion people by 2100. Back in 2011, the world population reached 7 billion people [8].

The development of agricultural production is largely determined by the technological modernization of the industry, the development of new intensive agricultural methods that increase the harvest and diversity of crops while protecting the soil through the use of environment-friendly renewable energy sources, conservation of water resources, etc. [9, 10]. Currently, many countries specify the transition to green energy as their national priorities. To implement this complex task, various concepts, numerous applied developments, technological solutions and equipment for the modernization of energy supply systems based on various renewable energy sources have already been proposed [11, 12].

One of the cleanest energy sources is solar energy, which is safe for the environment and does not cause global warming. Solar photovoltaic stations, which are the basis for the development of low-cost autonomous power supply systems, are now used to generate energy in many countries. A significant large area of roofs and walls of houses, including business buildings, as well as the availability of free territories may contribute to getting and collecting large amounts of free energy.

In the context of agriculture, technologies of solar energy are applicable in every sector of the agro-industrial complex and may address many problems in this field of activity.

In the modern practice of crop growing, one of the innovative, but promising applications of solar energy is the combination of plants and solar energy production on one piece of land. The idea of integrating solar devices into agro-ecosystems, namely agrovoltaic, provides the possibility of

dual use of land, i.e. growing plants while generating electricity on the same land. Agro-electric systems are particularly effective in agriculture in countries that suffer from land scarcity and lack of areas for crops, as well as those with dry areas and high solar potential.

Various approaches to the implementation of the technology of combining solar energy and land use require a precise calculation of the features of shadows, taking into account the risks negatively affecting the growth and development of plants, the crop size, etc.

Many researchers around the world are now focusing on these studies, aimed at both the development of agriculture and the improvement of solar devices, including the development of alternative energy [13–20]. According to the results of studies and experiments, the combination of solar energy with crops, with the right scientific approach, may increase crop yields on the one hand, and generate environmentally friendly energy on the other [21].

In another study [19], the objective was to examine the performance of agrovoltaic systems, which produce crops and electricity simultaneously based on the installation of stilt-mounted PV panels on farmlands (**Fig. 5.1**).
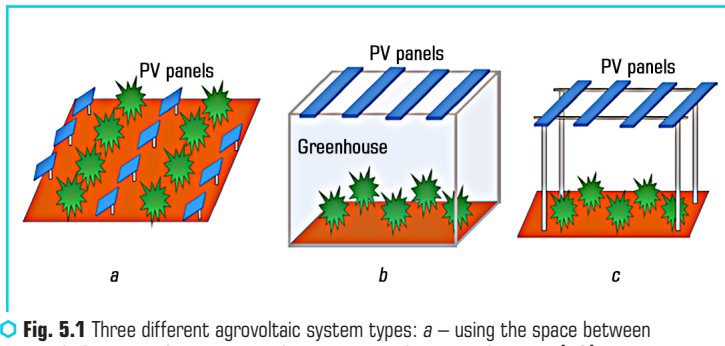
○ **Fig. 5.1** Three different agrovoltaic system types: *a* — using the space between PV panels for crops; *b* — a PV greenhouse; *c* — a stilt-mounted system [19]

The abovementioned studies consider three principles for the application of solar devices in agroecosystems:

1) emphasis on the agricultural crops that make up the agroecosystem;
2) emphasis on the solar energy production;
3) emphasis on the integration of solar panels into agroecosystems.

The first principle is aimed to maximize biomass production by minimizing changes in production systems. Devices for electricity production are installed on available lands and do not severely change agricultural production. The second principle attempts to maximize the generation of solar energy and minimize the changes in standard technologies in solar energy receiving, contributing to the agricultural growth around renewable energy facilities. The third principle efforts to merge both cases and benefit from the increase in biomass and energy capacity of solar devices.

CHAPTER 5

In this study, implemented within the framework of the third principle, we have made an effort to preserve and upsurge the productivity of agricultural crops while guaranteeing the highest power generation.

5.1 OUR APPROACH

This article explores the reasons for the transition of countries to a green economy through the prism of global climate change. An analysis of the state of development of environmentally friendly energy sources is performed on the example of two countries, i.e., Azerbaijan and Mexico, the energy sectors of which are mainly based on natural fuel. These countries, taking into account the values of their basic economic indicators, have upper-middle-income economies (4,046–12,535 USD) being referred to the group of developing countries and are gradually approaching the category of developed countries and also have a number of similar climatic, agrobiological and geographic relief features. More than 77 % of the world's population lives in developing countries, which make up about 4/5 of all countries in the world [22].

The main factors determining the relevance of the development of renewable energy sources in these countries are identified, with an emphasis on the use of the latter in agro-complexes. As the main segment of agriculture, crop production is considered, which is the leading field in ensuring food security and exports in both countries.

Taking into account the prospects of introducing agrovoltaics into crop production, this study considers the issues of creating integrated systems for electricity production and growing crops in one field through the use of solar energy.

Analysis of approaches to solving the problem of merging solar energy and agriculture, which makes it possible to identify two main problems when choosing a model for combining concentrators with certain types of plants. The first problem is related to the selection or development of solar concentrators that are most suitable for certain crops. The second factor is related to the choice of the mathematical model proposed to evaluate the most efficient placement of solar concentrators in the field in the combination with plants.

In **Fig. 5.2** we demonstrate flowchart of our model work. The model is subject to requirements of ease of use and versatility, providing simulation of various combinations of solar concentrators and agricultural fields. Another important point when choosing a model is to provide the ability to simulate various combinations of solar concentrators and plants without the need for empirical studies directly in the field. We can describe the general objective and specific objectives in the following way.

General objective is investigate the possibility of solar concentrator collocation between plants in agricultural fields.

Specific objectives:

1. Development of solar concentrators that are compact, light, and inexpensive. We selected parabolic solar concentrators with plane mirrors that approximate the parabolic surface.

CHAPTER 5

2. A methodology is proposed for the evaluation of the impact of combinations of solar concentrators together with certain agricultural crops. The proposed mathematical model is simple and can be implemented for different cases of a combination of solar concentrators and agricultural fields.

3. Parameter selection for solar concentrators (the characteristics taken into account in solar concentrators include their dimensions, weight, plate width or dish diameter, shade produced, mounting structure, the material of construction, quantity and distribution of solar concentrators).

4. Parameter selection for agricultural fields (the field area, its slope, soil type, humidity, spacing between the rows, crop type, crop density, maximum plant width, and plant height).

5. Creation of a computer program to realize the mathematical model.

6. Comparative analysis of Mexico and Azerbaijan and their possibilities to develop green energy.

7. Development of methods of automatic assembly of solar concentrators.

This article substantiates the expediency of choosing a linear model with two objective functions that make it possible to satisfy the specified requirements. Such a model can be effectively used in crop production in the countries with analogous characteristics and high solar radiation potential.
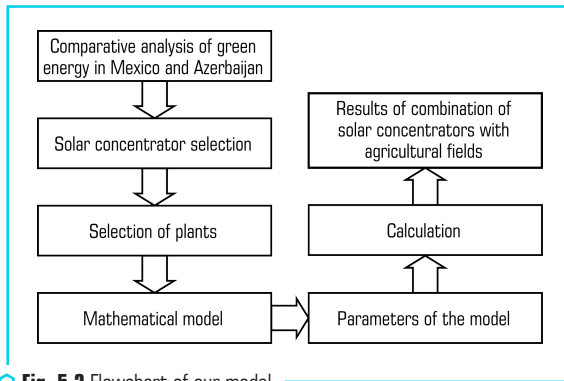
Fig. 5.2 Flowchart of our model

5.2 AZERBAIJAN AND MEXICO: DRIVERS FOR DEVELOPMENT OF GREEN ECONOMY

The main factors determining the need for the development of a green economy in Azerbaijan and Mexico may include:

1) global trend towards the decarbonization of energy and the need to fulfill obligations to reduce greenhouse gases;

2) climate policy of countries;

3) geographical location and landscape;

4) climatic conditions;

CHAPTER 5

5) along with traditional energy resources, presence of high potential of renewable energy sources;

6) priorities of social and economic development policy.

A comparative analysis of Azerbaijan and Mexico through the prism of factors that determine the relevance of the development of new types of renewable energy makes it possible to identify a number of similar features of these countries, which are listed below.

5.2.1 OIL AND GAS INDUSTRY

Azerbaijan and Mexico are the countries with a developed hydrocarbon industry. Huge reserves of oil and gas resources, which are produced on land and under the sea, have contributed to the attraction of large investments to these countries ensuring energy security, and became the main driving force of national economies, the most important source of foreign exchange earnings and a growth factor of the population's well-being.

However, as mentioned above, the extraction and refining of traditional energy resources are associated with environmental problems, and furthermore, fossil fuels are among the main sources of environmental pollution and global climate change. Therefore, in recent years, the importance of the transition to low-hydrogen and carbon-free energy sources has become specifically relevant. In this regard, Azerbaijan and Mexico, despite the large reserves of oil and gas, focus on the transfer of their energy systems to alternative, mainly renewable energy sources.

Currently, electricity generation in Azerbaijan and Mexico is mainly based on hydrocarbon resources. In recent years, both countries have been intensively converting traditional oil power plants into natural gas with cleaner burning.

Thus, in Azerbaijan, the share of gas in electricity production in early 2020 was estimated at 92 %. As of 2020, the country's share of electricity generation from environmentally friendly sources (mainly through the generation of energy from hydroelectric power plants) in the total amount of energy produced in the country amounted for 17 %.

In accordance with the Paris climate agreement, Azerbaijan has committed to reduce the level of gas emissions and a thermal effect by 35 % by 2030 compared to the base year 1990 [23]. In November 2021, at the COP26 conference held in Glasgow, Azerbaijan made a new commitment to reduce emissions by 40 % by 2050 and create a "Net Zero Emissions" zone in the territories liberated from occupation [24].

Positive demographic and economic trends played an important role in the growth of annual emissions in Mexico between 1990 and 2010, increasing by 33 %, and led to an increase in energy demand [25]. To prevent unsafe climate change and the development of low-carbon energy, the Mexican government has adopted a series of climate measures, due to which, in early 2020, 70.1 % of the installed net power capacity in Mexico came from thermal gas power plants. Energy production from low-carbon nuclear power plants in Mexico accounted for 2.1 %, while electricity

generation from clean renewable sources accounted for 27.8 % of the total electricity produced in the country [26].

Under the Paris Climate Agreement, Mexico's greenhouse gas reduction commitments are among the most ambitious in the world, compared to those of many developed countries and most other Latin American countries. Thus, Mexico's national greenhouse gas (GHG) emission reduction goals are to provide for bringing electricity generation from environmentally friendly sources to 35 % by 2024, and by 2035 to achieve a share in electricity generation with zero or low emissions up to 40 %. In the long term, it is planned to continue increasing the capacity of the energy sector by up to 50 % by 2050, including both renewable energy sources and low-carbon nuclear and fossil fuels [25].

Fig. 5.3, based on the BP Statistical Review of World Energy, shows the results of various types of energy consumption in Azerbaijan and Mexico. To concern from primary direct energy consumption, an inefficient factor has been applied or fossil fuels (i.e. the "substitution method") [27].
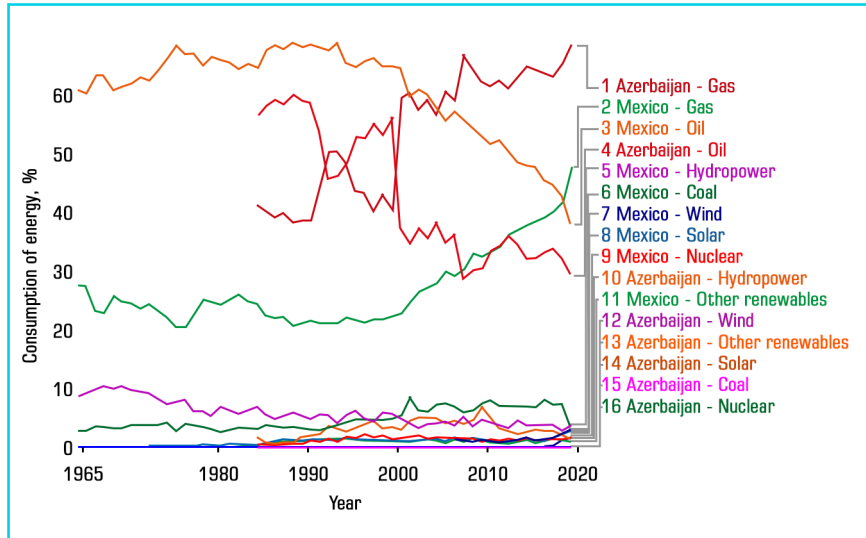

Fig. 5.3 Consumption of various types of energy (in Azerbaijan and Mexico in 2021 [27])

5.2.2 CLIMATE CHANGE POLICY

The growth of the renewable energy sector necessitates the enhancement of the policy and institutional environment in this field. Therefore, both countries have recently adopted relevant laws and regulations.

It should be mentioned that the establishment of the Azerbaijan Renewable Energy Agency under the Ministry of Energy of the Republic of Azerbaijan in 2020 [28], as well as the adoption of the law of the Republic of Azerbaijan "On the use of renewable energy sources in the production of electricity, in 2021 [29], significantly contributed to the growth of renewable energy.

The institutional and programme framework for national climate change mitigation policy in Mexico is specified in the 2012 General Law on Climate Change. Mexico [30] and the National Climate Change Strategy adopted in 2013. In 2021, the Mexican Ministry of Energy (Secretaría de Energía, SENER) prepared the Law on New Electric Industry in Mexico and the National Electricity System Development Programme for 2022–2036 [31].

5.2.3 GEOGRAPHICAL POSITION AND RELIEF DIVERSITY OF THE COUNTRIES

The territories of Azerbaijan and Mexico are characterized by a unique geographical position and diversity of relief.

The Republic of Azerbaijan is located in the east of the South Caucasus, to the southwest of the Caspian Sea. The total area of the country is 86,600 km^2. The population of Azerbaijan as of March 1, 2022 reached 10,164,464 people, the population density is 117 people per km^2 [32].

Azerbaijan has a unique geographical position, being at the crossroads of Europe and Asia, which gives it certain advantages and shapes the relief. Up to 60 % of the total area of the country is occupied by mountains, of which 43 % have a height of more than 1000 m, and 17 % of the area is occupied by low mountains and foothills. The rest of the country's territory, i.e., 40 % of the area, covers plains and lowlands with high mountains, intermountain depressions, valleys, and volcanic highlands. At the same time, 18 % of flats and lowlands are located 28 m below sea level [33].

Given the complexity of the landscape and suitability for agriculture, Azerbaijan refers to the category of land-poor countries in the world. According to the State Committee on Property Issues of the Republic of Azerbaijan, only 55.2 % of the country's land fund is suitable for agriculture, of which only 44.4 % of arable land is used for agriculture and perennial crops. The situation with arable land has become even more complicated by the fact that 20 % of the territories of Azerbaijan were under occupation for almost 30 years. Ecocide of agricultural lands as a result of burning land and forests, destruction of flora and fauna, widespread contamination of liberated territories with mines and other illegal actions led to the degradation of fertile lands in Karabakh.

Mexico is located in the south of North America and occupies most of Central America. To the west and south, the country is washed by the Pacific Ocean and to the east by the Gulf of Mexico and the Caribbean Sea. Mexico is the northern part of Latin America and the most populous country.

Mexico covers an area of 1,972,550 km^2 and is the 13th largest country in the world. The population of the country is 132,838,093 people, and the population density in Mexico is 67.6 per km^2 [34]. The relief of the country is made up of high mountain ranges, low coastal plains, high mountain plateaus, and deserts. Most of the territory of Mexico lies 1000 m above sea level.

Mountainous regions and highlands occupy almost 2/3 of the country's area. At the same time, the highlands, which occupy most of Mexico, in places rise above 3000 m or consist of vast depressions with gentle slopes. The lowlands and plains account for only 25 % of the country's territory. Thus, Mexico is also characterized by a lack of land and the predominance of remote mountainous regions with hard-to-reach settlements [35].

According to the World Bank's set of development indicators, generated from officially renowned sources, agricultural land (% of land area) in Mexico was 54.99 % in 2018 [36]. Agricultural lands are the territories which are arable, and occupied by permanent crops and permanent pastures.

5.2.4 THE CLIMATE

The characteristic topographical features and the main landscape types determined the diversity of climatic conditions in Azerbaijan and Mexico.

Azerbaijan, being a predominantly mountainous country, at the same time has vast lowlands, valleys, sea and other water resources that shape the country's climate. The country is protected from the invasion of cold air masses from the north by the main Caucasian ridge. Depending on the height above the level, several types of climate, namely semi-desert and dry steppe climate types are observed in Azerbaijan, which are characterized by hot summers and mild winters with little precipitation due to intense evaporation; humid subtropical type with warm-temperate climate and dry summers; cold climate with ample rainfall, which is distinctive for the Alpine zone of the greater and Lesser Caucasus, and others. Northern winds observed on the Absheron Peninsula sometimes even reach the strength of a hurricane [37, 38].

Mexico is also distinguished by its diverse landscape and unique geographical position, being a mountainous country, and possessing significant marine and other water resources that shape the country's climate. In the north of Mexico, the climate is subtropical, in the rest of the country it is predominantly tropical, on the coastal plains it is humid and hot [35, 39].

On the Pacific coast, daytime temperatures throughout the year do not fall below +30 °C degrees, and nighttime temperatures range from 21 to 24 °C. Temperatures are cooler on the Caribbean coast. In the winter months, during the day, the air warms up to +24 °C, and in the summer – up to +31 °C, at night, about 19 °C of heat is observed in winter and 25 degrees of heat in summer.

In the central highlands of Mexico, the climate is sharply continental, with a maximum temperature in April and May (+27 °C), and at night in the same months the air cools down to +11 or +13 °C. In winter, daytime air temperatures rise to +21 °C, at night it is about 7 °C.

In Mexico, an altitudinal zone is well expressed. Thus, in the northern part of the country, which is the driest region of the country, at the altitudes in winter, the temperature can drop below 0 degrees. The rainy season lasts from May to October, when powerful tropical cyclones often occur. The greatest amount of rainfall is observed in the southern regions of the country.

CHAPTER 5

The geographical positions and climates of Azerbaijan and Mexico cause abundant solar radiation and heat, creating an opportunity for the cultivation of many crops and the production of solar electricity. Vegetation in both countries is distributed in altitudinal steps depending on the zonal changes in climate and soil.

5.2.5 NON-OIL SECTOR

The main priorities of the policy of both Azerbaijan and Mexico in the socio-economic sphere are aimed at diversifying the economy through the development of the non-oil sector. Alternative energy, agriculture, and "green economy" successfully fit this concept.

Today, a significant part of the remote highlands of Mexico does not have a centralized electricity supply. The population of these areas lives in the rural areas and most of them are engaged in subsistence farming. Connecting rural settlements to the centralized electrical systems is complicated due to the high capital costs for laying expensive heating networks and the construction of power lines, as well as the complexity of the terrain and the lack of infrastructure. Under these conditions, solutions for the autonomous power supply to the residents of remote and hard-to-reach areas of Mexico are uncontested.

The program adopted and implemented by the government of Mexico to provide modern clean energy to almost three million people in remote rural areas of the country without access to electricity, as well as to reduce the use of traditional biomass for domestic purposes, will certainly play an important role in improving the quality of life of villagers, increasing the productivity of rural economy, development of the regional economy, and achievement of the country's goals in the field of clean energy [26, 31].

The pace of "green energy" development in Mexico has enabled the country's energy companies to offer the lowest prices for solar energy. This allows for increasing access to electricity to all segments of the population [40]. In recent years, Azerbaijan has been focusing on the development of the "green economy" in agriculture, the second most important sector of the country after the oil industry. "Clean Environment and Green Growth" has been propagated as one of the top five national priorities [41]. The territories of the country liberated from occupation were declared a "green energy" zone [42] and an action plan for the establishment of a "green zone" in the territories of the Republic of Azerbaijan liberated from occupation in 2022–2026 was approved [43].

Furthermore, a number of factors have been taken into account. Consequently, firstly, the liberated territories, declared "green" energy zones, are predominantly agricultural. Secondly, in the process of reintegration of 1,670.3 thousand hectares of territories liberated from occupation into the country's economy, the area of agricultural land is estimated to increase by 680.8 thousand hectares of suitable arable land and 10.7 thousand hectares of household land, 247.3 thousand hectares of forests [44]. Thirdly, the policy of agricultural development in the liberated territories of Azerbaijan is based on the use of environmentally friendly and safe technol-

ogies. The country has already initiated a number of projects in the field of solar and wind energy production in the liberated territories with the involvement of investors.

5.2.6 SOLAR ENERGY

Currently, the technical potential of solar energy is estimated to be the highest among renewable energy sources, particularly in the countries with significant annual solar radiation resources.

The Mexican Republic has a huge and diverse renewable energy resource base that can provide a significant increase in clean energy capacity. Mexico's national renewable technical potential includes 24,918 GW of solar Photovoltaic power, 3,669 GW of wind power, 2.5 GW of conventional geothermal power, and 1.2 GW of additional capacity from existing hydropower facilities [45]. There are about 3126.3 solar hours during the year [35]. The level of solar radiation is 5.2 kWh/m^2 [46]. Mexico receives high levels of solar radiation over much of its territory (**Fig. 5.4**).
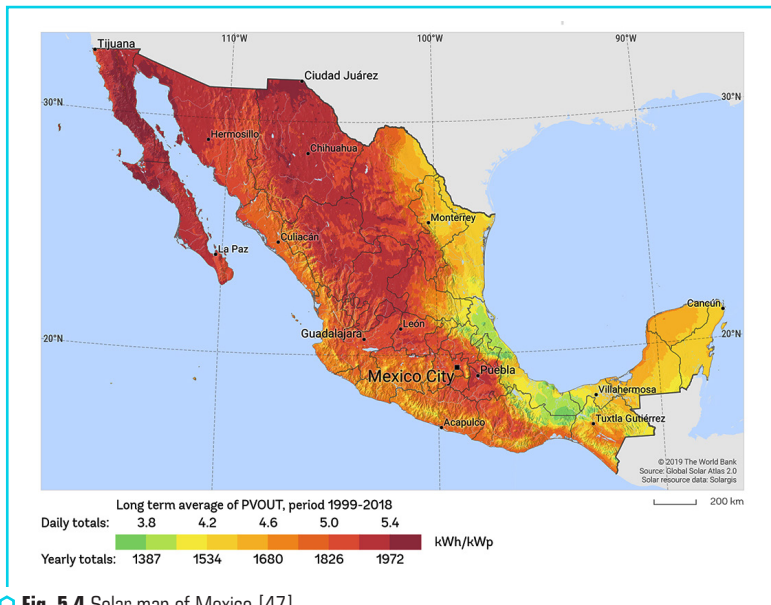

Fig. 5.4 Solar map of Mexico [47]

The Ministry of Energy of the Republic of Azerbaijan estimates the potential of economically practical and technically reasonable renewable energy sources in the country as 27,000 MW, including 23,000 MW of solar power, 3,000 MW of wind power, 380 MW of bioenergy potential,

CHAPTER 5

520 MW of mountain river potential [24, 48]. Solar radiation in Azerbaijan is 2400–3200 hours per year and is well comparable with the international indicators. The sunshine duration on the Absheron Peninsula and in the coastal areas of the Caspian Sea is about 2500 hours, and in the Nakhchivan Autonomous Republic – about 2900 hours [49]. **Fig. 5.5** demonstrates the solar radiation high level in these areas.
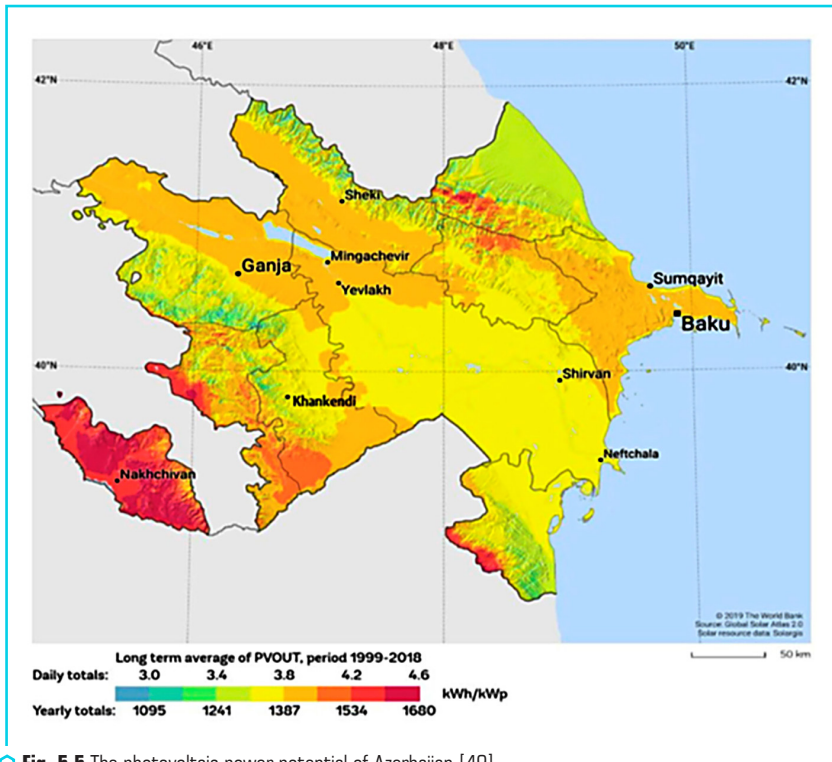
○ **Fig. 5.5** The photovoltaic power potential of Azerbaijan [49]

With sufficient investment and improved regulatory frameworks, Mexico and Azerbaijan are capable to rapidly realize this potential in short term, meet the country's electricity needs, and achieve their energy goals in the field of clean energy production. The use of solar energy is the most cost-effective way to solve the problems associated with the energy supply of rural settlements, remote and hard-to-reach areas of both Azerbaijan and Mexico, which have complex landscapes suffering from the lack of land. Along with power generation, solar installations may assist to improve agricultural systems by reducing wind erosion as well as saving water.

5.2.7 PRACTICAL EXAMPLES

The company "Gecko Logic Mexico" offers renewable energy systems that can be interconnected to the Mexican electrical net system now available in Mexico [46]. The solar panel systems are designed to capture energy from the sun (**Fig. 5.6**). The hypothesis is based on the idea of placing solar devices in areas occupied by crops in such a way that the mutual influence between them is minimal, and thus one could benefit from solar devices for crops.

○ **Fig. 5.6** Solar farm [46]

Azerbaijan has favorable climatic conditions, sufficient amount of heat and light, which enable growing and harvesting some agricultural crops twice a year. The main trends of agricultural production in the country include crop production, as well as grain-growing, vegetable-growing, fodder crops, tea-growing, potato-growing and various types of fruits [38].

Crop production is also the leading branch of Mexican agriculture, and the main crops grown include wheat, corn, soybeans, rice, beans, coffee, tomatoes, fruits, and cotton [50].

For the first time in Azerbaijan, as part of the "Agrovoltaics" pilot project, various agricultural plants were sown on a plot with solar panels in the village of Sarygamysh, Samukh region. Vegetables (peas, onions, red beets, carrots) were sown in the inter-panel space on an area of 1.2 hectares [51].

A group of Stanford University researchers recommends using solar-panels in agricultural fields that cultivate agave (**Fig. 5.7**), the plant that is used to make tequila [50]. Solar panels have to be washed to keep off the dust in the desert and maintain efficient electricity production. From this point of view, it seems that water is wasted. However, agave plants need water, and co-locating

CHAPTER 5

them together proves beneficial. One of the major issues is that most of the food crops do not grow in deserts because of low water availability, and soil not being very fertile. But agave and aloe are adapted to desert landscapes.

Azerbaijan and Mexico already have experience in installing and operating solar power plants. Thus, in Azerbaijan, solar power plants operate in Gobustan, in the villages of Surakhani and Sahil (**Fig. 5.8**), on the island of Pirallahi, in the regions Samukh and Garadagh, Sumgayit and Nakhchivan.

A wide network of solar power plants installed in various regions of Mexico is available [52]. Many of the proposed solar installations consist of large photovoltaic systems [18].

○ **Fig. 5.7** Agave for production of tequila [50]

○ **Fig. 5.8** Surakhani, Azerbaijan

5.3 CHALLENGES OF COMBINING SOLAR ENERGY AND AGRICULTURE

As photovoltaic plants continue to grow, the use of land for solar farms upsurges the competition for land resources between food production and clean energy [53]. Although photovoltaic systems require less land than other renewable energy options [54], in fact, commercial photovoltaic power plants can occupy a significant area of land locally.

One of the first experiments recorded and described in the literature to develop an agro-power plant on a farm was the system in Montpellier, France, in 2013 [55]. The system grew lettuce in combination with a system consisting of photovoltaic modules mounted on 0.8 m wide piles. The same piece of land was used for electricity and food production. The results of the experiments showed that the shades of the PV matrices had no significant effect on lettuce yield.

To date, three types of agro-electric systems have been proposed for the simultaneous growth of crops and electricity production on agricultural lands. The first type was proposed in the early 1980s using photovoltaic panels in the spaces between crop rows [56]. The second type is the photovoltaic greenhouse, in which a part of the transparent roof is replaced by photovoltaic panels [57]. The third type is the photovoltaic systems mounted on poles above the crops, which consist of pipes and rows of photovoltaic panels. They are installed on the ground and located at regular intervals allowing enough sunlight to reach the plants for photosynthesis.

An example of the placement of solar concentrators is described in [58, 59]. In 2019–2020 we have proposed to collocate our solar concentrators with different types of plants [58, 59]. In **Fig. 5.9** we demonstrate the proposed structure.

a *b*
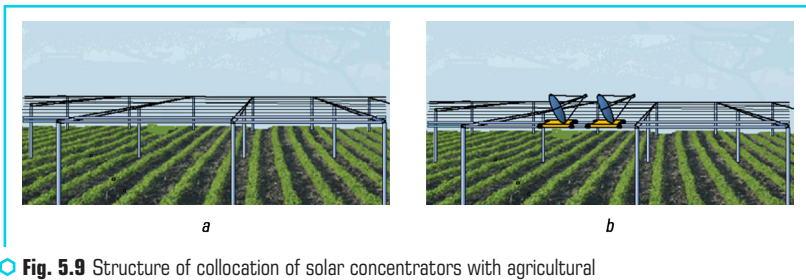
○ **Fig. 5.9** Structure of collocation of solar concentrators with agricultural fields: *a* – Structure; *b* – Structure with solar concentrators [58]

In 2018, Amaducci and Colauzzi [60] proposed an agro-electric system, solar tracking, mounted on suspended structures (piles). The horizontal main axle is mounted on frames, on which the secondary axles supporting the solar panels are pivotally connected. The two shafts rotate driven by interconnected electric motors through an innovative wireless communication and control system.

To simulate the growth and production of crops in the shade of the Agro voltaic system, Scilab [61] develops a software platform combining the radiation and shading model with the

CHAPTER 5

universal plant growth simulator GECROS [62]. The GECROS agricultural crop model predicts biomass and yield depending on climatic factors (radiation, temperature, wind speed and humidity) and available water and nitrogen amount in the soil.

We propose using the solar concentrators in the fields of Mexico and Azerbaijan. For Mexico, these can be systems together with common crops such as beans, corn, and agave. For Azerbaijan, these can be plantations of early vegetables, fields of potatoes or beets. The spaces between plant rows can be used to install solar concentrators. Moreover, the parabolic surface dimensions do not affect the plants at all.

Global demand for energy leads to an increase in the need for the use of green energy for irrigation, domestic purposes, etc. The studies [13–19, 53–55] describe the solar concentrators installed in combination with an agricultural field infrastructure. They show the economic feasibility of these systems in some rural areas and their opportunities for the electrification of the latter, while stimulating their economic growth.

The first problem required to be solved for combining solar energy with agriculture is the choice of solar concentrators and the most suitable crops for such concentrators.

The need for solar energy varies for different crops depending on their metabolism and the timing of sunlight use. The design of solar concentrators and the mounting methods (distance and height of frames) can generate different amounts of energy according to the requirements of selected crops.

One of the motivating options can be obtained using parabolic dish solar concentrators covered with flat triangular or square mirrors. For example, the studies [63–67] present the development of such concentrators. The cost of such a solar concentrator is low due to the modeling of a parabolic surface by flat mirrors, and small dimensions (from 2 to 3 meters in diameter). Such a concentrator operates in two modes:

1) capturing solar energy, when the parabolic dish axis is directed towards the sun;

2) in the minimum shadow, when the parabolic dish axis is fixed perpendicular to the sun's direction.

The hypothesis is based on the idea of placing solar devices in areas occupied by crops, so that the interaction between them is minimal, thus, benefitting from solar devices for crops.

5.4 SOLAR CONCENTRATOR PROTOTYPES

Before discussing the mathematical model for the evaluation of solar concentrators and agricultural plants we present several prototypes of solar concentrators and discuss the existing problems.

We have developed several prototypes of solar concentrators. As an example of solar concentrators, we selected parabolic solar concentrators with plane mirrors that approximate the parabolic surface. This decision is based on our experience in developing new solar concentrator prototypes that are compact, light, and inexpensive.

During the last decades we have developed several variants of solar concentrators with parabolic surfaces. To decrease their cost, we propose to approximate the parabolic surface using flat triangular or square mirrors. For this purpose, a special support frame was developed. **Fig. 5.10** shows the support frame simulated using SolidWorks [68]. The structure consists of bars and nodes [69–71].
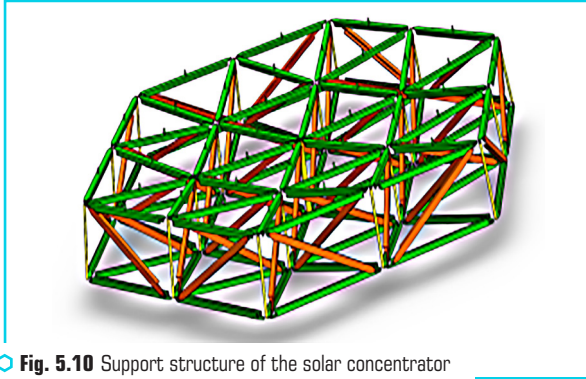
○ **Fig. 5.10** Support structure of the solar concentrator with triangular mirrors

The bars are made from aluminum angles that are connected by screws (**Fig. 5.11**).

a

b
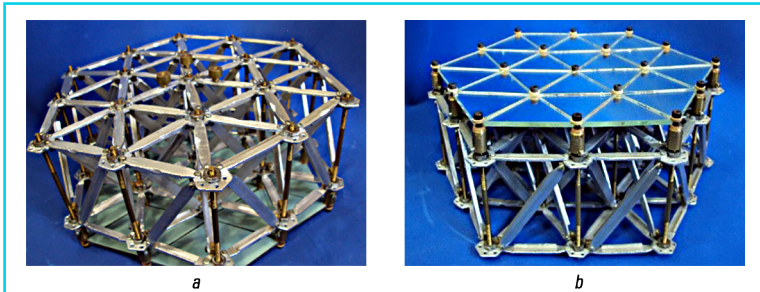
○ **Fig. 5.11** Structure of the first prototype: *a* – backside of the concentrator; *b* – right side of the concentrator with flat triangular mirrors

Prototype of a solar concentrator

The first solar concentrator prototype was developed, as shown in **Fig. 5.11**. It contains 24 triangular flat mirrors. **Fig. 5.11, *a*** displays the backside of the solar concentrator. The structure of the support frame is clearly presented in this figure. The aluminum bars are connected to

CHAPTER 5

each other by screws and form a triangular structure where it is possible to collocate the flat triangular mirrors, as exhibited in **Fig. 5.11, *b***. This prototype was made manually. It is a labor-intensive assembly. Therefore, it is very important to automatize this process.

We propose prototypes of solar concentrators with flat triangular or square mirrors. These concentrators have a support frame from bars and nodes. To automatize the structural construction process, we propose an automatic assembly system that can be used for the construction of the solar concentrator support frame. The first step is to simulate the structure and the two main modules (manipulator and computer vision) using SolidWorks. The results of the simulation will be used to fabricate real prototypes in the future.

5.5 MATHEMATICAL MODEL FOR EVALUATION OF SOLAR CONCENTRATORS AND AGRICULTURAL PLANTS

The main aim of this study is to develop a methodology for evaluating the effectiveness of possible models for combining solar concentrators with a certain type of plant. The methodology we propose in solving two tasks. The first task is to develop a mathematical model, which includes two important steps. The first step implies the development of an analytical model with the parameters characterizing agricultural fields. The second step is to evaluate the characteristics of the solar concentrator.

The second task implies the computer implementation of the developed model and virtualizes the interaction process of crops on an agricultural field and the placement of solar concentrators on it to obtain the maximum productivity of both.

The hypothesis is based on the idea of placing solar devices in areas occupied by crops, so that the interaction between them is minimal, thus, benefitting from solar devices for crops (**Fig. 5.12**).

Detailed implementation of the first task is described below.

The parameters taken into account in the fields include the field area, its slope, soil type, humidity, spacing between the rows, crop type, crop density, maximum plant width, and plant height. Irritability of plants to external agents (light, temperature, humidity, etc.) and plant development are determinable by the timing of sowing, germination, growth and harvesting.

The objective function may include all of these parameters or some of the most important in a particular situation. The simplest model is the linear model. In this case, the objective function has the following form:

$$f_1\left(x\right) = \sum_{i=1}^{N} a_i x_i,$$ (5.1)

where x_i – the selected parameters for the field and plants; a_i – the coefficients obtained by calculation or experiment for a specific task; $i = 1, \ldots, N$.
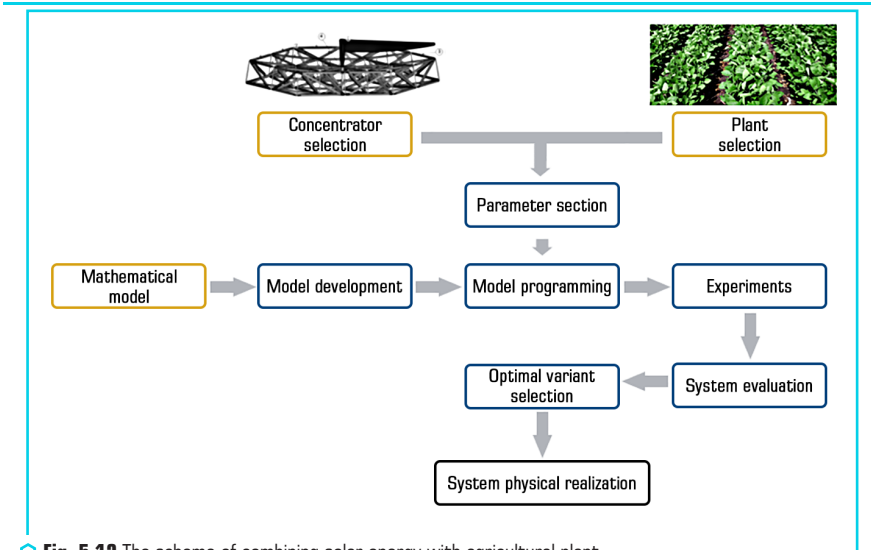
Fig. 5.12 The scheme of combining solar energy with agricultural plant

The characteristics taken into account in solar concentrators include their dimensions, weight, plate width or dish diameter, shade produced, mounting structure, material of construction, quantity and distribution of solar concentrators. The type of objective function is selected depending on the specific task. In this case, the objective function can be presented as follows:

$$f_2(y) = \sum_{j=1}^{M} b_j y_j,$$

(5.2)

where y_j – the selected parameters of the characteristics of solar concentrators; b_j – the coefficients obtained by calculation or experiment; $j = 1, \ldots, M$.

Some of these parameters can be obtained from various statistical tables, for example, the yield rate of certain crops. Certain parameters require additional mathematical calculations, for example, how many concentrators can be placed on a field with a predetermined distance between the poles (supports), etc. Some values can be obtained during the operation of the first real prototype of the combined system.

The efficiency of the system functioning is evaluated by two main criteria. The first criterion is the maximization of yield per field, and the second criterion is the maximum number of solar concentrators distributed per field.

Based on these goals, the first objective functions and models are constructed. Taking into account these functions and the ratio of the parameters of solar concentrators and cultivation fields, secondary goals can be obtained.

CHAPTER 5

Based on these objective functions, new functions will be defined to determine the relationship between field parameters and concentrators' characteristics. For example, determination of the stability of solar concentrator support on the ground or the amount of shadow by solar concentrators on plants throughout the day. The computer system can be developed by model developers, or available software systems can be used, for example, software modules described in [66].

5.6 DISCUSSION OF POSSIBLE OPTIONS FOR THE MODEL IMPLEMENTATION

A holistic system combining renewable energy sources and agricultural fields may use new designs of solar concentrators. **Fig. 5.13** shows several prototypes of solar concentrators developed and patented in Mexico, Spain and the United States of America [17, 63–67]. The developed prototypes are 1 meter in diameter. Since the support structure is made of aluminum poles, it is not heavy. The cost of prototype materials is low. For example, flat mirrors are now available on market for about 3 USD per square meter. The only expensive and time-consuming step is assembling. This stage is estimated to require automation in the future, which will significantly reduce the cost of the assembling process.
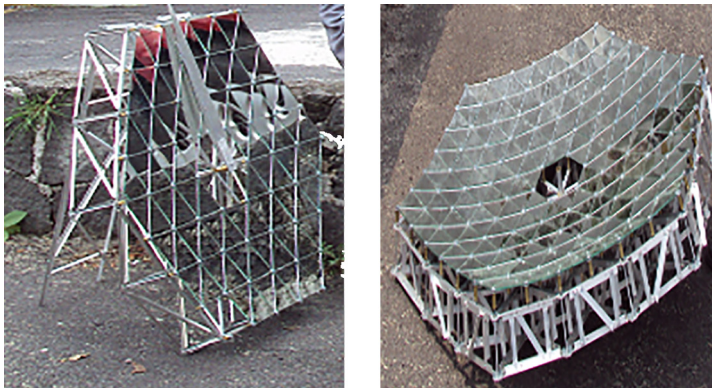
○ **Fig. 5.13** Prototypes of flat mirror solar concentrators

Equipment technology (MET) has been developed over the past few years [72]. The task of manufacturing solar concentrators was chosen as an application of MET. Various types of solar concentrators with flat mirrors and their prototypes have been developed so far. These concentrators can be installed on the horizontal roofs of buildings, as are in many cities and towns in Mexico. Installing solar concentrators in agricultural fields is a new trend. This study proposes, as an ex-

CHAPTER 5

ample, to use these solar concentrators in potato fields in Azerbaijan and agave fields in Mexico to achieve dual benefits such as power generation and minimal crop losses.

The main problem is the automatization of the assembly process of these solar concentrators. Thus, we propose two methods of assembly, which is, using a parabolic rule and using a robotic arm with a stereoscopic vision system. Both methods are described in this article.

Parabolic surface adjustment

The concept of easily constructing a parabolic surface was patented in the USA, Mexico, and Spain [69–71]. The tool used is the parabolic rule, as illustrated in **Fig. 5.14** (the parabolic rule is colored red). This rule is installed on the center of the support structure (central tube) and can rotate over the surface. In the screw location, the screw must be rotated until it contacts the parabolic rule. This procedure is performed for all screws of the support frame structure. Thus, the screw heads will have different heights and the screw heights will approximate the parabolic surface.
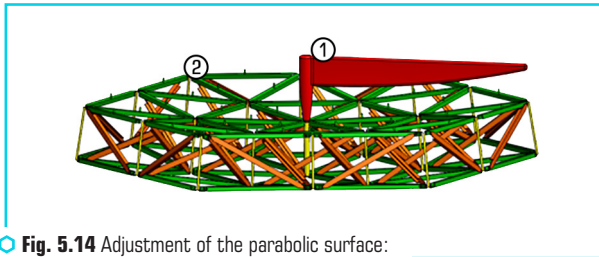
Fig. 5.14 Adjustment of the parabolic surface:
1 – parabolic rule; 2 – solar concentrator

The parabolic rule can also be used to prepare the structure of a solar concentrator to collocate the flat mirrors.

Manipulator and computer vision system

To automatize the process, it is proposed to use a robot manipulator with a computer vision system. The proposed robot manipulator is depicted in **Fig. 5.15**.

Fig. 5.15 Adjustment of parabolic surface using:
1 – the parabolic rule; 2 – the manipulator

CHAPTER 5

The second task implies the computer implementation of the developed model and virtualizes the interaction process of crops on an agricultural field and the placement of solar concentrators on it to obtain the maximum productivity of both.

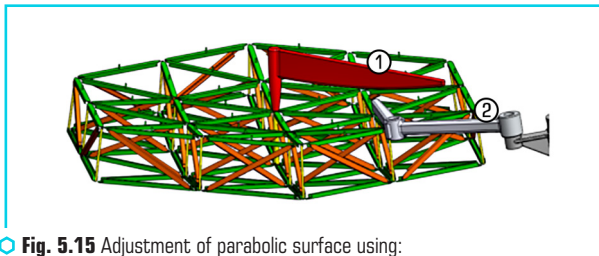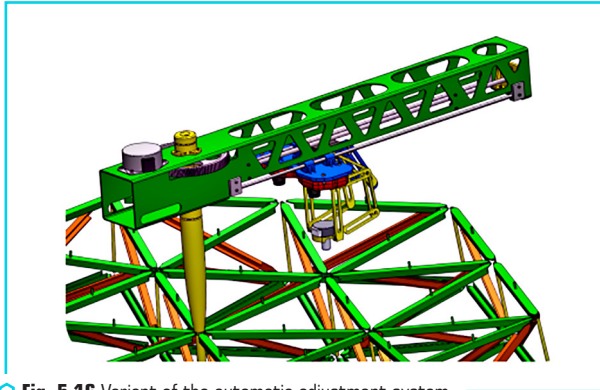Another variant of the system for an automatic adjustment that we propose is displayed in **Fig. 5.16**. In this system, a central tube is installed as a guide for a special type of manipulator.

○ **Fig. 5.16** Variant of the automatic adjustment system

Components of the system for automatic adjustment

A more detailed view of the guide showing the different components is presented in **Fig. 5.17**. This guide contains two important components: the manipulator and the computer vision block.

○ **Fig. 5.17** Components of the system for automatic adjustment

The computer vision system contains two cameras to implement a stereoscopic vision, which is used to evaluate the distance to the point of the screw position. A stereoscopic kit with two digital cameras is depicted in **Fig. 5.18**.

Fig. 5.18 Stereoscopic kit with two digital cameras

To recognize better the position of the screw, we propose to use a mark, as indicated in **Fig. 5.19**.
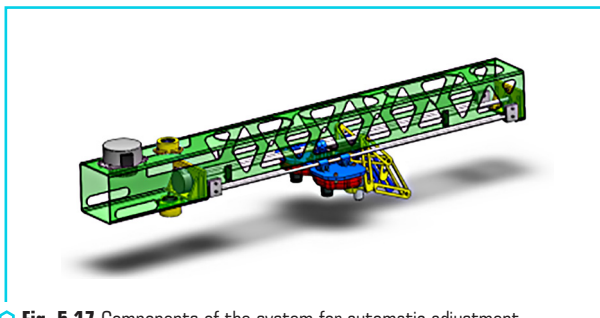

Fig. 5.19 Example of a mark for screw detection

Another variant of the system for an automatic adjustment we propose is displayed in **Fig. 5.15**. In this system, a central tube is installed as a guide for a special type of manipulator.

The prototypes of solar concentrators with flat triangular or square mirrors have the support frame from bars and nodes. The goal is to automatize the structural construction process. We propose an automatic assembly system that can be used for the construction of the solar concentrator support frame. The first step is to simulate the structure and the two main modules (manipulator and computer vision) using SolidWorks. The results of the simulation will be used to fabricate real prototypes in the future.

In Azerbaijan, the period of active agricultural activity, for example, for planting potatoes or beets, depending on the region, starts from late February to April. Potato varieties are distinguished depending on how many days after planting the tubes are dug out: early – after 50–65 days; medium early – after 65–80 days; mid-season – after 80–95 days; medium-late – after 95–110 days; late – after 110 or more days. Planting rows are often wide enough to install solar concentrators.

In Mexico, cultivation starts in April and ends in October or November [55]. Solar concentrators can be used during this 7-month period. In early May, plants do not consume much solar

CHAPTER 5

energy, and during this period, the solar concentrators can be placed easily. However, by the end of the second month, the plants are fully grown and need more sunlight. In this case, solar concentrators can be removed from the field and put into storage. In the period from November to April, concentrators can be installed throughout the field.

Fig. 5.20 shows the extent of agricultural activity during the twelve months of the year in Mexico. It is possible to compare the season in Mexico with season in Azerbaijan (**Fig. 5.21, *a***). The harvest periods correspond to the grayscale rectangles in **Fig. 5.21, *a***.
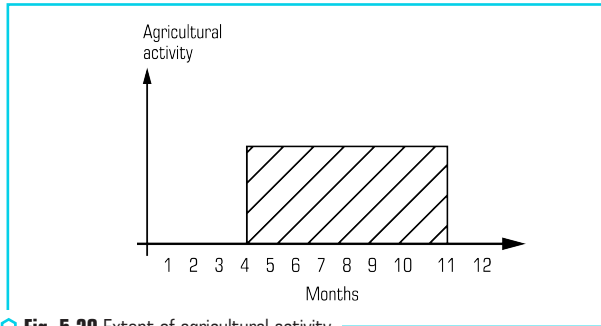
Fig. 5.20 Extent of agricultural activity
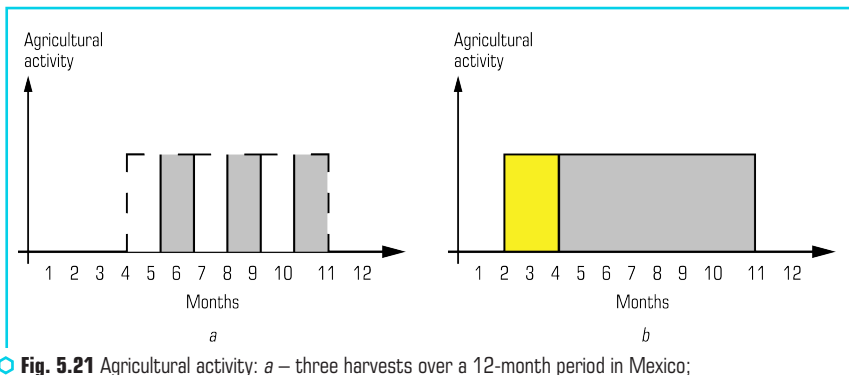
Fig. 5.21 Agricultural activity: *a* – three harvests over a 12-month period in Mexico; *b* – one harvest period in Azerbaijan

The maximum number of solar collectors could be placed in the field during the November-April period (**Fig. 5.20**). The crop is harvested two or three times during the April-November period when agricultural activity recommences; thus, three harvests were considered in the present study (**Fig. 5.21, *a***).

Each harvest was divided into two periods. The first period corresponded to when the plants are small and solar concentrators can be used, while the second period corresponded to when the plants are mature, during which all concentrators are removed.

Secondly, the situation with potato fields in Azerbaijan, characterized by only one harvest period per year is shown in **Fig. 5.21, *b***.

CONCLUSIONS

We have developed several prototypes of solar concentrators that are compact, light, and inexpensive. We selected parabolic solar concentrators with plane mirrors that approximate the parabolic surface.

We proposed the creation of integrated systems for electricity generation and agricultural products on one field of land through the use of solar energy. The proposed models, without any need for empirical studies directly on the field, made it possible to evaluate the distribution of solar concentrators, to avoid their assembly in the field, and to obtain results without conducting experiments on real sowing and harvesting cycles.

The next stage of the study includes the development of an optimal strategy for placing solar concentrators among crops and the production of new prototypes of solar concentrators with the parameters obtained after experimental trials. The proposed system includes a dual source of income for farmers, employment opportunities for both solar and crop production, rural electrification, and the availability of electricity for local agricultural processing.

Due to the geospatial positions of Azerbaijan and Mexico located in privileged regions of solar radiation, they have many opportunities for the practical use of solar energy.

The main problem of the proposed solar concentrators is the automatization of their assembly. We analyzed two approaches for the assembly automatization of solar concentrator frames. The both methods can be further realized and do inexpensive the solar concentrator manufacturing.

CONFLICT OF INTEREST

The authors declare that they have no conflict of interest in relation to this research, whether financial, personal, authorship or otherwise, that could affect the research and its results presented in this paper.

ACKNOWLEDGMENTS

CHAPTER 5

REFERENCES

1. Analysis of climate policies of the countries of Eastern Europe, Caucasus and Central Asia (EECCA) (2020). CAN, 36. Available at: https://infoclimate.org/wp-content/uploads/2020/12/overview-of-climate-policies-eecca.pdf Last accessed: 19.08.2022

2. The Paris Agreement (2015). Available at: https://unfccc.int/process-and-meetings/the-paris-agreement/the-paris-agreement Last accessed: 19.08.2022

3. FAO Strategy on Climate Change (2017). Food and Agriculture Organization of the United Nations. Rome. Available at: https://agris.fao.org/agris-search/search.do?recordID=XF2018000291 Last accessed: 19.08.2022

4. Viana, C. M., Freire, D., Abrantes, P., Rocha, J., Pereira, P. (2022). Agricultural land systems importance for supporting food security and sustainable development goals: A systematic review. Science of The Total Environment, 806, 150718. doi: https://doi.org/10.1016/j.scitotenv.2021.150718

5. Majumdar, D., Pasqualetti, M. J. (2018). Dual use of agricultural land: Introducing 'agrivoltaics' in Phoenix Metropolitan Statistical Area, USA. Landscape and Urban Planning, 170, 150–168. doi: https://doi.org/10.1016/j.landurbplan.2017.10.011

6. Skuras, D., Psaltopoulos, D. (2012). A broad overview of the main problems derived from climate change that will affect agricultural production in the Mediterranean area. Building Resilience for Adaptation to Climate Change in the Agriculture Sector, 23, 217–260.

7. Zhu, X., Zhang, Z., Chen, X., Jia, F., Chai, Y. (2022). Nexus of mixed-use vitality, carbon emissions and sustainability of mixed-use rural communities: The case of Zhejiang. Journal of Cleaner Production, 330, 129766. doi: https://doi.org/10.1016/j.jclepro.2021.129766

8. World Population Prospects 2022. (2022). United Nation, 54. Available at: https://www.un.org/development/desa/pd/sites/www.un.org.development.desa.pd/files/wpp2022_summary_of_results.pdf Last accessed: 19.08.2022

9. Global Report on Food Crises (2019). Food Security Information Network. Available at: http://www.fsinplatform.org/global-report-food-crises-2019 Last accessed: 19.08.2022

10. Dinesh, H., Pearce, J. M. (2016). The potential of agrivoltaic systems. Renewable and Sustainable Energy Reviews, 54, 299–308. doi: https://doi.org/10.1016/j.rser.2015.10.024

11. Global Renewables Outlook: Energy Transformation 2050 (2020). International Renewable Energy Agency. Abu Dhabi.

12. Weselek, A., Ehmann, A., Zikeli, S., Lewandowski, I., Schindele, S., Högy, P. (2019). Agrophotovoltaic systems: applications, challenges, and opportunities. A review. Agronomy for Sustainable Development, 39 (4). doi: https://doi.org/10.1007/s13593-019-0581-3

13. Santra, P., Pande, P.C., Kumar, S., Mishra, D., Singh, R. K. (2017). Agri-voltaics or solar farming: the concept of integrating solar PV based electricity generation and crop production in a single land use system. International Journal of Renewable Energy Research, 7 (2), 694–699. doi: https://doi.org/10.20508/ijrer.v7i2.5582.g7049

14. Coşgun, A. E. (2021). The potential of Agrivoltaic systems in Turkey. Energy Reports, 7, 105–111. doi: https://doi.org/10.1016/j.egyr.2021.06.017

15. Zainol Abidin, M. A., Mahyuddin, M. N., Mohd Zainuri, M. A. A. (2021). Solar Photovoltaic Architecture and Agronomic Management in Agrivoltaic System: A Review. Sustainability, 13 (14), 7846. doi: https://doi.org/10.3390/su13147846

16. Cho, J., Park, S. M., Park, A. R., Lee, O. C., Nam, G., Ra, I.-H. (2020). Application of Photovoltaic Systems for Agriculture: A Study on the Relationship between Power Generation and Farming for the Improvement of Photovoltaic Applications in Agriculture. Energies, 13 (18), 4815. doi: https://doi.org/10.3390/en13184815

17. Kussul, E., Baydyk, T., Estrada, A. E., González, M. T. R., Wunsch II, D. (2019). Solar concentrators manufacture and automation. Open Physics, 17 (1), 93–103. doi: https://doi.org/10.1515/phys-2019-0011

18. Ravi, S., Macknick, J., Lobell, D., Field, C., Ganesan, K., Jain, R., Elchinger, M., Stoltenberg, B. (2016). Colocation opportunities for large solar infrastructures and agriculture in drylands. Applied Energy, 165, 383–392. doi: https://doi.org/10.1016/j.apenergy.2015.12.078

19. Sekiyama, T., Nagashima, A. (2019). Solar Sharing for Both Food and Clean Energy Production: Performance of Agrivoltaic Systems for Corn, A Typical Shade-Intolerant Crop. Environments, 6 (6), 65. doi: https://doi.org/10.3390/environments6060065

20. Alemán-Nava, G. S., Casiano-Flores, V. H., Cárdenas-Chávez, D. L., Díaz-Chavez, R., Scarlat, N., Mahlknecht, J. et al. (2014). Renewable energy research progress in Mexico: A review. Renewable and Sustainable Energy Reviews, 32, 140–153. doi: https://doi.org/10.1016/j.rser.2014.01.004

21. Agostini, A., Colauzzi, M., Amaducci, S. (2021). Innovative agrivoltaic systems to produce sustainable energy: An economic and environmental assessment. Applied Energy, 281, 116102. doi: https://doi.org/10.1016/j.apenergy.2020.116102

22. World Bank list of economies (2021). Available at: https://cdn.ymaws.com/www.autism-insar.org/resource/resmgr/docs/world_bank_lists/world_bank_list_of_economies.pdf Last accessed: 19.08.2022

23. In-depth Review of the Energy Efficiency Policy of the Republic of Azerbaijan (2020). Available at: https://www.energycharter.org/what-we-do/energy-efficiency/energy-efficiency-country-reviews/in-depth-review-of-energy-efficiency-policies-and-programmes/in-depth-review-of-the-energy-efficiency-policy-of-the-republic-of-azerbaijan Last accessed: 19.08.2022

24. The use of renewable energy resources in Azerbaijan. Ministry of Energy of the Republic of Azerbaijan (2022). Available at: https://minenergy.gov.az/en/alternativ-ve-berpa-olunan-enerji/azerbaycanda-berpa-olunan-enerji-menbelerinden-istifade Last accessed: 19.08.2022

25. Veysey, J., Octaviano, C., Calvin, K., Martinez, S. H., Kitous, A., McFarland, J., van der Zwaan, B. (2016). Pathways to Mexico's climate change mitigation targets: A multi-model analysis. Energy Economics, 56, 587–599. doi: https://doi.org/10.1016/j.eneco.2015.04.011

CHAPTER 5

26. Energy Resource Guide. Mexico – Renewable Energy (2021). Available at: https://www.trade.gov/energy-resource-guide-mexico-renewable-energy Last accessed: 19.08.2022

27. Our World in Data based on BP Statistical Review of World Energy (2021). Available at: https://ourworldindata.org/energy/country/

28. Azerbaijan Renewable Energy Agency (2020). Decree No. 1159 of the President of the Republic of Azerbaijan dated 22 September 2020. Available at: https://minenergy.gov.az/en/ministry/nazirliyin-tabeliyinde-olan-qurumlar Last accessed: 20.08.2022

29. On the use of renewable energy sources in the production of electricity (2021). The law of the Republic of Azerbaijan No. 339-VIQ. 31.05.2021. Available at: https://minenergy.gov.az/en/qanunlar Last accessed: 20.08.2022

30. General Law on Climate Change Mexico. Available at: https://iea.blob.core.windows.net/assets/imports/events/13/GeneralClimateChangeLaw_Englishversion.pdf Last accessed: 20.08.2022

31. Development Program of the National Electrical System, 2022–2036 (2022). Secretaría de Energía. Available at: https://www.gob.mx/sener/articulos/programa-para-el-desarrollo-del-sistema-electrico-nacional-304042 Last accessed: 20.08.2022

32. Population. Available at: https://stat.gov.az/source/demoqraphy/?lang=en Last accessed: 20.08.2022

33. General information on nature of Azerbaijan. Available at: https://azerbaijan.az/en/information/201 Last accessed: 20.08.2022

34. Mexico population. Available at: https://countrymeters.info/en/Mexico#population_2022 Last accessed: 20.08.2022

35. Geography of Mexico. Available at: http://worldfacts.us/Mexico-geography.htm Last accessed: 20.08.2022

36. Agricultural land (% of land area). Available at: https://tradingeconomics.com/mexico/agricultural-land-percent-of-land-area-wb-data.html Last accessed: 20.08.2022

37. Climate-Azerbaijan. Available at: https://www.azerbaijans.com/content_457_en.html Last accessed: 20.08.2022

38. RAE Aliyev, Z. H. (2018). Agriculture in Azerbaijan and its Development Prospects. JOJ Sciences, 5, 555–572.

39. A Mexico Climate Overview. Available at: https://focusonmexico.com/climate-mexico/ Last accessed: 20.08.2022

40. Mexico sets world's lowest solar price; Energy storage to hit 125 GW by 2030. Available at: https://www.reutersevents.com/renewables/pv-insider/mexico-sets-worlds-lowest-solar-price-energy-storage-hit-125-gw-2030 Last accessed: 20.08.2022

41. Azerbaijan 2030: National Priorities for Socio-Economic Develpment (2021). Order of the President of the Azerbaijan Republic 02.02.2021. Available at: https://president.az/en/articles/view/50474 Last accessed: 20.08.2022

42. On measures in connection with the creation of a "green energy" zone in the liberated territories of the Republic of Azerbaijan (2021). Order of the President of the Republic of Azerbaijan No. 2620. 03.05.2021. Available at: https://president.az/az/articles/view/51355/print Last accessed: 20.08.2022

43. On approval of the Action Plan on establishment of a "green zone" in the territories of the Republic of Azerbaijan liberated from occupation in 2022–2026 (2022). Order of the Cabinet of Ministers No. 357. 21.06.2022. Available at: https://nk.gov.az/az/document/6209/ Last accessed: 20.08.2022

44. Valiyev, A.H. (2020). Evaluation of the potential of agricultural soils in the occupied territories. Agricultural economics, 3 (33), 60–70.

45. Mexico Clean Energy Report – Executive Summary (2021). NREL, 64. Available at: https://www.nrel.gov/docs/fy22osti/82580.pdf Last accessed: 20.08.2022

46. Industrial solar power plant and solar farms in Mexico. Available at: https://www.solarenergymexico.com/solar-energy-industrial-use/ Last accessed: 20.08.2022

47. Solar resource maps of Mexico. Available at: https://solargis.com/maps-and-gis-data/download/mexicot

48. Mustafayev, F., Kulawczuk, P., Orobello, C. (2022). Renewable Energy Status in Azerbaijan: Solar and Wind Potentials for Future Development. Energies, 15 (2), 401. doi: https://doi.org/10.3390/en15020401

49. The photovoltaic power potential of Azerbaijan (2021). The World Bank Group Global Solar Atlas. Global Solar Atlas. Available at: http://www.globalsolaratlas.info/ Last accessed: 20.08.2022

50. A Solar Farm That Doubles As A Tequila Plant Operation (2014). Sidney Brownstone. Fast Company. Available at: https://www.fastcompany.com/3029260/a-solar-farm-that-doubles-as-a-tequila-making-operation Last accessed: 20.08.2022

51. As part of the «Agrivoltaics» pilot project, various agricultural plants sown on a plot with solar panels. Available at: https://agro.gov.az/az/news/aqrovoltaika-layihesi-cercivesinde-guenes-panelleri-olan-erazide-muextelif-kend-teserruefati-bitkilerinin-sepini-heyata-kecirilib Last accessed: 20.08.2022

52. Renewable Energy Prospects: Mexico (2015). REmap2030. Available at: https://www.irena.org/publications/2015/May/Renewable-Energy-Prospects-Mexico Last accessed: 20.08.2022

53. Nonhebel, S. (2005). Renewable energy and food supply: will there be enough land? Renewable and Sustainable Energy Reviews, 9 (2), 191–201. doi: https://doi.org/10.1016/j.rser.2004.02.003

54. Fthenakis, V., Kim, H. C. (2009). Land use and electricity generation: A life-cycle analysis. Renewable and Sustainable Energy Reviews, 13 (6-7), 1465–1474. doi: https://doi.org/10.1016/j.rser.2008.09.017

55. Marrou, H., Guilioni, L., Dufour, L., Dupraz, C., Wery, J. (2013). Microclimate under agrivoltaic systems: Is crop growth rate affected in the partial shade of solar panels?

CHAPTER 5

Agricultural and Forest Meteorology, 177, 117–132. doi: https://doi.org/10.1016/j.agrformet.2013.04.012

56. Goetzberger, A., Zastrow, A. (1982). On the Coexistence of Solar-Energy Conversion and Plant Cultivation. International Journal of Solar Energy, 1 (1), 55–69. doi: https://doi.org/10.1080/01425918208909875

57. Scognamiglio, A. (2014). Photovoltaic Greenhouses: A Feasible Solution for Islands? Design, Operation Monitoring and Lessons Learned from a Real Case Study. The 6th World Conf. on Photovoltaic Energy Conversion. Kyoto.

58. Kussul, E., Baydyk, T., Olvera-Tapia, O., Rodríguez Andrade, J. (2019). Comparison of Collocation of Solar Concentrators with Bean Fields in Mexico and Potato Fields in Canada and Micromechanical Equipment for Their Production. Journal of Energy and Power Engineering, 13 (1), 24–31. doi: https://doi.org/10.17265/1934-8975/2019.01.002

59. Kussul, E., Baydyk, T., Garcia, N., Velasco Herrera, G., Curtidor Lopez, A. V. (2020). Combinations of Solar Concentrators with Agricultural Plants. Journal of Environmental Science and Engineering B, 9 (5), 168–181. doi: https://doi.org/10.17265/2162-5263/2020.05.002

60. Amaducci, S., Yin, X., Colauzzi, M. (2018). Agrivoltaic systems to optimise land use for electric energy production. Applied Energy, 220, 545–561. doi: https://doi.org/10.1016/j.apenergy.2018.03.081

61. Scilab Enterprises and Consortium Scilab. Digiteo. Scilab: Free and Open Source software for numerical computation (OS, Version 5.4.1) (2012). Available at: http://www.scilab.org Last accessed: 20.08.2022

62. Yin, X., Van Laar, H. (2005). Crop systems dynamics: an ecophysiological simulation model for genotype-by-environment interactions. Wageningen Academic Pub. doi: https://doi.org/10.3920/978-90-8686-539-0

63. Kussul, E., Baidyk, T., Makeyev, O., Lara-Rosano, F., Saniger, J. M., Bruce, N. (2007). Development of Micro Mirror Solar Concentrator. WSEAS Trans on Power Systems, 8 (2), 188–194.

64. Kussul, E., Baidyk, T., Makeyev, O., Lara-Rosano, F., Saniger, J. M., Bruce, N. (2008). Flat Facet Parabolic Solar Concentrator with Support Cell for One and More Mirrors. WSEAS Trans on Power Systems, 8 (3), 577–586.

65. Kussul, E., Makeyev, O., Baidyk, T., SanigerBlesa, J., Bruce, N., Lara-Rosano, F. (2011). Adjustment of Solar Concentrator Support Frame. Proc. of the Intern. Conf. on Innovative Technologies. Bratislava, 314–316.

66. Kussul, E., Makeyev, O., Baidyk, T., Blesa, J. S., Bruce, N., Lara-Rosano, F. (2011). The Problem of Automation of Solar Concentrator Assembly and Adjustment. International Journal of Advanced Robotic Systems, 8 (4), 150–157. doi: https://doi.org/10.5772/45685

67. Kussul, E., Makeyev, O., Baidyk, T., Blesa, J. S., Bruce, N. (2012). Ericsson Heat Engine with Microchannel Recuperator for Solar Concentrator with Flat Mirrors. International Journal of Energy Research, 4, 165–177.

CHAPTER 5

68. Rodríguez Mendoza, J. L. (2011). Sistema robótico para ajuste de concentradores solares, Tesis para obtener el grado de Maestro en Ingeniería Mecánica-Mecatrónica. UNAM.

69. Kussul, E., Baidyk, T., Lara-Rosano, F., Saniger Blesa, J. M., Ascanio, G., Bruce, N. (2011). Pat. No. US 8,631,995 B2. Method and Device for Mirrors Position Adjustment of a Solar Concentrator, Notice of Allowance. 02.03.2010 (Mexico), 02.03.2011 (USA).

70. Kussul, E., Baydyk, T., Saniger Blesa, J. M., Bruce Davidson, N. Ch., Lara Rosano, F., Rodríguez Mendoza, J. L. (2015). Pat. No 334742. Dispositivo de soporte para concentrador solar con espejos planos, 7.02.2012. Instituto Mexicano de Propiedad Industrial. Solicitud MX/a/2012/001598. Fecha de expedición 9.10.2015.

71. Kussul, E., Baydyk, T., Saniger Blesa, J. M., Bruce Davidson, N. Ch., Lara Rosano, F., Rodríguez Mendoza, J. L. (2015). Pat. No. ES2525276 Dispositivo de soporte para concentrador solar con espejos planos, 21.07.2014, Oficina Española de Patentes y Marca. Solicitud P201490078l. Fecha de la concesión 25.09.2015.

72. Kussul, E., Baidyk, T., Ruiz-Huerta, L., Caballero-Ruiz, A., Velasco, G., Kasatkina, L. (2002). Development of micromachine tool prototypes for microfactories. Journal of Micromechanics and Microengineering, 12 (6), 795–812. doi: https://doi.org/10.1088/0960-1317/12/6/311

ENERGY FACILITIES: MANAGEMENT AND DESIGN AND TECHNOLOGICAL INNOVATIONS

Andriy Polishchuk, Volodymyr Kulyk, Vira Teptya, Sviatoslav Vishnevskyi, Yurii Hrytsiuk,
Iryna Hrytsiuk, Viacheslav Komar, Petro Lezhniuk, Vladyslav Lesko, Yuliya Malogulko,
Volodymyr Netrebskyi, Olena Sikorska, Volodymyr Khomenko, Oksana Chernysh,
Viacheslav Barsukov, Viktor Tverdokhlib, Arkadij Berezovskij, Volodymyr Slobodianyk,
Natalia Minska, Roman Shevchenko, Vasyl Servatyuk, Valery Strelets,
Victoria Lukashenko, Yaroslav Kalchenko, Ernst Kussul, Tetyana Baydyk,
Masuma Mammadova, Jorge Luis Rodriguez Mendoza

Collective monograph

Technical editor I. Prudius
Desktop publishing T. Serhiienko
Cover photo Copyright © 2022 Canva